The Planar Entry Flow Behavior of Polymer Melts: An Experimental and Numerical Analysis

by

Scott Alex White

Dissertation submitted to the Faculty of the
Virginia Polytechnic Institute and State University
in partial fulfillment of the requirements for the degree of
Doctor of Philosophy
in
Chemical Engineering

APPROVED:

Donald G. Baird, Chairman

Garth L. Wilkes

William L. Conger

Kenneth Konrad

Dean T. Mook

May 15, 1987

Blacksburg, Virginia

The Planar Entry Flow Behavior of Polymer Melts: An Experimental and Numerical Analysis

by

Scott Alex White

Donald G. Baird, Chairman

Chemical Engineering

(ABSTRACT)

The planar entry flow behavior of polystyrene, LDPE, and HDPE has been observed experimentally. The purpose of the work was to determine the cause of vortex growth and explain why this phenomenon occurs in some polymers but not in others. To accomplish this a die was constructed in which nearly any flow geometry could be formed by means of inserts. Flow visualization and flow birefringence experiments were performed using this die with 4:1 and 8:1 abrupt planar contraction geometries for τ_{12w} up to 7×10^4 Pa and $\dot{\gamma}$ from 1 to 80 sec^{-1}. From these experiments it was determined that vortex growth in a polymer is caused by the resistance to flow under the influence of extensional strain. Although extensional viscosity measurements give an indication of whether or not vortices will form, the flow behavior is best correlated by the ratio of the centerline extensional stress to the downstream wall shear stress, $\frac{\tau_{11} - \tau_{22}}{\tau_{12w}}$, measured in the entry region. The magnitude of this ratio was approximately 2 for LDPE, which exhibited vortex growth, but was approximately 1 for polystyrene, which did not exhibit vortex growth.

Based on the experimental results, the numerical work was directed towards the use of a constitutive equation which could predict the extensional properties of the polymers being modelled. The Phan-Thien Tanner model was found to give adequate rheological property predictions and was used with the penalty finite element method to simulate the entry flow behavior of LDPE and polystyrene. Both qualitative (streamline patterns) and quantitative (extensional stress ratio) agreement was found between the experimental and numerical results. Vortex growth was predicted for LDPE, but incorporation of a zero relaxation time at the corner elements was necessary to increase the limit of convergence to the point where vortex

growth was predicted. Support for the relation between vortex growth and extensional properties was given by the numerical results. It was found that, holding all other rheological properties the same, an increase in the predicted extensional viscosity of a fluid results in the prediction of larger vortices.

Acknowledgements

The author wishes to express his appreciation to Professor Donald G. Baird for his support, suggestions, and criticisms throughout the completion of this work. He would also like to express appreciation to Professor Garth L. Wilkes for his interest and suggestions concerning various aspects of this study. In addition, thanks go to Professors Conger, Konrad, Mook, and Reddy for serving on the advisory committee.

The author would like to express his appreciation to the following:

- Dr. Alex Gotsis whose finite element code made possible the comparison of experimental and numerical results in this work. His interest in entry flow provided additional direction not only to the numerical work but also to the experimental studies.
- Dr. Mike Read and who provided invaluable assistance in regards to performing flow birefringence experiments and operating equipment.
- for his expertise in machining the entry flow die and for solving other mechanical problems encountered in this work.
- for the line drawings presented in this and other work which was completed often under tight time constraints.
- The General Electric Company which provided support by donation of material and through extending the author a three year leave of absence.

• Finally, the members of Professor Baird's research group who provided advice and assistance.

Original Contributions

The author considers the following as his original contributions in this study of entry flow:

1. The design of a die for performing flow visualization and flow birefringence experiments on polymer melts. Nearly any flow geometry can be examined in the die by means of inserts.

2. The fundamental explanation of vortex formation where vortex growth has been attributed to a polymer's restriction to flow in extension relative to that in shear and recirculation has been attributed to the transfer of momentum from the bulk fluid flow across the vortex cell interface.

3. The finding that changes in M_w and MWD of a polymer or changes in the geometry of the flow region which lead to differences in flow behavior can be related to the extensional nature of entry flow.

4. The finding that the experimentally determined relation between vortex growth and extensional properties is supported numerically by the prediction of larger vortex size for a fluid with the prediction of higher extensional viscosities.

Table of Contents

List of Illustrations

List of Tables

1.0 INTRODUCTION

Simulation of polymer flow has been of great interest in the plastics industry for several years now. This is apparent from the widespread use of computer programs which simulate the flow and solidification of polymers in injection molding. The importance of such software lies in its ability to provide process design information, avoiding the typical trial and error method of design. As tooling costs for the fabrication of large plastic parts can easily approach $100,000, the value of methods which accurately design such equipment prior to machining is significant. However, the software available today provides only rough approximations of actual flow behavior, as might be expected if one considers the complexity of a transient, non-isothermal process such as injection molding.

In recent years much work has been devoted to the accurate simulation of non-Newtonian fluid flow by means of constitutive equations which more thoroughly describe the fluid's rheological properties. However the flow problem becomes quite complex due to the non-linearity which is imparted by the constitutive equation on the differential equations which govern the flow. The resulting equations can not be solved analytically and require the use of the approximation methods, such as the finite element method, in their solution. This is true even in relatively simple flow geometries in which the flow is both isothermal and at steady-state. In light of this fact, entry flow has been the subject of most numerical simulation studies.

See p27

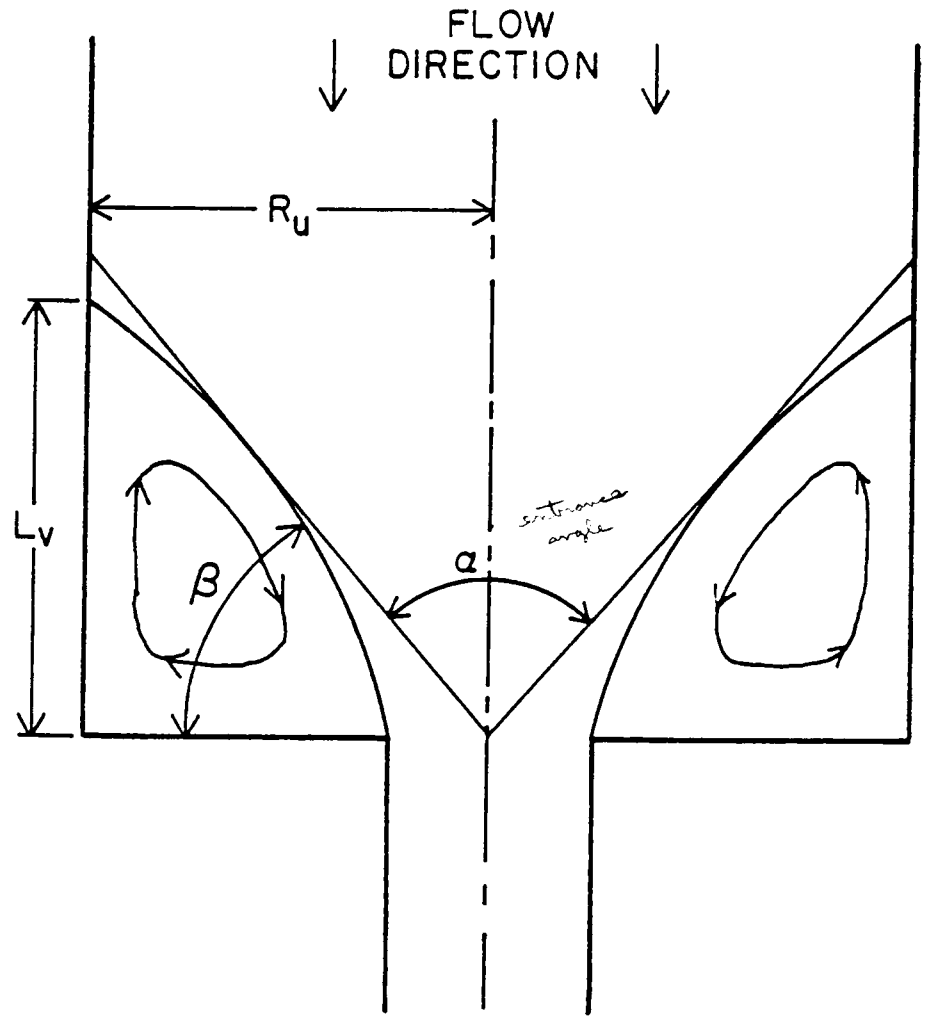

Figure 1. Entry Flow Geometry

The flow of fluid through an abrupt contraction makes use of a simple flow geometry but at the same time manifests the significantly different flow behavior of Newtonian and non-Newtonian fluids. Typically, under creeping flow conditions, Newtonian fluids will flow radially through the entry region into the contraction sweeping out the corners in the upstream channel. Even at higher rates the flow behavior changes only slightly with recirculation occurring only in a very small corner region. However, many non-Newtonian fluids will form vortices in the corners of the upstream channel as diagrammed in Figure 1 on page 2. It is this latter behavior which is being attempted to be simulated. The presence of secondary flow in non-Newtonian fluids results in different pressure drops and stress fields than would be found in Newtonian fluids. The accurate prediction of these quantities will ultimately lead to improvement of predictions of polymer flow in such processes as extrusion and also in injection molding where the complex flow can involve numerous contractions and expansions.

The work on the simulation of entry flow behavior however, has only had limited success. In most studies the numerical method has failed at Deborah numbers on the order of 1. The Deborah number represents the ratio of a characteristic relaxation time of the fluid to the time scale of the flow. Therefore, failure is occurring at the point where the non-Newtonian character of the fluid is becoming apparent. In many cases failure of the calculations has been attributed to approximation error. Approximation error refers to the inability of the numerical method to approximate the set of governing differential equations. It is believed that approximation can be improved by proper choice constitutive equation. Most of the equations used to date give unrealistic predictions of the extensional viscosity and since large stress gradients are predicted at the corners of the entrance, failure of the method may be due to the constitutive equation's inability to reflect the fluid's rheological properties correctly.

In order to understand the failure of numerical methods it is necessary to understand entry flow and what rheological properties are important in determining flow behavior. As with the numerical studies of entry flow, experimental studies have largely ignored the importance of extensional flow in the entry region. For studies of both polymer solutions and polymer melts rheological characterization of any kind has been minimal. In those cases where

rheological properties have been presented it has been limited to the measurement of shear viscosity and the primary normal stress difference.

From examination of the previous studies it is seen that entry flow has largely been considered a shear flow in spite of the fact that there is a significant extensional component in the flow due to the acceleration of the fluid through the contraction. Also, vortex growth is correlated with shear properties. This has typically involved correlating secondary cell size with the Weissenberg number (i.e. the ratio of the primary normal stress difference to twice the shear stress). Although the size of vortices appears to order with the Weissenberg number for a given material, this type of correlation provides no fundamental explanation of why vortices occur in the first place. In general, explanation of the formation of vortices has been lacking. Only recently have any explanations been presented and these have related the presence of vortices to the extensional properties of the fluid. Therefore, it appears that in understanding entry flow it will be necessary to account for the extensional properties of the fluid and this may ultimately explain the failure of numerical methods based on their inability to predict the extensional properties of the fluid. It will be the purpose of the present study to evaluate the importance of extensional flow properties on the entry flow behavior polymer melts. It is proposed to 1) provide a fundamental explanation of the origin of vortices, 2) based on this explanation provide an understanding of the effects of molecular, rheological, and geometrical parameters on entry flow behavior, and 3) based on the importance of the above parameters provide a direction towards the better prediction of entry flow behavior by numerical methods.

2.0 LITERATURE REVIEW

In this chapter the numerous studies on entry flow behavior will be organized into a progression from the early experimental studies up through the most recent numerical simulations of the flow. In section 2.1 and 2.2 the experimental studies will be reviewed. Section 2.1 will cover studies of polymer solutions and section 2.2 will be concerned studies of polymer melts. The choice of whether to study polymer solutions or melts represents one of the fundamental decisions on how to approach the entry flow problem. Each has its own advantages and disadvantages. There are differences in rheological characterization, experimental techniques, and ultimately differences in interpretation of the observed behavior. By examining both solution and melt studies it should become clear why the choice in the present study has been to examine the entry flow behavior of polymer melts.

It will also be shown in these sections that although many of the past studies have been quite well done there is in general a lack of thorough rheological characterization of the materials studied and specifically a lack of extensional flow data provided. As a result, proper correlation of rheological properties to entry flow behavior may not have been achieved.

Because of the importance of extensional flow in the entry region section 2.3 will provide a review of what is known about the rheological properties of polymers in elongational flow. It is believed this will result in a better understanding of the flow patterns observed in the entry

region and also a firmer basis upon which to make the choice of constitutive equation to use in the numerical simulation of the flow. Section 2.4 will address the computational aspect of entry flow in regards to what constitutive equations have been used, the numerical techniques used, and the results obtained.

2.1 Experimental Studies of Entry Flow: Polymer Solutions

As can be seen by comparing Table 1 on page 7 and Table 2 on page 8, studies of polymer solutions began after that of polymer melts. Although they are only approximations to true polymer behavior they do have some distinct advantages. First, the flow experiments can be conducted at room temperature. This eliminates the difficulties of isothermal control of polymer melts at elevated temperatures. Also, because of their low viscosity it is possible to evaluate the elasticity of the solutions in terms of the primary normal stress difference (N_1), at relatively high shear rates (1000 sec^{-1}). In addition, some of the fluids can be controlled, by means of composition, with regard to shear thinning and magnitude of N_1.

Several types of polymer solutions have been used including polyisobutylene (1-4) and polyethylene oxide (5,6) solutions. However, the most widely used have been the polyacrylamide (PAA) based solutions. Both aqueous and syrup based solutions have been used, the latter being commonly referred to as Boger fluids (7). Although aqueous solutions were used initially, their low viscosity led to inertial effects, which are absent with high viscosity polymers.

Boger devised his fluids such that their viscosity would be high enough to eliminate inertial effects. Typical compositions are 0.02 - 0.1% PAA, 1 - 4 % water, and 96 - 99% glucose or maltose syrup. Also, depending on the composition, shear thinning effects due to the

Table 1. Entry Flow Studies: Polymer Solutions

INVESTIGATOR	YEAR	MATERIAL	RHEOLOGY	FLOW VISUALIZATION
Vinogradov & Manin (63)	1964	Al naphthalate/gasoline	-	Polarized light
Adams et.al. (88)	1965	PS/Aroclor	τ_{12}-$\dot{\gamma}$	Flow Birefringence
Fields & Bogue (10)	1968	PS/Aroclor	τ_{12}, N_1-$\dot{\gamma}$	Air bubble tracer
Giesekus (1)	1968	PAA/water, PIB/decalin	-	Streak photography
Metzner (16)	1969	PAA/water	-	Streak photography
Boles et.al. (2)	1970	PIB/mineral oil	-	Flow birefringence
Ballenger & White (3)	1970	PIB/mineral oil	-	Carbon black tracer
Ballenger et.al. (35)	1971	PIB/mineral oil	-	Carbon black tracer
Boger & Rama Murthy (64)	1972	PAA/water, Methocell/water	τ_{12}, N_1-$\dot{\gamma}$	Streak photography
Oliver & Bragg (15)	1973	PAA/water	-	Dye tracer
Pearson & Pickup (65)	1973	PAA/glycerine-water	-	Streak photography
Tomita & Shimbo (5)	1973	PEO solution	η, N_1-$\dot{\gamma}$	Not specified
Rama Murthy (86)	1974	PAA/glycerine-water	η-γ	Streak photography
Southern & Paul (11)	1974	PS/benzene	η, N_1-$\dot{\gamma}$	Flow birefringence
Strauss & Kinast (66)	1974	PAA/water	-	Streak photography
Busby & MacSporran (87)	1976	PAA/water	-	LDA
Cable & Boger (8)	1978	PAA/water	τ_{12}, N_1-$\dot{\gamma}$	Streak photography
Nguyen & Boger (7)	1979	Boger fluid	τ_{12}, N_1-$\dot{\gamma}$	Streak photography
Cochrane et.al. (17)	1981	Boger fluid, PAA/water	τ_{12}, N_1-$\dot{\gamma}$	Streak photography
Walters & Webster (18)	1982	Boger fluid, PAA/water	τ_{12}, N_1-$\dot{\gamma}$	Streak photography
Eisenbrand & Goddard (12)	1982	PAA/glycerol-water	η-γ	Streak photography
Shirakoshi et.al. (67)	1983	PAA/water	η, N_1-$\dot{\gamma}$	Streak photography
Evans & Walters (93)	1986	Boger fluid, PAA/water	η, N_1-γ	Streak photography
Boger et.al. (95)	1986	Boger fluid, PIB/kerosene	η, η', N_1,G'-$\dot{\gamma}$	Streak photography

Table 2. Entry Flow Studies: Polymer Melts

INVESTIGATOR	YEAR	POLYMER	RHEOLOGY	FLOW VISUALIZATION
Tordella (32)	1957	LDPE	-	Carbon black filled PE
Clegg (36)	1958	LDPE, HDPE	η-$\dot{\gamma}$	Colored core
Schott & Kaghan (33)	1959	LDPE	-	Pigmented resin
Bagley & Birks (34)	1960	LDPE, HDPE	-	Carbon black threads
Bagley & Schreiber (68)	1961	LDPE	-	Carbon black threads
Tordella (69)	1963	LDPE, HDPE	-	Flow birefringence
Insarova (70)	1969	PS	-	Flow birefringence
Ballenger & White (3)	1970	LDPE, HDPE, PS, PMMA, PP, Nylon 66, PB	-	Colored threads
Den Otter (37)	1970	Linear & branched PDMS	-	Streak photography
Ballenger et.al. (4)	1971	LDPE, PS, PP	η-$\dot{\gamma}$, ΔP_{ent}	Colored threads
Oyanagi & Yamaguchi (71)	1971	HDPE	η-$\dot{\gamma}$	Not specified
Vinogradov et.al. (72)	1972	Polybutadiene	η-$\dot{\gamma}$	Flow birefringence
Cogswell (26)	1972	LDPE, PMMA, PP	η-$\dot{\gamma}$, η_E	Colored threads
Han & Drexler (29)	1973	HDPE, PS, PP	η-$\dot{\gamma}$	Streak Photography
Oyanagi (73)	1973	HDPE	-	Flow birefingence
White & Kondo (23)	1977	LDPE, PS, HDPE	η, N_1-$\dot{\gamma}$	Colored threads
Isayev & Upadhyay (74)	1985	Polyisobutylene	η, N_1-$\dot{\gamma}$	Flow birefringence
Ma et.al. (27)	1985	Carbon black filled LDPE	η-σ	Colored threads

polyacrylamide could be nearly eliminated by the large amount of the high viscosity Newtonian syrup. With this control over properties it was possible to compare the entry flow behavior of a Newtonian fluid (syrup alone) to an elastic fluid of constant viscosity to an elastic fluid of the same initial viscosity which exhibited shear thinning.

2.1.1 Rheological Characterization

Initially, rheological characterization of the fluids studied in entry flow was something which either was not done or was limited to the measurement of viscosity. Over the past six or seven years the importance of the rheological properties on entry flow has been realized. However, the scope of the characterization is still limited, for the majority of cases, to measurement of viscosity and N_1 as functions of shear rate.

Typical shear stress and normal stress plots can be found in the literature for aqueous polyacrylamide solutions and Boger fluids (8,54,55). These fluids exhibit significant elasticity as determined by the ratio of normal stress to shear stress. The values of this ratio, typically referred to as the Weissenberg number ($N_1/2\tau_{12w}$), are comparable to those of polymer melts.

However, the magnitude of the viscosity is not of the same order as that of melts. In the case of aqueous PAA solutions the viscosity is quite low being in the order of 1 Pa-s (8). As mentioned previously, this low viscosity leads to inertia effects becoming significant at the high flow rates encountered in the entry region. The Boger fluids have eliminated this problem with their higher viscosity (10-100 Pa-s) yet it is still not comparable to that of polymer melts for which the viscosity is in the range of 10^3-10^5Pa-s.

Beyond measurement of shear stress and normal stress nothing has been done to further characterize aqueous PAA solutions. However, there has been some further characterization of Boger fluids. As Boger fluids have been used as the basis for many numerical simulations of entry flow it has been necessary to further characterize these fluids in order to determine the proper constitutive equation to use to describe their rheological behavior. In support of this

effort data has been published in regards to Boger fluids' dynamic properties (L1) and extensional flow properties (9). The dynamic data, although pertinent to the choosing of constitutive equations, provides little new information concerning entry flow behavior. The extensional viscosity, measured using a spin-line rheometer, was at best an average of the true viscosity. No interpretation of Boger fluids' entry flow behavior based upon this data has appeared in the literature.

2.1.2 Experimental Methods

Complete characterization of the entry flow field involves measurement of stresses, velocities, and streamlines within the region. Characterization of this type provides information not only for understanding the flow behavior but also for comparison with numerical predictions. Measurement of stresses is typically done using a birefringence technique however, the evaluation of velocities and streamlines has been done in a multitude of ways. In the following paragraphs some of the methods that have been used for characterizing the flow field will be examined.

Surprisingly, the measurement of stresses in polymer solutions in entry flow has not been done extensively. There have only been a few studies to date (2,10-12,88) and those mostly dealt with polystyrene and polyisobutylene solutions. Only the most recent (12) has addressed the measurement of stresses in a polyacrylamide solution. However, the method of measurement of stresses, birefringence, is common to all the studies and with only minor differences, the technique is also the same. A light beam is directed through a polarizer from which it travels to an entry flow die. The polarized light impinges perpendicular to the 1 - 2 plane of the flow. The light beam then exits the die, passes through an analyzer, and the resulting fringe patterns are recorded. Based on the fringe patterns the stresses can be calculated. (Theory of the method is provided in Appendix B). In none of the above mentioned studies

were the stress measurements used to explain the flow behavior of the solution but were used merely as an indicator of the behavior.

The measurement of velocities in the entry region has progressed over the years to the point where it is now possible to determine the values quite accurately. In early studies of velocity profiles the measurement technique was rather simple. Halmos and Boger (13) used a multiple flash technique in which flash tubes were triggered at preset time intervals. The result was a double exposure showing the reflection of light off of tracer particles at two different times. Measuring the distance moved in the set amount of time gave the velocity.

More recent methods using laser scattering techniques have given more accurate measurement of velocities in the entry region. Binnington et. al. (14) used a laser speckle technique in their study of Boger fluids in entry flow. The method involves sending a chopped laser beam through a flow field containing tracer particles.The beam is scattered off the particles and the side-scattered light is recorded on film as speckle-particle images. A laser beam is passed through the developed image in the region of interest. The result is a fringe pattern from which the velocities of the particles can be determined based upon fringe spacing.

Finally, Laser Doppler Anemometry (LDA) has been used to determine velocities in the entry region (6). With this method a laser beam is split into two parallel beams and then sent into the flow region. When a tracer particle passes through the beams an interference pattern is set up. This Doppler signal is sent to a storage oscilloscope from which frequency of the Doppler signal can be determined. The velocity of the signal is directly proportional to this frequency. Of the three techniques used for measuring velocities the latter is the most accurate. However it suffers from being the most expensive. The laser speckle technique described by Binnington et.al. was proposed as a low cost velocity measurement method and of the three it is the most cost efficient means of obtaining accurate velocities.

The determination of streamlines by flow visualization methods has been the main objective of studies of entry flow and is the main objective of this study. In an effort to determine streamlines in polymer solutions several methods have been used (Table 1 on page 7) Oliver and Bragg (15) injected dye into their polyacrylamide solution. Ballenger and White (3,4) used

carbon black tracers in their study of polyisobutylene solutions. In the latter case the flow patterns were observed as the solution flowed through a glass extension on a capillary rheometer. However, the most common method that has been used to observe flow patterns in polymer solutions is the streak photography technique.

The streak photography technique is based on the scatter of light off of tracer particles within the fluid. Several types of tracers have been used including air bubbles (10,16), bismuth oxychloride compound and titanium dioxide coated mica flakes (8), and high density polyethylene powder (17,18). The light scattering takes place by sending a narrow sheet of light into the center of the 1-3 plane of flow. The sheet of light is typically generated by passing a beam of light through a cylindrical lens which forms a plane of light and then through a spherical lens which collimates it. The light passes through slits in a viewing box which surrounds the test section. When the beam enters the test section the flow field is illuminated. A camera, mounted at 90^0 to the light source, records the flow pattern in the 1-2 plane as streaks. The technique is quite versatile in that it illuminates a cross section of the flow and therefore can be used for both planar and axisymmetric flow. Also, the same apparatus can be used for velocity measurements (laser-speckle photography) by placing a beam chopper in front of the light source.

2.1.3 Observation of Entry Flow Behavior

In the previous sections the discussion has been concerned with the different types of polymer solutions that are used in entry flow studies, how they are rheologically characterized, and finally how their flow fields are observed. In this section the actual observations of previous studies will be reviewed. The findings of these researchers will be presented in

terms of how they found the viscoelasticity of the fluids and the geometry of the entry flow region affected the flow behavior of the solutions.

Although there have been several studies of entry flow behavior only a few have attempted to explain the observed behavior (7,8,17-19). Several of the earlier papers were just concerned with the measurement of stresses within the flow region (10,16,88). Although these researchers were aware of the presence of of vortices within the entry region it was not their objective to interpret this phenomenon. Even some of the more recent work in this area has only been concerned with stress and velocity measurements in the entry region (6,12,20,21).

2.1.3.1 Viscoelastic Effects

The first major work to address the growth of vortices in viscoelastic polymer solutions was Cable and Boger (8). Cable and Boger studied the behavior of aqueous polyacrylamide solutions in axisymmetric flow. Several solutions of various elasticity were used and all were shear-thinning. Rheological characterization included measurement of the shear stress and the first normal stress difference. Based on these measurements comparisons were made between the rheological properties of the solutions and and those of typical polymer melts. It was found that although the shear stress of polymer melts was up to four orders of magnitude higher than that of the solutions their Maxwellian relaxation times ($\theta = N_1/2\tau_{12w}\dot{\gamma}$) were comparable at high shear rates. Cable and Boger stated that the similarity of relaxation times justified the use of their solutions as a model for polymer melts.

Flow patterns were observed by the streak photography method described previously. Secondary cell size was described in terms of the detachment length, Lv, shown in Figure 1 on page 2. The detachment length is the distance upstream from the contraction where the flow detaches from the tube wall. In this and later studies the detachment length was expressed in dimensionless form as

$$X = \frac{L_v}{D_u} \tag{2.1}$$

For the polyacrylamide solutions tested vortices were always present under the conditions reported. Cable and Boger did not explain why vortices occurred for these solutions but did address their growth in terms of flow rate and rheological properties. Two flow regimes were identified. The first, the vortex growth regime, was characterized by a smoothly convergent entry flow and increasing detachment length with flow rate. The second, the divergent flow regime, occurred at higher flow rates and was characterized by divergent flow at the detachment plane and decreasing vortex size with increasing flow rate. This latter phenomenon was attributed to inertia effects occurring at Reynolds numbers greater than 50. Since polymer melts have significantly higher viscosity than polymer solutions inertia effects are negligible and the divergent flow behavior that Cable and Boger observed should not become apparent.

Although the divergent flow regime is not likely to apply to polymer melts, Cable and Boger did postulate a theory for vortex growth which has been the basis of several subsequent papers. Cable and Boger stated that vortex growth was directly related to the elasticity of the fluid. The elasticity of the fluid was expressed by a Weissenberg number, $Nws = \theta V/D$, where V and D are the velocity and tube diameter measured downstream of the contraction. Cable and Boger found that the fluids with greater elasticity exhibited larger vortices. Justification for the use of elastic properties as opposed to viscous properties as the basis for vortex growth was given by comparing two fluids of equal viscosity but different levels of elasticity. The fluid with the higher elasticity was found to exhibit larger vortices and based on the work of Dudas and Verentas (22) it was stated that shear thinning of fluids only resulted in relatively minor enhancement of vortex size.

Nugyen and Boger (7) had two objectives in their study of the relationship between vortices and elasticity. The first was to eliminate inertia effects. This was accomplished by using Boger fluids instead of the aqueous polyacrylamide solutions. As described previously,

the Boger fluids are composed of PAA, water, and some type of maltose or fructose syrup. The syrup, which is Newtonian, is high in viscosity and comprises 96-99% of the solution. The result is a highly elastic, viscous polymer solution for which inertia effects are negligible.

Nugyen and Boger's second objective was to separate out the different effects of elasticity and shear thinning. This was accomplished in the same way that inertia effects were eliminated. The syrup used in the Boger fluids was high enough in viscosity to mask any shear thinning in the polyacrylamide. Therefore, Nugyen and Boger were able to compare the entry flow behavior of a Newtonian fluid (syrup) with a non-shear thinning, elastic fluid (Boger fluid) with a highly shear thinning, elastic fluid (aqueous PAA solution).

For the inelastic Newtonian fluid Nugyen and Boger found that the flow into the entry region was nearly radial. There were only very small vortices in the corners and their size did not increase with flow rate. The detachment length of the vortices was comparable with that predicted for creeping flow. The behavior of the Boger fluids was quite different. At very low shear rates the size of the vortices was comparable with that of the Newtonian fluid but as the shear rate was increased the size of the vortices increased significantly. Again the vortex size was explained in terms of the elasticity of the fluid. It was found that an increase in Nws from 0.218 to 0.263 resulted in a 100% increase in the detachment length.

2.1.3.2 Correlation to Rheological Properties

In an attempt to correlate vortex size with rheological properties of the fluid, Cable and Boger (8) presented plots of the dimensionless detachment length (X) versus Nws. It was found that there was a linear relationship between the two variables within the vortex growth regime. Plots of Nws/X versus the Reynolds number gave a single curve for all the fluids tested regardless of differences in viscosity and elasticity. This relationship between vortex size and elasticity was pursued in Nugyen and Boger's study.

In Nugyen and Boger's (7) study the vortex growth was related to rheological properties by means of the Weissenberg number, however they used different parameters than Cable and Boger to correlate the data by plotting it as BNws/X versus Nel. The first parameter is similar to what Cable and Boger used however, it takes into account the contraction ratio (B) used in the flow. The second term is an elasticity number defined by $Nel = \eta\theta/\rho D^2$ where η is the apparent viscosity and ρ is the fluid density. The reasoning behind the choice of this parameter is not explained. However when plotted the data for the fluids tested, including the shear thinning elastic solution, fall on the same curve. Nugyen and Boger use this as the basis of the statement that secondary cell size is a unique function of the fluid relaxation time.

Although Cable and Boger and Nugyen and Boger correlate vortex growth with fluid elasticity Nugyen and Boger go beyond this and state why they believe vortices form in some fluids and not in others. In their study, Nugyen and Boger compared a Newtonian fluid with an elastic, non-shear thinning fluid of identical shear viscosity. Because the elastic fluid exhibited vortex growth and the Newtonian fluid did not, Nugyen and Boger stated that this offered "conclusive proof that elasticity is the factor responsible for the formation and growth of the secondary cell in the entry flow of viscoelastic fluids."

It appears that vortex growth can be correlated to elasticity, however, Nugyen and Boger's statement that it is responsible for vortex formation is not supported by the work of White and Kondo (23) on polymer melts, which Nugyen and Boger cite in their paper. In their study, White and Kondo state that low density polyethylene and polystyrene show vortices but high density polyethylene does not. Nugyen and Boger state that elasticity is responsible for vortex formation and that shear thinning enhances this behavior. However, high density polyethylene is both elastic and shear thinning but White and Kondo did not observe vortices in this fluid. Therefore, there is a contradiction between what Nugyen and Boger have stated and what White and Kondo have observed. This appears to leave open the question of why vortices form. In a recent paper Boger et.al. [5] state that entry flow behavior cannot be characterized by steady and dynamic shear properties and that knowledge of the extensional properties of the fluid may be necessary to explain the flow behavior.

2.1.3.3 *Geometric Effects*

Realizing that there was some relation between flow behavior and fluid elasticity, Walters and Webster (18) and Walters (56) examined the effect of geometry on the formation of vortices. Walters and Webster specifically examined planar and axisymmetric entry flow. Also, the response of the fluids to geometric asymmetries (rounded entrance corner) was observed. Again a Newtonian fluid (maltose syrup), a non-shear thinning, elastic fluid (Boger fluid), and a shear thinning, elastic fluid (aqueous PAA solution) were examined. The flow visualization method used was streak photography and the fluids were rheologically characterized by measuring the shear stress and N_1 as functions of $\dot{\gamma}$.

For the Newtonian fluid the results were as expected with little or no vortices in the corners for both the planar and axisymmetric cases. No change was observed with increasing flow rate. In the cases where small vortices were observed, rounding of the corners caused a slight reduction in cell size. Results for the Boger fluids were significantly different. In the axisymmetric geometry vortices were observed. The cell size was found to increase initially with flow rate and then decrease corresponding to the vortex growth and and divergent flow regimes observed by Cable and Boger. The rounding of the corners led to smaller vortices on the rounded corner side and larger vortices on the opposite side. Surprisingly, in the planar geometry there was little difference in the entry flow behavior of the Boger fluid and the Newtonian fluid. Corner vortices were either absent or very small even at the higher flow rates.

In order to understand the difference in behavior of the Boger fluids in axisymmetric and planar flow and whether this behavior applied to all elastic fluids, Walters and Webster examined the flow behavior of an aqueous polyacrylamide solution in the two geometries. With the aqueous solution vortices were observed in both geometries, but recirculation within the cells was very weak. Furthermore the vortices for the aqueous solution were significantly larger than those for the Boger fluid. Again, the rounded corner resulted in smaller recircu-

lating regions. It was observed that this reduction was greater for the planar geometry than for the axisymmetric geometry.

Overall, Walters and Webster's results are interesting but unexpected. It was found that aqueous polyacrylamide solutions exhibit vortices in both planar and axisymmetric flow but Boger fluids exhibit vortices only in axisymmetric flow. Walters and Webster could find no explanation for this behavior. However, a reason may be found in examining the fluids themselves. Although fluid compositions were not provided, it was stated that the Boger fluid was a mixture of PAA, water, and maltose syrup. In a previous section it was shown that the syrup results in the fluid's high viscosity and to do this it typically comprises over 96% of the fluid. The Boger fluid in this study had a zero shear rate viscosity of 2.25 Pa-s. However, the aqueous polyacrylamide solution had a zero shear rate viscosity of over 100 Pa-s and this was accomplished without the use of syrup. Therefore, it is likely that this fluid had a much higher concentration of polyacrylamide than the Boger fluid. Since polyacrylamide has a molecular weight on the order of 1-2 x 10^6 it is likely that the aqueous solution has far greater chain entanglement which could alter flow behavior under the extensional stretching imposed in the entry region. However, without knowing about fluid composition and extensional flow properties, the behavior can not be fully explained. It should also be noted that Nugyen and Boger stated that elasticity was responsible for vortex formation. Yet the Boger fluids upon which they based this statement were the same type of fluids which Walters and Webster found to show no vortices in planar entry flow.

In another study, Walters and Rawlinson (89) again examined Boger fluids in planar geometries. Again, no vortices were observed in the planar slit contraction. However, Walters and Rawlinson also examined the flow behavior of the fluid in going from a large square upstream channel to a smaller square downstream channel. This square/square geometry more closely resembled an axisymmetric contraction rather than a planar slit contraction of the previous work. In this geometry the Boger fluids exhibited vortices as were seen in the axisymmetric case studied by Walters and Webster.

The difference in flow behavior of Boger fluids in planar and axisymmetric geometries is not understood but, the work of James and Saringer (90,91) and Chakraborty and Metzner (92) on sink flow may give some insight. James and Saringer examined planar and axisymmetric sink flow of polyethylene oxide solutions. Sink flow, which can be approximated by the flow of a fluid through an orifice, is essentially shear-free and therefore the pressure drop through the orifice gives a relative measure of the extensional stress in the contraction region. James and Saringer found, in comparing the flow through planar and axisymmetric contractions, that the pressure drop in the axisymmetric case was several times higher than in the planar case. This behavior was predicted numerically by Chakraborty and Metzner. Therefore, the different flow behavior of Boger fluids in planar and axisymmetric entry flow may be related to the development of larger extensional stresses in axisymmetric flow than in planar flow.

The contraction ratio, B, also affects the entry flow behavior of polymer solutions. In two recent papers by Evans and Walters (93) and Boger et.al. (94) the effect of B on vortex growth was examined. Evans and Walters studied the entry flow behavior of aqueous polyacrylamide solutions in planar contractions of different B. They found that for $B=4$ the intensity of the vortex increased with flow rate and a corresponding movement of the vortex center occurred. However, with $B=16$ it was found that the corner vortex increased in intensity with flow rate but also extended in a finger like shape towards the re-entrant corner at which another vortex had formed. At higher flow rates the two vortices merged, with the vortex at the re-entrant corner being dominant. Therefore, two types of vortex formation were found to be possible for a given fluid depending on B.

The presence of an additional vortex at the re-entrant corner was also observed by Boger et.al. (94). In this study Boger fluids and polyisobutylene solutions were observed in axisymmetric entry flow. It was found that for $4 \leq B \leq 16$ that the mechanism of vortex growth in Boger fluids was the same. At low flow rates the detachment length, X, remained constant however, in this range of flow rates the vortex center shifted towards the re-entrant corner and the shape of the vortex changed from concave to convex with increasing flow rate. After this rearrangement X again increased with flow rate. Similar behavior was observed for the

polyisobutylene solution in the 16:1 contraction. However, in the 4:1 contraction a different mechanism of vortex growth was observed. As the flow rate was increased the corner vortex was found to decrease in size. Simultaneously a new vortex formed at the re-entrant corner. With increasing flow rate the re-entrant corner vortex grew into the diminishing corner vortex and X then increased with flow rate. This behavior is similar to that reported by Dembek (95) who also examined the flow behavior of polyisobutylene solutions. Dembek found that depending on the concentration of the solution the mechanism of vortex formation was altered. For low concentrations large corner vortices formed but at higher concentrations vortices initially formed at the re-entrant corner and then grew into the corners.

From these studies of polymer solutions it is seen that the entry flow behavior of different fluids has been well documented. The effects of elasticity, shear thinning, and flow geometry have also been examined in detail. Yet, the reasons why the observed behavior occurs has not been determined. The same is true of the studies of polymer melts.

2.2 *Experimental Studies of Entry Flow: Polymer Melts*

As was seen in the previous section, the study of polymer solutions in entry flow has resulted in as many new questions as it has answered. The same can be said about the studies of polymer melts. However, the evolution of research on polymer melts has taken a somewhat different path. Although some of the same correlations between vortex growth and rheological properties are used, different explanations of the origin of vortices appear.

By comparing Table 1 on page 7 and Table 2 on page 8 it can be seen that polymer melts in entry flow were studied long before polymer solutions. Also, they were studied more extensively up through the early seventies. In the mid seventies, much of the work on entry flow shifted from melts to the study of aqueous polyacrylamide solutions and Boger fluids. The Boger fluids allowed for the tailoring of rheological properties in a manner such that effects

of shear thinning and elasticity could be separated out. Since the advent of Boger fluids there have only been a few studies on polymer melts.

Although the study of Boger fluids in entry flow may be justified for the development of numerical methods, it may not be justified as a replacement of studies of polymer melts. Because the rheological properties of Boger fluids can be controlled to some extent it becomes easier to find a comparatively simple constitutive equation which describes these properties (such as the Oldroyd B equation (9,24,25)). This has provided the means to concentrate on the complex numerical methods to simulate the entry flow behavior without the additional burden of the complicated constitutive equations necessary to describe polymer melts.

However, the equating of the behavior of Boger fluids to polymer melts is not completely valid. It should be remembered that Boger fluids are just polymer solutions and that the polyacrylamide within them typically comprises less than 0.1% of the fluid. It is here where the inherent advantage of the study of polymer melts lies. Polymer solutions are just approximations of polymer melts. In past studies of polymer solutions it was not possible to evaluate the effects of topology, chain entanglement, molecular weight, and molecular weight distribution on entry flow. These are polymer characteristics which could be expected to have a significant effect on flow in the entry region. Also, the accurate measurement of the extensional properties of polymer solutions is not yet possible. This may be a fundamental property, as indicated by others (23,26,27), necessary to the understanding of entry flow behavior.

2.2.1 Rheological Characterization

Rheological characterization of polymer melts, as with polymer solutions, was something that was not done in the early studies on entry flow. Not until the studies of Ballenger et. al. (4) were rheological data considered necessary for understanding and correlating entry flow behavior. Still, in those studies where the melts were characterized the measurements were limited to viscosity and some other property related to the elasticity of the material.

Because of the nature of polymer melts the measurement of the primary normal stress difference (N_1), which is related to polymer elasticity, is not possible at higher shear rates. Therefore, in order to evaluate the elasticity of the polymer, in terms of the Weissenberg number ($N_1/2\tau_{12w}$), it was necessary to find some approximation of N_1. In one of the studies (4) this was done by measuring ΔP_{ENT} which is the sum of the entrance and exit pressure losses in capillary flow. It had been shown by Philippoff and Gaskins (28) that N_1 and ΔP_{ENT} were proportional. Other approximations of the Weissenberg number have involved extrapolation of data of N_1 versus shear stress (23). Difficulties have arisen in that it is not known whether the relation between N_1 and shear stress is linear at high rates and since extrapolation may be necessary over a decade or more the error could be significant. Therefore, in all studies to date the evaluation of the Weissenberg number, at flow rates of interest, have only been approximate.

The extensional properties of the melt, as stated previously, have been considered to be fundamental in understanding entry flow behavior. For a number of years there have been methods for accurately determining these properties for polymer melts. This data has been reported in the literature, and will be discussed in a later section, yet only one study (26) has presented extensional data along with entry flow patterns and only two others (23,27) have made reference to such data. Also, in the study which presented the extensional data, the measurements were based on manipulation of capillary flow data and therefore only represented a rough approximation of the true extensional data.

Comparison of rheological characterization of polymer solutions and polymer melts shows that evaluation of fluid elasticity is more accurately defined for polymer solutions. For melts, the fluid elasticity can only be considered in terms of approximations at high shear rates. However, accurate measurement of extensional properties, although possible for melts, can not be achieved for solutions. As extensional flow properties may prove to be a more important property than elasticity, polymer melts may be the more likely candidate for entry flow studies from a rheological point of view.

2.2.2 Experimental Methods

Techniques for characterizing the the entry flow field for polymer melts are, for the most part, very similar to those described earlier for polymer solutions. Specifically, those methods used to determine the stress and velocity fields for the two types of fluids are identical. The only differences are in regards to die design and melt delivery systems which must be built such that they can withstand the high pressure and elevated temperatures associated with polymer melts (see for example Han and Drexler (29)).

The methods used for determining the streamlines in polymer melts are significantly different than those used for polymer solutions. For polymer solutions the most commonly used method of flow visualization was streak photography (reflective tracers were placed in the flow and the flow patterns were recorded by photographing side scattered light from the tracers). In the studies of polymer melts, streak photography has been less frequently used except in the measurement of velocities in the entry region (30,31). Typically, flow patterns in melts have been observed by introducing some type of colored material into the melt and observing the patterns formed by the colored tracer.

Tordella (32) was one of the first to observe flow patterns in polymer melts and the apparatus that he used has been the basis for even the most recent work. The apparatus consisted of a gas driven capillary rheometer to which a glass capillary was attached to observe the flow. This glass extension of the rheometer barrel was maintained at temperature by an air thermostat and was capable of withstanding pressures of up to 1000 psi. Flow patterns were observed in transparent polymers by back-lighting the capillary and recording the flow of opaque tracer material through the entry region.

Tordella's method of observing flow patterns in polymer melts has remained the same for most subsequent studies. However, the type of tracer used and the method of its introduction into the flow has changed. Originally, Tordella used carbon black filled polyethylene particles (20-50 mesh). Those particles which had a higher viscosity than the material being studied

provided point sources of the flow while those with a lower viscosity extended and a provided a streak pattern. Later, Schott and Kaghan (33) used colored resin. The capillary was fed by an extruder and the flow pattern was formed by alternating the feed between the natural and pigmented resins. Bagley and Birks (34) and later Ballenger and White (3,57) used colored resin, however, it was introduced into the flow by another method. First the material to be examined was molded into a rod having the dimensions of the rheometer barrel. Then holes were drilled perpendicular to the long axis of the rod and threads of the colored material were placed into the holes. The rod was then extruded through the capillary with the pigmented tracer deforming to give streak patterns of the flow. In the case of opaque polymers (27) after extruding the polymer for a period of time the polymer was cooled under pressure in the capillary. The polymer rod was then removed from the capillary and longitudinally sectioned to reveal the flow patterns.

Although streak photography has not been used often with polymer melts, there is no reason why it should not be. Han and Drexler (30,31) used this method, although not to observe flow patterns, and found it useful in determining velocities. Streak photography should actually provide some advantage in that the flow patterns should be clearer than those obtained using colored tracer. This aspect will be discussed in the following section.

2.2.3 Observations of Entry Flow Behavior

Many of the early studies on polymer solutions were concerned more with the measurement of stresses and velocities rather than with explaining flow patterns. With polymer melts the original concern was the occurrence of melt fracture. However, in interpreting melt fracture it was necessary to understand the entry flow behavior. Therefore, even with the early studies on polymer melts there was an attempt to relate melt fracture to the observed entry flow behavior. However, no explanation was given for the formation of vortices. Over the years there has been a steady progression in the correlation of vortex size with rheological prop-

erties. There has also been a steady development of the reasoning for the origin of vortices. Much of the progress in this area can be attributed to J.L. White and his co-workers.

In this section the behavior of individual polymer melts will be summarized initially. For the most part there is a consensus on the behavior of most polymer melts. Any discrepancies will be discussed. The bulk of this section will be concerned with what was found in regards to correlation of flow behavior with rheological data and how the origin of vortices was explained.

2.2.3.1 Flow Patterns

The behavior of polymer melts in entry flow, with regards to vortex formation, is summarized in Table 3 on page 26. Considering the number of studies, the agreement is very good. Differences in observations occur for low density polyethylene (LDPE), polystyrene (PS), and polypropylene (PP). For LDPE and polystyrene, the discrepancy results because of differences in flow geometry. Vortices are observed in abrupt contraction flow but not in tapered flow . This may be expected based on the taper filling the region where vortices would usually form. For polypropylene it is stated in an early paper by Ballenger and White (3) that polypropylene exhibits vortices. However, in a later study by the same authors (35) it is stated that no vortices are exhibited by isotactic polypropylene. In the second study it is pointed out that the polypropylene is isotactic but no explanation is given as to whether it is the tacticity or some other variable which is responsible for the differences.

2.2.3.2 Interpretation of Vortices and Correlation to Rheological Data

As stated previously, the first studies of entry flow behavior of polymer melts were concerned with melt fracture. As such, no explanation was given for the observed formation of vortices by some polymers. Tordella (32), Schott and Kaghan (33), Clegg (36), and Bagley et.

Table 3. Vortex Formation: Polymer Melts

MATERIAL	VORTICES	REFERENCE
LDPE	Yes	3,4,23,26,27,32-34,36
	No	68 (Tapered entry)
HDPE	No	3,23,29,34,71,73
PS	Yes	3,4
	No	29 (Tapered entry)
PP	Yes	3
	No	4,26,29
PMMA	Yes	3,26
PB	No	72
PDMS Branched	Yes	37
Linear	No	37

al. (34) were among the first to observe the flow behavior of polymer melts in the entry region. In all cases the polymers were observed in abrupt axisymmetric entry flow and Schott and Kaghan also examined tapered entry flow. The observations reported in all the studies were in agreement that LDPE exhibited vortices. Bagley and Birks also found that high density polyethylene (HDPE) did not exhibit vortices. However, in none of the studies was an explanation given as to why the vortices occurred and in the case of Bagley and Birks no explanation was given for the difference in behavior of LDPE and HDPE. Schott and Kaghan were the only ones to provide rheological data on the polymer studied, but there was no attempt to correlate the data with the observed flow behavior.

After the studies of the late fifties and early sixties little new was reported on the entry flow of polymer melts until the early seventies. In this new series of studies a molecular explanation of vortices was given and there was an attempt to correlate flow behavior with rheological data. Ballenger and White (3) were the first to give a comprehensive study of several polymer melts. In this study LDPE, HDPE, polypropylene, polystyrene, Nylon 66, polymethylmethacrylate, and polybutadiene were studied in axisymmetric contraction flow. This study represents the first attempt to quantify entry flow by use of the observed entrance angle. The angle, α, represented the natural entrance angle exhibited by a polymer at the entrance to the contraction (Figure 1 on page 2). However, this method for quantifying the size of vortices is different than the detachment length used by Cable and Boger in their study of polymer solutions and points out the fallibility of Ballenger and White's flow visualization method. First, since the entry flow pattern is typically curved it is difficult to determine at which point the angle should be measured. Also, Ballenger and White state in their paper that the angles are approximate due to the blurred outline of the secondary cell interface. Finally, Nugyen and Boger state (7) that at higher rates the entrance angle remains constant while the detachment length still varies making the detachment length a better parameter to characterize vortex size.

Beyond measurement of the entrance angle, Ballenger and White suggest the correlation of α with some form of the Weissenberg number. The Weissenberg number is traditionally

represented as N_1 over twice the shear stress. However, due to measurement techniques, N_1 can not be measured at high rates. Based on this Ballenger and White suggest the use of a Weissenberg number based on the ratio of the capillary entrance pressure loss to the shear stress. The proportionality of N_1 to ΔP_{ENT} came from the work of Philippoff and Gaskins (28). Although they do not present any correlation between α and Nws this does represent the first attempt to correlate rheological properties with entry flow behavior.

In a later study, Ballenger and White (35) did present a correlation between α and Nws. They also observed the entry flow behavior of three polymers over a wide range of shear rates. Based on this work they state that at low shear rates all polymers flow radially into the contraction and that only at higher rates do some polymers exhibit vortices. Plots of α versus shear rate are presented in support of this. At low rates the entrance angle seems to approach a constant value in the range of 130^0-150^0 for the polymers tested. As the shear rate is increased the entrance angle decreases and appears, at high rates, to level off again. The latter observation supports Nugyen and Boger's criticism of using the entrance angle rather than the detachment length.

In order to test the correlation between α and Nws that they had suggested in their previous paper, Ballenger and White present a plot of α versus Nws where Nws is taken as the ratio of capillary entrance pressure loss to shear stress. The data for three polymers are plotted together and a semilogarithmic equation is used to correlate α to Nws. A single curve is used for all the data on all polymers and the fit is at best moderate. Also, the relation is only good for a particular geometry (i.e. changing the contraction ratio would change the correlation). However, this type of relation would be the basis of further study.

In his studies of melt fracture, den Otter also studied the entry flow behavior of polymers (37). Using planar contraction flow he examined both a linear and a branched polydimethylsiloxane (PDMS). Den Otter found that the branched PDMS exhibited vortices but the linear PDMS did not. In addition it was found that the melt fracture behavior of the branched PDMS was similar to that of LDPE while that of the linear PDMS was similar to that of HDPE. Based on this he speculated the entry flow behavior of the linear and branched

PDMS's would be similar to the linear (high density) and branched (low density) polyethylenes.

Although he did not correlate rheological data with entry flow behavior, den Otter did propose a molecular mechanism for the presence or absence of vortices in different materials. It was stated that secondary flow was due to the splitting up of material before the entrance and therefore occurred in materials with low levels of coherence. However, the logic of this hypothesis is not immediately apparent. Den Otter found that the branched PDMS exhibited vortices but the linear PDMS did not. Yet it would be expected that the branched polymer would be more entangled, and therefore more coherent, than the linear polymer.

In support of his hypothesis den Otter states that lowering the molecular weight of a polymer or diluting it in solution would result in lower cohesion and therefore result in larger vortices. He comments that experimental results confirm this but none of the results are presented in the paper. Although den Otter's belief that entanglement is responsible for entry flow behavior is reasonable, it seems as though the data indicate that greater entanglement leads to vortices and not the opposite which den Otter puts forth. Based on the behavior of the branched PDMS and LDPE and the linear PDMS and HDPE, higher levels of cohesion should result in vortices.

The results of Cogswell (26) also serve to contradict the hypothesis of den Otter and at the same time introduce the concept of using extensional properties to understand entry flow behavior. In his study Cogswell examined the flow behavior of LDPE, polymethylmethacrylate, and polypropylene. His findings were in agreement with those of Ballenger and White with vortices exhibited by LDPE and polymethylmethacrylate but none by polypropylene.

Cogswell provided a simplified analytical analysis of converging flow. The method involved splitting entry flow into both shear and extensional components. Based on this analysis, Cogswell was able to estimate the extensional viscosity of a polymer based on capillary flow data. It was found that those polymers which exhibited vortices in entry flow had extensional viscosities which increased with stress. Although the extensional viscosity was only approximate, Cogswell had pointed out the importance of extensional flow in the entry region.

For the first time a non-shear flow property had been used to interpret the occurrence of vortices.

Cogswell's findings also explains the results of den Otter's work on branched and linear PDMS. According to Cogswell's data vortices are found in polymers with increasing extensional viscosity. It would be expected that increasing extensional viscosity would be due to increasing restriction of entanglements within the polymer. This would agree with Cogswell's data since LDPE, which exhibits vortices and increasing extensional viscosity, is highly branched and therefore highly entangled. Also, polypropylene, which does not exhibit vortices and has a decreasing extensional viscosity, is linear and therefore less entangled. Although this contradicts den Otter's hypothesis, that less entanglement results in vortices, it does agree with his experimental results for branched and linear PDMS.

In a review paper, White (38) mentions Cogswell's explanation of vortices and also presents his own. He states that at low shear rates polymer melts behave as Newtonian fluids and flow radially into the contraction. At higher rates the fluid deviates from Newtonian behavior as the viscoelasticity of the polymer becomes apparent. White states that increasing deviation from Newtonian behavior ultimately results in vortices in the entry region and that the Weissenberg number is the important parameter in interpreting this deviation. However, White does not provide a molecular explanation of why vortices occur. Nor does he explain why physically it would be better to use a parameter based on shear flow properties rather than one based on extensional flow properties especially when flow in the entry region is predominantly extensional. As for comparison of his hypothesis with that of Cogswell, White stated that there was insufficient information to distinguish between them.

In a later study White and Kondo (23) do accept Cogswell's interpretation of entry flow behavior in terms of extensional properties, but shear flow parameters are still used to correlate the behavior. In this study several LDPE's and polystyrenes of different molecular weight and a HDPE were observed in axisymmetric contraction flow. As in earlier studies, entrance angle was plotted versus Weissenberg number. The entrance angle, β, is shown in Figure 1 on page 2. The Weissenberg number in this study was not based on the capillary

entrance pressure loss but the primary normal stress difference. Values were obtained at high rates by extrapolation of the Maxwellian relaxation time, $\theta = N_1/2\tau_{12w}\dot{\gamma}$. The data were plotted as β versus $\theta\dot{\gamma}$. It was found that for a given polymer with a wide range of molecular weights and different flow rates the data correlated well. However, different correlations were obtained for different polymers. Therefore, it was not possible to explain why some polymers exhibited vortices and others did not.

White and Kondo stated that a parameter, in addition to the Weissenberg number, was necessary in order to correlate vortex size. They chose a parameter which reflected the deformation-rate dependence of the relaxation spectra. The reasoning given was that the deformation-rate dependence would be important since "the die entry flow patterns involve significant elongational flow components". Calculation of the parameter roughly ordered the polymers according to the size of vortices exhibited.

In their paper, White and Kondo had recognized that there was significant elongational flow in the entry region. In addition they had accepted Cogswell's idea that entry flow behavior can be interpreted in terms of the extensional flow properties of the melt. They stated that polymer melts which have rapidly rising extensional stresses will exhibit vortices and that these vortices are essentially a stress relief mechanism within the flow. Although they accepted the importance of extensional flow properties, White and Kondo still correlated entry flow behavior with parameters that were based upon shear flow properties. It would seem that the logical approach would be to correlate the behavior based on the extensional flow data.

The most recent paper on entry flow, co-authored by White (27), examines the behavior of carbon black filled LDPE. Although flow behavior is not correlated with extensional data it is explained in terms of extensional viscosities. It is stated that "only materials with clearly strong increasing elongational viscosities as a function of stretch rate exhibit vortices." Whether or not this is true is not proven with applicable data. What is significant is that in this paper entry flow is interpreted in terms of extensional properties only. There is no mention of any relation between flow behavior and shear flow properties, which had been the basis of nearly all previous studies on polymer melts and solutions.

2.2.4 Summary

In these first two sections experimental studies of entry flow have been reviewed for both polymer solutions and melts. Comparison of studies on solutions and melts reveals that rheological characterization has been minimal in both cases. Even in the most recent work measurement of rheological properties have been limited to those of viscosity and primary normal stress difference. In light of the recent work on polymer melts it appears that measurement of extensional properties should also be included.

With regards to correlation of entry flow behavior with rheological properties, the Weissenberg number has been the primary parameter. Although Nws has been used successfully to correlate vortex size for a given material it has not been successfully used to explain the origin of vortices. For the most part, an explanation of vortex origin has been missing from nearly all studies on solutions and melts. Correlation of vortex size with fluid parameters is important but the method of correlation can not be justified without a fundamental understanding of vortex formation as its basis. Again, the study of polymer melts indicates that the origin of vortices may be a stress relief mechanism related to chain entanglement and reflected in extensional properties.

Because of the importance attached to extensional flow in entry flow behavior it would seem that further studies on polymer melts would be warranted since accurate experimental techniques for measuring extensional properties are available for melts but not for solutions. Also, the importance of branching and molecular weight on entry flow behavior would favor the study of polymer melts.

In the next section the extensional flow properties of polymer melts and how they may relate to entry flow behavior will be examined.

2.3 *Extensional Rheology of Polymer Melts*

From the discussion in the previous section it is evident that extensional flow plays an important role in the development of vortices in polymer melts. Therefore, in the prediction of the lack of or presence of vortices it is necessary to measure the extensional rheological properties of the polymers being studied. White and Kondo (23) found that it was not possible to correlate the size of the vortices with shear properties alone. It was necessary to also use a parameter which reflected the effects of the extensional deformation in the entry region. In White and Kondo's study the parameter was the deformation rate dependence of the relaxation spectra. White and Kondo went on to say that the origins of vortices may be due to the development of large extensional stresses in the entry region and that vortices are formed as a stress relief mechanism. However, White and Kondo did not present any extensional data on the polymers they studied, but just referenced a previous study in which the extensional properties of some of the polymers had been measured.

Cogswell's study (26) also addressed the relationship between vortices and extensional properties. He attributed vortices to polymers which exhibited extensional viscosities which increased as a function of stress. Although extensional data were presented, the method by which it was obtained, as decribed previously, is questionable because it was based on capillary entry flow results.

What is apparent from these studies is that the extensional flow properties of the polymer are considered important in determining whether or not vortices will occur. Also apparent is that neither study has rigorously examined the relationship between extensional data and the occurrence of vortices. Part of this can be attributed to lack of experimental methods for accurately measuring the extensional rheological properties at the time of these studies. It has only been recently that these methods have been developed and that meaningful information on the extensional deformation of polymers has been obtained.

It will be the purpose of this section to review what is known about the extensional rheological properties of polymer melts. As it is the magnitude of extensional stresses which may be important in determining whether or not vortices occur, the effects of strain and strain rate on stress growth will be examined since both vary in the entry region. Also, the effects of molecular parameters on extensional stress will be reviewed. As there is still much controversy over the extensional behavior of polymer melts, this review will be limited to those studies which employed isothermal and constant strain rate or constant stress deformation techniques. The results of early studies using non-isothermal, variable rate extension are too prone to error to be considered in comparison to recent studies.

2.3.1 General Behavior

Extensional rheometry involves the stretching of a molten polymer in a uniaxial, biaxial, or multiaxial manner. Different techniques for accomplishing this are described elsewhere (39-41). Since the stretching flow encountered in the entry region is uniaxial only this type of deformation will be considered. Uniaxial extensional rheometry involves stretching the polymer either at a constant strain rate or with a constant applied stress. If a steady-state deformation is obtained the two tests give the same results. That is, if steady-state is achieved in a constant strain rate test a steady-state stress is measured. If this stress is then applied in a constant stress experiment the resulting steady-state strain rate that is measured will be equivalent to that of the constant strain rate experiment. The similarity of the techniques is pointed out here since different workers use different techniques. However, it should be kept in mind that the results from constant strain rate and constant stress experiments are directly comparable.

The results of extensional tests can be used to calculate the extensional viscosity. This quantity is defined as the the ratio of stress to strain rate ($\eta_E = \frac{\sigma_E}{\dot{\varepsilon}} = \frac{\tau_{11} - \tau_{22}}{\dot{\varepsilon}}$). Also, of interest is the transient growth of stress (or strain rate). The steady-state extensional viscosity

provides a common basis for making comparisons between different polymers. However, the stress growth is important in understanding the behavior of polymers in entry flow because of the transient nature of the flow.

Despite the amount of work that has been done it has not been resolved as to how different polymers actually behave in extensional flow. Most of the controversy is in regards to the transient extensional stress growth at high strain rates and also how the steady-state extensional viscosity varies with applied stress. It is generally agreed upon that there exists a steady-state viscosity at very low rates of extension. Also, this viscosity is related to the zero rate shear viscosity by the Trouton ratio which states $\eta_\varepsilon = 3\eta_0$. The only contradictory results (42-44) could be attributed to not testing the polymer at low enough strain rates and/or not extending to high enough strains. In one study the inability to achieve steady-state was attributed to the material. Au-Yeung and Macosko (45) found that steady-state could be achieved with a linear hydrogenated polybutadiene (HPB) but not with the star material. They stated that this was due to the high entanglement of the four-arm star structure. Although highly branched LDPE can achieve steady-state, Au-Yueng and Macosko believe the star structure has a higher level of entanglement which prohibits extension.

Although it is accepted that there is a steady-state extensional viscosity at low strain rates this is not important in the die entry region. What is important is the transient stress growth at high extension rates and how the viscosity varies with strain rate (stress). However, it is this behavior which is the least agreed upon. In regards to transient stress growth there is a difference in opinion even for the most commonly studied polymers. For polystyrene, Ide and White (42) report that the stress growth is unbounded at high extension rates and that steady-state only occurs at low rates. However, Franck and Meissner (46) and Münstedt (47,48) report that steady-state can be achieved even at high strain rates. This discrepancy is also found for HDPE (42,44,48-50) and linear low density polyethylene (LLDPE) (43,44,51). For LDPE three types of stress growth have been reported. Ide and White (42) stated that the material strain-hardened and exhibited unbounded stress growth, Münstedt (48) and Münstedt and Laun (50) found that at high strains the stress leveled off to a steady-state value, and Raible

et.al. (52) observed that beyond the plateau reported by Münstedt the stress decreased and therefore the material did not exhibit a steady-state stress.

Although there does not appear to be a consensus in regards to stress growth behavior, most of the differences can be attributed to experimental technique. For polystyrene, HDPE, and LDPE Franck and Meissner (46), Münstedt (47,48), and Münstedt and Laun (50) find that the stress levels off if the deformation is continued to high enough strains. Also, it has been observed (39,45-48,50) that if the deformation is performed under constant stress, as opposed to constant strain rate, the strain required to achieve steady-state is less. In most of the studies where a steady-state stress was not observed one or both of the above observations could be used to dispute the results. As for the behavior of LDPE, Münstedt states that the stress decrease observed by Raible et. al. was due to nonhomogeneous deformation at high strain and therefore did not represent the true behavior of LDPE.

Also important in the entry region is the manner in which extensional viscosity varies with strain rate (stress). Since the strain rate increases towards the entrance to the contraction, the flow behavior could be significantly different for polymers whose extensional viscosity increases with strain rate than for those for which the viscosity remains constant or decreases. Again, contradictory results are found in the literature.

The extensional viscosity of LDPE has been reported to increase (42,49) and also to go through a maximum and then decrease with strain rate (48,50). The same behavior has been reported for polystyrene by the same authors. HDPE has been observed to have a viscosity which goes through a maximum (48,50), remains constant (42,48-50), and decreases (42,44,49). For LLDPE increasing or constant (43) and decreasing (44) viscosity has been reported.

Part of the discrepancy can be attributed to the calculation of the viscosity from the extensional stress growth data. As discussed previously, some workers did not find a steady-state stress and therefore measurement of the viscosity was done at some arbitrary level of stress, typically the maximum value. Values such as these could be expected to be erroneous. However, the major reason for the differences in observed behavior is due to lack of proper molecular characterization of the polymers studied. It has been found in recent studies that

stress growth and viscosity rate dependency is related to branching and molecular weight parameters and that lack of proper characterization could explain reported differences. The importance of branching and molecular weight will be discussed next.

2.3.2 Branching Effects

There are two forms of branching in polymers: 1) long chain branching (LCB) and 2) short chain branching (SCB). SCB usually refers to branches of only a few atoms as found in LLDPE whereas LCB describes branches of a much greater scope as found in the random tree like structure of LDPE. For the most part it has been found that SCB has little effect on extensional stress growth behavior (45,49). Kalyon and Moy (51) did find the viscosity to increase slightly with the length of the branches. In this study they measured the viscosity of LLDPE's that had butene, hexene, and octene as the comonomers. However, the polymers were commercial resins and no molecular weight data was provided. Without proper characterization the differences can not be fully explained.

LCB, as opposed to SCB, has been found to significantly effect not only the stress growth behavior but also the rate dependency of the viscosity. In general it is accepted that LCB results in rapid strain hardening as exhibited by LDPE (49,51,58). Strain hardening is observed in non-branched polymers such as HDPE, however, it is of a much lower magnitude. In the extreme, LCB can prevent the attainment of steady-state as in the case of Au-Yeung and Macosko's star branched HPB (45).

The magnitude of the viscosity and its rate dependency can also be altered by LCB. Muller et. al. (43) created long chain branches in LLDPE by peroxide reaction. The amount of branching was small enough that the GPC results indicated no change in molecular weight from that of the original LLDPE. However, the extensional viscosity was found to increase significantly according to the amount of LCB in the polymer. Münstedt and Laun (50) compared the extensional viscosities of LDPE's and an HDPE of similar zero shear rate viscosity. They

found that the magnitude of the maximums in extensional viscosity versus stress plots could be related to the degree of branching in the polymer. Although the degree of branching is a structural variable which must be considered in the measurement of extensional viscosity, its effects have been found to be not as great as those due to the average molecular weight and the distribution of molecular weight within a specific polymer.

2.3.3 Molecular Weight Effects

In recent studies (46-48,50) the weight average molecular weight, M_w, and the molecular weight distribution, MWD, have been found to be the most important factors in explaining the differences in observed extensional behavior of polymer melts. Earlier studies (49,53) have referred to the effects of MWD but their results are contradictory to those of more recent studies. Again, discrepancies can most likely be related to the experimental methods used at the time. The work of Franck and Meissner (46) and Münstedt (47,48) and Münstedt and Laun (50) has shown not only that the low strain rate extensional viscosity is proportional to M_w but also that the MWD can explain deviations from linear deformation behavior and also the increase or decrease of the extensional viscosity from that of the Trouton ratio (i.e. $3\eta_0$).

Münstedt conducted the first comprehensive work on the effects of molecular weight on extensional behavior (47,48). In his study, four polystyrenes of different M_w and MWD were examined. The main differences in extensional behavior were found to be related to the presence or absence of high molecular weight components in the distribution. Under constant strain rate deformation it was found that those polymers which had a high molecular weight tail in their MWD either did not obtain steady-state or did so at high strain. In particular, one polystyrene, which had a bimodal MWD, appeared to reach steady-state at one level but as the strain increased the stress again increased and seemed to approach steady-state at a much higher level. Münstedt attributed this behavior to the high molecular weight material which was represented by the second peak in the bimodal distribution.

At higher strain rates the effect of the higher molecular weight component became more apparent. Although the polystyrenes without a significant high molecular weight tail exhibited bounded stress growth the bimodal polystyrene exhibited unbounded stress growth similar to that of LDPE. Plots of extensional viscosity as a function of stress showed that the bimodal polystyrene exhibited a maximum several times higher than the Trouton value. Comparison with the other polystyrenes showed that those which had a significant high molecular weight tail in their distribution also exhibited maxima although much lower in magnitude than that of the bimodal polymer. The one polystyrene which had no detectable high molecular weight component did not show any deviation from the Trouton value within the range of stresses tested.

In explaining the observed behavior, Münstedt states that the high molecular weight components represent long chains which act as a far reaching network within the matrix of smaller chains. At low strains the stress necessary to deform the polymer is representative of the shorter chains. However, at higher strains the entanglements of the longer chains become significant resulting in higher stress. It is apparent that it is not necessary to have a bimodal distribution to obtain this behavior. Even those polymers which have only a small amount of long chains, as exhibited by a high molecular weight tail, will have an increase in extensional viscosity as a function of applied stress.

In a later study, Franck and Meissner (46) also examined this behavior in polystyrenes. Their study was different in that they examined blends of polystyrenes of different M_w and of narrow MWD. It was found that blending polystyrenes, which individually exhibited nearly linear deformation, resulted in significant deviation from linearity at higher strains. In other words, at high strains the extensional viscosity deviated from a steady-state value. As with Münstedt, this behavior was attributed to the interaction of chains of different lengths. In addition it was found that the strains at which the deviation occurs increases with increasing difference in M_w of the components of the blend.

The effect of the molecular weight parameters on the deformation behavior of LDPE and HDPE was also examined by Münstedt (48) and Münstedt and Laun (50). Several comparisons

of polymers of different M_w and MWD were made. First, LDPE's of similar zero shear rate viscosity and M_w were compared. Although the molecular weights were similar, the extensional viscosities were significantly different. It was found that the LDPE which had the most significant high molecular weight tail exhibited the greatest increase in extensional viscosity above the Trouton value. In another comparison, LDPE's of different M_w were examined. Although the magnitude of the extensional viscosity ordered with M_w, the maximum increase above the Trouton value was attributed to the presence of a high molecular weight component. However, differences in GPC traces were minimal.

The same problem was encountered in comparison of HDPE's of different M_w. It was found that two HDPE's exhibited maxima in extensional viscosity while two others did not. Yet comparison of GPC curves did not show a significant high molecular weight tail for those polymers which had a maximum in extensional viscosity. However, based on his previous study of polystyrenes and the comparison of the LDPE's of similar M_w, Münstedt believes that differences in extensional viscosity maxima can be attributed to high molecular weight components even though they may be too small to detect by conventional characterization methods.

2.3.4 Summary

Although Münstedt had difficulty in some cases in establishing the role of the high molecular weight components on extensional behavior, previous results and the work of Meissner strongly indicate knowledge of MWD is necessary in understanding extensional flow behavior. Also, Münstedt's theory could explain why there has been so much discrepancy in the reported behavior of polymer melts. His work on polystyrene points out that completely different stress growth behavior (bounded versus unbounded) can be obtained by variation of the MWD of the polymer.

Also, the findings are important in regards to entry flow behavior. If widely different extensional behavior can be attributed to MWD then it would not be unusual to observe differ-

ences in entry flow patterns of polymers of a given type but of different MWD. Therefore, since differences are reflected in extensional properties, rheological characterization of polymers studied in entry flow should include extensional data.

2.4 Numerical Studies

Over the past few years there has been an intense effort to attempt to numerically simulate the flow of non-Newtonian fluids through an abrupt contraction (Table 4 on page 42). Both planar and axisymmetric geometries have been examined (59). There are two reasons for the choice of geometry. First, converging flow is found in nearly all types of polymer fabrication processes. The ability to numerically simulate the flow and calculate the associated pressure losses would provide aid in the design of such processes. The second reason is that contraction flow represents a simple geometry which illustrates the dramatic differences in flow behavior of Newtonian and non-Newtonian fluids. From the review of experimental studies it was found that Newtonian fluids flow radially through the contraction region. However, some non-Newtonian fluids exhibit secondary flow cells in the corners of the upstream channel. The presence of corner vortices can result in pressure drops significantly different than those found for their Newtonian counterparts. Hence, understanding this flow behavior from an experimental and numerical standpoint is of great importance.

Although several attempts have been made to numerically predict flow through a contraction difficulties encountered have hampered progress in this area. To begin with, the constitutive equation necessary for describing non-Newtonian fluids are non-linear and therefore the differential equations which describe the flow become non-linear. As these equations can not be solved analytically numerical techniques are required. Both finite difference and finite element methods have been used. Since these methods involve approximation of the solution of the differential equations some amount of error is inherent within

Table 4. References on the Numerical Simulation of Planar Entry Flow

MODEL	CONTRACTION RATIO	ELASTICITY LIMIT (De)	VORTICES	REFERENCE
Upper Convected Maxwell	2/1	?	yes	75
		0.9	yes(?)	77
	4/1	1.2	?	76
		0.11-0.87 depending on the mesh	no	79,97
Oldroyd-4	4/1	2.4	?	79
		0.5-1.75 depending on the mesh	yes(?)	80
		1.9-6.57 depending on shape functions and mesh	yes	110
White-Metzner	4/1	1.2	no	79
Phan-Thien Tanner	2/1	0.9	yes	77
	4/1	0.5-1.75 depending on the mesh	yes	80
		1.2-7.8 depending on mesh and shape functions	yes	111
Leonov	6.8/1	only at 0.66	yes	74
	4/1	??	?	81
Leonov-like	4/1	0.41-4.55 depending on the mesh	yes	97,112
CEF and modified GNF	4/1	4.5 and ∞ depending on the model	depended on the model	82-84

them. Also, the constitutive equations are approximations to the complex behavior of non-Newtonian fluids and therefore sources of error may be within them. Finally, there is the possibility that there is a mathematical loss or multiplicity of the solution.

Whatever the source of error, the result is that the numerical procedures fail to converge for Deborah numbers (De) on the order of 1. The Deborah number represents the ratio of a characteristic relaxation time of the fluid to the time scale of the flow. The fact that failure occurs at this point is significant in that it represents the point at which elastic stresses become comparable with viscous stresses (i.e. the non-Newtonian character of the fluid becomes important). As most polymer processes of interest involve Deborah numbers greater than one, solving this convergence problem is of great importance and has been the focus of several studies.

2.4.1 Non-Convergence Due to Bifurcation or Limit Points

As mentioned previously, failure of numerical techniques to converge could be due to a mathematical loss (limit point) or multiplicity (bifurcation) of the solution. Both of these possibilities have been studied (60-62). Mendelson (60) describes the above failure in relation to a regular solution. At a given level of De, a regular point is one which is a single-valued function of De and is locally unique. This is the situation which is assumed in non-Newtonian flow problems but as Mendelson states there is no reason why a unique solution should result in light of the fact that there are no existence or uniqueness theorems for these problems.

At a bifurcation point the solution becomes multi-valued. Several families of solutions may extend from this point and convergence may be prevented due to their inability to discriminate between solutions. A limit point represents the situation in which the solution turns back on itself. Beyond this point there is no solution and therefore convergence can not occur.

Mendelson could not determine the presence of bifurcation or limit points in his work. The failure of his calculations was attributed to approximation error which will be discussed in the

next section. However, bifurcation was addressed by Josse (62) and limit points were investigated by Yeh et. al. (61). In Yeh's study it was found that turning points in the solutions were inherent in the upper convected Maxwell model and the axisymmetric contraction and were not due to numerical artifacts associated with approximation error. Approximation error was not considered the source of failure because of the lack of oscillation in the solution before the limit point was reached.

2.4.2 Non-Convergence Due to Approximation Error

Approximation error was described by Mendelson (60) as 1) the inability of the weighted residual method of the finite element method to approximate the set of differential equations and boundary conditions governing the problem or 2) the inability of the discretization, in terms of elements, to describe local behavior of the dependent variables. The former kind of approximation error is possible because there are no convergence proofs for viscoelastic constitutive equations. The latter arises when functions with steep gradients are approximated with low-order interpolation polynomials and coarse meshes.

Mendelson finds failure of the upper convected Maxwell fluid and the second-order fluid to describe the flow in a planar contraction to be due to approximation error. Specifically, failure is attributed to the inability to approximate the stress field. It was stated that the discontinuity at the corner resulted in oscillation of the stress and pressure. Also, as the value of De increased additional oscillations were calculated as a result of the inability to approximate the large gradients in stress and pressure at the corner. Vortex growth was calculated for the second-order fluid, but, this was interpreted as being numerical artifact due to approximation error.

Yeh et.al. (61) examined the effect of using higher order interpolation polynomials on reducing approximation error. By using quadratic interpolation polynomials (versus linear) it

was found that approximation error could be reduced and oscillations, although still present, were damped out more quickly.

2.4.3 Effects of Mesh Refinement

Another possible means of improving convergence may be by mesh refinement. However, from the published results it is not clear whether finer meshes improve convergence or actually cause the solution to deteriorate. Davies found (96) that a fine mesh decreased the oscillations in the prediction of planar entry flow of a Maxwell fluid. However, Mitsoulis and Vlachopolous (82), using a CEF model, found the opposite with an increase in the convergence limit with finer meshes. Also, Keunings and Crochet (80) found an improvement in convergence when corner elements were decreased in size. For the Phan-Thien Tanner (PTT) model they found that the convergence limit increased from $De=0.7$ to $De=1.75$ when the corner element size was decreased by a factor of five. However, it was not known whether this solution improvement with mesh refinement might have been constitutive equation dependent. The PTT model incorporates a retardation term which is known to stabilize the solution. Also, the PTT model has a bounded value of the extensional viscosity whereas for the Maxwell fluid, for which Davies found finer meshes decreased convergence, the extensional viscosity goes to infinity at some critical value of the strain rate.

The effect of mesh refinement on convergence limit was made much clearer by Keunings (97) in a more recent paper. In this study the Maxwell and Leonov models were used with meshes of increasing degree of refinement with up to 40974 degrees of freedom. Keunings found that although there was some initial improvement in convergence limit with mesh refinement both models experienced a sharp drop in convergence limit with the finest meshes. The results implied that earlier studies which indicated better convergence with mesh refinement were just in the initial region of improvement and further refinement would have resulted

in a drop in the convergence limit. This study also indicates that there should be an optimum mesh size, depending on the constitutive equation used, for carrying out simulations.

2.4.4 Extensional Viscosity Predictions of the Constitutive Equation

Another means of reducing approximation error and improving convergence could be proper choice of constitutive equation. Mendelson (60) does not believe improvement will result based on failures of other constitutive equations. However, both of the constitutive equations used in his study give unrealistic predictions of extensional viscosity behavior. In the case of the convected Maxwell model the extensional viscosity goes to infinity when the strain rate equals 1/2De. The second-order fluid predicts extensional viscosity increases linearly with strain rate. In light of the review of extensional behavior of polymer melts neither of these predictions is valid. Also, based on the large stress gradients which were calculated correct prediction of extensional viscosity would seem necessary.

Other than the Maxwell and second-order fluid models the Oldroyd-4, White-Metzner, PTT, and Leonov models have been used in the simulation of planar entry flow. However, only the PTT and Leonov models predict bounded values of the extensional viscosity. The other models predict that η_E will go to infinity at some critical value of the strain rate. In addition, both the PTT and Leonov models incorporate adjustable parameters which control the predictions of extensional properties. In the PTT model the adjustable parameter controls the magnitude of the steady-state extensional viscosity and therefore, to some extent, the stress growth behavior. In the Leonov model a parameter is provided for control over the strain hardening behavior. As the PTT and Leonov models also give adequate predictions of viscometric properties it would seem that there use would would be preferred in numerical simulations.

2.5 Research Objectives

In the previous sections it was seen that although considerable work has been done on the entry flow problem, there is still confusion in regards to the flow behavior of polymeric fluids. Although the flow geometry is simple the behavior of non-Newtonian fluids is quite complex with vortices occurring with some fluids but not with others and the degree of secondary flow varying in those fluids which do exhibit vortices. The work of Boger and co-workers (7,8,20,21) and the early work of White and co-workers (3,35,57) suggest that entry flow behavior can be related to fluid elasticity expressed quantitatively by the Weissenberg number. It was observed that secondary cell size increased with increasing magnitude of the Weissenberg number and therefore, vortex growth was attributed to fluid elasticity. However, Walters and Webster (18) and White and Kondo (23) presented results which questioned this interpretation. Both Walters and Webster and White and Kondo found that some fluids did not exhibit vortices even though they were highly elastic. In addition, Walters and Webster discovered that entry geometry affected flow behavior. Also, White and Kondo found that although vortex size ordered with fluid elasticity, different correlations were obtained for different fluids suggesting the need of a parameter in addition to the Weissenberg number to correlate entry flow behavior. The work of Cogswell (26) and the most recent work of White (27) point to the extensional properties rather than the shear properties as being the most influential in regards to entry flow behavior. Although White did not present extensional data and Cogswell's data is questionable, other more thorough studies seem to indicate that extensional properties vary widely from polymer to polymer. It is possible that this may explain differences in observed flow behavior.

In addition to the lack of understanding of the entry flow behavior there is an absence of any fundamental explanation of the origin of vortices. The studies to date have been primarily concerned with the growth of vortices rather than explaining why vortices occur in the first place. Without a fundamental explanation the choice of rheological property with which to

correlate entry flow behavior becomes somewhat arbitrary. This then leads to problems with the numerical predictions of entry flow since it is not known what rheological properties must be accurately described by the constitutive equation. Therefore, it is proposed in the present study to 1) provide a fundamental explanation of the origin of vortices, 2) based on this explanation provide an understanding of the effects of molecular, rheological, and geometrical parameters on entry flow behavior, and 3) based on the importance of the above parameters provide a better prediction of entry flow behavior by numerical methods. In order to achieve these goals, observation of of the entry flow behavior of several polymers using different geometries will be made. From these observations an explanation of vortex formation will be derived.

Only polymer melts will be examined in this study. As stated in the previous chapter, polymer solutions are only approximations of polymer melts. Also, with polymer melts the effect on entry flow of molecular parameters such as topology, molecular weight, and molecular weight distribution can be examined. Rheological characterization of the polymers will be done in both shear and extensional flow. From the shear tests the elasticity of the polymers can be evaluated as $N_1/2\tau_{12w}$. and G'/G''. The latter value will be used to approximate the Weissenberg number at higher rates where it is not possible to measure N_1. Of particular importance in the extensional measurements will be the stress growth behavior of the materials. This should most closely relate to the transient conditions in the entry region.

Characterization of the flow field will include measurement of the stresses and streamlines within the entry region. Measurement of stresses will be accomplished by birefringence and observation of flow patterns will employ the method of streak photography. Both methods have been described previously in the literature review. Stress and streamline measurement will be used for comparison with numerical predictions and in interpreting vortex formation.

In the past the Weissenberg number has been used to correlate the vortex growth behavior exhibited by some non-Newtonian fluids. Although vortex size was found to increase with increasing Weissenberg number for a given material, no explanation was given for why vortices initially formed. In this study it will be attempted to explain the origin of vortices in

terms of the extensional stresses which develop in the material. The Weissenberg number, expressed as $N_1/2\tau_{12w}$ and G'/G'', will be compared with extensional stress to see if the occurrence of vortices can be related to the growth and magnitude of the extensional stress rather than to the magnitude of the Weissenberg number. It is believed that since there is considerable acceleration in the entry region that extensional properties will provide a better explanation of observed flow behavior than shear properties.

If it is found that the extensional properties of the polymer play a significant role in entry flow behavior then several new variables become important in trying to understand this behavior. As was discussed in the previous chapter, the extensional properties of a polymer can be significantly altered by changes in branching, molecular weight, and molecular weight distribution. It would be expected that these parameters would also affect the entry flow behavior. In this study molecular weight effects will be examined in two ways. First, a series of polymers will be studied to see how their rheological properties and their flow behavior in the entry region is altered with increasing molecular weight. Second, a polystyrene's M_w and MWD will be changed by the addition of a high molecular weight fraction. According to the work of Münstedt and co-workers (47,48,50) and Meissner (46,58) and co-workers small changes in the high molecular weight tail of a polymer's MWD results in large changes in the polymer's extensional properties. In this study it will be determined if changes in the high molecular weight tail also result in significant changes in the polymer's entry flow behavior.

Again, if extensional properties are important in determining entry flow behavior then changes in flow geometry, which would affect the extensional strains and strain rates imposed in the entry region, would be expected to influence the flow behavior. For this reason the effect on entry flow of changes in contraction ratio will be examined. It is expected that those geometries which reduce strain and strain rate will minimize vortex formation while those which increase strain and strain rate will enhance secondary flow.

The previous paragraphs described the methods which will be employed to evaluate the significance of extensional properties on entry flow behavior and also provide the information necessary to derive a fundamental explanation of vortex formation. The results of this work

will determine the direction of the work on numerical predictions of entry flow behavior. The numerical work will involve using an existing finite element code to the describe the behavior of different polymers in different flow geometries and comparing the results with experimental data.

3.0 EXPERIMENTAL APPARATUS AND PROCEDURE

Details of the materials investigated and the procedures used in this study are presented in this chapter. Section 3.1 describes the polymers used in regards to structure, M_w, MWD, and with respect to the polystyrene blends, the blending methods. In section 3.2 the apparatuses used for rheological characterization will be reviewed. In section 3.3 is detailed the design and construction of the two dies used in this study and in section 3.4 is described the polymer feed system for the die. Finally, in sections 3.5 and 3.6 flow visualization and flow birefringence techniques will be described with the operating procedures given in section 3.7.

3.1 Polymers Studied

The polymers used in this study are listed in Table 5 on page 52 along with molecular weight data. The polystyrene used in this work, Dow STYRON 678, is a typical commercial resin chosen based on its use in previous studies which also provide extensive characteriza-

Table 5. Polymers Studied

POLYMER	MANUFACTURER/GRADE	M_w	$\frac{M_w}{M_n}$
Polystyrene	Dow/STYRON 678	238,000	2.6
LDPE	Norchem/NPE-952	-	-
	/NPE-953	-	-
HDPE	Phillips/EMN TR-885	45,000	3.0
	/HHM-5502	150,000	7.7
	/HXM-50100	200,000	10.5
Polystyrene Blend		335,000	3.34

tion of the melt. For similar reasons the LDPE NPE-952 was also used. In addition another LDPE, NPE-953, was studied. This latter polyethylene is identical to NPE-952 except none of the additives incorporated in NPE-952 are present. There was no measurable difference in rheological properties, but the optical clarity was much better for NPE-953 than for NPE-952. This improved clarity was found to be necessary in order to obtain clear birefringence patterns in the melt. In addition to the low density polyethylene, three high density polyethylenes were also studied. These materials were chosen such that flow behavior could be evaluated for a fairly wide range of molecular weight. As can be seen from Table 5 on page 52 M_w varies by a factor of over 4 from 45,000 to 200,000 and the polydispersity varies from 3.0 to 10.5. The final commercial resin studied was a medium viscosity polycarbonate.

In order to further examine M_w and MWD effects on flow behavior it was necessary to blend polymers of different molecular weights in order to get a polymer with the desired distribution. In the present work it was desired to produce a polystyrene with a bimodal distribution. This was achieved by using the STYRON 678 as a base resin and blending into it small amounts of a narrow MWD, high M_w polystyrene fraction. In order to obtain a second peak in the distribution at high molecular weight it was necessary to choose the fraction such that its M_w was in the high end tail of the base resin's distribution. From Figure 2 on page 54 it can be seen that the base resin's distribution ends at a $M_w \cong 3 \times 10^6$. Accordingly, the fraction chosen had $M_w = 1.75 \times 10^6$. The fraction, obtained from Polymer Laboratories, had a very narrow distribution with $M_w/M_n = 1.05$.

Blends of the two polystyrene were made using both solution and mechanical blending techniques. Small 5 gram batches were made initially by solution blending to determine what composition would be best to make up in large quantity for the flow visualization studies. Blends of the base resin with 5, 10, and 15% (by weight) of the fraction were made by dissolving the polymer in toluene in quantities of 5 gr/100 ml. The polymer was then precipitated out of solution by drop wise addition to agitated chilled methanol. Extensional viscosity measurements on the blends indicated that the 10% blend resulted in significant changes in

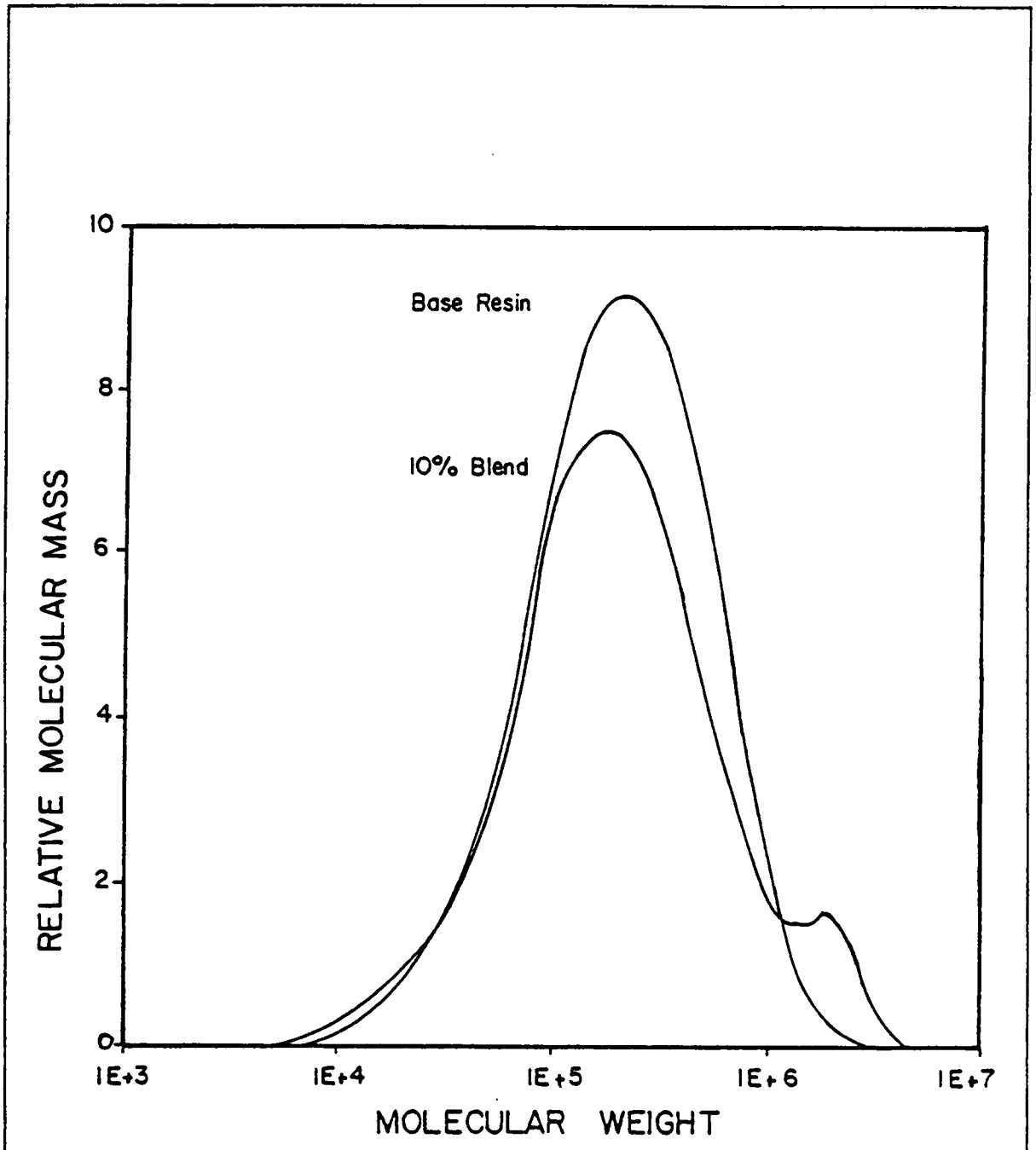

Figure 2. MWD of Polystyrene Blend and Base Resin

properties while being the lowest concentration at which the bimodal nature of the distribution became clear.

A mechanical blending technique was used to make up the 80 grams of the 10% blend necessary for doing the flow visualization work. A small bench top extruder (Maxwell Mixer) was used to blend the two polystyrenes. A melt temperature of 170° C was used and two passes were made through the extruder to ensure adequate mixing. The distribution of the blend is compared with that of the base resin in Figure 2 on page 54 and it is clear that the desired bimodal distribution has been achieved. For this blend $M_w = 335{,}000$ and $M_w/M_n = 3.34$.

3.2 *Rheological Characterization*

Rheological characterization of the test fluids was carried out in both shear and extensional flow fields. Although shear flow properties may be enough to characterize a melt in many processes, the highly extensional nature of contraction flow requires the additional knowledge of the extensional properties in order to fully understand the flow behavior. As will be shown later, although polymers may have similar shear properties, their entry flow behavior can be significantly different if their extensional properties differ appreciably.

3.2.1 Shear Flow Properties

Polymer melt viscosities were measured using both the Rheometrics Mechanical Spectrometer (Model RMS 605) and the Instron Capillary Rheometer (ICR, model 3211). The RMS is a cone-and-plate rheometer from which rheological properties are determined based upon the torque required to shear the fluid between the cone and the plate and the normal force which may result from this shearing. In the capillary rheometer viscosity is determined

based on the pressure drop required to force the fluid through a capillary of known diameter and length. Complete descriptions of these rheometers can be found elsewhere (98). It was only possible to obtain steady-shear viscosity values at rates up to 5 sec^{-1} in the RMS. Beyond this rate there was loss of fluid out from between the plates. Measurement of viscosity at higher rates was obtained from the capillary rheometer and from the RMS operated in the dynamic mode.

In addition to viscosity, measurement of the primary normal stress difference (N_1) was also made. As with viscosity, the measurement of N_1 above 5 sec^{-1} was not possible. Since it was necessary to have some measurement of fluid elasticity at higher rates, measurements of the storage modulus (G′) and loss modulus (G″) were also made. In the limit of low shear rate $N_1=2G'$. This relation holds at higher rates for some polymers and is used as the basis for determining fluid elasticity at high shear rates in this study.

3.2.2 Extensional Flow Properties

Extensional stress growth and steady-state extensional viscosity were measured using the Rheometrics Extensional Rheometer (Model RER 9000). This rheometer is based upon the Münstedt design (109) in which the polymer (molded into a cylindrical sample) is suspended in a heated oil bath between a fixed lower arm and a movable upper arm (Figure 3 on page 57). The oil is chosen such that its density is the same as that of the polymer at the test temperature so that no deformation of the sample occurs due to buoyancy effects. The sample is then deformed uniaxially at a constant strain rate. The force required to extend the sample is measured by a transducer attached to the lower end of the sample by means of a leaf spring. Assuming uniform deformation the true stress can be calculated based on this force and the dimensions of the sample. Knowing the stress and the strain rate, the extensional viscosity can be determined from, $\eta_E=\tau_{11}-\tau_{22}/\dot{\varepsilon}$ where $\tau_{11}-\tau_{22}$ is the measured stress and $\dot{\varepsilon}$ is the strain rate. The polymers in this study were tested at strain rates from 0.05-1.0 sec^{-1} and were ex-

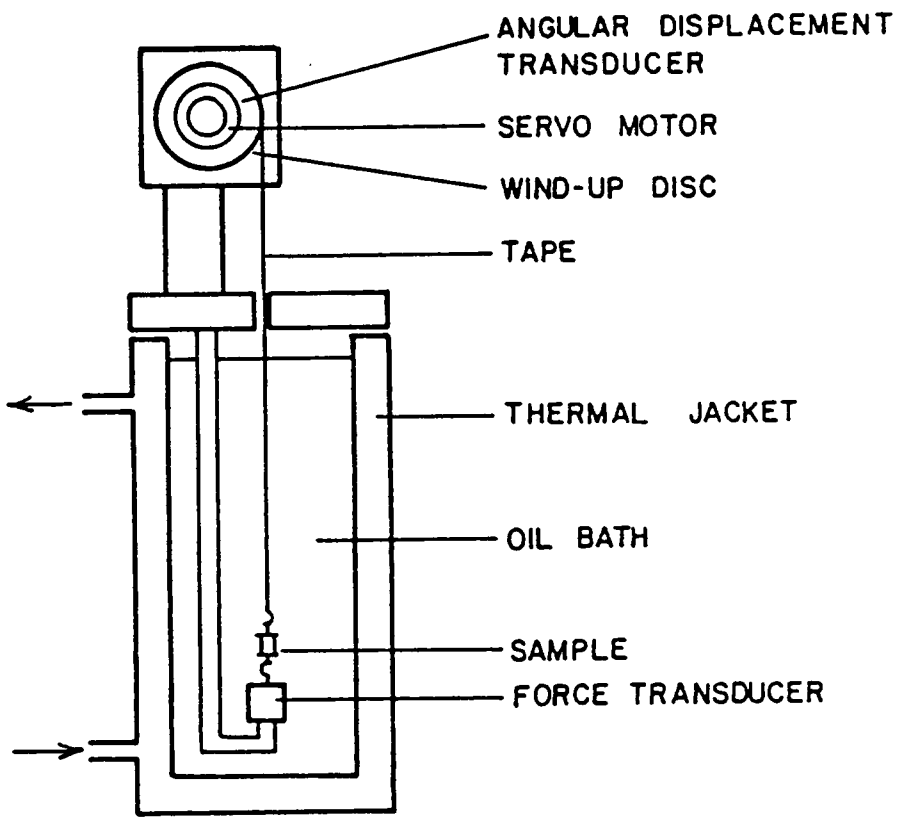

Figure 3. Extensional Rheometer Design

tended up to Hencky strains of 3. For those polymers which exhibited a steady-state extensional viscosity this value was compared with the zero-shear rate viscosity according to Trouton's rule: $\eta_E = 3\eta_0$.

3.3 *Slit Dies*

Two slit dies were used in this study. Slit die 1 was relatively small in size and utilized the capillary rheometer as a polymer melt feed system. It was used primarily for flow visualization studies of polymers which were available only in small quantities. Slit die 2 was used for the majority of the experiments. It utilized a 25.4 mm single screw extruder as the polymer melt source which increased the range of attainable flow rates. This die was designed such that both flow visualization and flow birefringence experiments could be carried out with it. Information on the design and construction of the two dies follows.

3.3.1 Slit Die 1

Slit die 1 was an existing die which was modified for the current study. The features and dimensions of the die are presented in Figure 4 on page 59. The die is constructed of two symmetrical halves which, when bolted together, form a 5.8:1 contraction. (The height of the downstream channel being 2.54 mm and that of the upstream channel being 14.88 mm.) The length of the upstream channel is 53.98 mm allowing for fully developed flow to occur after the entrance to the die and before reaching the contraction.

For observing the flow two 25.4 mm circular windows were placed on opposite sides of the contraction. This resulted in a viewing region 1.07 L/D upstream and 4.06 L/D downstream. In order to secure the windows, threaded circular adapters were made which screw into the

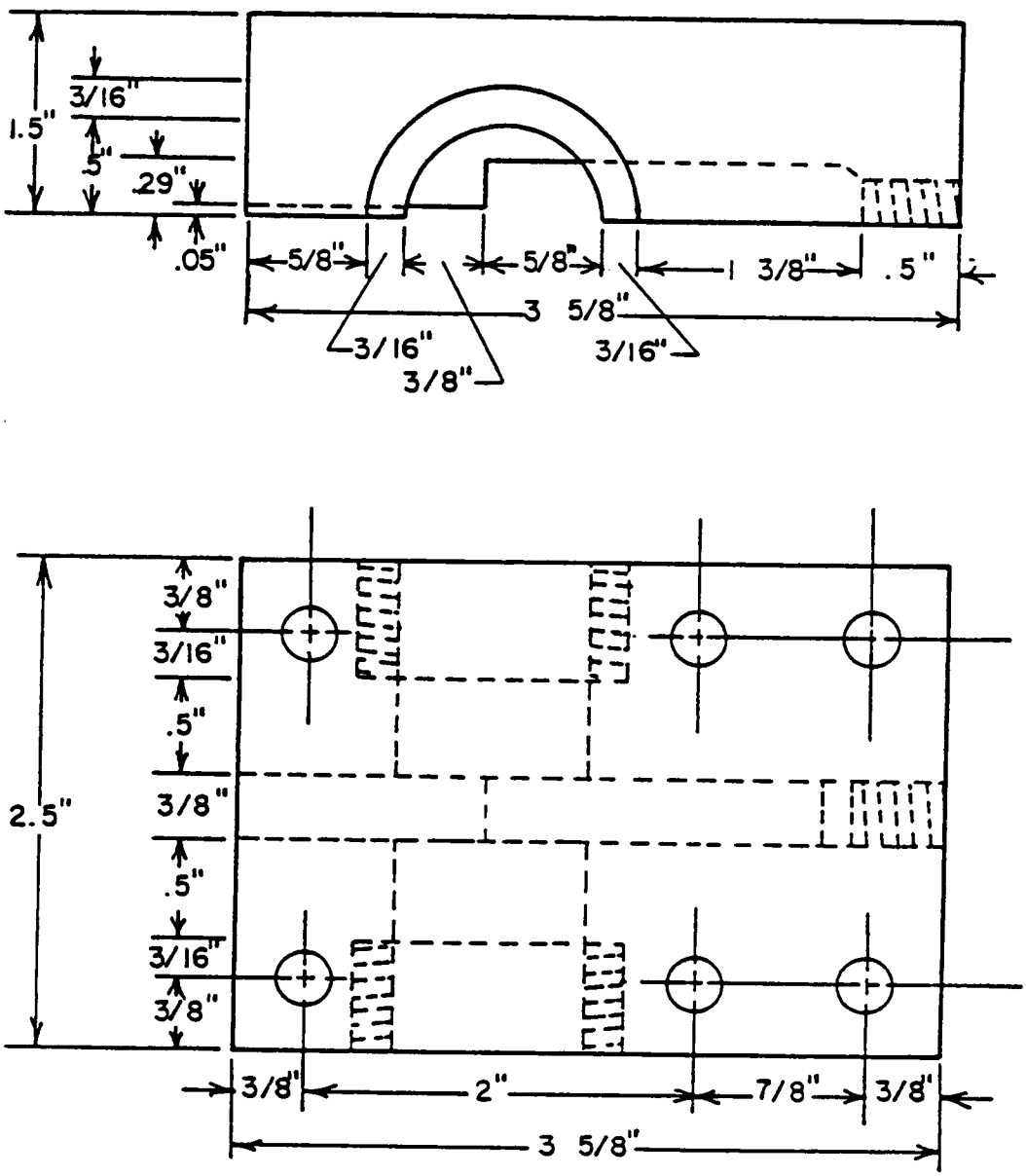

Figure 4. Design of Slit Die 1

side of the die providing a compression fit against the window. To prevent the damage which would result from a metal to glass seal, silicone gasket material (CHR Industries, CHOR 500) was inserted between the window and the securing adapter.

The heating of the die was accomplished with four strip heaters (Watlow) with two on the top half and two on the bottom half of the die. The heaters being 25.4 mm by 63.5 mm covered all available surface area on the top and bottom surfaces of the die. The heaters were secured to the surface by means of an aluminum clamp. Control of the temperature within the die was achieved with a single proportional type controller (Omega model 4001JC) with an iron-constantan (J-type) thermocouple. The thermocouple was positioned in the bottom half of the die such that its tip was within 3 mm of the slit wall right at the contraction corner.

The die assembly was attached to the capillary rheometer by means of a threaded capillary. The upper half of the capillary was similar to most conventional capillaries and was attached to the rheometer by inserting into the lower part of the barrel and securing with the lock screw. A three inch section of the capillary extended down below the rheometer and was heated with a single band heater which was controlled by a second controller. The bottom part of the capillary was threaded for attachment of the die.

3.3.2 Slit Die 2

Slit die 2 was designed specifically for this study. It was built for the purpose of carrying out flow visualization and flow birefringence studies in various flow geometries. The features and dimensions of the die are presented in Figure 5 on page 61. The top and bottom halves are identical except for thermocouple and pressure transducer placement (see Figure 6 on page 62 and Figure 7 on page 63). The die was machined from two rectangular pieces of 316 stainless steel. A slot 25.4 mm wide and 19.05 mm deep was machined into both halves of the die for placement of inserts which form the flow geometry when the two halves of the die are bolted together. With this design nearly any planar flow geometry is possible. The inserts

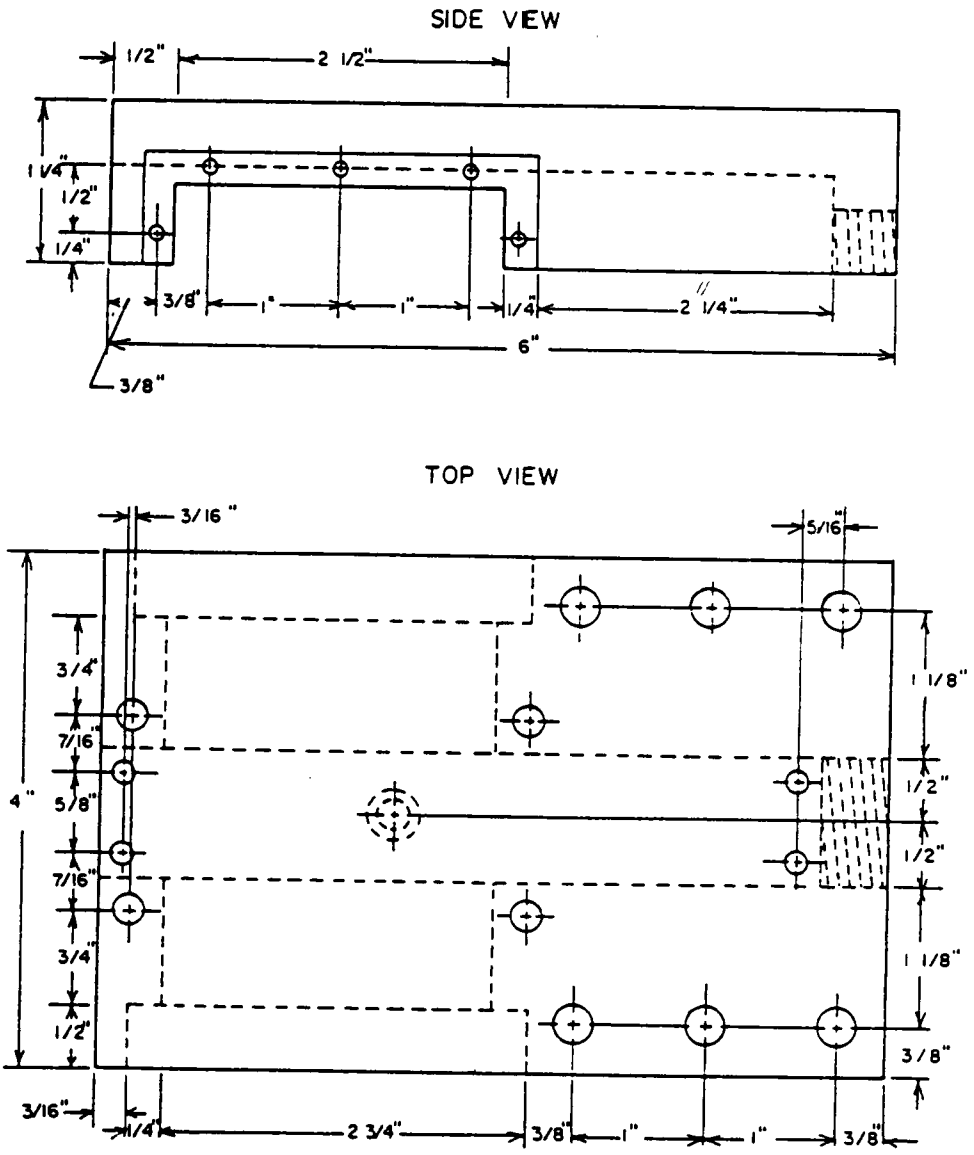

Figure 5. Design of Slit Die 2

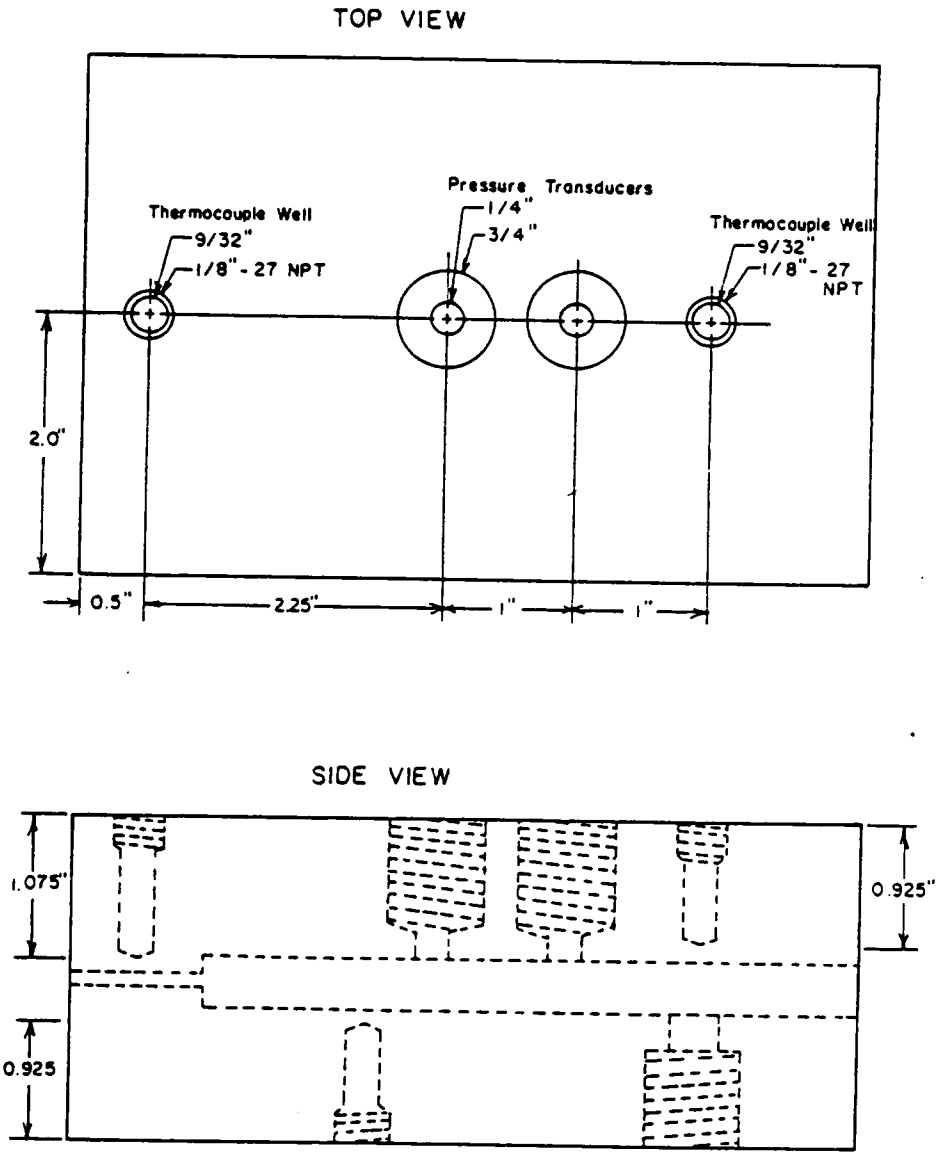

Figure 6. Thermocouple and Pressure Transducer Placement: Top and Side View

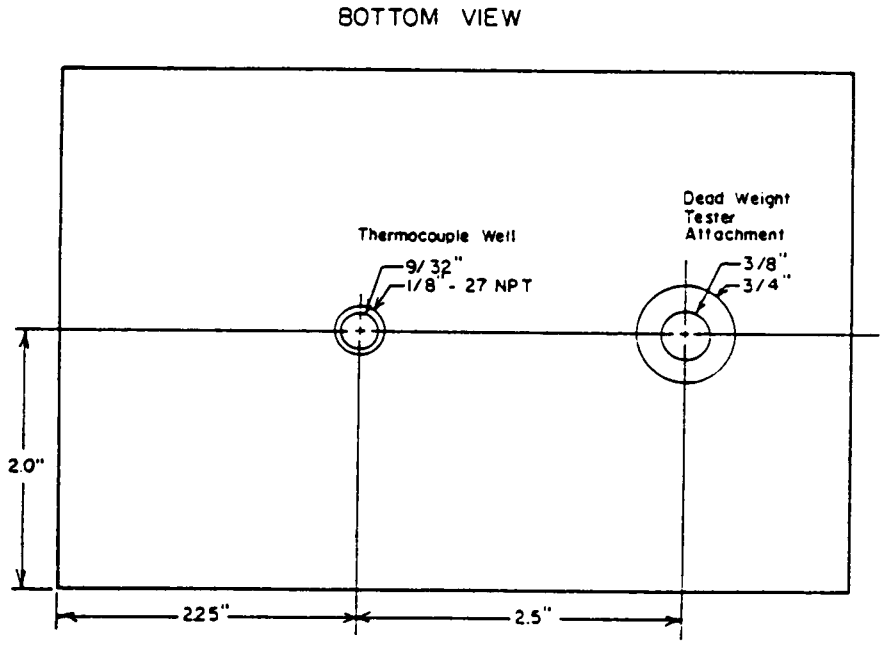

Figure 7. Thermocouple and Pressure Transducer Placement: Bottom View

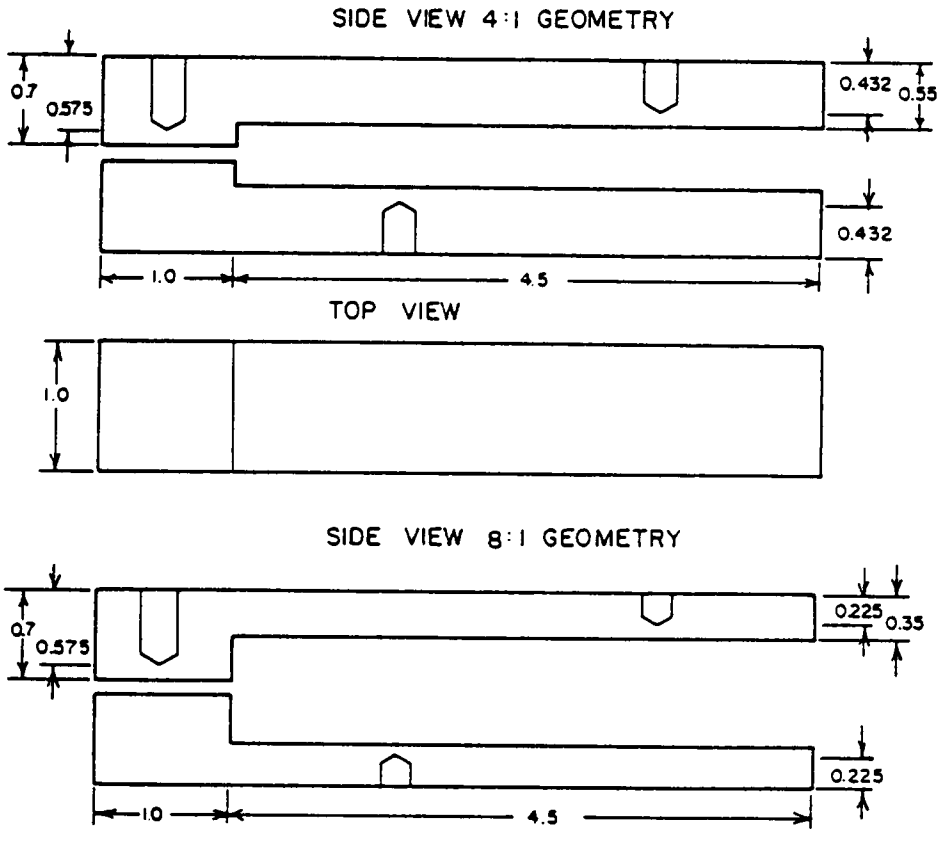

Figure 8. Insert Geometry

used in this study are shown in Figure 8 on page 64. The two inserts represent 4:1 and 8:1 abrupt planar contractions when assembled in the die. In both cases the channel width is 25.4 mm and the downstream channel height is 2.54 mm. The length of the downstream channel is 25.4 mm and that of the upstream channel is 114.3 mm allowing for fully developed flow to occur before the contraction. The tolerance in the machining of the inserts was 0.026 mm.

Two rectangular windows were positioned on opposite sides of he entry region. The windows were 25.4 x 31.75 x 63.5 mm pieces of commercial quartz obtained from Dell Optics. The thickness was chosen such that the quartz could withstand the high pressures attained at the higher flow rates. The height and length were chosen such that the fully developed flow region and the entry region could be observed for inserts with a wide range of shapes and contraction ratios. The windows were secured in place by a retaining bracket bolted against their outside face. Silicone gasket material was placed between the windows and the retaining brackets to avoid damage to the window surface.

Openings for two pressure transducers were provided in the top half of the die. The transducers were flush mounted by means of a custom bushing. With this design (99) the transducer is threaded into the bushing and then the bushing is machined such that the transducer will be flush with the slit wall. In this way the transducers can be used with different inserts of different channel height by merely machining a new bushing. The openings for the transducers were located at 69.85 mm and 95.25 mm from the die exit. Room was made available to put in two additional transducers further downstream if this is deemed necessary in later studies. In the present study transducers were used only in the 4:1 geometry. The dimensions of the insert were such that the transducers were located 44.45 mm and 69.85 mm upstream of the contraction which is well within the region of fully developed flow. The transducers used were Dynisco model PT422A. Transducer design and calibration procedures are described in detail elsewhere (99).

The heating of the die was accomplished with three independently controlled sets of strip heaters. The strip heaters, obtained from Industrial Heater Co., were secured to the top and bottom surfaces of the die by mounting bolts. Each zone consisted of a set of four strip heaters

the first of which heated the first 50.8 mm of the die, the second heated the middle 69.85 mm, and the third heated the final 25.4 mm. Each zone was controlled by a proportional type controller with a J-type thermocouple located in the center of the zone. The thermocouples were of the spring loaded bayonet type so that with different height inserts the thermocouple well could be drilled so that the tip of the probe was always within 3 mm of the slit surface. Insulation of the die was accomplished by covering the outside surfaces with alumina-silica fiber board.

3.4 Polymer Feed System

As mentioned previously the polymer feed for slit die 1 was provided by the capillary rheometer however, for slit die 2 the polymer feed system was based on an extruder-gear pump arrangement. A schematic diagram of the system is provide in Figure 9 on page 67. The melting and initial pumping of the polymer was accomplished with a Killion 25.4 mm extruder driven by a 1 horsepower motor. The polymer was delivered through 19.05 mm steel piping to a gear pump (Zenith model HPB-5556). A valve was inserted in the line between the extruder and the gear pump to act as a bleed when the flow rate from the extruder was greater than that from the gear pump. The gear pump was driven by a 1/4 horsepower motor (U. S. Electrical Motors) which operated in a range of RPM from 11-113. To obtain lower flow rates a gear reducer (Renold Limited) was placed between the drive motor and the gear pump. This effectively reduced the RPM and therefore the flow rate, by a factor of 21.4. The polymer from the gear pump was delivered through 19.05 mm steel piping to the entrance of the slit die.

Heating of the polymer feed system was accomplished in five independent zones of the die. The first two were within the extruder itself with the barrel being heated by two independently controlled sets of heater bands with thermocouples reading barrel temperature. The line from the extruder to the gear pump was the third zone. It was heated by glass in-

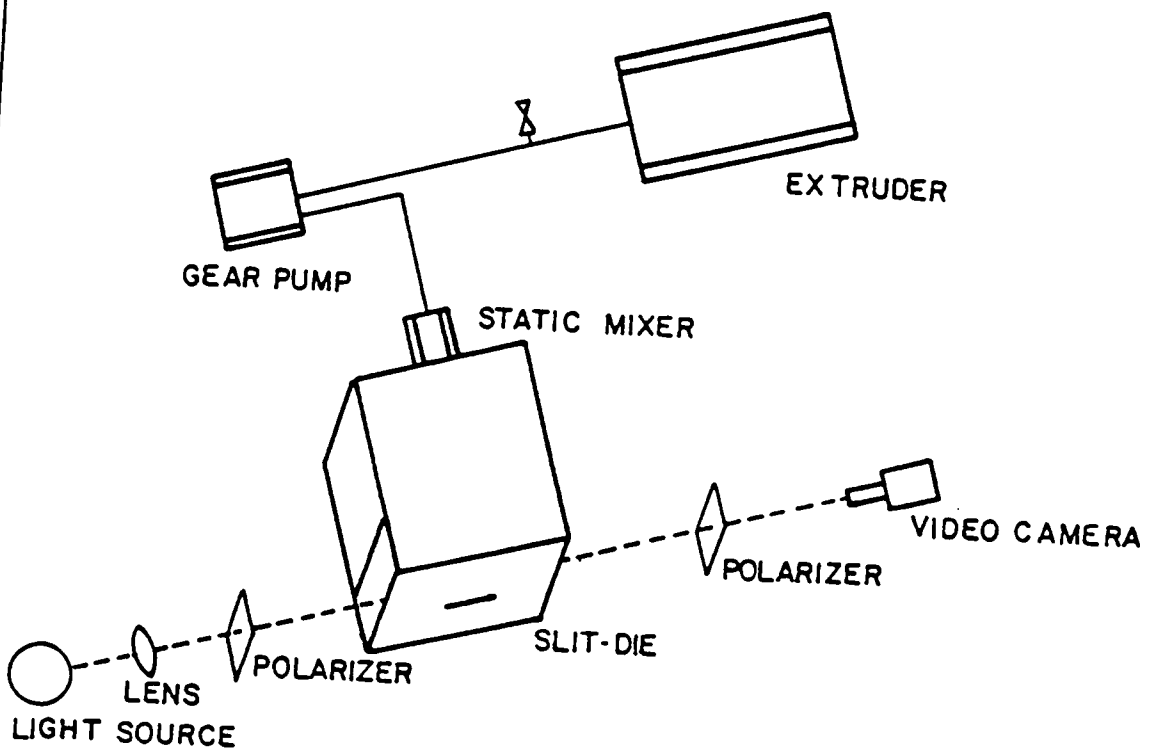

Figure 9. Schematic Diagram of the Polymer Feed System

sulated heating tape (Fisher Scientific) controlled with reference to a thermocouple inserted within the melt flow midway between the extruder and the gear pump. The gear pump represented the fourth zone and it was heated by two heater bands (Industrial Heater Co.) wrapped around the pump and the mounting block. This zone was controlled with reference to the temperature of the melt exiting the gear pump and in addition the temperature of the pump was monitored by means of a thermocouple inserted through the mounting block. The final heating zone was the line from the gear pump to the slit die. It was heated in a manner similar to that for zone 3.

Shear rates in the die were calculated based on the measured flow rates. Two methods of determining flow rates were used depending on the flow rate range. At low throughputs the flow rate was measured by determining the RPM of the gear pump shaft. Knowing the RPM and the volume pumped per revolution (fixed for a given gear pump, in this case 1.752 cm^3/rev) the volumetric flow rate could be calculated. In addition, the flow rate was also calculated by measuring the mass flow rate and dividing by the melt density. Agreement between the two methods was very good (within 3%). At higher throughputs it was no longer possible to accurately determine the RPM of the gear pump shaft. In these cases the flow rate was determined using just the latter method described above.

3.5 *Flow Visualization Technique*

In order to obtain the streamline pattern of the polymer flowing through the convergent region a streak photography flow visualization technique was used. As described in the previous chapter, this involved mixing a tracer in with the polymer and then reflecting light off the particles as they flowed through the viewing region and recording the flow on videotape. In this study two types of tracers were used. For slit die 1 and the 4:1 geometry of slit die 2 powdered nickel (Alfa Products) with a size distribution of -100 to +150 mesh was used. For

the 8:1 geometry it was found that a larger particle size was needed. Therefore, in this case a powdered iron (Alfa Products) with a size distribution of -40 to +70 mesh was used. The tracer was mixed with the polymer in amounts of 0.5% by weight (0.06% by volume). A white light source was aimed at the viewing region at approximately a 45° angle to obtain reflection off the particles. The window on the opposite side of the die was covered so that the tracer particles would appear as bright spots on a black background. A video camera (Panasonic model WV-3100) with close-up lenses attached to the camera's zoom lens was used to record the flow pattern. In order to obtain better contrast between the tracer and the dark background the iris setting on the camera was set between 1/4 and 1/2 closed.

To obtain the streamline pattern in the convergent region it was necessary to take time lapse photographs of the flow from the video recording. To do this a 35 mm camera (Olympus OM-1) was used with a low ISO black and white film. It is best to use a low ISO film (in this case Kodak Panatomic, ISO 32) as this allows for longer exposure times which are necessary, especially for low flow rates. With this film it was possible to obtain exposure times of 8 minutes and with the video playback running at 2x speed this corresponded to 16 minutes of flow on a single exposure. The exposures were taken off the television monitor while in the darkroom. In order to obtain better contrast it was necessary to cover the slit die walls by attaching electrical tape or black cardboard to the monitor. Depending on the lighting conditions that were used, the intensity of the light reflected off the slit die surfaces could be much greater than that from the tracer particles. By covering these areas only the light from the tracer particles entered the camera thereby improving contrast.

3.6 *Flow Birefringence Measurement*

In this study birefringence methods were used to evaluate the stress field in the convergent region of slit die 2. As discussed in the previous chapter and Appendix B, when polarized

light is passed through the polymer melt in the entry region the light is resolved into two components along the principal axes in the viewing plane. If the region is viewed, before flow is initiated, through a second polarizer (with its axes rotated 90^0 relative to the first polarizer) no light is transmitted due to the isotropic nature of the fluid. However, when flow begins orientation of molecules in the melt occurs giving rise to different indices of refraction along the two principal axes. Because of this difference the two components of light will exit the melt out of phase relative to each other giving rise to interference patterns. This phase difference can be expressed as,

$$\delta = \frac{2\pi L \Delta n}{\lambda} \tag{3.1}$$

or in terms of the number of relative wavelengths of retardation (N),

$$N = \frac{\Delta n L}{\lambda} \tag{3.2}$$

Equations B.18 and B.19 then become

$$\tau_{12} = \frac{N\lambda \sin 2\chi}{2LC} \tag{3.3}$$

and

$$\tau_{11} - \tau_{22} = \frac{N\lambda \cos 2\chi}{LC} \tag{3.4}$$

In this study L was the width of the slit (25.4 mm), λ was the wavelength of the laser light source (Spectra Physics model 155, $\lambda = 632.8$ nm), and C was the stress optic coefficient taken to be $4.54 \times 10^{-9}\ Pa^{-1}$ for polystyrene (100) and $2.0 \times 10^{-9}\ Pa^{-1}$ for LDPE (101).

The extinction angle (or isoclinic angle) , χ, could only be evaluated at low flow rates since at high rates the patterns became much to broad and diffuse to be of any quantitative use. As such, quantitative measurement of the shear stress was not possible. However, it

was possible to obtain values for the normal stress at the centerline. By squaring and summing equations 3.3 and 3.4 and knowing that the shear stress is zero at the centerline one gets

$$\tau_{11} - \tau_{22} = \frac{N\lambda}{LC} \tag{3.5}$$

Therefore, only values of N are needed as χ has been eliminated from the equation. It should be noted that this equation is an expression for the extensional stress and not N_1. The equation is obtained on the assumption that there is no shear stress.

Two techniques were used to obtain values of N. When monochromatic polarized light was passed through the flowing melt the resulting interference pattern consisted of light and dark fringes which represented different values of N. These patterns are referred to as isochromatic patterns. If plane polarized light was used (dark field pattern), the dark fringes took on values of N=0,1,2,... where N=0 corresponded to the centerline fringe (where $\sigma_{xy}=0$) and the value of N at each fringe increased going outward towards the wall. If circularly polarized light was used (light field pattern) then the dark fringes took on values of N=1/2, 3/2, 5/2,... again numbered outward from the centerline.

The optical arrangement used in this investigation to obtain the isochromatic patterns is shown schematically in Figure 9 on page 67 and Figure 10 on page 72. An optical rail was used to keep the lenses and video camera aligned relative to each other and the die. The laser light source and collimating lens could not be attached to the rail and were manually aligned with the other optics. The light from the laser initially passed through a 10x microscope objective lens to enlarge the beam to a spot large enough to illuminate the flow region. The light then passed through a lens which collimated and focused the beam. The light then went through the first polarizer, the slit die, and the second polarizer. The resulting fringe pattern was recorded on the video camera.

The alignment of the laser and collimating lens involved using the fact that the angle of reflected light is equal to the angle of the incident beam. The laser was initially aimed at the re-entrant corner of the slit die. The laser was then adjusted until the reflected beam returned

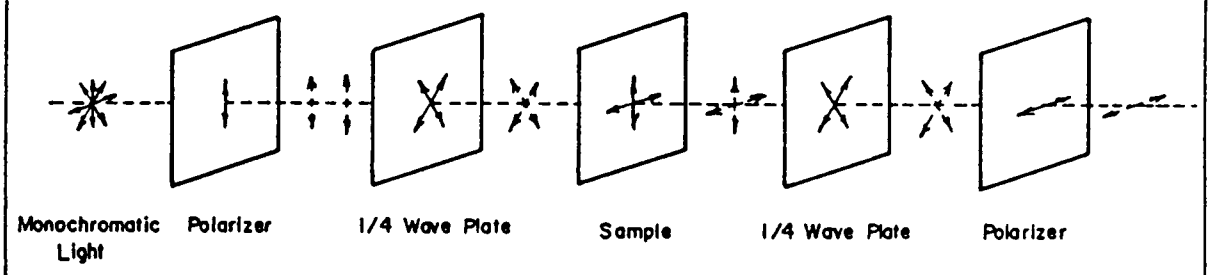

Figure 10. Optical Arrangement for Flow Birefringence Experiments

directly into the light source. The collimating lens was also adjusted such that when placed between the laser and slit die the reflected beam still returned directly into the light source. It was also positioned laterally such that the laser was at the focal point of the lens. The 10x objective lens and the polarizers were adjusted such that they were perpendicular to the light beam.

In order to obtain the dark and light field patterns mentioned above it was necessary to use two pairs of polarizers. The dark field pattern was obtained by passing the beam through two plane polarizers (Figure 10 on page 72) (Oriel Linear Film Polarizers) oriented at 90^0 with respect to each other. The light field pattern was obtained by inserting a pair of quarter wave plates between the two plane polarizers. The quarter wave plates were oriented with the principal optic axis at 45^0 to the axes of the plane polarizers and such that their fast axes were parallel. Combination plane polarizer-quarter wave plate lenses (Oriel Circular Film Polarizers), in which the quarter wave plate was laminated to the plane polarizer, were used.

3.7 Operating Procedure

In the next three sections step-by-step instructions are given which summarize the procedures for operating the polymer feed system and slit die, for obtaining flow visualization data, and for obtaining birefringence data. The procedure for slit die operation and birefringence measurement are as described by Pike (99) and Read (100).

3.7.1 Slit Die Operating Procedure

1. Turn on the main power and slowly bring the temperature of the equipment up to the desired operating temperature. The die temperature should be increased no faster than 40^0

C/hour to prevent cracking of the windows due to unequal thermal expansion. In heating the gear pump be sure to monitor the temperature of the probe in the pump. The control thermocouple for the pump is downstream from the pump and therefore will not indicate the true temperature in the pump during heat-up. In heating the extruder be sure cooling water is provided to the extruder throat so that melting of the polymer does not occur in the conveying zone.

2. After the temperature in the die has reached steady-state initialize the pressure measurement system. Zero the strip chart recorder and then set the zero and span adjustments of the transducers using the potentiometers found in the pressure signal amplifier.

3. Check the temperature distribution within the die using a thermocouple probe. Adjust the set points as necessary.

4. Check all temperature readings before starting the extruder. Make sure the gear pump monitor thermocouple reads the proper temperature even if the control thermocouple indicates a temperature higher than desired.

5. Start the extruder and gear pump drive. Adjust the gear pump to the desired speed. Adjust the extruder speed and bleed valve as necessary.

6. Purge the system of degraded material (10-20 minutes) and let the temperatures equilibrate under flow conditions. At high flow rates it may be necessary to adjust the set points down due to heat generation within the polymer by viscous dissipation.

7. Record pressure traces and determine the flow rate by weighing timed extrudate and from determining the gear pump RPM if possible.

8. Record the flow pattern or stress pattern.

9. Repeat steps 5-7 for additional flow rates.

10. When experiments are completed turn the bleed valve to full open and return the gear pump drive motor and the extruder to there lowest speed positions before turning off. The speed of these drives can be set only when the motors are running. Therefore, if they are inadvertently turned off at a high speed damage may result upon restarting.

11. Shut down all other equipment except for the slit die. Cool the die at 20°C/hour to prevent cracking of the windows.

3.7.2 Flow Visualization Procedure

1. Perform steps 1-7 outlined in section 3.7.1.

2. Add tracer particles to the feed polymer in the amount of 0.5% by weight.

3. Align the video camera with the slit die and orient the light source to get the maximum reflection from the tracer particles. Increased contrast is achieved by blacking out the opposite window and partially closing the camera's iris.

4. Allow the polymer to flow until the tracer particles are distributed throughout the viewing region.

5. Record the flow for 5 minutes; 20 minutes if below 10 sec^{-1}.

6. Repeat at different flow rates.

7. Obtain streamline patterns by taking time lapse photographs from the television monitor. For ISO 32 film a setting of f=16 and exposure times of 1-4 minutes should suffice. For shear rates below 10 sec^{-1} increase the exposure time and use the 2x replay speed.

3.7.3 Flow Birefringence Procedure

1. Align the optic system while performing steps 1-7 outlined in section 3.7.1.

2. Obtain the light field stress patterns by inserting the circular polarizers on either side of the die. Be sure the quarter wave plates face each other.

3. Obtain the dark field stress patterns by replacing the circular polarizers with the plane polarizers. Be sure the polarizers are crossed at 90° relative to each other.

4. If isoclinics are to be obtained replace the laser with the white light source and realign. Rotate the polarizers from -45^0 to $+45^0$ in 5^0 increments.

5. Repeat steps 2-4 for different flow rates.

6. To obtain a mapping of the fringe patterns take a photograph of the stress patterns from the television monitor. Insert the negative in the enlarger in the darkroom and enlarge to an appropriate size. Trace the image on graph paper.

4.0 NUMERICAL METHODS

Simulation of the flow of a polymer through a contraction was accomplished in this study by the use of the finite element method (FEM). Specifically, this was done using the FEM code NONEWT developed by Gotsis (85) based on a general two-dimensional code written by Reddy (102). The finite element method is a numerical technique used for the solving of differential equations in 1, 2, or 3-dimensions. The procedure is based upon dividing the continuum over which the set of differential equations are being solved into finite elements. The value of the variables of the problem are then obtained at each element using interpolation (approximation) functions. The interpolation functions are incorporated into the governing set of differential equations to give a linear system of equations which approximate the solution at each element. The system of equations for each element are then assembled over the entire domain (based on knowledge of the connectivity of the elements) to give a global set of linear equations which, when simultaneously solved, give the nodal values of the variables of the governing equations. If the governing differential equations contain nonlinear terms or if the problem is time dependent then an iterative technique is necessary in which the global set of equations are updated and repeatedly solved until some convergence criteria is met.

In this chapter the application of the finite element method to the simulation of the flow through a contraction is described. Section 4.1 provides the formulation of the governing dif-

ferential equations for contraction flow. These being the equations of change relating to mass and momentum and the constitutive equation. In section 4.2 the particular constitutive equation which was used in this study, the Phan-Thien Tanner model, is described and predictions of the model are presented. Finally, in section 4.3 a description of the implementation of the finite element method is given.

4.1 The Finite Element Formulation for Fluid Flow

For a general isothermal fluid flow problem the differential equations governing the flow are given below,

$$\frac{\partial \rho}{\partial t} = -(\vec{\nabla} \cdot \rho\vec{v}) \tag{4.1}$$

$$\frac{\partial \rho\vec{v}}{\partial t} = -[\vec{\nabla} \cdot \rho\vec{v}\vec{v}] - [\vec{\nabla} \cdot \underline{\pi}] + \rho\vec{g} \tag{4.2}$$

$$h(\underline{\tau}, \underline{\dot{\gamma}}, ...) = 0 \tag{4.3}$$

where ρ is density, $\vec{v}$ is velocity, $\underline{\pi}$ is the total stress tensor and $\vec{g}$ is gravitational acceleration. For the constitutive equation, h is either an integral or differential operator which acts on the extra stress tensor, $\underline{\tau}$, and the rate of deformation tensor, $\underline{\dot{\gamma}}$. In the above notation tensor quantities are underscored and vector quantities are overscored.

For the current problem, in which the flow is assumed to be incompressible (i.e. ρ =constant) and of low enough Reynolds number such that the inertia terms of the equation of momentum can be ignored, equations 4.1 and 4.2 can be rewritten as,

$$\vec{\nabla} \cdot \vec{v} = 0 \tag{4.4}$$

$$[\vec{\nabla} \cdot \underset{\sim}{\pi}] = 0 \tag{4.5}$$

Incorporation of indicial notation and the definition of the total stress tensor as $\underset{\sim}{\pi} = P\underset{\sim}{\delta} + \underset{\sim}{\tau}$ gives equations 4.4, 4.5, and 4.3 as,

$$v_{\alpha,\alpha} = 0 \tag{4.6}$$

$$\tau_{\beta\alpha,\beta} + P_{,\alpha} = 0 \tag{4.7}$$

$$h(\tau_{\alpha\beta}, \dot{\gamma}_{\alpha\beta}, v_{\alpha}, \ldots) = 0 \tag{4.8}$$

where for the current 2-D problem α and β take on values of 1 and 2. The above set of differential equations represents the governing system of equations used to describe contraction flow. There are six unknowns in this "mixed" method: P, v_1, v_2, τ_{11}, τ_{12}, and τ_{22}.

The finite element formulation of the equation of momentum (Eq. 4.7) can now be achieved by first obtaining the variational (weak) form of the equation. The variational form is obtained by multiplying the equation by a test function, w_i, and integrating over the element domain:

$$\int_{\Omega^e} w_i[\tau_{\beta\alpha,\beta} + P_{,\alpha}]d\Omega^e = 0 \tag{4.9}$$

Shifting the derivative onto w_i and then applying the gradient theorem gives,

$$\int_{\Omega^e} [w_{i,\beta}\tau_{\beta\alpha} + w_{i,\alpha}P]d\Omega^e = \int_{\Gamma^e} (w_i t_\alpha)d\Gamma^e \tag{4.10}$$

Equation 4.10 represents the formulation of the equation of momentum that would be used in the "mixed" method. However, the FEM code NONEWT makes use of the "penalty" method. In the penalty method the mass equation (Eq. 4.6) is used as a constraint on the momentum equation. The result is that the pressure is eliminated as a variable in the equation of momentum and can be expressed as,

$$P = -\gamma_p v_{\alpha,\alpha} \tag{4.11}$$

This results in the elimination of the mass equation from the system of governing equations and more importantly reduces the number of unknowns at each node to five. This is quite significant in large meshes with several hundred nodes for which computer storage requirements can be reduced substantially by reducing the number of degrees of freedom at each node by one.

Choice of the value of the penalty parameter, γ_p should be related to the magnitude of the viscosity according to Reddy (102). Problems result when the value is either too small or too large. If γ_p is too small the constraint is not satisfied however, if γ_p is too large then computer round-off errors can lead to the trivial solution. Reddy suggests values of γ_p in the range,

$$\gamma_p = \mu \times 10^6 \leq 10^{13} \tag{4.12}$$

In the current study the penalty parameter was taken as $\gamma_p = \eta_0 \times 10^6$.

In order to obtain the variational formulation of the equation of momentum using the penalty method, equation 4.11 is incorporated into equation 4.10. Substituting 4.11 and employing the mechanics sign convention, which is used in NONEWT, gives,

$$\int_{\Omega^e} [w_{i,\beta}\tau_{\beta\alpha} + \gamma_p w_{i,\alpha} v_{\beta,\beta}] d\Omega^e = \int_{\Gamma^e} (w_i t_\alpha) d\Gamma^e \tag{4.13}$$

The formulation is then completed by substituting the approximation functions, φ_i for the test function and replacing the variables of the governing equations with,

$$v_\alpha = \sum_{j=1}^{n} \varphi_j v_{\alpha j} \tag{4.14}$$

$$\tau_{\alpha\beta} = \sum_{j=1}^{n} \varphi_j \tau_{\alpha\beta j} \tag{4.15}$$

where the summation is over the number of elements, n. The resulting finite element formulation is,

$$\sum_{j=1}^{n} \{ \int_{\Omega^e} [\varphi_{i,\beta}\varphi_j \tau_{\alpha\beta j} + \gamma_p \varphi_{i,\alpha}\varphi_{j,\beta} v_{\beta j}] d\Omega^e - \int_{\Gamma^e} (\varphi_i t_\alpha) d\Gamma^e \} = 0 \tag{4.16}$$

Equation 4.16 represents the penalty finite element formulation for the momentum equation. Having eliminated the mass equation as a constraint on the momentum equation by the penalty method, only the formulation of the constitutive equation remains to be done to complete the problem. As this formulation is similar to that outlined above it will not be given here (a description of the constitutive equation used in this study will be given in the next section). The three components of the constitutive equation can be solved simultaneously with the two components of the above momentum equation to obtain the five unknowns of the problem. As can be seen the momentum equation is linear in $\underset{\sim}{\tau}$ and $\vec{v}$, but it will be shown that the constitutive equation is not. Therefore, solution of the problem involves linearization of the constitutive equation and iteration of the set of momentum and constitutive equations until convergence is met.

4.2 The Phan-Thien Tanner Constitutive Equation

As mentioned in the previous section, in addition to the equations of change it is necessary to have a constitutive equation (an equation which expresses the relation between stress and strain) in order to solve for the unknown velocities and stresses. Care must be taken in choosing a constitutive equation since it is the link between the real fluid and the mathematical representation of its behavior. In choosing a constitutive equation attention should be paid to those rheological properties which are important to the particular flow problem which is being solved. In the current study of contraction flow it is known that only shear flow occurs

well upstream and downstream of the contraction. However, in the region of the contraction the flow is highly extensional in nature due to the acceleration of the fluid from the upstream channel to the smaller downstream channel. As it is in this area that the flow behavior of interest occurs it is necessary to choose a constitutive equation which not only predicts the viscometric properties of the polymer but also gives a realistic and quantitatively accurate prediction of the polymer's extensional properties. Primarily for this reason the Phan-Thien Tanner (PTT) model was chosen for use in the FEM simulation of entry flow.

The PTT model not only provides an adequate prediction of viscometric properties but also gives a good description of of both transient and steady-state extensional properties. There is also an adjustable parameter for changing the magnitude of the extensional viscosity while holding viscometric properties nearly constant. As will be seen later this allows for the direct evaluation of the effect of extensional properties on the prediction of vortex growth. In addition the PTT model does not have the problems of instability associated with the Leonov model (85). The Leonov model is capable of providing a better fit of the extensional properties of a polymer through an adjustable parameter which changes the strain hardening behavior, but this parameter is not present in the form of the equation used in NONEWT. In addition, it was found that the use of this equation in NONEWT was not as successful as that of the PTT model.

4.2.1 Model Derivation

The PTT model was derived (103,104) from a Lodge-Yamamoto type of network theory for polymeric fluids and incorporates the idea of nonaffine deformation of network junctions. An affine deformation is one in which network and fluid strains are the same. In the PTT model it is assumed that there is slip within the network and that there is a functional form of the creation and destruction rates of network junctions which depends on the average extension

of the network strand. Through this approach two adjustable parameters result which provide control over the predictions of the extensional properties and the elastic response of the fluid.

Phan-Thien and Tanner began their derivation by examining the rate of deformation between two network junctions (Figure 11 on page 84). This deformation was expressed by,

$$\frac{\partial \vec{p}}{\partial t} = \vec{\nabla}\vec{v} \cdot \vec{p} + \frac{\partial \vec{\alpha}}{\partial \vec{r}}\vec{p} \tag{4.17}$$

For affine deformation the slip tensor, $\frac{\partial \vec{\alpha}}{\partial \vec{r}}$, would be equal to zero. However, to incorporate slip into their constitutive equation, Phan-Thien and Tanner assumed that the slip tensor had a finite value which was a function of the stretching rate and the end-to-end vector $\vec{\rho}$. Using this assumption equation 4.17 was rewritten as,

$$\frac{\partial \vec{p}}{\partial t} = \vec{\nabla}\vec{v} \cdot \vec{p} - \sigma\vec{p} - \xi\dot{\gamma}\vec{p} \tag{4.18}$$

where σ and ξ are constants. Substituting the above equation into a conservation equation for the rate of creation and destruction of network junctions gives,

$$\frac{\partial f}{\partial t} + \vec{v} \cdot \frac{\partial f}{\partial \vec{r}} + (\vec{\nabla} \cdot \vec{p} - \sigma\vec{p} - \xi\dot{\gamma}\vec{p}) \cdot \frac{\partial f}{\partial \vec{p}} = g - hf \tag{4.19}$$

where *f* is the probability distribution expressing the number of junctions in a statistical volume, *g* is the rate of creation of junctions, and *hf* is the rate of destruction of network junctions. Equation 4.19 in combination with the definition of the stress tensor obtained from Gaussian network theory gives,

$$\lambda[\frac{d\underline{\tau}}{dt} - \underline{L} \cdot \underline{\tau} - \underline{\tau} \cdot \underline{L}^{t}] + H(tr\underline{\tau})\underline{\tau} = \eta\dot{\gamma} \tag{4.20}$$

where $\underline{L} = \vec{\nabla}\vec{v} - \frac{\xi}{2}\dot{\gamma}$, *H* represents the rate of destruction of network junctions, and λ is the relaxation time. Incorporating the definition of $\underline{L}$ into equation 4.20 the PTT model can be written in terms of the convective derivative, $\underline{\tau}_{(1)}$, as,

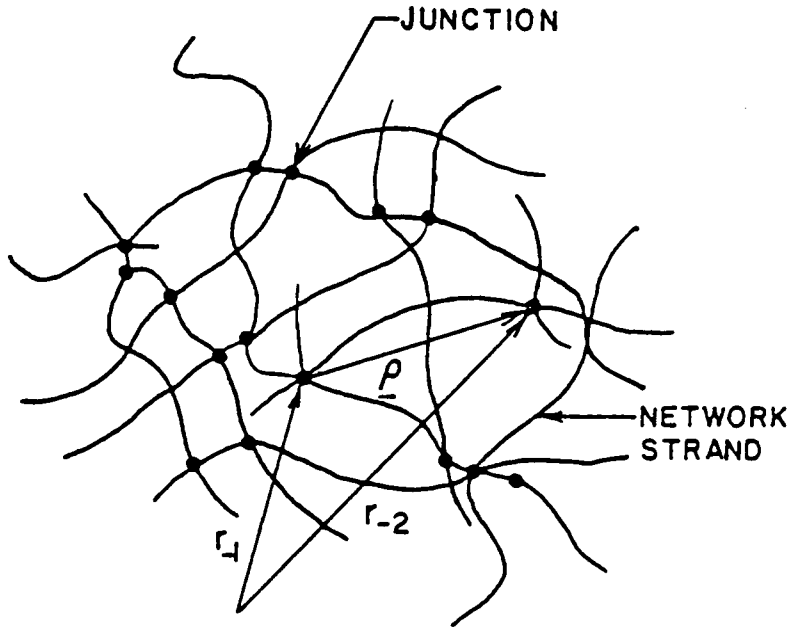

Figure 11. Polymer Network Representation Used for PTT Model Derivation

$$H(tr\underline{\tau})\underline{\tau} + \lambda\underline{\tau}_{(1)} + \frac{\lambda\xi}{2}(\underline{\dot{\gamma}}\cdot\underline{\tau} + \underline{\tau}\cdot\underline{\dot{\gamma}}) = \eta\underline{\dot{\gamma}} \tag{4.21}$$

Two forms of the function $H(tr\underline{\tau})$ have been presented by Phan-Thien and Tanner. The most physically realistic is the exponential form given as,

$$H(tr\underline{\tau}) = \exp[\frac{\lambda\varepsilon}{\eta}tr\underline{\tau}] \tag{4.22}$$

In this exponential form the model predicts that the extensional viscosity will start off at the Trouton value at low extension rates and then increase and go through a maximum with the ultimate magnitude of the extensional viscosity being determined by the adjustable parameter ε. This shape of the extensional viscosity-strain rate curve is in agreement with experimental data for most polymers.

Although the PTT model also gives adequate predictions of viscometric properties, at high rates it predicts a much greater rate of shear thinning than is realistically possible. The result is that the shear stress goes through a maximum and decreases rather than being a monotonically increasing function of shear rate. To avoid this problem a retardation term, $\underline{\tau}^2$, is incorporated in the extra stress tensor,

$$\underline{\tau} = \underline{\tau}^1 + \underline{\tau}^2 \tag{4.23}$$

Here the stress is written in terms of a viscoelastic component, $\underline{\tau}^1$, obtained from the constitutive equation (Eq 4.21) and a purely viscous component, $\underline{\tau}^2$, expressed as,

$$\underline{\tau}^2 = \eta_2\underline{\dot{\gamma}} \tag{4.24}$$

The result is that at higher rates the retardation term dominates causing the viscosity to level off to a constant value, η_2, and keeping the stress a monotonically increasing function of shear rate. It has been found (105) that to prevent the maximum in shear stress, η_2 must be chosen such that $\eta_1 \leq 8\eta_2$ where $\eta = \eta_1 + \eta_2$

4.2.2 Model Summary and Predictions

The PTT model presented in the previous section can be summarized by the following set of equations:

$$\underline{\tau} = \underline{\tau}^1 + \underline{\tau}^2 \tag{4.23}$$

$$H(tr\underline{\tau}^1)\underline{\tau}^1 + \lambda\underline{\tau}^1_{(1)} + \frac{\lambda\xi}{2}(\underline{\dot{\gamma}}\cdot\underline{\tau}^1 + \underline{\tau}^1\cdot\underline{\dot{\gamma}}) = \eta_1\underline{\dot{\gamma}} \tag{4.21}$$

$$H(tr\underline{\tau}^1) = \exp[\frac{\lambda\varepsilon}{\eta_1}tr\underline{\tau}^1] \tag{4.22}$$

$$\underline{\tau}^2 = \eta_2\underline{\dot{\gamma}} \tag{4.24}$$

In this section the equations for the rheological predictions of the PTT model in both shear flow and extensional flow are provided. These will be referenced in the next chapter where the degree of fit by the model to the rheological properties of the polymers studied will be evaluated.

4.2.2.1 Shear Flow Predictions

In steady shear flow the model makes the following predictions,

$$\eta = \frac{\eta_1}{1 + \xi(2-\xi)(\lambda\dot{\gamma})^2} + O(\varepsilon) \tag{4.25}$$

$$N_1 = \frac{2\eta_1\lambda\dot{\gamma}^2}{1 + \xi(2-\xi)(\lambda\dot{\gamma})^2} + O(\varepsilon) \tag{4.26}$$

$$N_2 = -\frac{\xi}{2}N_1 \tag{4.27}$$

In small amplitude oscillatory shear flow the predictions are,

$$G' = \frac{\omega^2\eta\lambda}{1 + (\omega\lambda)^2} + O(\varepsilon) \tag{4.28}$$

$$G'' = \frac{\omega\eta\lambda}{1 + (\omega\lambda)^2} + O(\varepsilon) \tag{4.29}$$

All of the above equations were obtained by assuming $\varepsilon = 0$ which should be valid since the magnitude of network strain should be relatively small in shear flow. The term $O(\varepsilon)$ was added to represent the fact that the term $H(tr\underline{\tau})$ will have an effect on the predictions for large values of ε.

4.2.2.2 *Extensional Flow Properties*

For the case of extensional flow it is no longer possible to obtain an analytical solution for the rheological properties. To obtain η_ε it was necessary to simultaneously solve a pair of nonlinear equations for the two normal stress components. To obtain the transient extensional stress growth, σ_ε^+, it was necessary to solve a coupled pair of differential equations. The two sets of equations used in these calculations are given below where $\dot{\varepsilon}$ is the strain rate.

Steady-state extension:

$$\exp\left[\frac{\varepsilon\lambda}{\eta_1}(\tau_{11} + 2\tau_{22})\right]\tau_{11} - 2\lambda\dot{\varepsilon}(1 - \xi)\tau_{11} = 2\eta\dot{\varepsilon} \tag{4.30}$$

$$\exp\left[\frac{\varepsilon\lambda}{\eta_1}(\tau_{11} + 2\tau_{22})\right]\tau_{22} + \lambda\dot{\varepsilon}(1 - \xi)\tau_{22} = -\eta\dot{\varepsilon} \tag{4.31}$$

Transient stress growth:

$$\exp[\frac{\varepsilon\lambda}{\eta_1}(\tau_{11} + 2\tau_{22})]\tau_{11} + \lambda\frac{d\tau_{11}}{dt} - 2\lambda\dot{\varepsilon}(1 - \xi)\tau_{11} = 2\eta_1\dot{\varepsilon} \tag{4.32}$$

$$\exp[\frac{\varepsilon\lambda}{\eta_1}(\tau_{11} + 2\tau_{22})]\tau_{22} + \lambda\frac{d\tau_{22}}{dt} + \lambda\dot{\varepsilon}(1 - \xi)\tau_{22} = -\eta_1\dot{\varepsilon} \tag{4.33}$$

4.3 *Implementation of the Finite Element Method*

In the previous two sections the finite element formulation of the momentum equation has been presented along with the constitutive equation with which it is coupled. These are the governing equations which have been used to simulate the entry flow behavior of different polymers using the finite element method. In this section the computer programs necessary to implement the method are described. The discussion is broken down into three sections covering the input data, the FEM code NONEWT, and the reduction of output data from the program. All of the programs discussed were developed by Gotsis (85) except for the mesh generation program written by Pelletier (106) and the PTT extensional property prediction programs and some plotting routines developed by the author.

4.3.1 Input Data

In order to implement the FEM code it is first necessary to generate the input data which describes the flow domain of the problem, the rheological properties of the fluid, and the initial conditions of the flow. The flow domain is described by the finite element mesh. Mesh generation was accomplished using the program GEN2D developed by Pelletier (106). The user defines the number and location of subdivisions of the domain and the program creates an

output file which lists the connectivity matrix of the mesh along with coordinates of each node in the domain. This file is then used as an input file to the program FILTER which rearranges it into a form compatible for input into the FEM code.

In addition to describing the flow domain it is necessary for the computer to be able to mathematically describe the rheological properties of the polymer. This is achieved through the use of the constitutive equation presented in the previous section. For the PTT model it is necessary to specify values of the parameters η_1, η_2, λ, ξ, and ε.The first four parameters are determined from viscometric data while the latter parameter is obtained from extensional data. Program PTTFIT determines the value of η_1, η_2, λ, and ξ by fitting the equation to experimentally measured values of the shear viscosity and N_1. Only ξ is adjustable and its value is chosen based either on the fit of normal stress data or the shift between η and η' data. The value of the adjustable parameter ε is determined from the fit of steady-state extensional viscosity data and extensional stress growth data. Programs PTTEXTS and PTTEXTG are used to accomplish this.

The final information needed for input is that which describes the boundary conditions for the flow and the initial conditions which will be used as the starting point of the iterations. This information is obtained from the program INIT which calculates the values of the velocity, stresses, and stream function at several points along the inlet and outlet planes of the flow domain. In mesh generation the flow domain should be chosen such that the inlet and outlet planes are far enough away from the contraction to be in the fully developed flow region as INIT's calculations are based on steady shear pressure flow between parallel plates.

4.3.2 FEM Code: NONEWT

Having developed the necessary input file which describes the flow problem of interest it is possible to solve the problem using the FEM source code. In this study the program NONEWT was used. This program, based on Reddy's two-dimensional FEM code FEM2D (102),

was designed by Gotsis (85) to solve flow problems involving viscoelastic fluids. As it is described in detail elsewhere (85) only its general characteristics are given here.

Since NONEWT determines the solution for viscoelastic fluids using the penalty finite element method, five primary variables are calculated (i.e. two components of the velocity vector and three components of the stress tensor). Other than the Newtonian case, solutions can be found for a choice of five non-Newtonian constitutive equations including the Generalized Newtonian, White-Metzner, Upper Convected Maxwell, Phan-Thien Tanner, and Leonov-like models. In addition to calculating nodal values of the primary variables, elemental values of pressure, shear rate, viscosity, extension rate, vorticity, and birefringence are determined. Finally, the processor section is run again for calculation of the stream function as this requires the finite element method for solution.

4.3.3 Output Data

Output data from NONEWT is presented either as hardcopy output listings of nodal and elemental values of variables or as two-dimensional plots of selected variables. Several plotting routines have been developed, based on the SURFACE2 package, for presenting streamline and birefringence data the results of which are presented in the following chapter.

5.0 RESULTS AND DISCUSSION

In this chapter the results of the study of entry flow will be presented. The chapter will be divided into two main sections: the first covering the experimental aspects of the study and the second covering the numerical results. In the experimental section the purpose will be to fulfill the first two objectives of this study 1) to provide a fundamental explanation of why vortices form in some viscoelastic fluids but not in others and 2) provide an understanding of the effects of molecular, rheological, and geometrical parameters on entry flow behavior. In doing this, streamline patterns of several polymer melts will be presented along with key rheological data in an attempt to explain and correlate the flow behavior. This will be done by providing a rather thorough study of LDPE and polystyrene in section 5.1. These two polymers best exemplify the two extremes in flow behavior exhibited by viscoelastic fluids in contraction flow and will provide the means for introducing the reasons for vortex growth. In sections 5.2 and 5.3 examination of the flow behavior of polymers of different molecular weight and MWD will be presented. Through these sections it will be possible to relate flow behavior to molecular characteristics. To complete the discussion of experimental work, section 5.4 will present the birefringence data obtained in this study. Through this data it will be possible to provide additional support for the ideas presented in the previous sections on vortex growth.

Numerical results will be presented in the last sections of the chapter. The purpose of the numerical work will be to determine if numerical simulation of entry flow can be improved by use of a constitutive equation which better describes those rheological properties which have been found to be key to vortex growth. Also, it will be seen that the numerical simulations provide independent support of the explanation of vortex growth derived from experimental data. In section 5.5 the fit of the rheological properties of the polymers of this study by the Phan-Thien Tanner (PTT) model will be evaluated. This section will provide justification of the use of the PTT model in the numerical simulations. Mesh design and refinement effects will be briefly described in section 5.6. Section 5.7 will show to what extent the finite element method and the PTT model can predict the flow behavior of polymer melts in the entry region. Comparison will be made between numerical and experimental streamlines and the effect on flow behavior of the variation of a fluid's extensional flow properties will be examined. Finally, in section 5.8 a quantitative comparison between numerical and experimental results will be made by examining the stresses in the fluid as it flows through the contraction.

5.1 Comparison of the Entry Flow Behavior of LDPE and Polystyrene

As stated previously, LDPE and polystyrene most clearly demonstrate the two different types of flow behavior encountered in entry flow and as such have been the major focus of this study both experimentally and numerically. In the following section the flow patterns obtained for these polymers will be presented along with the quantification of the flow in terms of the detachment length. This will be followed by a discussion of the flow behavior and its relation to rheological properties. Based on this a theory for the cause of vortex growth will be proposed.

5.1.1 Streamline Patterns of LDPE and Polystyrene

The flow behavior of LDPE and polystyrene was observed under a multitude of conditions using slit die 2. The downstream wall shear rate range covered was from 1 to 80 sec^{-1}. Both the 4:1 and 8:1 geometries were used and the tests were run at melt temperatures of 150° C for LDPE and 165° and 190° C for polystyrene.

In Figure 12 and Figure 13 the flow patterns for LDPE in the 4:1 geometry are presented. Figure 12 shows the vortex growth which is typical of some viscoelastic fluids in entry flow. At low flow rates the entry flow patterns of all polymers has been found to be Newtonian in nature, with the fluid exhibiting no vortices, and this is seen to be true for LDPE. At a shear rate of 1 sec^{-1} it is seen that the fluid flows deep into the corners and there is no apparent recirculation even for this exposure which represents 16 minutes of flow time. However, when the rate is increased to 2.5 sec^{-1} vortex growth begins with the fluid streamlines rising slightly out of the corners and recirculation beginning. It can be seen that recirculation is quite weak as this photograph also represents 16 minutes of flow. As the rate is increased to 5 sec^{-1} and then to 10 sec^{-1}, it is seen that the vortex continues to grow and the recirculation intensifies. (The exposure time at 5 sec^{-1} was 8 minutes while that at 10 sec^{-1}, and for all remaining streamline patterns presented in this study, was 4 minutes.) In this vortex growth region (from 1 to 10 sec^{-1}) it should also be noted that the vortex boundary changes in shape. At 1 sec^{-1} and 5 sec^{-1} the boundary between the vortex and the bulk fluid flow is concave whereas on increasing the rate to 5 sec^{-1} and then to 10 sec^{-1} the boundary changes from a concave to a convex shape. Above 10 sec^{-1} negligible vortex growth occurs (Figure 13). The size and shape of the vortex, which grew between 1 sec^{-1} and 10 sec^{-1}, changes very little. Despite an increase in shear rate up to 80 sec^{-1} the only noticeable change is in the intensity of the recirculation.

Much the same type of behavior was observed for LDPE in the 8:1 geometry (Figure 14). At 1 sec^{-1} the flow is essentially Newtonian in nature but at 5 sec^{-1} indications

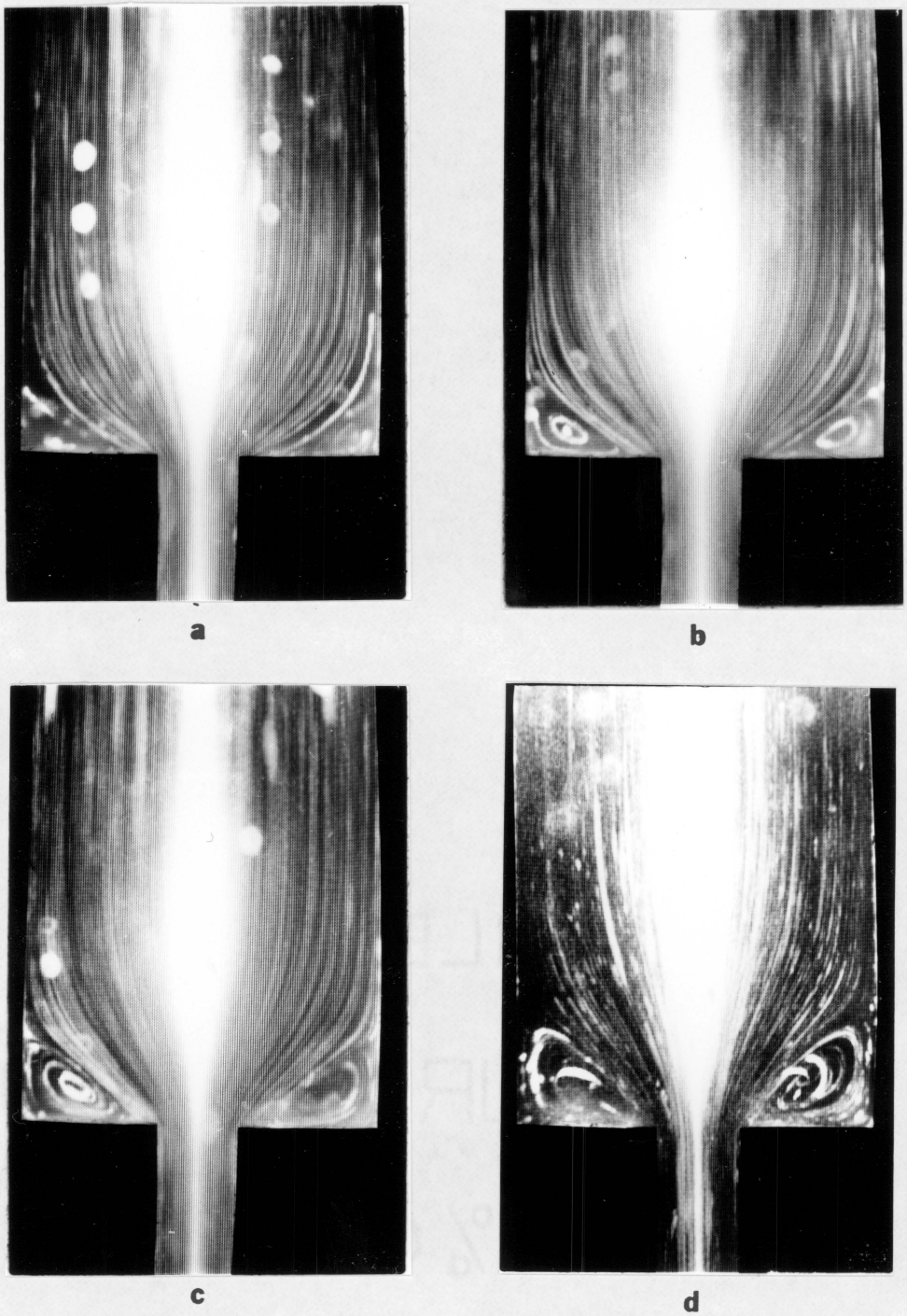

Figure 12. Streamline Patterns of LDPE, 4:1 Contraction: a) $\dot{\gamma} = 1\ \text{sec}^{-1}$, $We = 0.876$ b) $\dot{\gamma} = 2.5\ \text{sec}^{-1}$, $We = 1.01$ c) $\dot{\gamma} = 5\ \text{sec}^{-1}$, $We = 1.11$ d) $\dot{\gamma} = 10\ \text{sec}^{-1}$, $We = 1.21$

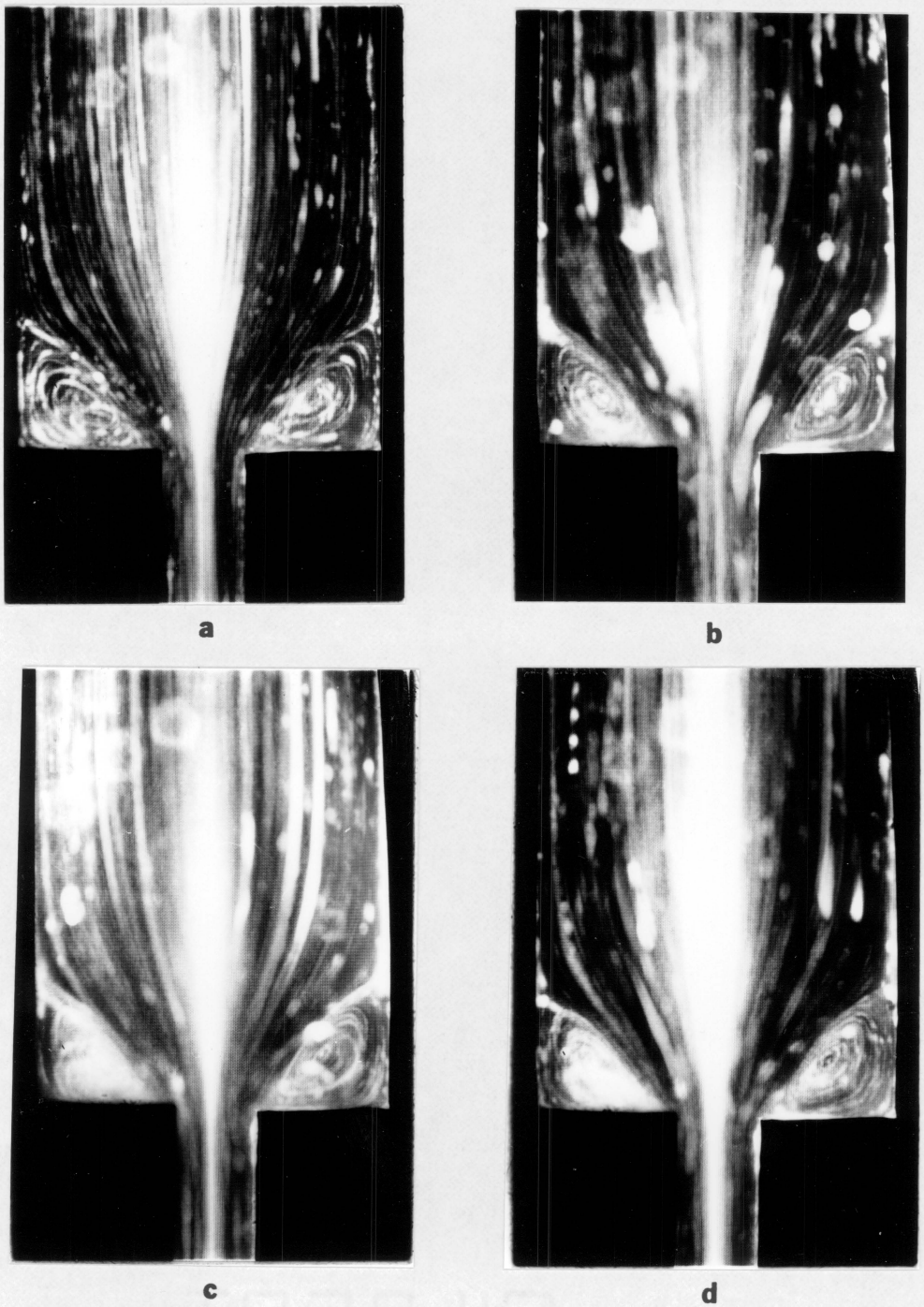

Figure 13. Streamline Patterns of LDPE, 4:1 Contraction: a) $\dot{\gamma} = 20\ \text{sec}^{-1}$, $We = 1.29$ b) $\dot{\gamma} = 40\ \text{sec}^{-1}$, $We = 1.35$ c) $\dot{\gamma} = 60\ \text{sec}^{-1}$, $We = 1.38$ d) $\dot{\gamma} = 80\ \text{sec}^{-1}$, $We = 1.38$

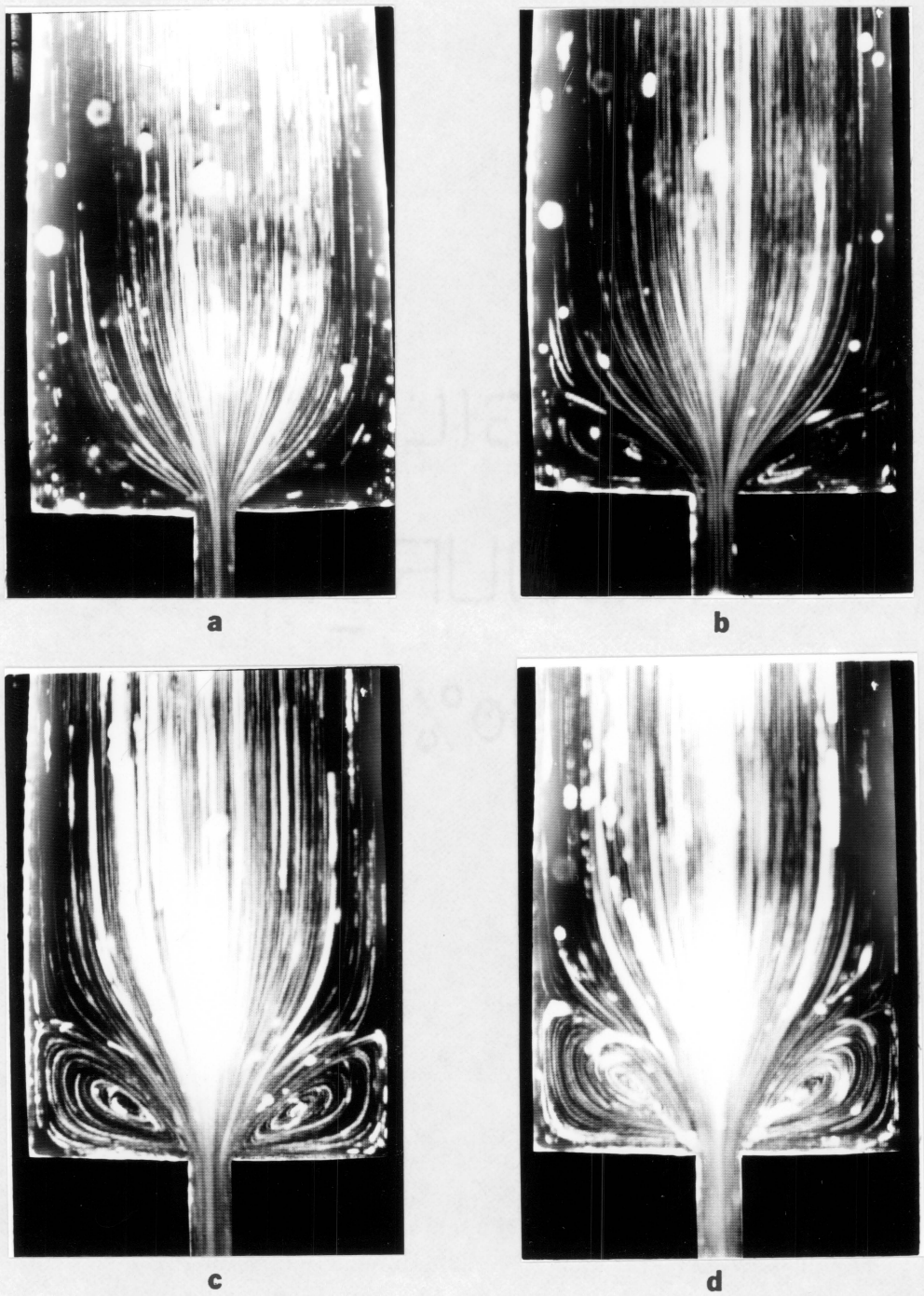

Figure 14. Streamline Patterns of LDPE, 8:1 Contraction: a) $\dot{\gamma} = 1\ sec^{-1}$, $We = 0.876$ b) $\dot{\gamma} = 5\ sec^{-1}$, $We = 1.11$ c) $\dot{\gamma} = 10\ sec^{-1}$, $We = 1.21$ d) $\dot{\gamma} = 20\ sec^{-1}$, $We = 1.29$

of recirculation appear. (The streamlines in these two cases are not as well defined as those in the 4:1 geometry since in the 8:1 geometry the height of the upstream channel is twice as large leading to correspondingly lower velocities.) Increasing the rate to 10 sec^{-1} leads to a rapid increase in vortex size and recirculation intensity. Again, above 10 sec^{-1} it appears that vortex growth stops, with only recirculation rate increasing. Comparison between the flow patterns obtained in the 4:1 and 8:1 geometries indicates larger vortices occur in the 8:1 geometry when compared at similar shear rates.

The flow behavior of polystyrene at 190° C is significantly different than that observed for LDPE (Figure 15 on page 98). At low rates the flow patterns of the two polymers are similar in that both are Newtonian in nature. However, this is where the similarity ends. At higher rates LDPE exhibits vortex growth but the shape of the flow pattern of polystyrene does not change for shear rates from 1 to 80 sec^{-1}. The only noticeable change is the occurrence of weak recirculation at the higher rates. However, even though recirculation is observed, there is no measurable increase in the size of this corner region even at the highest rate. Similar behavior was observed for polystyrene in the 8:1 geometry. There was no vortex growth and in addition there was not even the recirculation that was observed at higher rates in the 4:1 contraction.

When the melt temperature was lowered to 165° C there was a change in the flow behavior of the polystyrene (Figure 16 on page 99). In both the 4:1 and 8:1 geometries it was found that at shear rates in the range from 10-30 sec^{-1} vortex growth had occurred. Due to the high viscosity of the fluid at this temperature recirculation within the vortex was quite weak. In addition, because of this weak recirculation it was not possible to observe vortex growth at lower rates as was done for LDPE. Recirculation within the corners is necessary to define the size of the vortex so that without recirculation vortex growth cannot be followed with increasing flow rate. It is believed that since the vortex size remains the same in the 10-30 sec^{-1} shear rate range that vortex growth has already occurred and this represents the region, found for LDPE, where vortex size no longer increases.

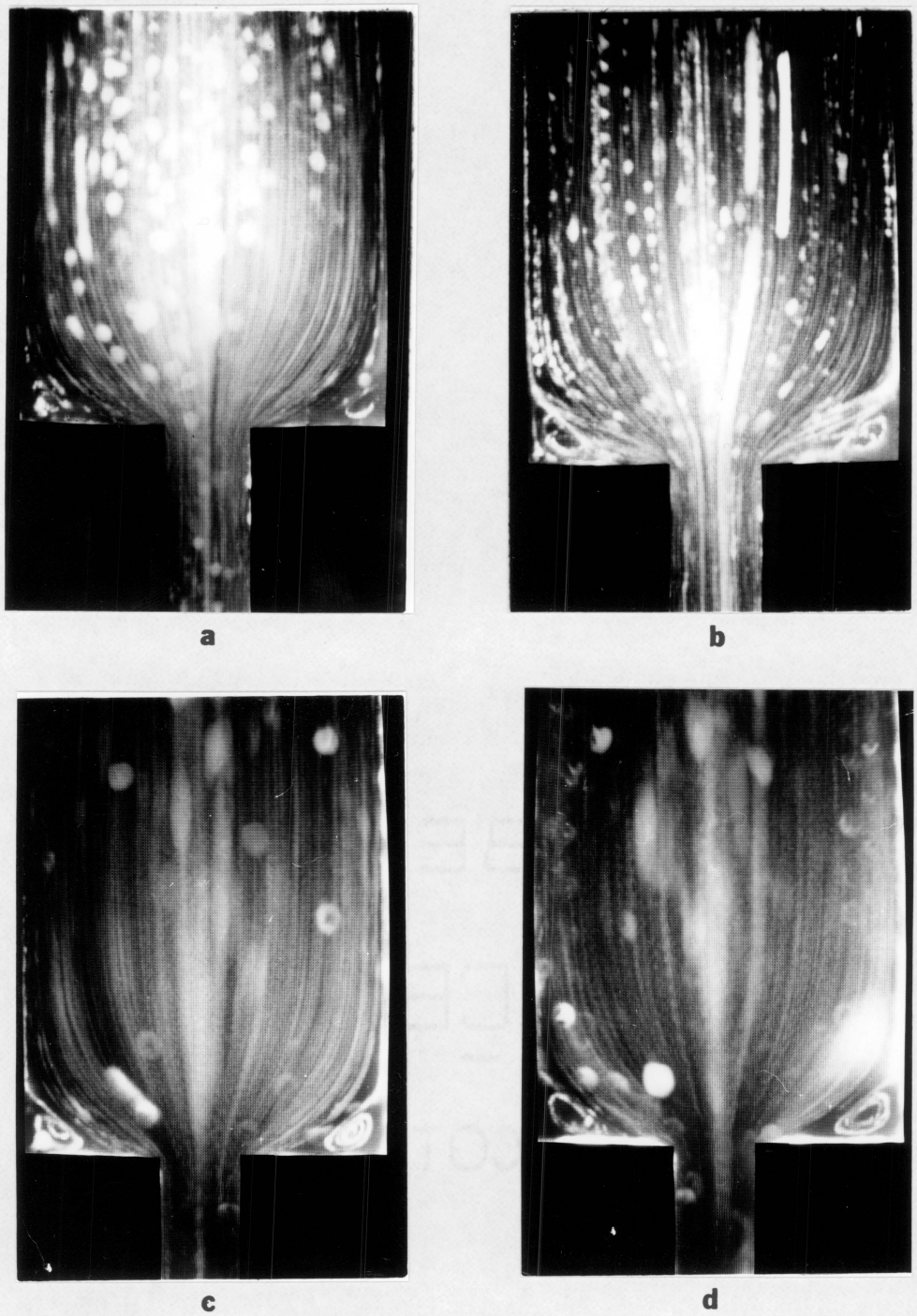

Figure 15. Streamline Patterns of Polystyrene, 4:1 Contraction, 190° C: a) $\dot{\gamma} = 5\ \text{sec}^{-1}$, $We = 0.823$ b) $\dot{\gamma} = 20\ \text{sec}^{-1}$, $We = 1.19$ c) $\dot{\gamma} = 40\ \text{sec}^{-1}$, $We = 1.39$ d) $\dot{\gamma} = 80\ \text{sec}^{-1}$, $We = 1.62$

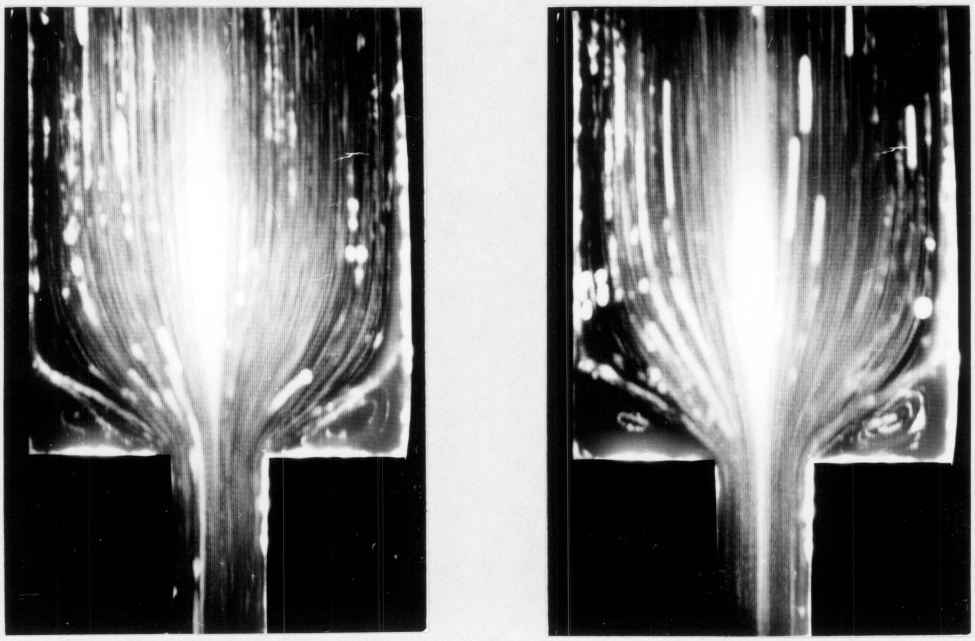

a b

Figure 16. Streamline Patterns of Polystyrene, 4:1 Contraction, 165° C: a) $\dot{\gamma} = 15\ \text{sec}^{-1}$, $We = 1.73$ b) $\dot{\gamma} = 25\ \text{sec}^{-1}$, $We = 2.07$

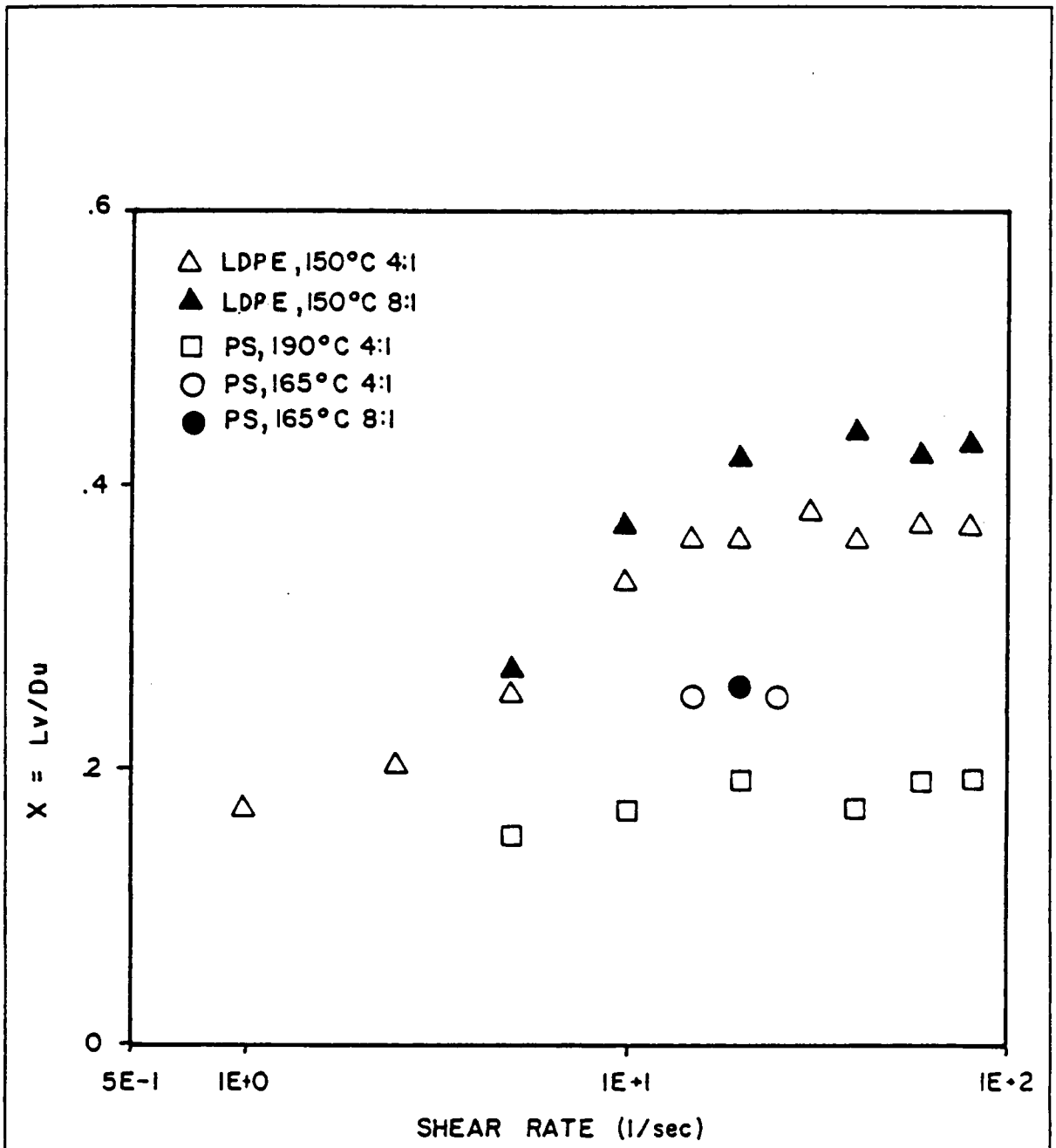

Figure 17. Detachment Length Versus Shear Rate for LDPE and Polystyrene

Vortex growth or the lack thereof, is quantified in Figure 17 on page 100 for LDPE and polystyrene. In this plot the detachment length is as defined previously:

$$X = \frac{L_v}{D_u} \tag{2.1}$$

where L_v is the distance upstream of the contraction at which the flow detaches from the wall (see Figure 1 on page 2) and D_u is the height of the upstream channel. The plot summarizes the major points that were made based on the streak photographs. It is seen that for polystyrene the detachment length remains at a constant value of $X \cong 0.18$ and that this is the value that LDPE asymptotically approaches at low rates. The detachment length for polystyrene at 165° C is higher at $X \cong 0.25$ and if it were possible to obtain values of X at lower rates it is expected that these would also asymptotically approach $X = 0.18$. For LDPE the effect of contraction ratio becomes apparent. For both the 4:1 and 8:1 geometries the detachment length appears to initially grow along the same curve and then at higher rates deviation occurs with the 8:1 geometry giving larger values of X. At the end of the vortex growth region, $\dot{\gamma} \cong 10 - 20 sec^{-1}$, both curves level off to constant values of X. In the 4:1 geometry the ultimate vortex size is $X = 0.37$ and in the 8:1 geometry it is $X = 0.43$.

5.1.2 Interpretation of the Entry Flow Results for LDPE and Polystyrene

In the previous section the entry flow behavior of LDPE and polystyrene was presented. It was made apparent that the flow behavior of these two polymers is distinctly different and in this section an explanation for the behavior will be given. The approach to this problem will be simplistic at first by comparing the viscometric properties of the two fluids. In Figure 18 on page 102 the viscosity and primary normal stress difference is given for LDPE at 150° C and polystyrene at 190° C. It is seen that the viscosity, and therefore the shear stress, is higher for LDPE than for polystyrene under these conditions. Correspondingly the normal stresses are

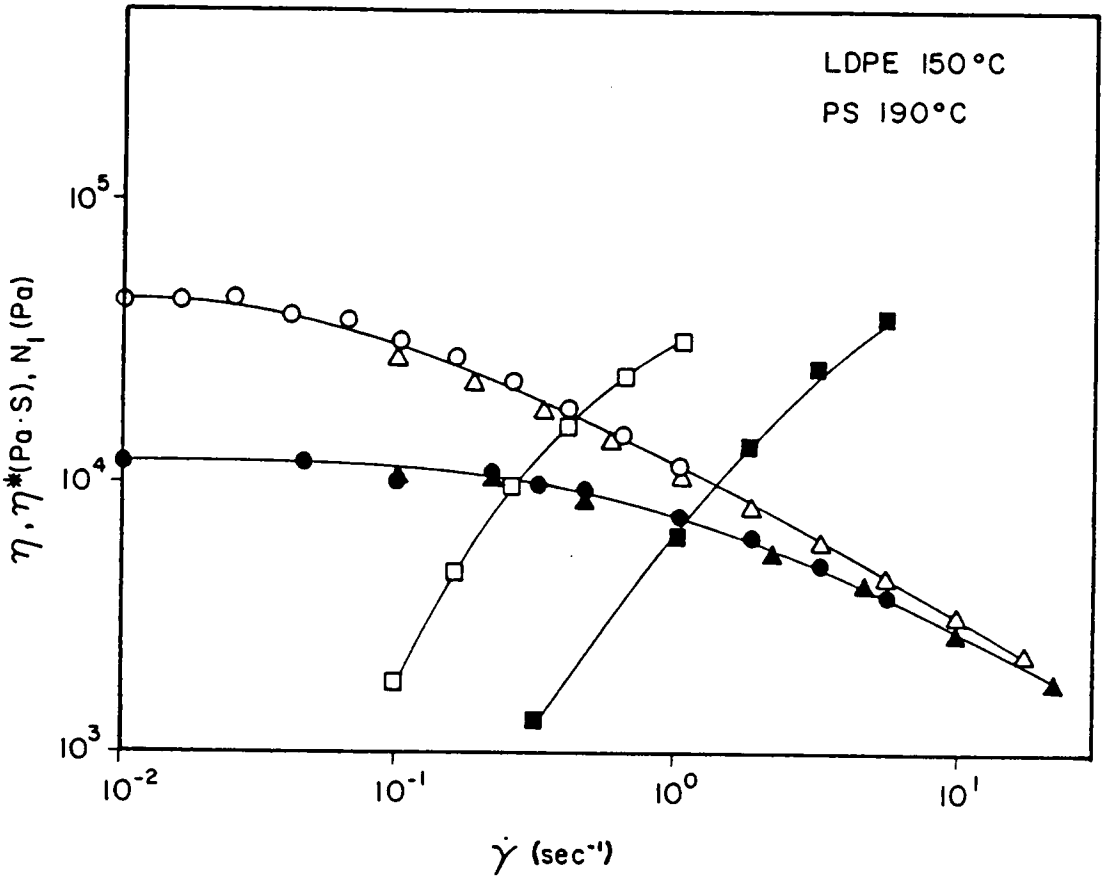

Figure 18. Viscometric Properties of LDPE at 150° C and Polystyrene at 190° C: Open symbols- LDPE●,○-η, ▲,△-η*, ■,□-N_1

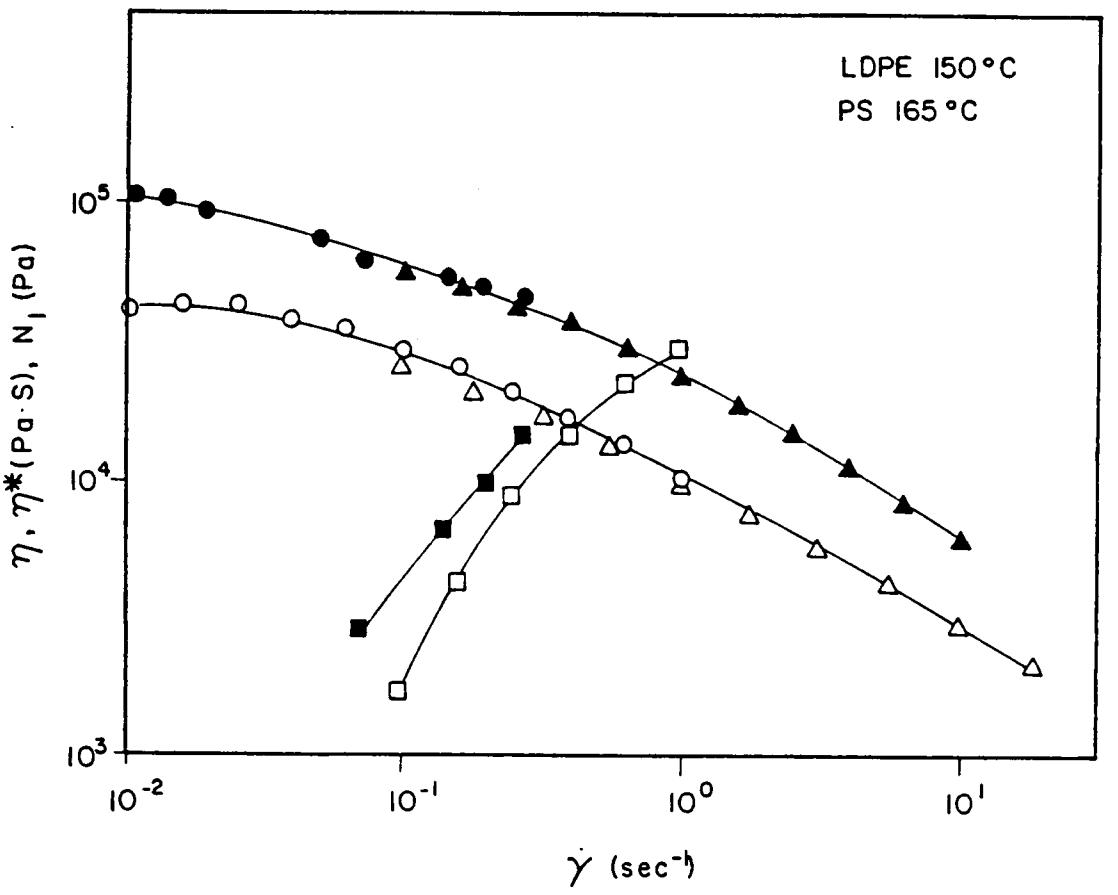

Figure 19. Viscometric Properties of LDPE at 150° C and Polystyrene at 165° C: Open symbols-LDPE ●,○-η, ▲,△-η^*, ■,□-N_1

also higher for LDPE. Therefore, it might be expected that the difference in entry flow behavior of the two polymers could be related to the development of higher levels of shear stress in LDPE than in polystyrene at comparable shear rates. However, this simplistic approach can be quickly dispelled by comparing the viscometric properties of LDPE at 150° C with those of polystyrene at a lower temperature of 165° C. From Figure 19 on page 103 it can be seen that the relative position of the curves has switched compared to those in Figure 18. Under these conditions the shear stresses in polystyrene will be higher than those in LDPE at similar shear rates. However, referring back to the detachment length plot (Figure 17 on page 100) shows that even at 165° C the vortex size of polystyrene is considerably smaller than that in LDPE despite the higher level of shear and normal stresses in polystyrene. Therefore, these shear properties taken alone give no insight into the differences in observed flow behavior.

The next step in trying to explain vortex growth is to follow up on the findings of other workers in this area who have typically correlated entry flow behavior with fluid elasticity. As stated previously, fluid elasticity is usually given by the Weissenberg number (We) which is the ratio of the normal stress to twice the shear stress, $\frac{N_1}{2\tau_{12w}}$. However, since it is not possible to obtain N_1 for polymer melts at the shear rates that the flow experiments were carried out at, it is necessary to use an approximation of We. In this study We is given as G'/G''. Justification is based on the fact that in the limit of low shear rates the two definitions of We are the same.

From a plot of We versus shear rate it can be seen that fluid elasticity also does not explain differences in flow behavior. Figure 20 on page 105 gives We for LDPE at 150° C and polystyrene at 165° and 190° C. It can be seen that although LDPE has a higher level of elasticity at lower rates, when one moves to the rates where vortex growth was observed (1-10 sec^{-1}) it is seen that polystyrene at 165° C has the higher level of elasticity and at the highest rates polystyrene at 190° C also has a higher level of elasticity than LDPE. But again, it should be remembered that LDPE had a much larger detachment length than polystyrene at either 165° C or 190° C but its relative elasticity is less. Therefore, elasticity also does not explain differences in flow behavior.

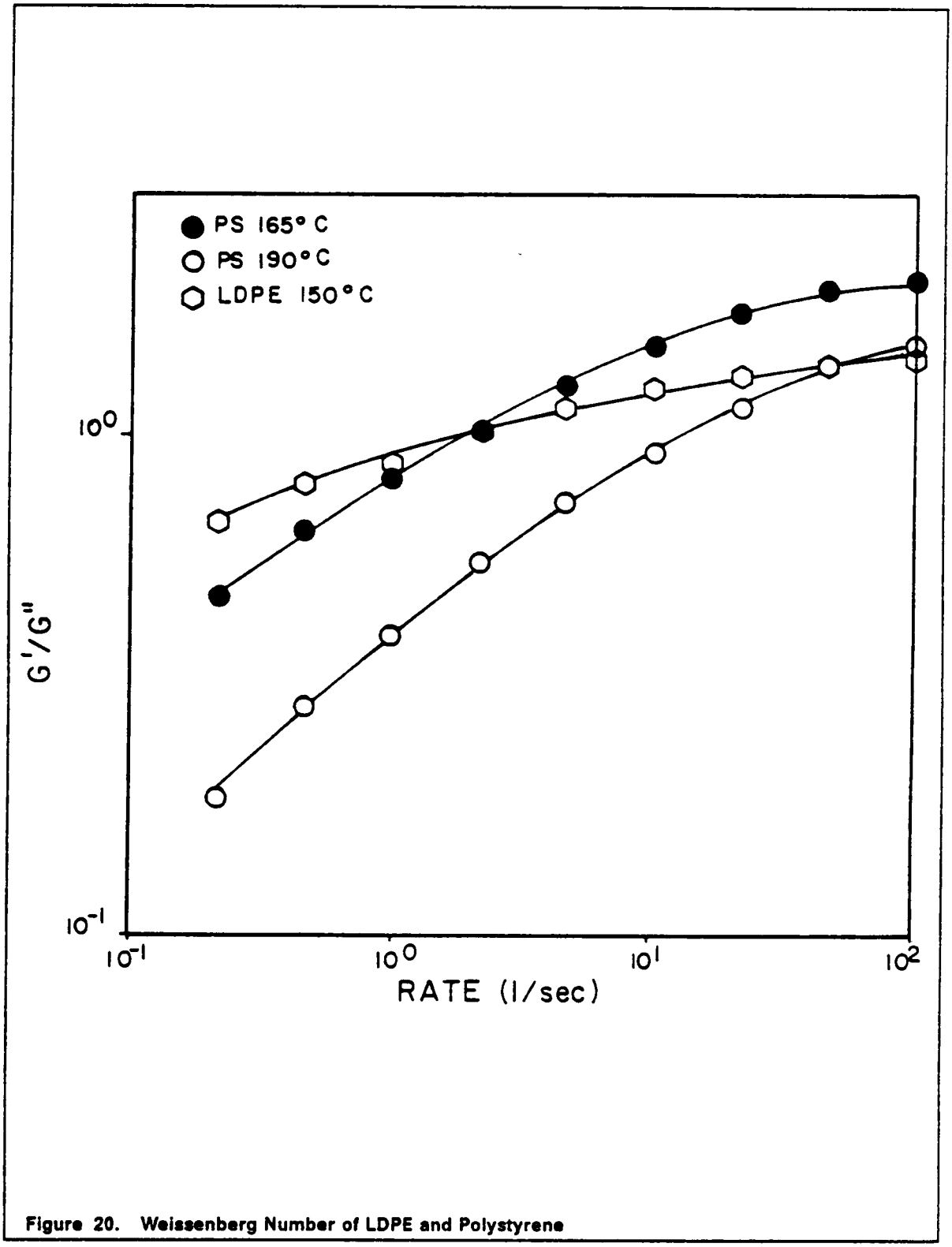

Figure 20. Weissenberg Number of LDPE and Polystyrene

It should be pointed out, however, that although elasticity cannot be used to distinguish between the flow behavior of different types of polymers it can be used to correlate flow behavior for a given type of polymer. This is what was typically done in the studies of Nugyen and Boger (7) and White and Kondo (23). In Nugyen and Boger's case, flow behavior was correlated with elasticity for polyacrylamide solutions and White and Kondo did the same with polymer melts. Both reported that vortex could be correlated with fluid elasticity. However, White and Kondo found that the correlations did not hold for different types of polymers which is the case in this study. The difference in detachment length of polystyrene at 165° C and 190° C could be correlated with the difference in elasticity at the different temperatures but as stated in the previous paragraph, it does not explain the difference in flow behavior between polystyrene and LDPE.

The inability to correlate entry flow behavior with fluid elasticity can be verified by one last method. By plotting detachment length versus We the polymers can be compared on a common dimensionless basis. This type of plot would indicate if there is a critical value of We above which vortex growth would occur in any polymer. However, from Figure 21 on page 107 it is seen that there is not a critical value of We. It is seen that although LDPE exhibits vortex growth for $We > 1$, polystyrene at 190° C exhibits no vortex growth for values of We up to 1.6. Although it is not known at what value of We vortex growth occurs for polystyrene at 165° C, it still has a much smaller detachment length than LDPE although We is much higher.

In light of what has been stated in the previous paragraphs it is not possible to explain entry flow behavior in terms of shear properties alone and therefore, attention should be directed towards the extensional properties of the polymer. Figure 22 on page 108 and Figure 23 on page 109 present the transient growth behavior of the extensional viscosity of LDPE and polystyrene. Figure 22 on page 108 compares the two polymers for the case of polystyrene at 190° C. From this plot it can be seen that there is a significant difference between the two materials not only in regards to the magnitude of the viscosity but also in regards to the transient growth behavior. Polystyrene exhibits a bounded growth even at the highest strain rates. However, LDPE exhibits unbounded growth up to the highest strains

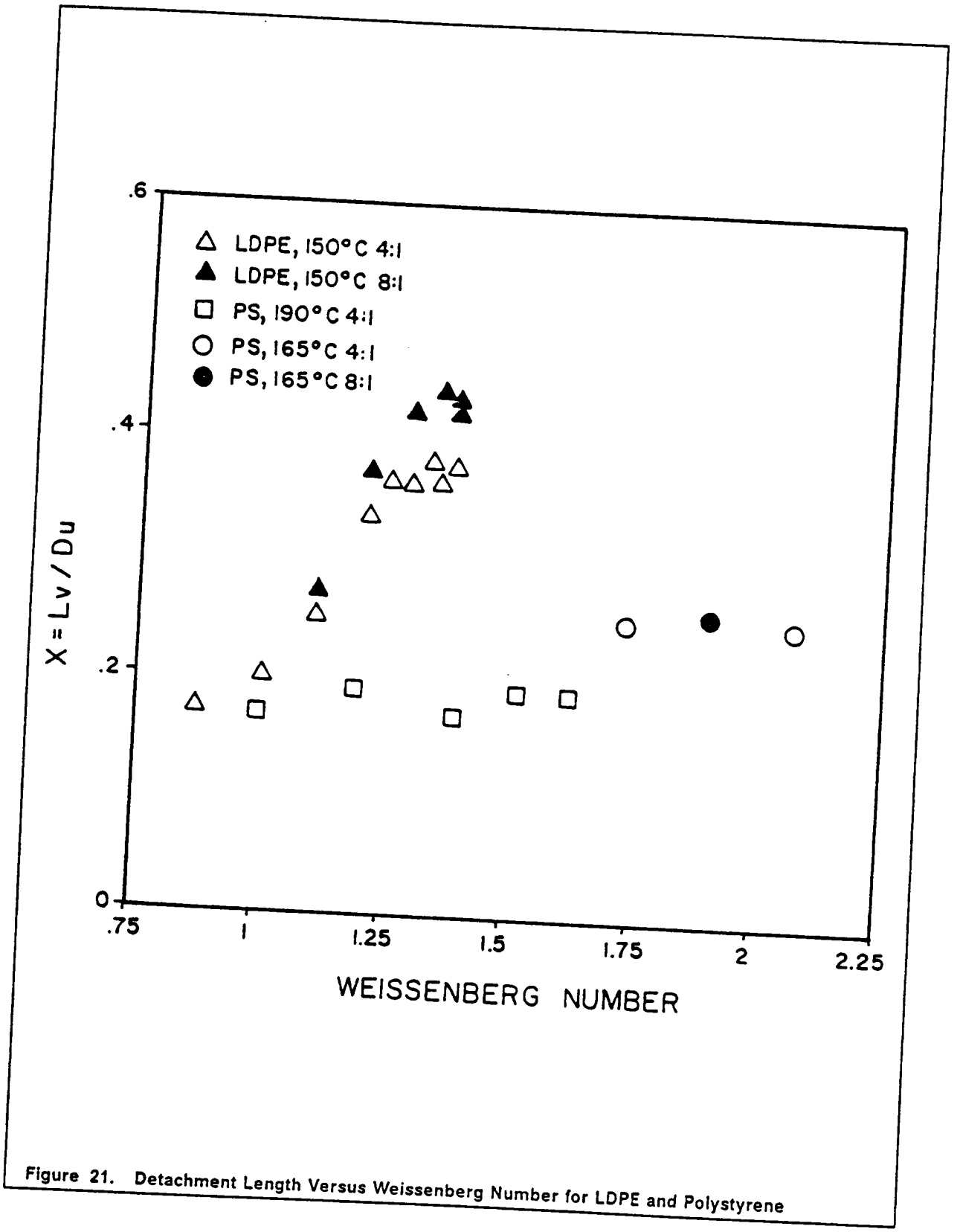

Figure 21. Detachment Length Versus Weissenberg Number for LDPE and Polystyrene

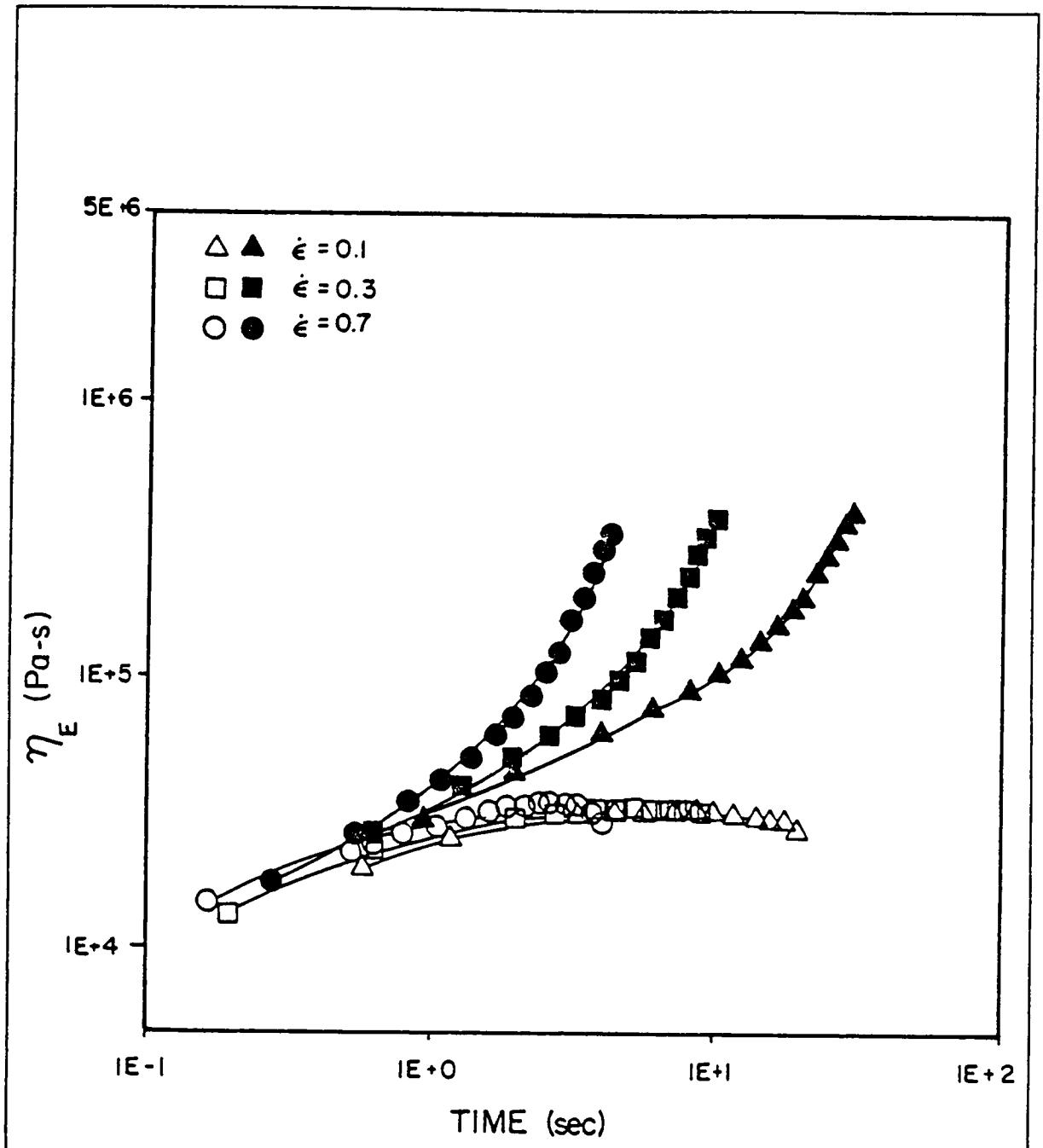

Figure 22. Extensional Viscosity of LDPE at 150° C and Polystyrene at 190° C: Closed symbols-LDPE

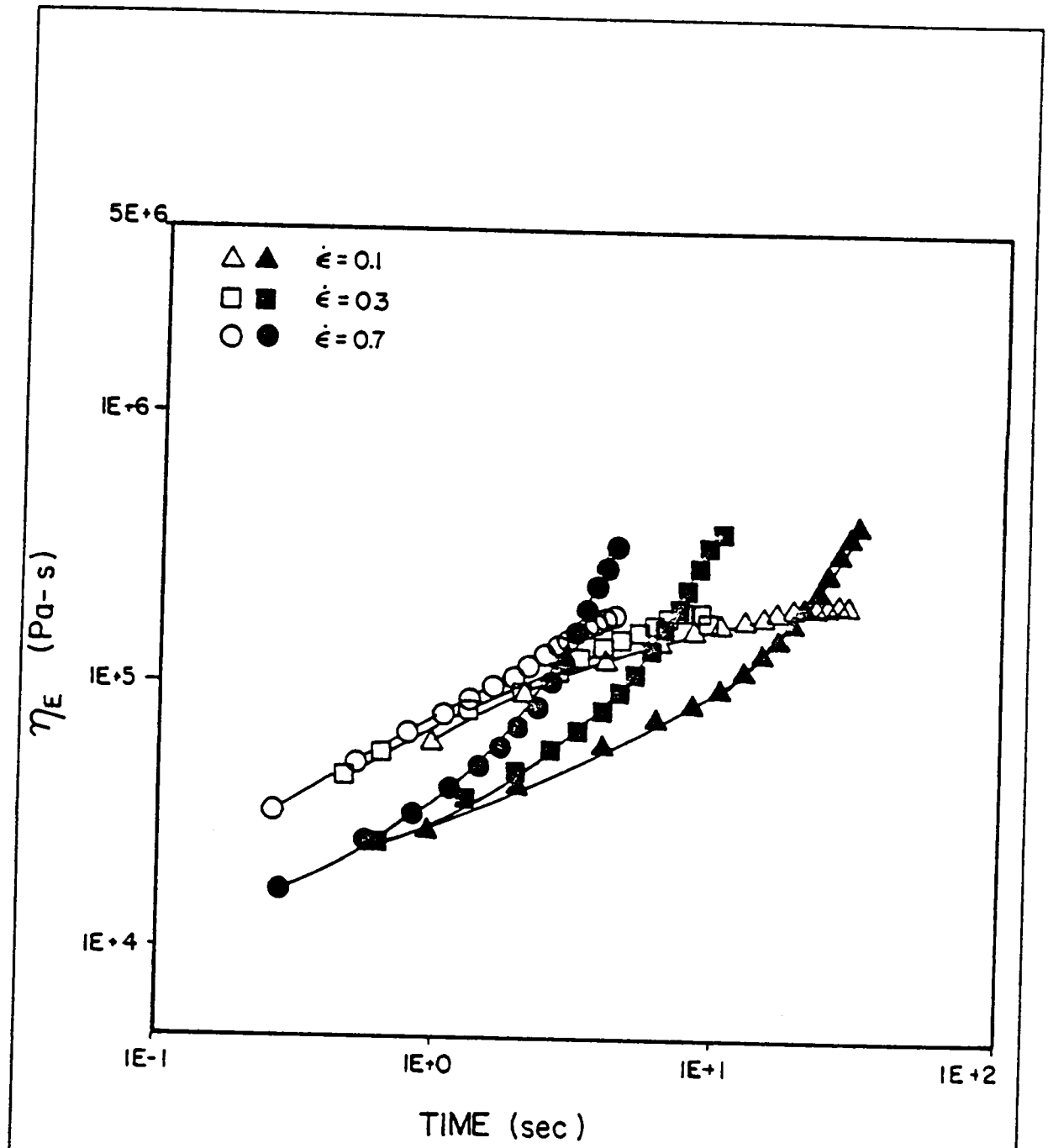

Figure 23. **Extensional Viscosity of LDPE at 150° C and Polystyrene at 165° C:** Closed symbols-LDPE

achievable with the extensional rheometer. The result is that although the viscosity of both materials start off at nearly the same value, the ultimate viscosity of the LDPE is over an order of magnitude higher than that of polystyrene. In addition, for the case of polystyrene at 165° C Figure 23 on page 109 shows that the viscosity of LDPE, although lower at low strains, becomes higher than that of polystyrene. Also, if it were possible to obtain higher strains in the rheometer it may indicate that the viscosity of LDPE attains values much higher than that shown in Figure 22 and Figure 23. Data reported in the literature indicate that the value of $\frac{\eta_E}{\eta_0}$ can be on the order of 10 for LDPE but only slightly over 3 for polystyrene.

Based on the behavior of the two polymers in extension it becomes apparent that there is a link between vortex growth and the extensional properties of the polymer. For polystyrene at 165° C the extensional viscosity and the detachment length are larger than at 190° C. This alone, however, does not show the link between vortex growth and extensional properties as both the elasticity and the shear stress are also larger at 165° C. What links the two is the fact that in comparison with polystyrene at 165° C, LDPE exhibits a greater detachment length and a larger extensional viscosity even though its shear viscosity and elasticity are lower than those of polystyrene. Therefore, based on comparison at similar flow rates, it would be expected that the LDPE would exhibit vortices and the polystyrene would not because of the development of larger extensional stresses in LDPE.

Not only does the above hypothesis make sense from a rheological point of view but also from a molecular point of view. It would be expected that in the entry region extensional strains would be imposed on the fluid as it accelerates into the contraction. At low flow rates the extensional strain rates in this region should be small and therefore, the flow should primarily be a shear flow. The result would be radial flow, as was observed for both LDPE and polystyrene at low shear rates. As the flow rate is increased the extensional strain rates encountered near the contraction should correspondingly increase resulting in a mixture of both shear and extensional flow. At this point differences should be observed for different fluids. It would be expected that those polymers which exhibit a large resistance to extension, as evidenced by their extensional rheological properties, would no longer exhibit a Newtonian

flow pattern, but in response to the extensional stress imposed upon it, pull up out of the corners and effectively funnel the fluid from the upper channel to the lower. This would explain the behavior of LDPE as it is a highly branched polymer for which the entanglement of these branches with other molecules would be expected to create a greater restriction to extensional flow than polystyrene, which is a linear molecule, and as such should have much less restriction to extension. The funneling of the polymer into the downstream channel would essentially smooth out the otherwise abrupt acceleration at the contraction over a larger entry zone avoiding the high extensional stress gradients which would occur.

Geometric effects can also be explained in terms of the above hypothesis. For LDPE it was observed that there was an increase in detachment length in going from the 4:1 to the 8:1 contraction ratio. Because of the greater change in velocities in the 8:1 geometry in going from the upstream channel to the downstream channel it would be expected that there would be greater extensional strain rates imposed on the fluid than are seen in the 4:1 geometry. Therefore, a polymer such as LDPE, whose extensional viscosity is a strong function of strain rate, would be expected to develop larger extensional stresses in the 8:1 than in the 4:1 geometry at similar flow rates and larger vortices would result. Referring to Figure 17 on page 100 it can be seen that the two curves for LDPE are similar at low flow rates where the extensional strain rates would be low but the curves diverge at high flow rates where the strain rates would become higher in the 8:1 geometry. In addition, comparison of polystyrene in the 4:1 and 8:1 geometries shows little difference in flow behavior. This would be expected since the polymer's extensional viscosity is relatively rate insensitive.

Finally, vortex recirculation must be addressed. The previous discussion has explained the formation of the vortex cell, but recirculation within the cell is believed to occur by a different process. Although there is an extensional component to the recirculation it is believed that the flow within the vortex cell is primarily a shear flow, largely attributable to the transfer of momentum from the bulk fluid flow through the cell interface, in a manner similar to cavity flow. For polystyrene this means weak recirculation since fluid velocity is quite low at the cell interface because the cell is deep in the corner and near the walls of the die. For LDPE this

means greater recirculation since the vortex cell projects much further in towards the center of the die where fluid velocity is higher.

In this section an explanation has been given for vortex growth and cell recirculation. Although recirculation has been related to shear flow at the cell interface it is believed that vortex growth is due to the degree of restriction to extensional flow of some polymers as evidenced by their extensional rheological properties. If this is true then changes in a given polymer type which would cause it to exhibit greater restriction to extension should be reflected in the polymer's entry flow behavior. This will be the subject of the following sections where the effect of changes in molecular weight and MWD on flow behavior will be examined.

5.2 *Molecular Weight Effects on Entry Flow Behavior: Polystyrene Blend*

The purpose of the work in this section is to examine the effect of relatively small changes in molecular weight and MWD on the entry flow behavior of polystyrene. The idea for this work developed from the findings of Münstedt (47) in regards to the extensional properties of polystyrenes of different M_w and MWD. As discussed in Chapter 2, Münstedt found that the main differences in the extensional behavior of the polystyrenes were related to the presence or absence of high molecular weight components in the distribution. Under constant strain rate deformation it was found that those polymers which had a high molecular weight tail in their MWD either did not obtain steady-state or did so at high strain. In particular, one polystyrene, which had a bimodal MWD, appeared to reach steady-state at one level but as the strain increased the stress again increased and seemed to approach steady-state at a much higher level. At higher strain rates the effect of the higher molecular weight component became more apparent. Although the polystyrenes without a significant high molecular weight

tail exhibited bounded stress growth the bimodal polystyrene exhibited unbounded stress growth similar to that of LDPE. Plots of extensional viscosity as a function of stress showed that the bimodal polystyrene exhibited a maximum several times higher than the Trouton value which is similar to the behavior of LDPE.

In explaining the observed behavior, Münstedt states that the high molecular weight components represent long chains which act as a far reaching network within the matrix of smaller chains. At low strains the stress necessary to deform the polymer is representative of the shorter chains. However, at higher strains the entanglements of the longer chains become significant resulting in higher stress.

Based on Münstedt's findings it was desired to learn if a bimodal polystyrene with extensional properties qualitatively similar to LDPE would also exhibit entry flow behavior similar to LDPE. However, the reduction of this idea to practice proved to be quite difficult. As will be seen, it was not possible to create a polystyrene with extensional properties similar to LDPE but it was possible to evaluate the effect of the presence of a high molecular weight component on entry flow behavior.

5.2.1 Streamline Patterns

The polystyrenes used in this study were a base resin, STYRON 678 described in the previous section, and a blend of the base resin and a narrow distribution, high molecular weight fraction. The blending procedure and molecular weight characterization of the polymers is given in Chapter 3. The result of the blending was a polystyrene with a MWD similar to that of the base resin but with the distinct presence of a second high molecular weight peak (Figure 2 on page 54).

To obtain flow patterns of the blend it was necessary to use slit die 1 as only a small quantity of the polymer was available. The flow patterns are presented in Figure 24 on page 114 for both the base resin and the blend. Both patterns were obtained at 190° C and a

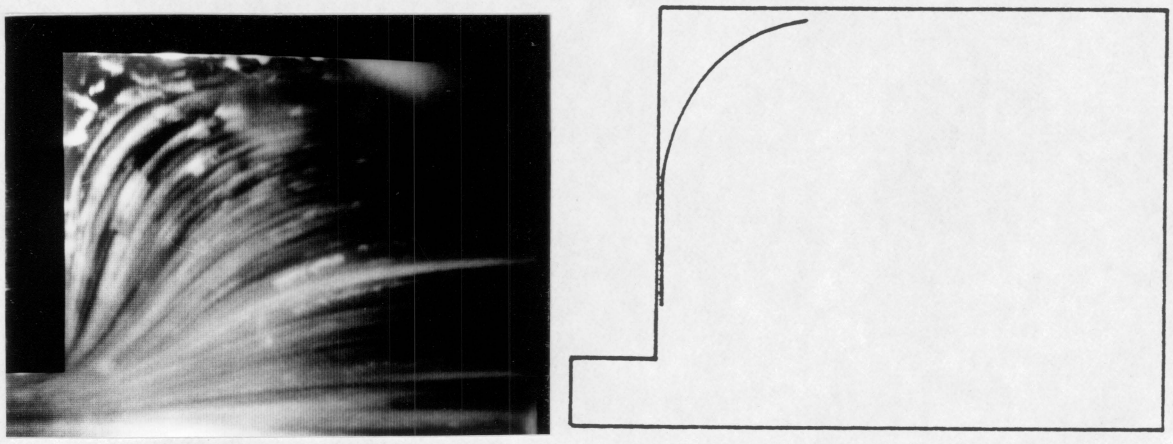

a

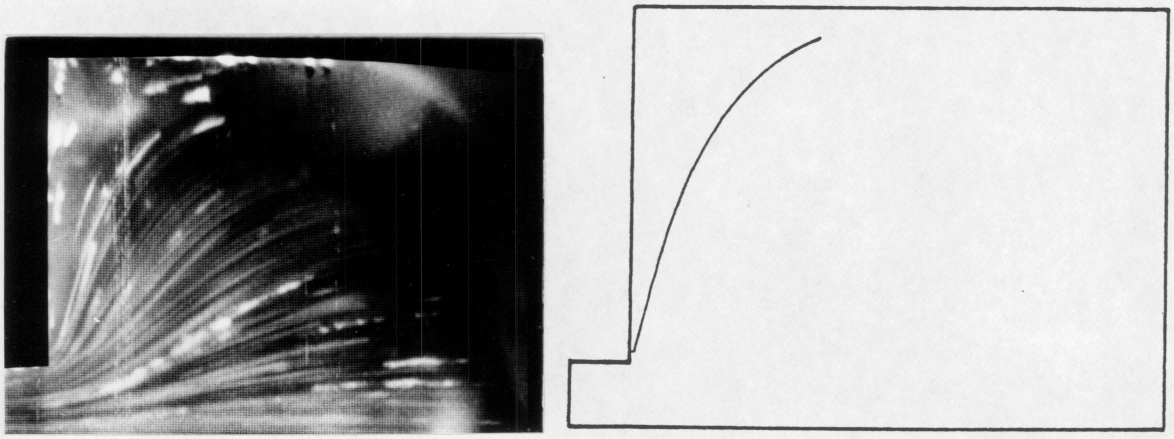

b

Figure 24. Streamline Patterns for Polystyrene and the Blend at 190° C: a) Base resin $\dot{\gamma} = 20\ \text{sec}^{-1}$ b) Blend $\dot{\gamma} = 20\ \text{sec}^{-1}$

downstream wall shear rate of 20 sec^{-1}. Only half of the entry region is shown in these photographs since illumination of the viewing zone was not possible. Symmetry of flow is assumed to apply to this situation. As can be seen there are only slight differences in the flow behavior of the two polymers and these are pointed out in the drawings above the photographs. It had been expected that a significant increase in the detachment length would result from the presence of a high molecular weight component but as shown in the figure there is only a small increase. However, even this small difference in flow behavior can be more readily attributed to the extensional properties of the polymer than to the shear properties.

5.2.2 Rheological Characterization

Rheological characterization of the polystyrene blend was similar to that presented for LDPE and the polystyrene base resin in the previous section. Figure 25 on page 116 and Figure 26 on page 117 provide the shear properties of of the blend in comparison with those of the base resin. Viscosity and normal stress are shown in Figure 25 on page 116. From this plot it can be seen that there are negligible differences between the two polymers especially at the shear rate at which the experiments were conducted. Also, the elastic response of the polymers (Figure 26 on page 117) is nearly identical. Based on these findings alone no difference in entry flow behavior would be expected.

Examination of the transient growth of the extensional viscosity does, however, indicate differences in the two polystyrenes. From the plot in Figure 27 on page 118 it can be seen that the magnitude of the extensional viscosity of the blend reaches a value twice as high as that of the base resin. In addition, the nature of the growth behavior of the polymers is also different. Although not clearly apparent in this figure, the difference in transient behavior can be seen in plots of the extensional stress growth shown in Figure 28 on page 119 for the base resin and in Figure 29 on page 120 for the blend. What is seen in comparing these figures is that the base resin more easily attains a steady-state stress than the blend. Even at the higher

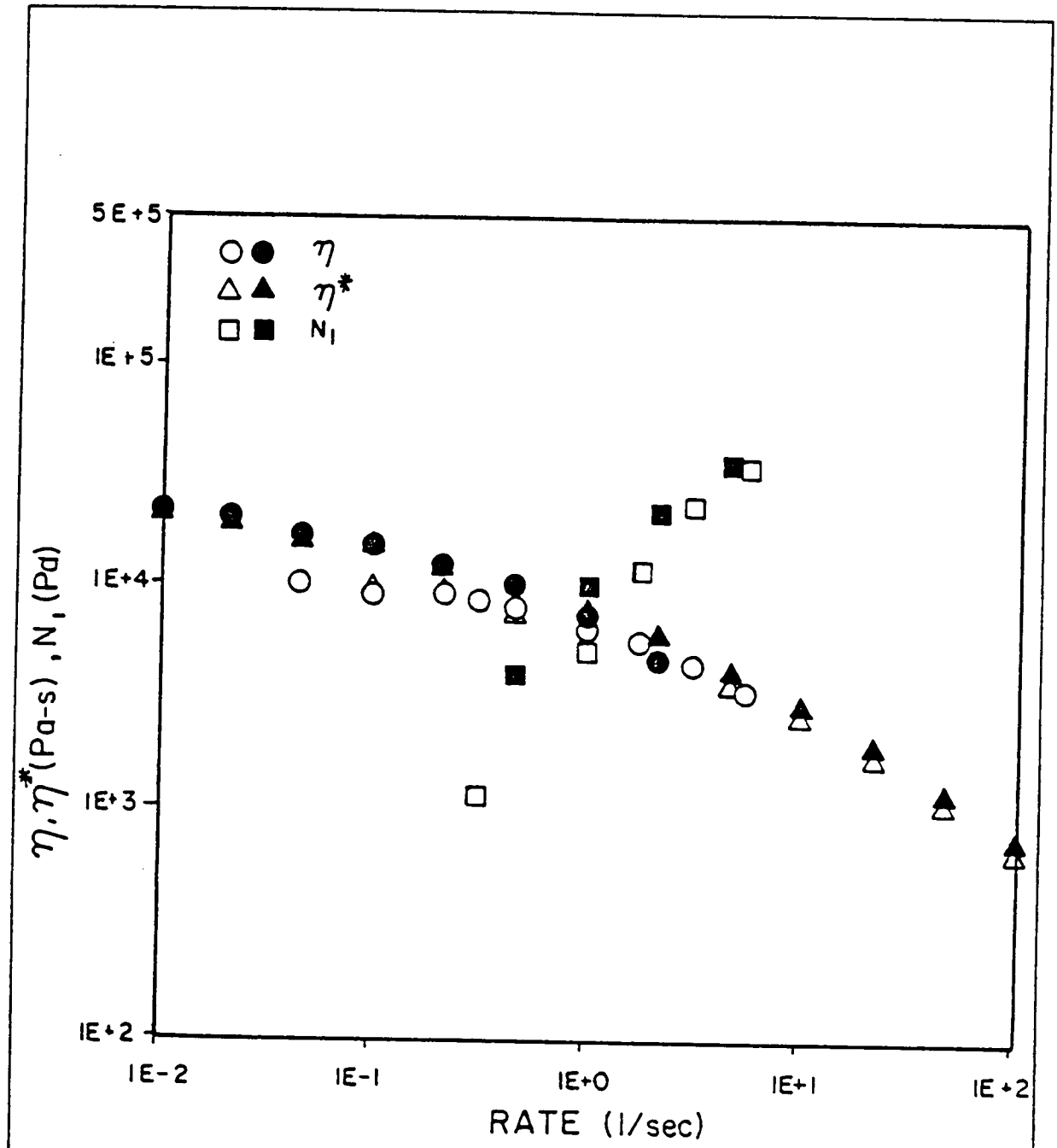

Figure 25. Viscometric Properties of Polystyrene and Blend at 190° C: Closed symbols- Blend

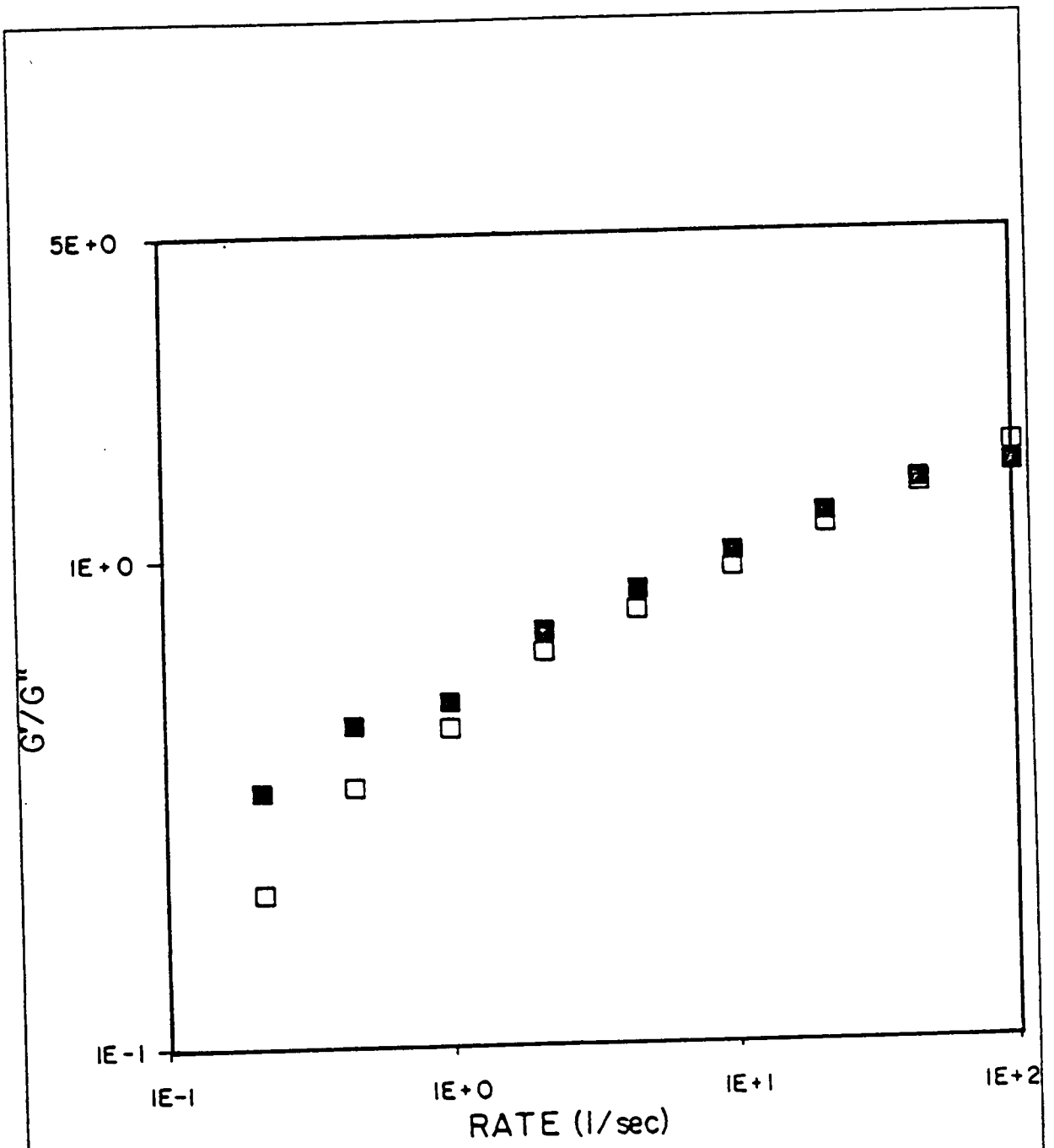

Figure 26. Weissenberg Number of Polystyrene and Blend at 190° C: Closed symbols- Blend

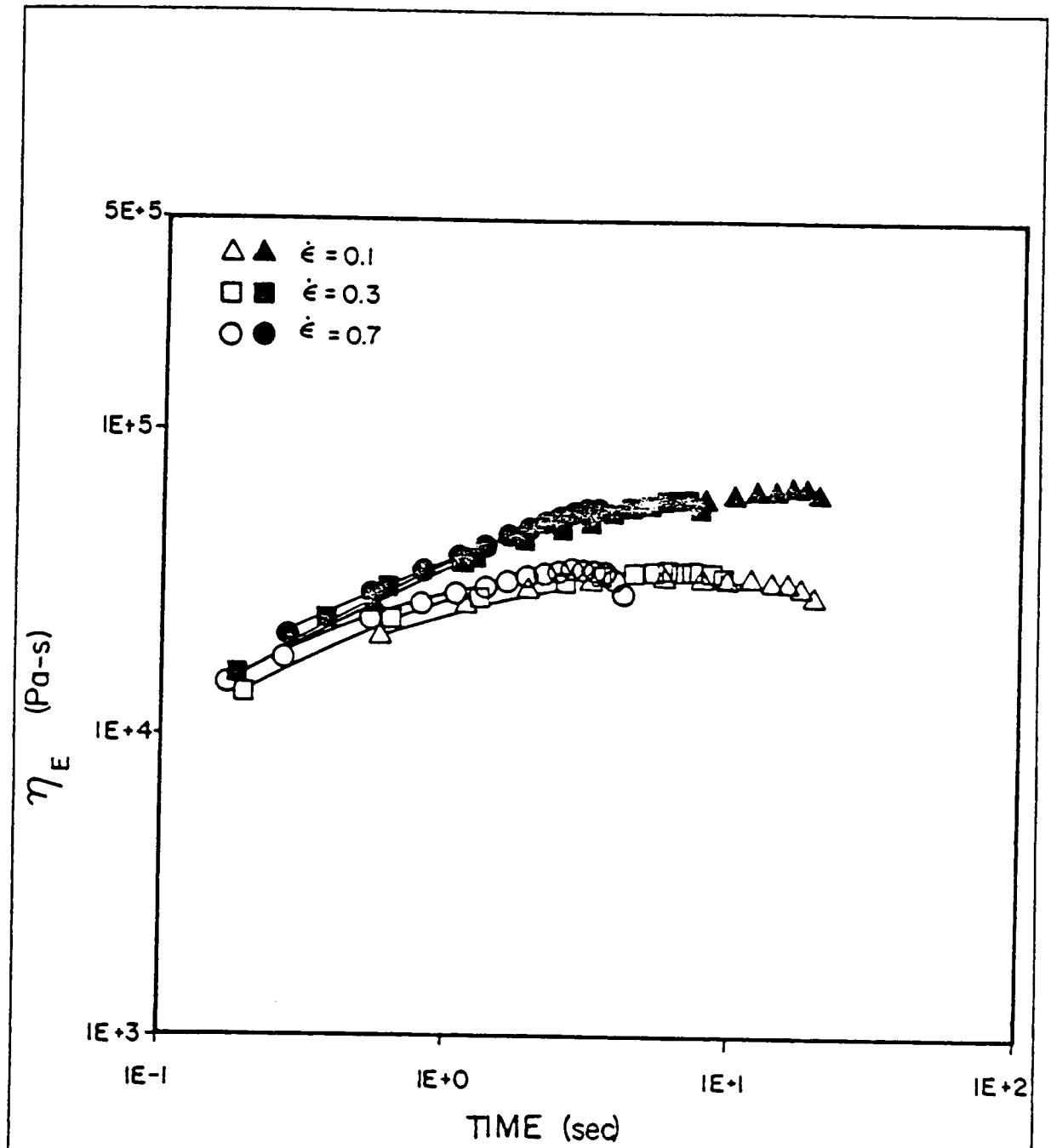

Figure 27. Extensional Viscosity of Polystyrene and Blend at 190° C: Closed symbols- Blend

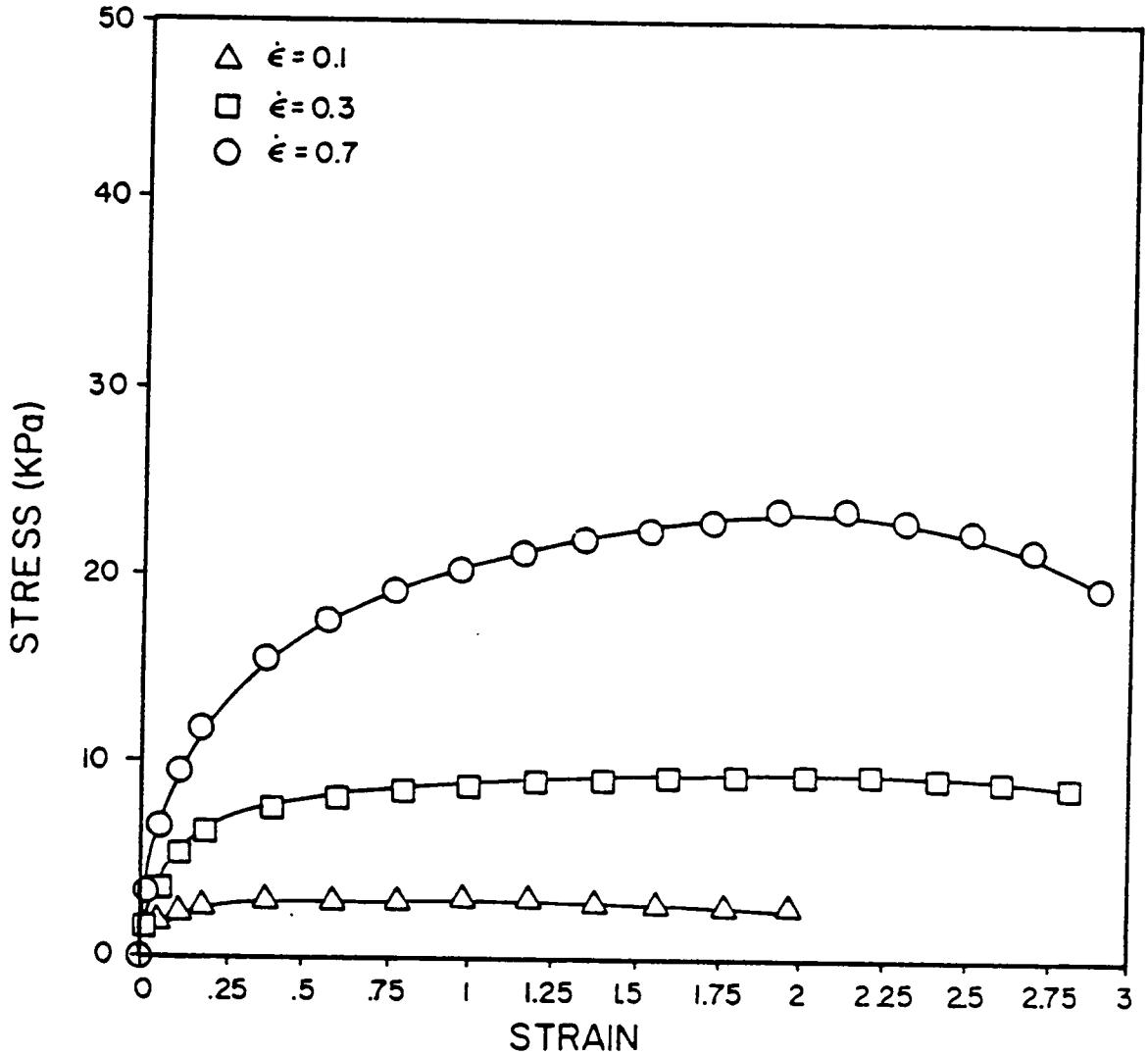

Figure 28. Extensional Stress Growth of Polystyrene at 190° C

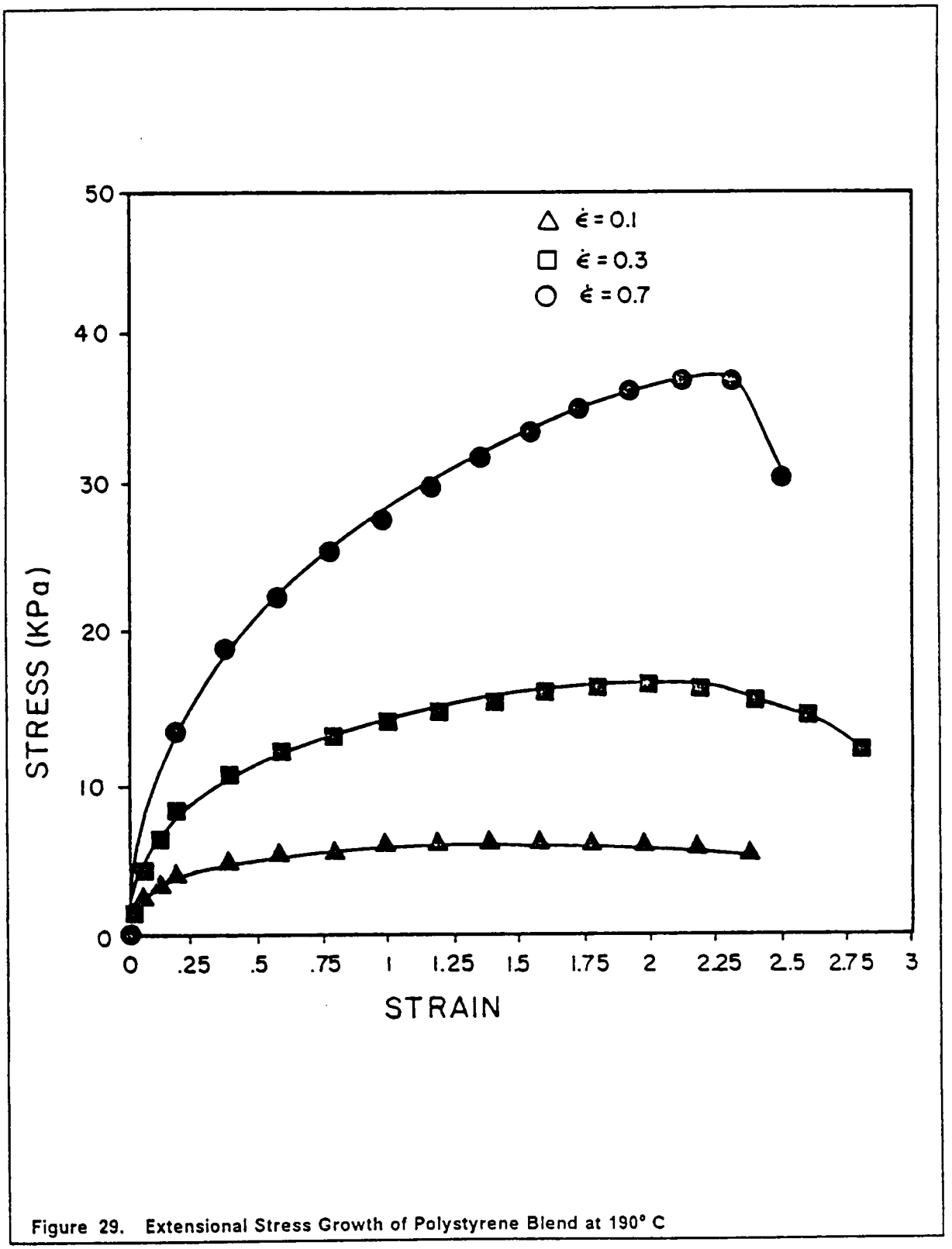

Figure 29. Extensional Stress Growth of Polystyrene Blend at 190° C

strain rates the base resin achieves steady-state but the blend exhibits what appears to be a weak strain hardening effect followed by necking of the sample. This type of stress growth behavior can be related to the presence of the high molecular component. As was reported by Münstedt, and as will be seen again in a later section examining HDPE's of different M_w, the high molecular weigh chains in the polymer act as a far reaching network, the effects of which are exhibited at higher strains. Although strain hardening and entry flow behavior similar to LDPE did not result, the findings of this work can still be used in support of the theory of vortex growth as discussed next.

5.2.3 Interpretation of Flow Behavior

It was postulated in section 5.1 that vortex growth can be attributed to the response of a polymer to extensional strain. In this section the same results were found. Although the differences in flow behavior and extensional properties are not as great between the base resin and the blend as they are between LDPE and polystyrene the increase in detachment length exhibited by the blend can still be attributed to its greater restriction to flow in extension. In LDPE the restriction to flow was caused by the presence of long chain branching which resulted in several possible points of restriction on each molecule. In the polystyrene blend the restriction to flow was caused by the high molecular weight chains which were added to the base resin. The smaller chains of the base resin by themselves do not pose much of a restriction to extension as evidenced by the extensional properties of the polymer. However, the presence of the high molecular weight chains in the blend provide greater restriction to extension since these longer chains can be entangled with other chains at more points along their length than the shorter chains of the base resin. The result is higher stresses in extension and the inability to reach a steady-state stress at higher strain rates. It is believed that the latter effect is due to the fact that at high strain rates the time available for the chain to disentangle itself is reduced and therefore, there are more entanglement points acting to in-

crease the stress and, in this study, this results in sample failure before steady-state stress can be reached. In shorter chains there are less points of restriction so that at comparable strain rates these chains have time to reduce the entanglement density and reach a steady-state stress.

The result of the restriction to flow caused by the long chains is negligible in shear flow but predominant in extensional flow. Shear properties such as viscosity and normal stress involve small strains in measurement, and therefore, the presence of the high molecular weight chains is only observed in the shift in η_0 corresponding to the shift in M_w. At the shear rates of concern in the flow experiments the differences in the shear properties and the elasticity (We) of the two polymers is negligible. Extensional properties involve large strains in measurement and therefore the difference between the two polystyrenes becomes apparent in these properties. In addition, flow through the contraction in the die involves extensional strains, and therefore, the differences in flow behavior can be attributed to their extensional properties.

5.3 Molecular Weight Effects on Entry Flow Behavior: HDPE

In the previous section the effect of relatively small changes in molecular weight on entry flow behavior was examined. In this section molecular weight effects will be examined again but for much larger differences in M_w. Again, the purpose will be to provide support for the belief that entry flow behavior is most closely related to the extensional properties of the fluid. In addition, reinforcement will be given to the statement that We can only be used to correlate entry flow behavior for polymers of a given type and not as a universal correlation for the entry flow behavior of all types of polymers.

In this work three HDPE's of different molecular weight were examined. M_w and polydispersity information is given in Table 5 on page 52. As can be seen M_w varies by over a factor of four for the three polymers and in addition polydispersity increases with increasing M_w indicating broader distributions for the higher molecular weight polymers. This means that with HXM-50100 the entry flow behavior will be affected not only by its high M_w but also by a high molecular weight tail in its distribution which indicates the presence of small amounts of very high molecular weight chains.

5.3.1 Streamline Patterns

The effect of molecular weight can be seen in the flow patterns of the three HDPE's (Figure 30 on page 124). All patterns were obtained at 190° C and at a shear rate of 20 sec^{-1} except for HXM-50100 for which the shear rate was 3.3 sec^{-1}. Due to the high viscosity of this material it was not possible to obtain higher flow rates without damage to the die windows. The three patterns show an increase in detachment length with increasing M_w. Although the streaks are faint, the flow behavior of the lowest molecular weight HDPE, EMN TR-885, is seen to be Newtonian-like. This behavior is very similar to what was seen for polystyrene. However, for the next higher M_w HDPE, HHM-5502, it is seen that a larger detachment length is exhibited and a large stagnant vortex cell is present. The highest molecular weight HDPE, HXM-50100, exhibits an even larger detachment length even though the streak pattern was obtained at a much lower rate than the other materials.

Although the two higher molecular weight materials exhibit large vortex cells, there is no apparent recirculation within them. There are two reasons for this. First, the flow patterns only represent about 30 seconds of flow time. Since these materials were run in slit die 1 the amount of material that could be fed to the die from the capillary rheometer was limited. Therefore, only short runs could be made and thereby time lapse photographs of the flow had to be relatively short in duration. There was enough time to establish the vortex cell but not

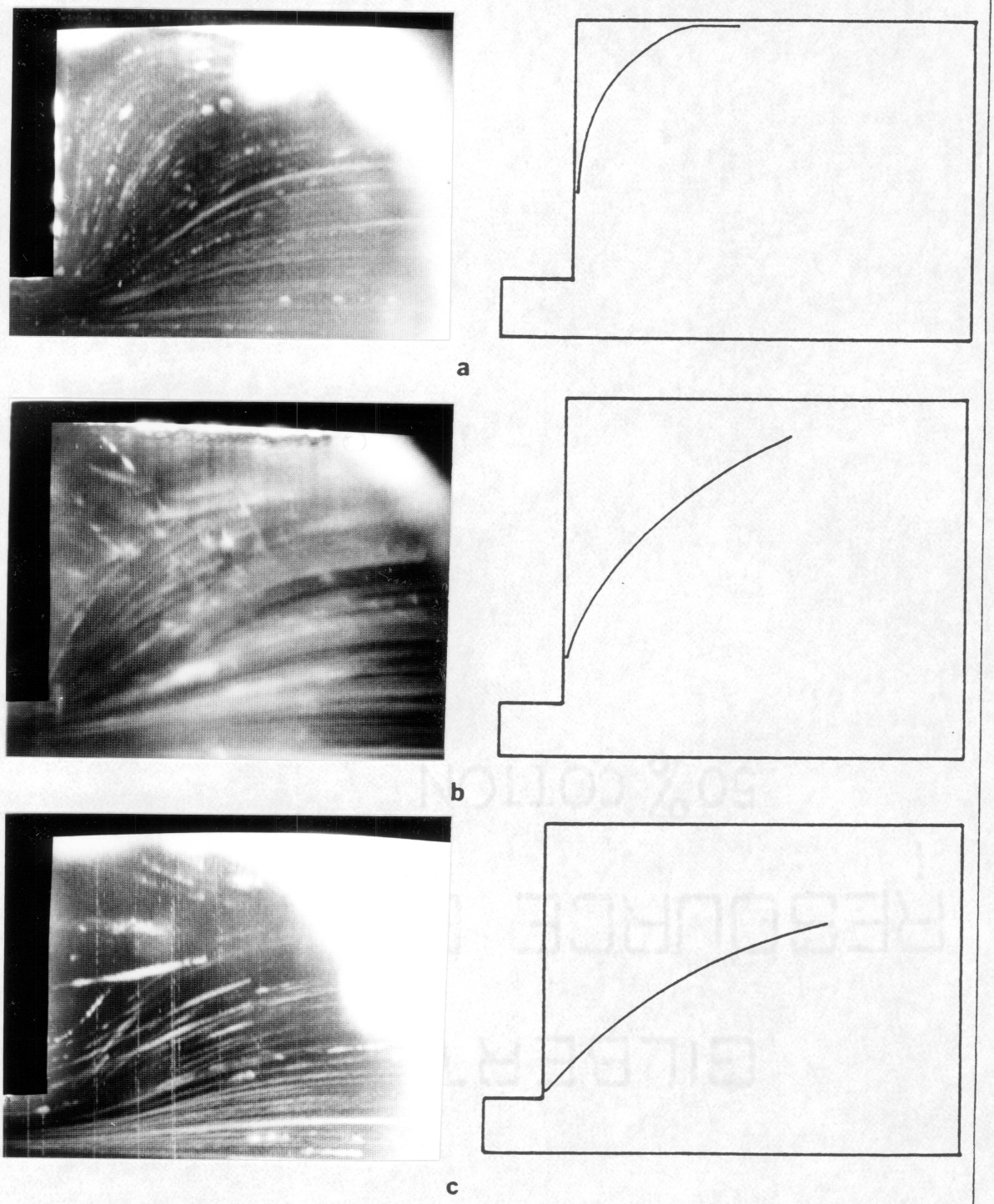

Figure 30. Streamline Patterns of Different Mw HDPE's at 190° C: a) EMN TR-885 $\dot{\gamma} = 20\ sec^{-1}$ b) HHM-5502 $\dot{\gamma} = 20\ sec^{-1}$ c) HXM-50100 $\dot{\gamma} = 3.3\ sec^{-1}$

enough time to set up recirculation within it. The second reason for the lack of recirculation is the high viscosity of the polymers. Even if there was enough time available to observe the flow, detection of recirculation would most likely be difficult. As with polystyrene at 165° C the rate of recirculation would be very low for these polymers at the conditions of the test. However, in this work the lack or presence of recirculation is not as important as the change in detachment length with M_w.

5.3.2 Correlation of Flow Behavior to Rheological Properties

As with the flow behavior of polystyrene at 165° C and 190° C, the increase in detachment length with increasing M_w of the HDPE's can be related to the elasticity of the polymer. This type of relation holds for a given type of polymer as shown by the plot of We of the HDPE's in Figure 31 on page 126. In this plot it is seen that elasticity increases with increasing M_w. It is no surprise that the detachment length exhibited in entry flow would increase with the elasticity of the polymer. However, as was seen when comparing LDPE and polystyrene, this relationship does not hold when comparing polymers of different types. This becomes clear when the data for LDPE and polystyrene at 190° C is added to Figure 31. The result, shown in Figure 32, is that there is no relation between elasticity and detachment length. From this figure it is seen that We for EMN TR-885 is much lower than that for polystyrene although their entry flow behavior is nearly identical. Also, We for the high M_w HDPE's is on the same order as that of polystyrene although the HDPE's exhibit significantly larger detachment lengths than the polystyrene. Therefore, from this figure it is again seen that elasticity cannot be used to correlate entry flow behavior.

Prediction of vortex growth is best derived from the extensional properties of the fluid. In Figure 33 on page 128 the extensional stress growth behavior of the different molecular weight HDPE's is presented along with that of LDPE and polystyrene at 190° C. From this figure it is seen that detachment length is more a function of extensional properties than it is of

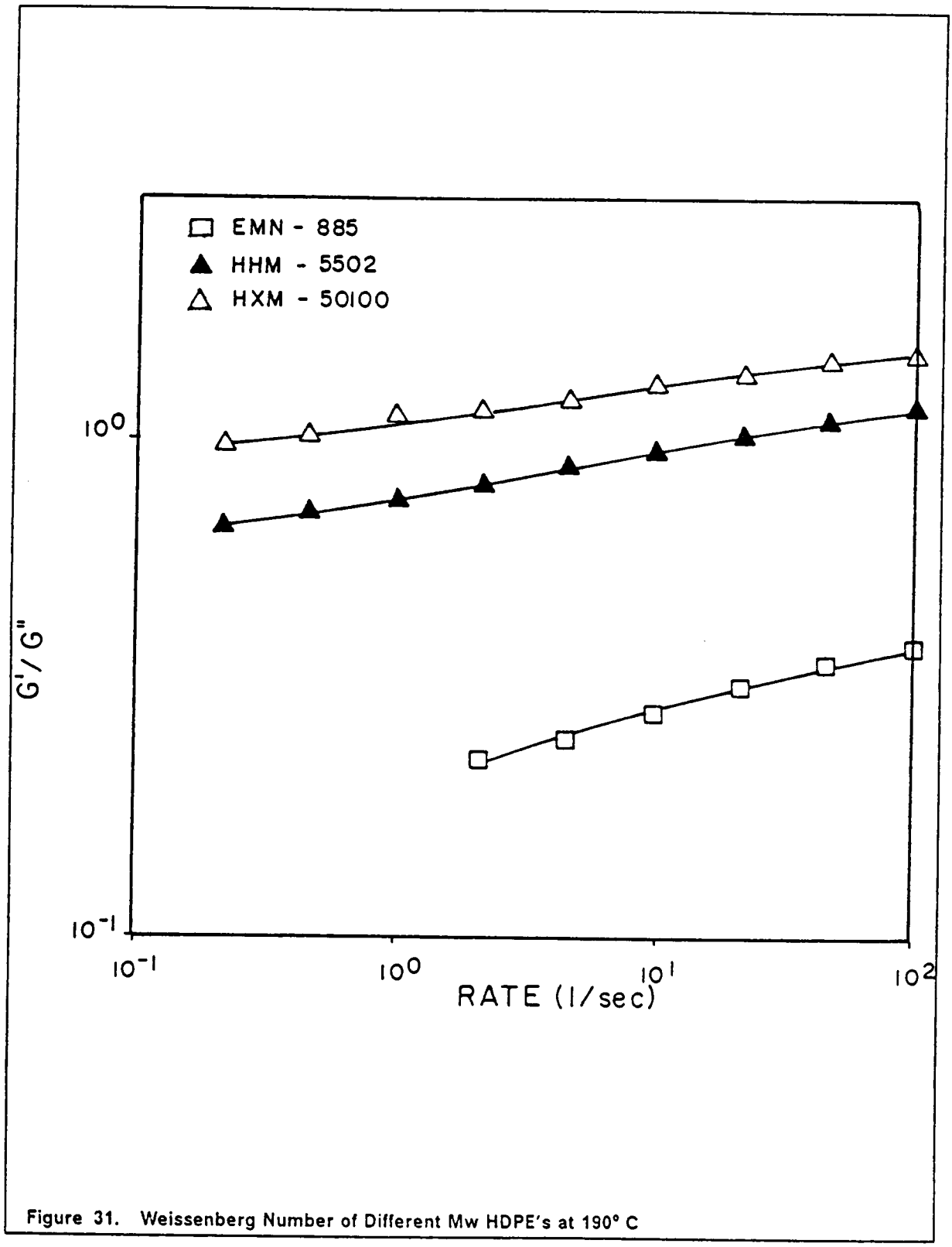

Figure 31. Weissenberg Number of Different Mw HDPE's at 190° C

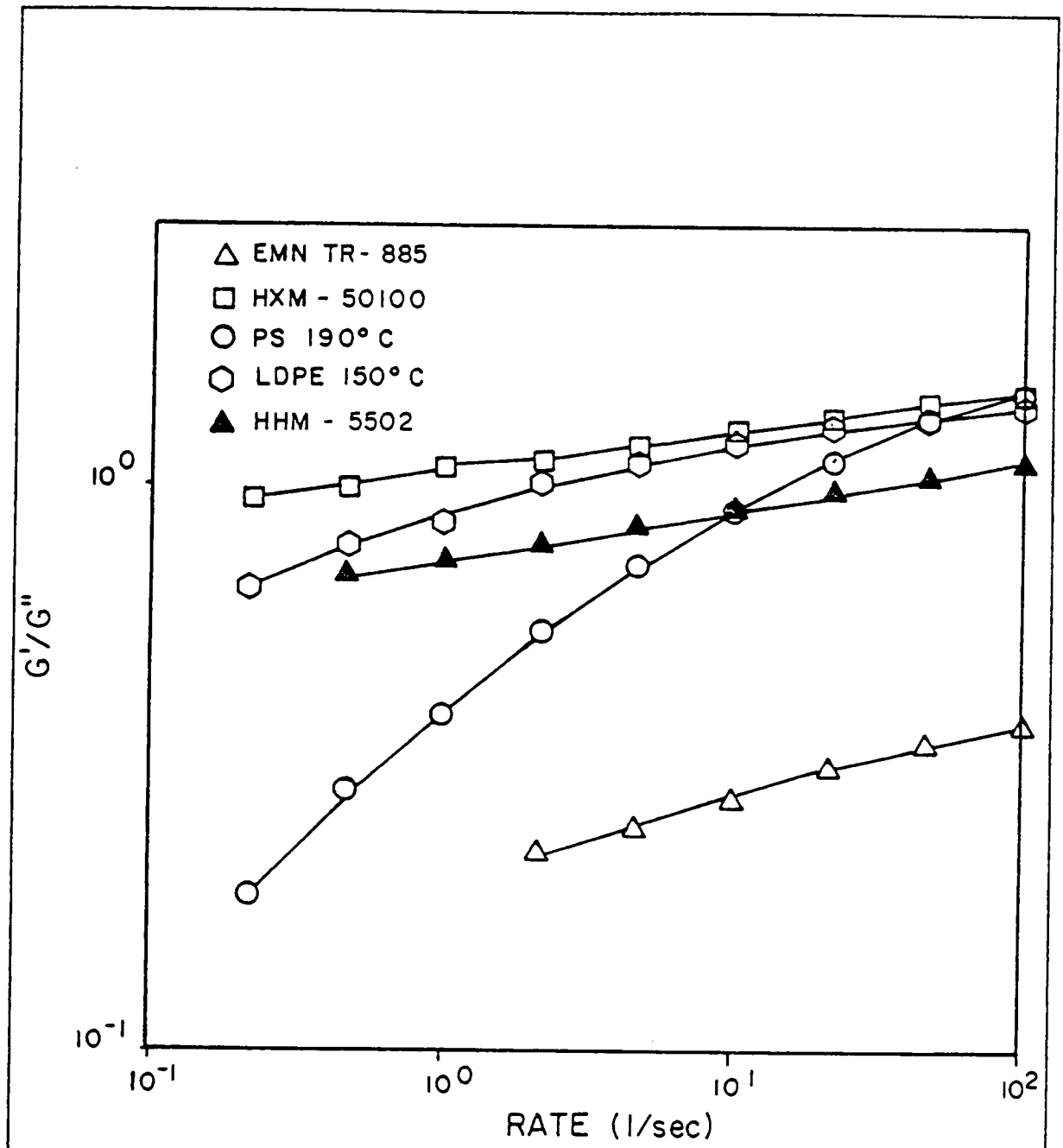

Figure 32. Weissenberg Number of Different Mw HDPE's, LDPE, and Polystyrene

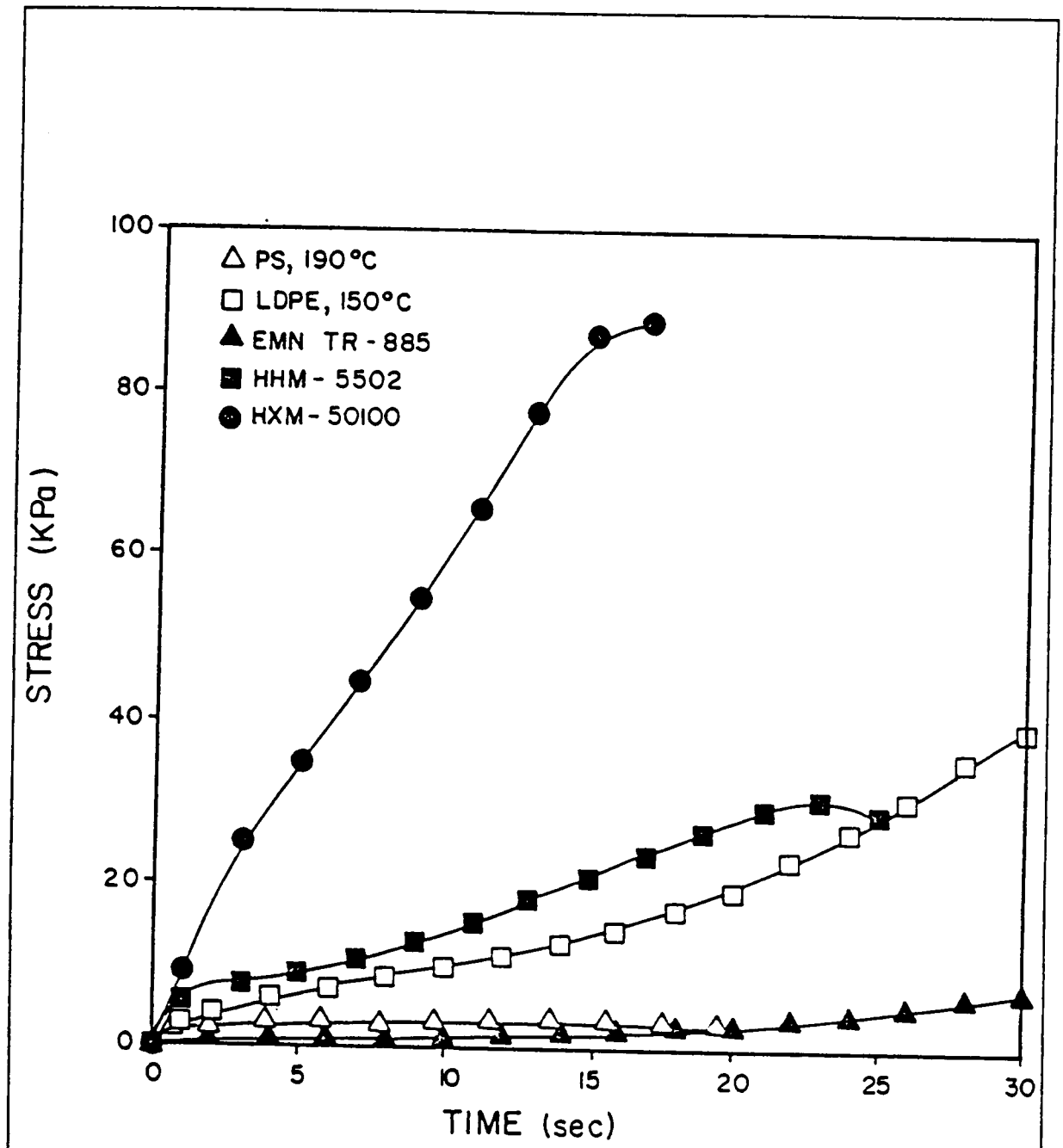

Figure 33. Extensional Stress Growth of Different Mw HDPE's, LDPE and Polystyrene

elasticity. In this figure the extensional stress growth was obtained at a strain rate of 0.1 sec^{-1} and at the temperature at which the flow patterns were obtained for each polymer. It is seen that for EMN TR-885 and polystyrene, which exhibited the same entry flow behavior, the magnitude of the stress is very low. In addition, HXM-50100, HHM-5502, and LDPE have significantly higher stresses and were shown to exhibit greater detachment lengths than the other two polymers. The effect of the high M_w chains in HXM-50100 is exhibited in this polymer's rapid strain hardening followed by sample necking and failure at higher strains. From this plot it is seen that there is a much better ordering of flow behavior with extensional properties than with elasticity.

In this section and in section 5.2 the purpose has been to provide support for the statement provided in section 5.1 that vortex growth in entry flow is related to the extensional properties of the fluid. Based on this statement it was assumed that changes in a polymer which would affect the polymer's extensional properties should be reflected in its entry flow behavior. In section 5.2 polystyrene was changed by adding a high molecular weight fraction to it. The result was a negligible change in shear properties but an increase in the extensional viscosity and an increase in the detachment length exhibited in entry flow. In this section HDPE's of different M_w were examined. The result was an increase in detachment length and extensional stress with increasing M_w. In both sections the increase in detachment length can be attributed to the restriction to flow caused by polymer chains of higher molecular weight. This restriction is not detected in low strain shear properties but in high strain extensional properties. These results from both sections have successfully provided support to the statements presented in section 5.1. Additional support will be provided in the next section on the basis of stresses measured within the entry flow die.

5.4 *Birefringence Measurements in the Entry Region*

Birefringence measurements were made on LDPE and polystyrene. Measurements were made over the same range of flow rates at which flow patterns were obtained. Although it was not possible to quantify the stress distribution throughout the entry region it was possible to make qualitative statements in regards to these patterns. However, it was possible to obtain quantitative measurements of the centerline extensional stresses in the entry region and this data will be used to support the views presented on the cause of vortex growth. Questions will arise in this analysis which will require the modification of the previous hypothesis of vortex growth.

5.4.1 Qualitative Observations Regarding Stress Patterns

A number of statements can be made about the different stress patterns of LDPE and polystyrene and how these patterns evolve with increasing flow rate. Isochromatic fringe patterns are presented for LDPE and polystyrene over a range of downstream shear rates in Figure 34 on page 131 and Figure 35 on page 132, respectively. The photographs are of the light field patterns and as such half order fringes are presented (i.e. N = 1/2, 3/2, 5/2,...).

One observation that can be made in regards to these photographs is how the fringe patterns change with increasing shear rate. For LDPE (Figure 34) it is seen that as the shear rate increases the fringes grow out into the upstream channel and at 15 sec^{-1} a triangular fringe begins to develop in the salient corner. At this rate only two sides of the triangle have appeared but on increasing the rate to 40 sec^{-1} it is seen that a closed triangular fringe is present. This fringe represents very low stress (N = 1/2), but it does roughly outline the recirculation cell observed in the streak photographs. This fringe pattern can be contrasted to that of polystyrene in Figure 35. It can be seen in these pictures that no corner fringe develops.

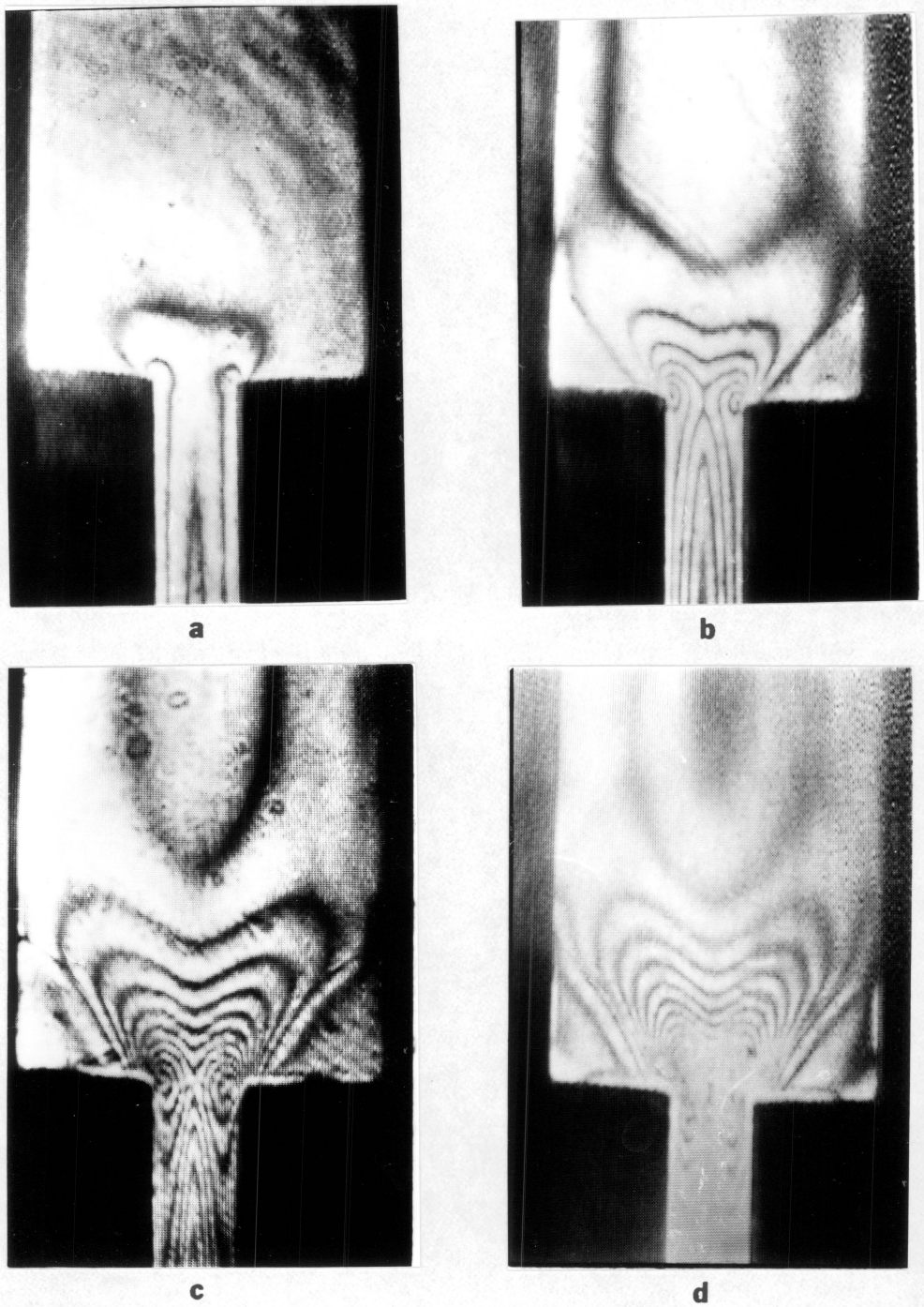

Figure 34. **Light Field Isochromatic Fringe Patterns of LDPE, 4:1 Contraction:** a) $\dot{\gamma} = 1\ \text{sec}^{-1}$ b) $\dot{\gamma} = 5\ \text{sec}^{-1}$ c) $\dot{\gamma} = 15\ \text{sec}^{-1}$ d) $\dot{\gamma} = 40\ \text{sec}^{-1}$

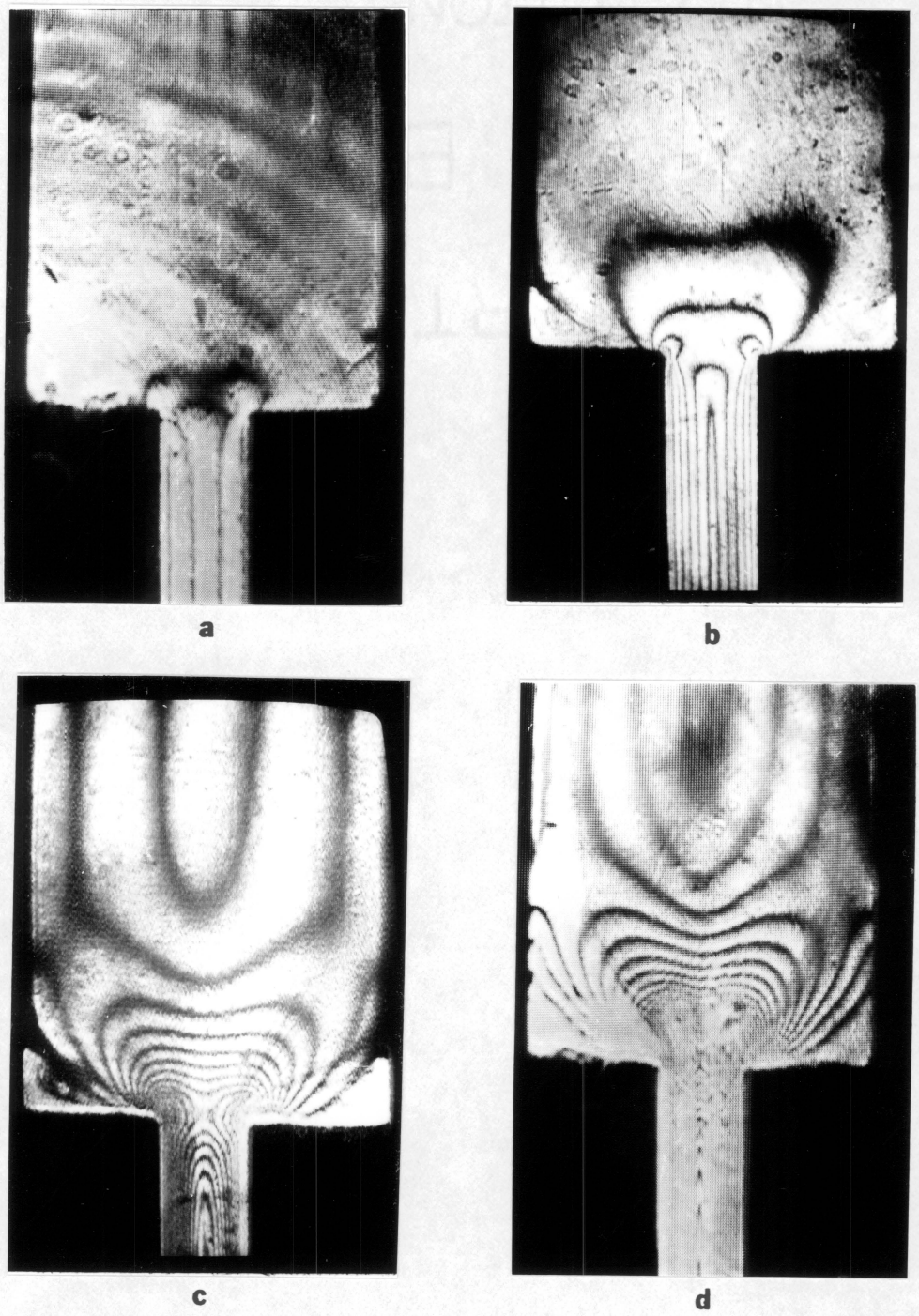

Figure 35. Light Field Isochromatic Fringe Patterns of Polystyrene at 190° C, 4:1 Contraction: a) $\dot{\gamma} = 1\ \text{sec}^{-1}$ b) $\dot{\gamma} = 5\ \text{sec}^{-1}$ c) $\dot{\gamma} = 20\ \text{sec}^{-1}$ d) $\dot{\gamma} = 40\ \text{sec}^{-1}$

At higher shear rates the developing fringes just lay into the corners giving no indication of recirculation. This should be expected since the flow patterns showed that recirculation within the corners was very weak, and therefore the stress in this region should be very low.

These observations regarding corner fringe development provide no new information regarding vortex growth. However, it is apparent that birefringence patterns can only be used as a rough indication of the presence of vortices. Some studies have used only birefringence measurements to indicate the presence of vortex motion. However, by comparing the fringe patterns of LDPE and polystyrene at 5 sec^{-1} there is no indication that vortices are present in either polymer, but examination of the streak patterns clearly indicates vortex growth is occurring in LDPE. The only means by which such low stress recirculation might be detected in birefringence patterns would be by incorporating a compensator into the optical system which could produce very low fractional order fringes.

Another observation can be derived from the fringe patterns in regards to the state of stress at the re-entrant corner. For both LDPE and polystyrene this corner represents the point of highest stress in the entry region and is where each higher order fringe originates. For LDPE at 5 and 15 sec^{-1} it can be seen that multiple higher order fringes occur at this corner than appear in the downstream channel implying that there is significant stress overshoot at the corner. These fringes appear as elliptical bands around the corner. At 5 sec^{-1} there are two such fringes and at 15 sec^{-1} there are four. This type of pattern indicates that steep stress gradients occur on either side of the corner as stress builds up rapidly on approach to the corner and then relaxes to the steady-state downstream stress going away from the corner. The situation, however, is different for polystyrene. There is still the rapid rise in stress on approach to the corner but there is much less overshoot. The higher level of stress overshoot in LDPE may contribute to the process of vortex growth, but it may also contribute to the failure of the numerical method at high shear rates. The numerical method may not be able to approximate the steep positive stress gradient leading up to the corner followed by the steep negative stress gradient going downstream of the corner. This situation will be addressed again later in the chapter.

A final qualitative observation can be obtained from the fringe patterns in regards to the attainment of steady-state flow in the downstream channel. As discussed in the previous paragraph stress overshoot occurs at the re-entrant corner for both polymers. However, the relaxation in stress beyond this point to the condition of steady-state flow takes significantly longer for LDPE than for polystyrene. Steady-state flow occurs at the point where all the fringes become parallel to the slit wall. These regions can be observed both prior to and after the contraction. However, by comparing the patterns of LDPE and polystyrene at 1 and 5 sec^{-1} it can be seen that the effect of the contraction is felt much further downstream in LDPE than in polystyrene. Steady-state flow occurs fairly quickly after the contraction in polystyrene but not in LDPE. Whether this downstream phenomenon affects vortex growth in the upstream channel or is just a reflection of the rheological nature of the polymers is not known. In the next section insight into vortex growth will be provided by a quantitative approach to birefringence data.

5.4.2 Extensional Stress Measurements in the Entry Region

As mentioned in Chapter 3 it was not possible to obtain the isoclinic patterns except at the lowest flow rates. Without the value of χ (isoclinic angle) it is not possible to obtain values of τ_{12} and $\tau_{11} - \tau_{22}$ from the fringe patterns. However, by knowing that the shear stress is zero at the centerline equations 3.3 and 3.4 can be combined to give,

$$\tau_{11} - \tau_{22} = \frac{N\lambda}{LC} \tag{3.5}$$

With this equation it was possible to determine the centerline extensional stress from knowledge of the fringe order N, the wavelength of the laser light source λ, the width of the slit L, and the stress optic coefficient of the polymer C. The value of the extensional stress obtained from this equation was then put in a dimensionless form by dividing by the downstream wall

shear stress. These values were then plotted versus x/H where x is the distance from the contraction and H is the height of the downstream channel.

Comparison of the extensional stress ratio for LDPE and polystyrene is presented in Figure 36 for the 4:1 geometry and in Figure 37 on page 136 for the 8:1 geometry. It is obvious that in both cases the extensional stress in LDPE is over twice as high as that in polystyrene. Also seen is the slow relaxation of the stress in LDPE downstream of the contraction. The effect of the contraction is felt much less by polystyrene for which the stress rises and falls more quickly on either side of the contraction. Finally, it should be noted that an increase in shear rate does not have a great effect on the ratio of the extensional stress to shear stress in the higher range of shear rates. For LDPE there is a large increase in going from 1 to 5 sec^{-1} (values for $\dot{\gamma}=1$ sec^{-1} are shown in Figure 38 on page 137) but there is a much smaller change in going from 5 to 20 sec^{-1}. The same type of behavior is observed for polystyrene.

In addition to comparison of the two polymers, comparison can be made between the two flow geometries. Extensional stress ratios are presented in Figures 27-29 for LDPE in the 4:1 and 8:1 geometries at shear rates of 1, 5, and 10 sec^{-1}, respectively. From these plots it is seen that the contraction ratio has a significant effect on the level of stress in the polymer. This is true even at the lowest flow rates. This behavior can be contrasted to that of polystyrene for which there is only a small effect on stress due to contraction ratio (Figure 41 on page 141 and Figure 42). Also, for both polymers there is a shift in the maximum in stress towards a position further upstream for the 8:1 contraction.

5.4.3 Relation Between Vortex Growth and Extensional Stresses in the Entry Region

In section 5.1 vortex growth was attributed to the extensional properties of the fluid. This statement was based on comparison of flow patterns and the shear and extensional

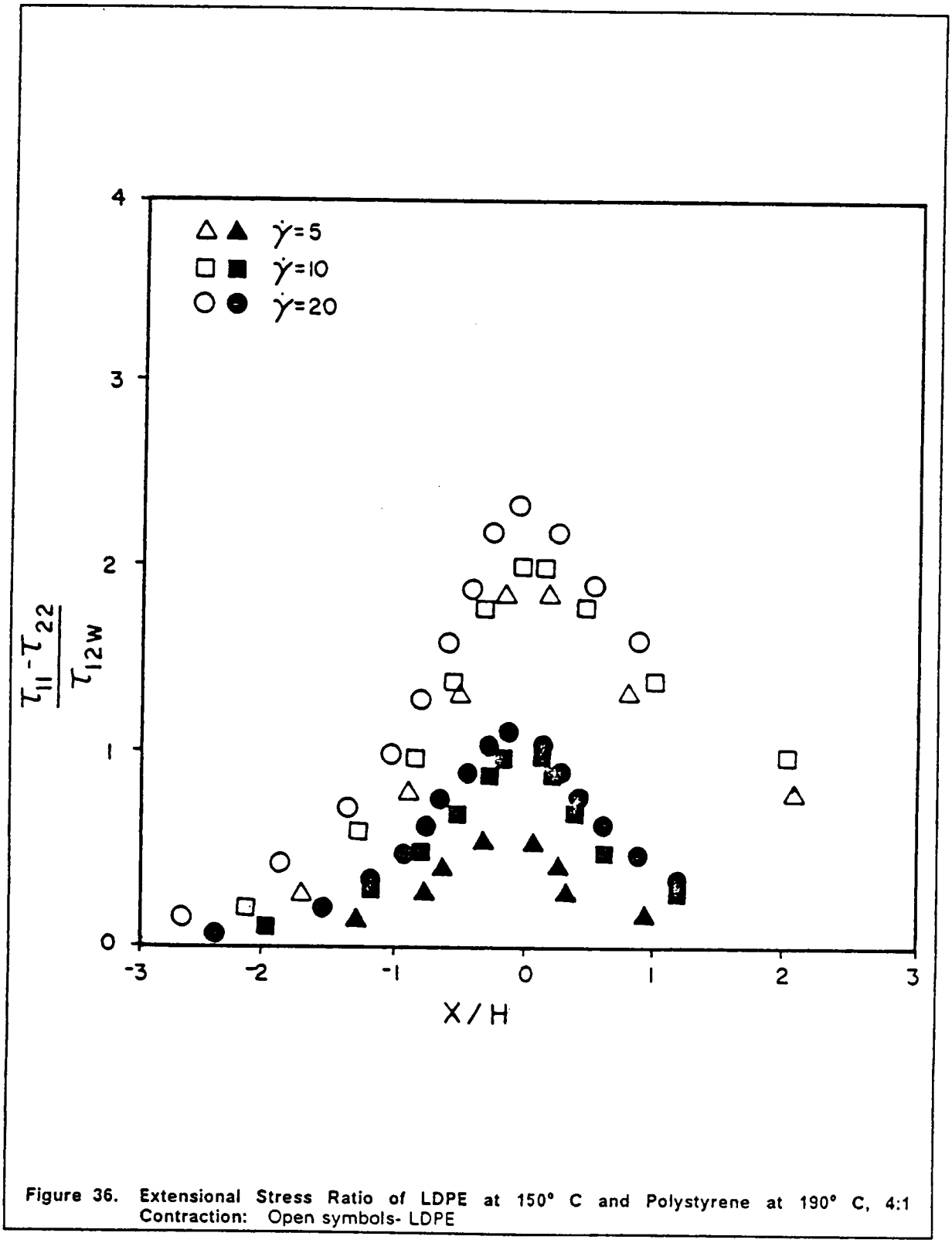

Figure 36. Extensional Stress Ratio of LDPE at 150° C and Polystyrene at 190° C, 4:1 Contraction: Open symbols- LDPE

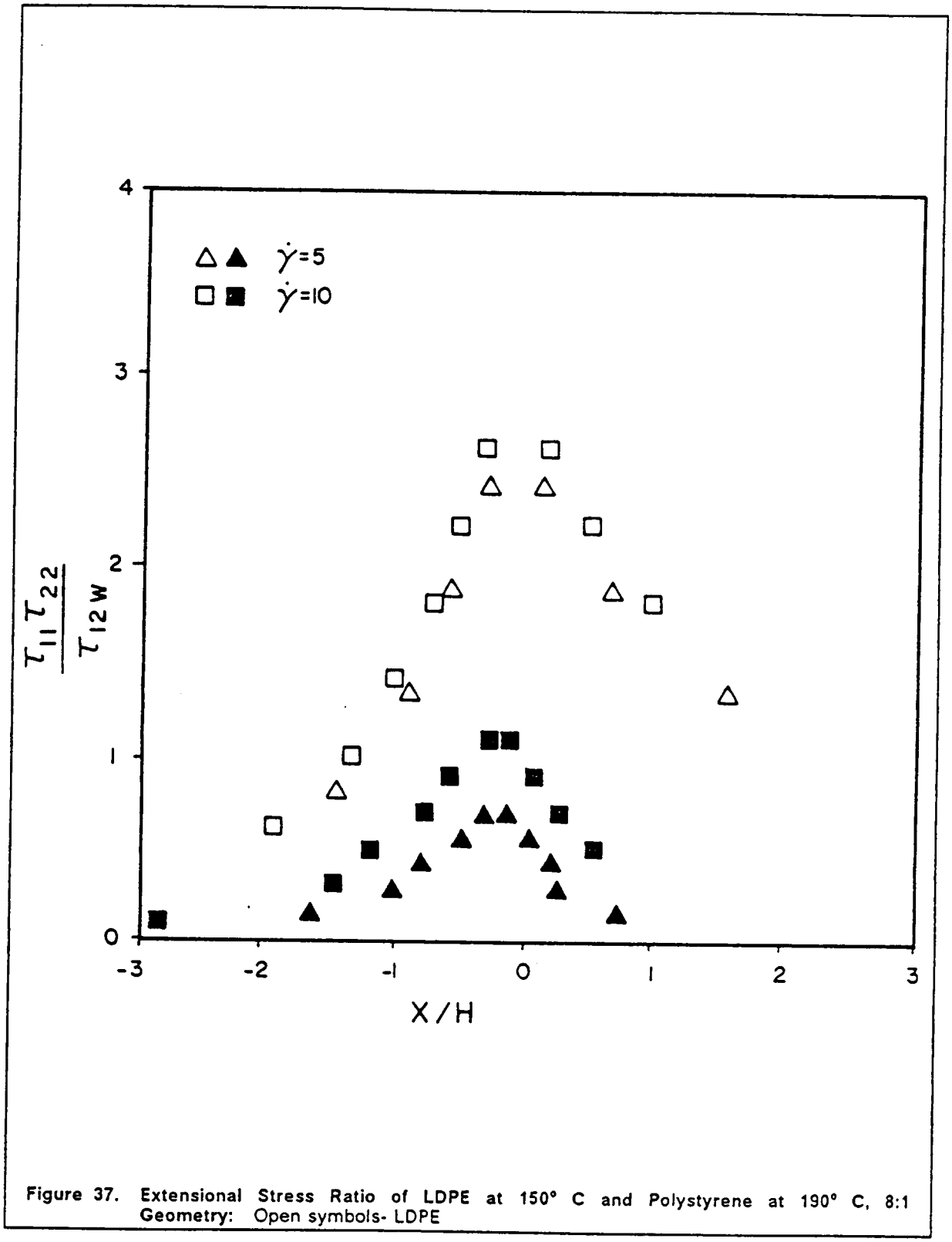

Figure 37. Extensional Stress Ratio of LDPE at 150° C and Polystyrene at 190° C, 8:1 Geometry: Open symbols- LDPE

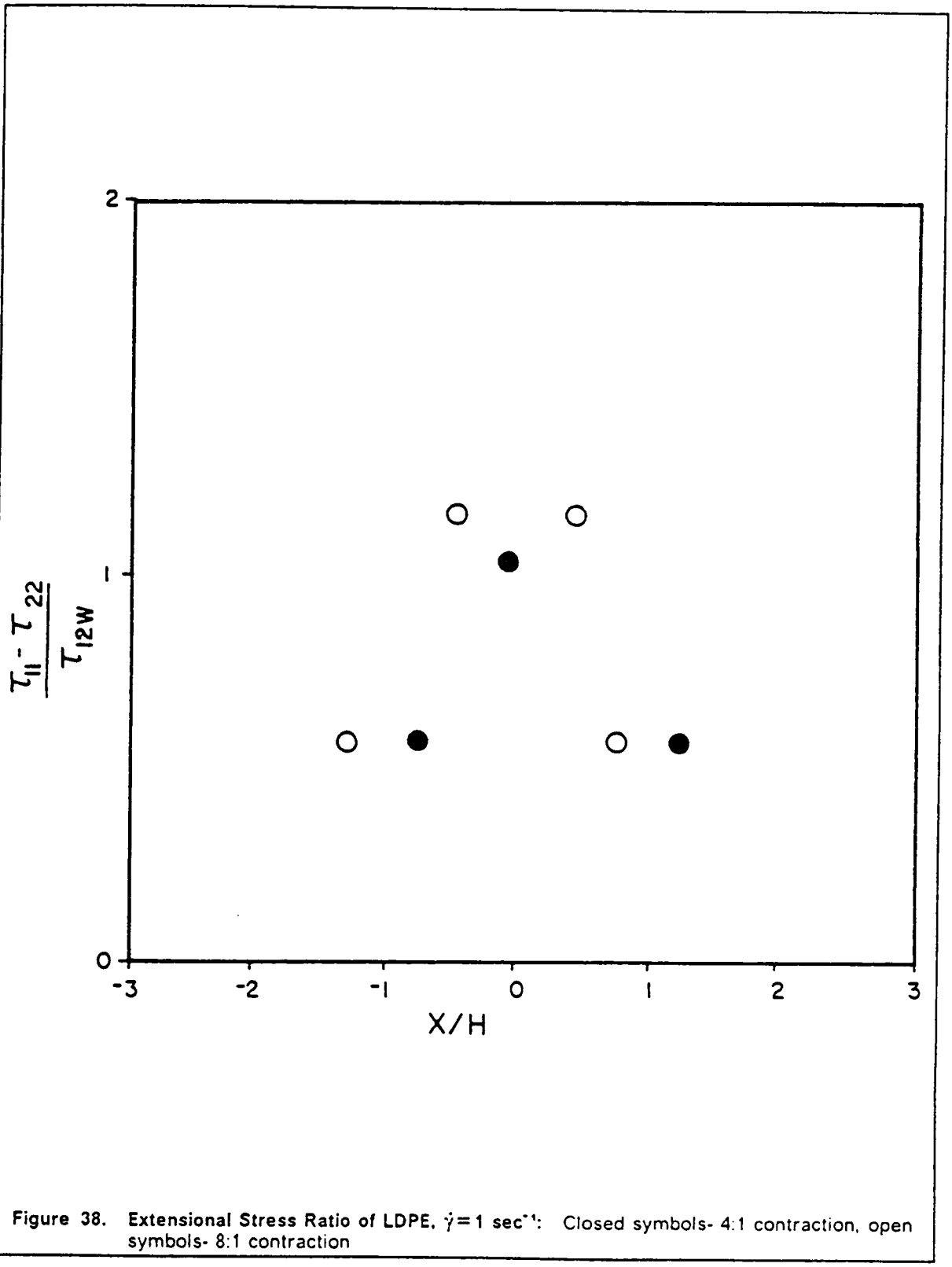

Figure 38. **Extensional Stress Ratio of LDPE, $\dot{\gamma} = 1$ sec^{-1}:** Closed symbols- 4:1 contraction, open symbols- 8:1 contraction

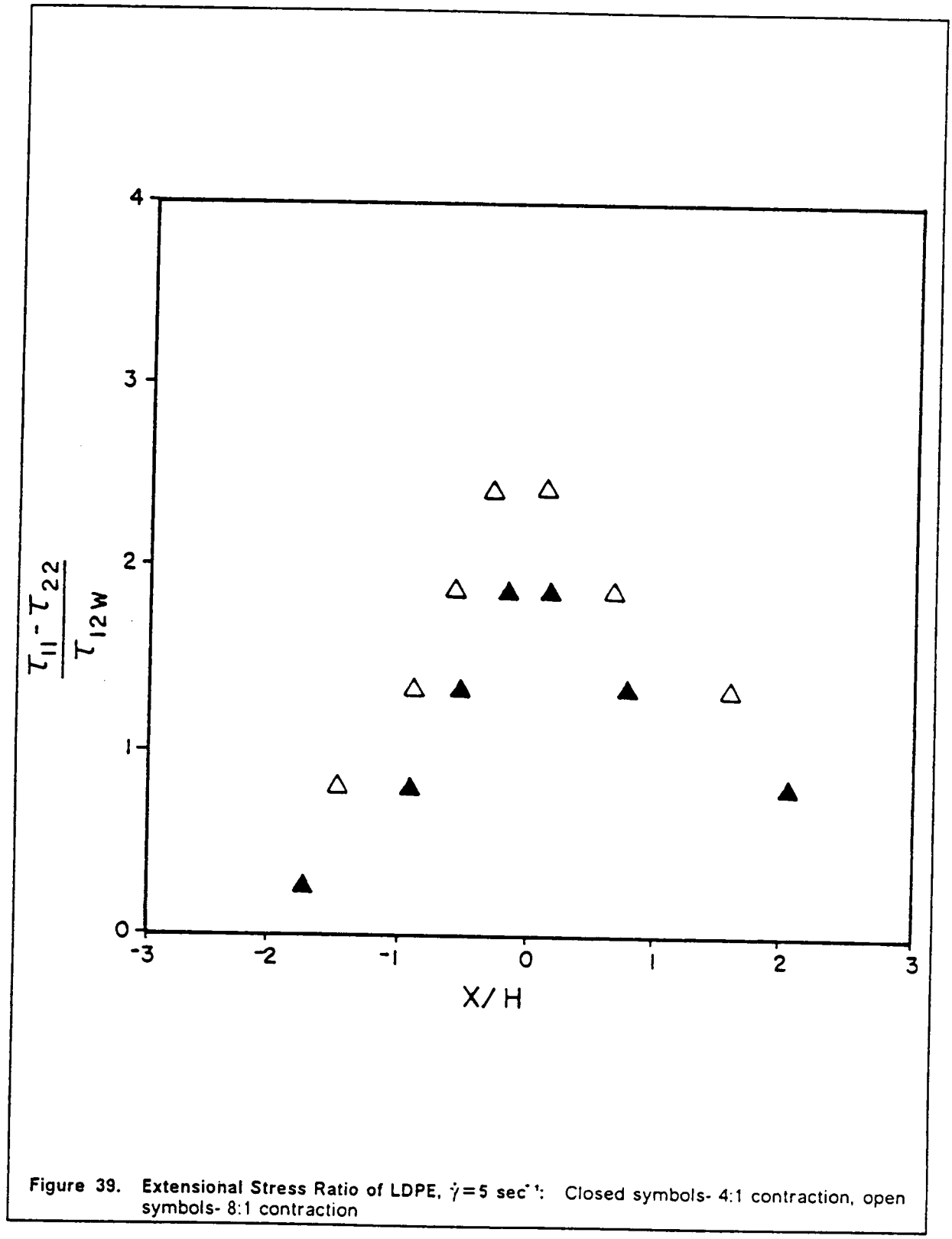

Figure 39. **Extensional Stress Ratio of LDPE, $\dot{\gamma}=5\ sec^{-1}$:** Closed symbols- 4:1 contraction, open symbols- 8:1 contraction

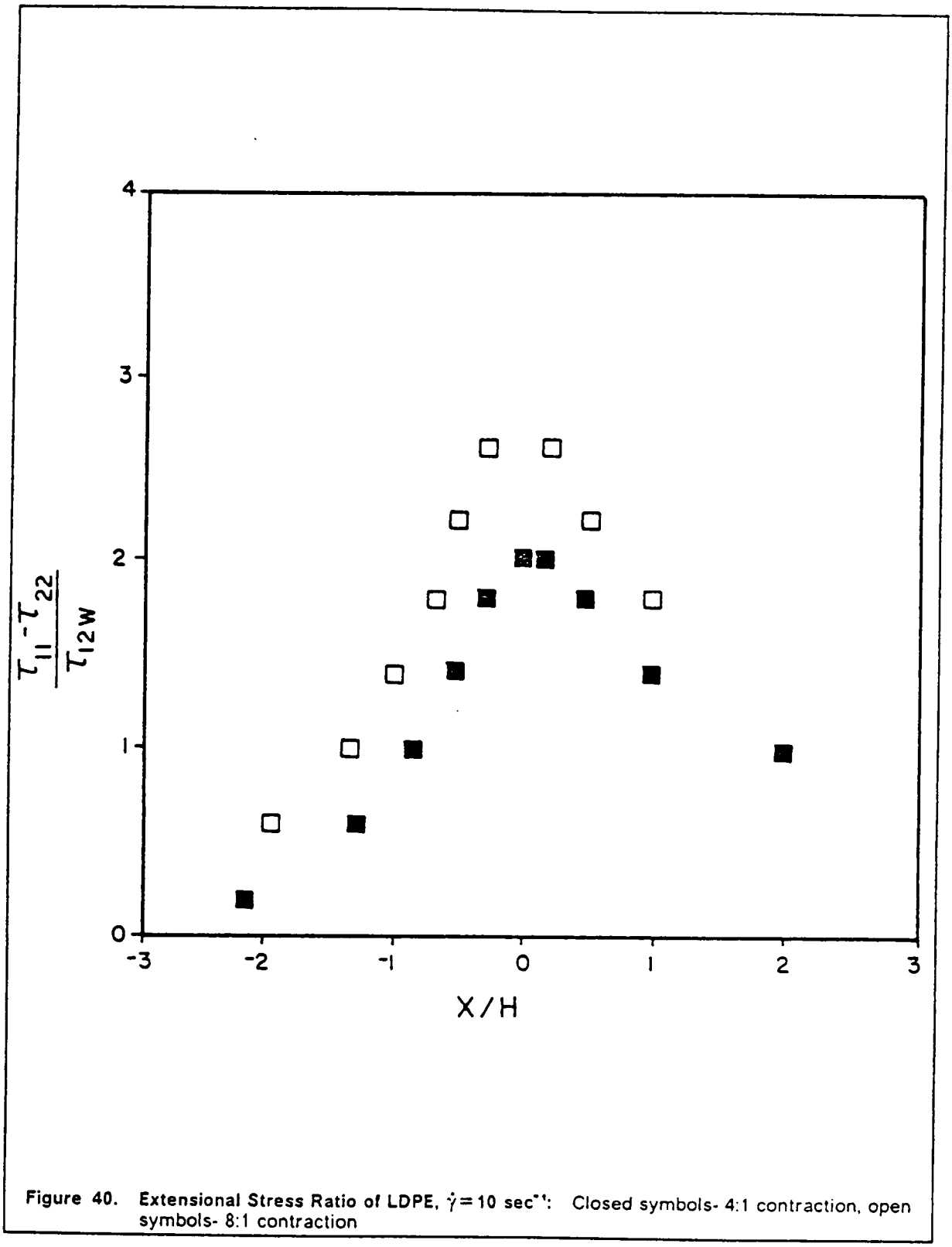

Figure 40. **Extensional Stress Ratio of LDPE, $\dot{\gamma}=10\ sec^{-1}$:** Closed symbols- 4:1 contraction, open symbols- 8:1 contraction

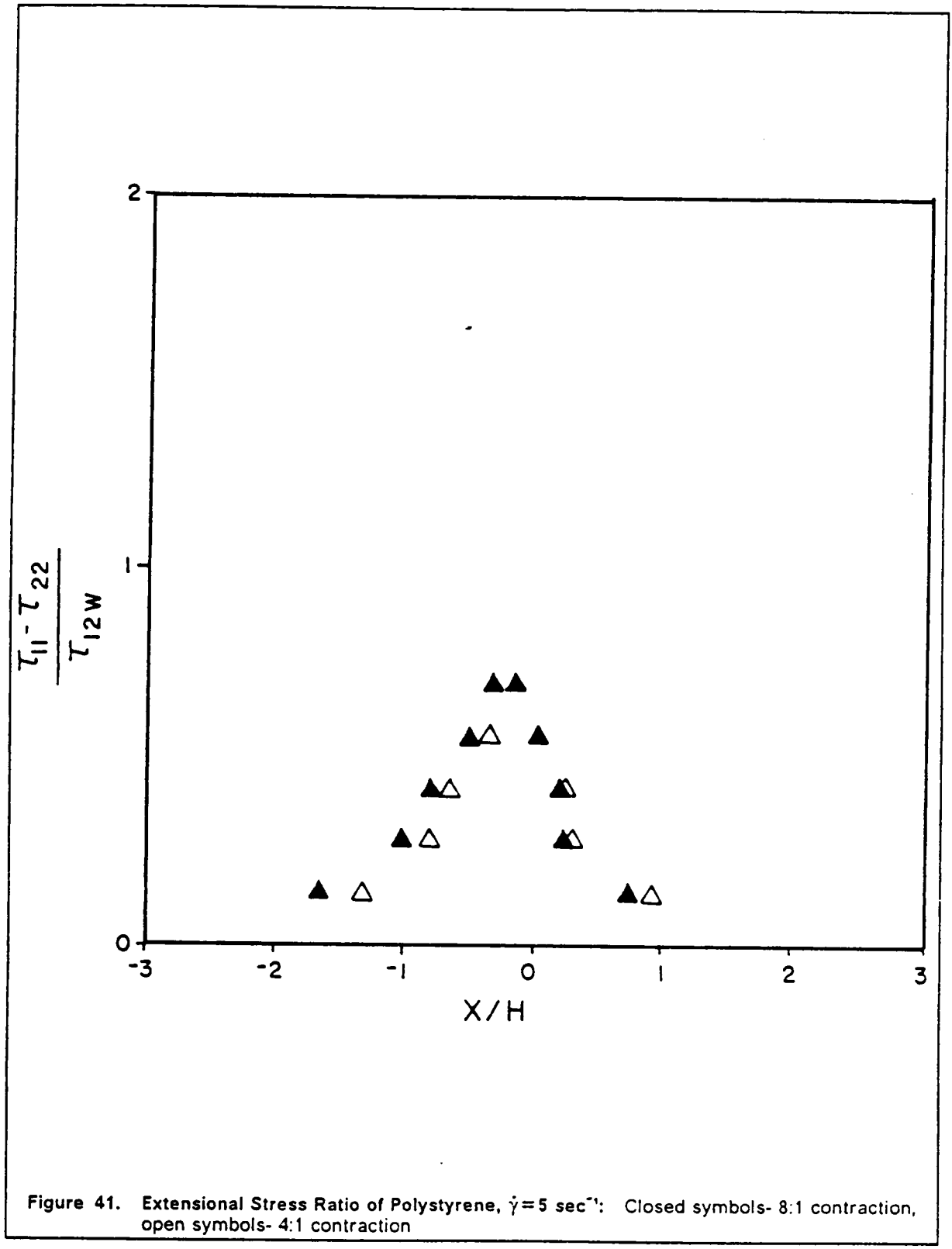

Figure 41. **Extensional Stress Ratio of Polystyrene, $\dot{\gamma}=5$ sec^{-1}:** Closed symbols- 8:1 contraction, open symbols- 4:1 contraction

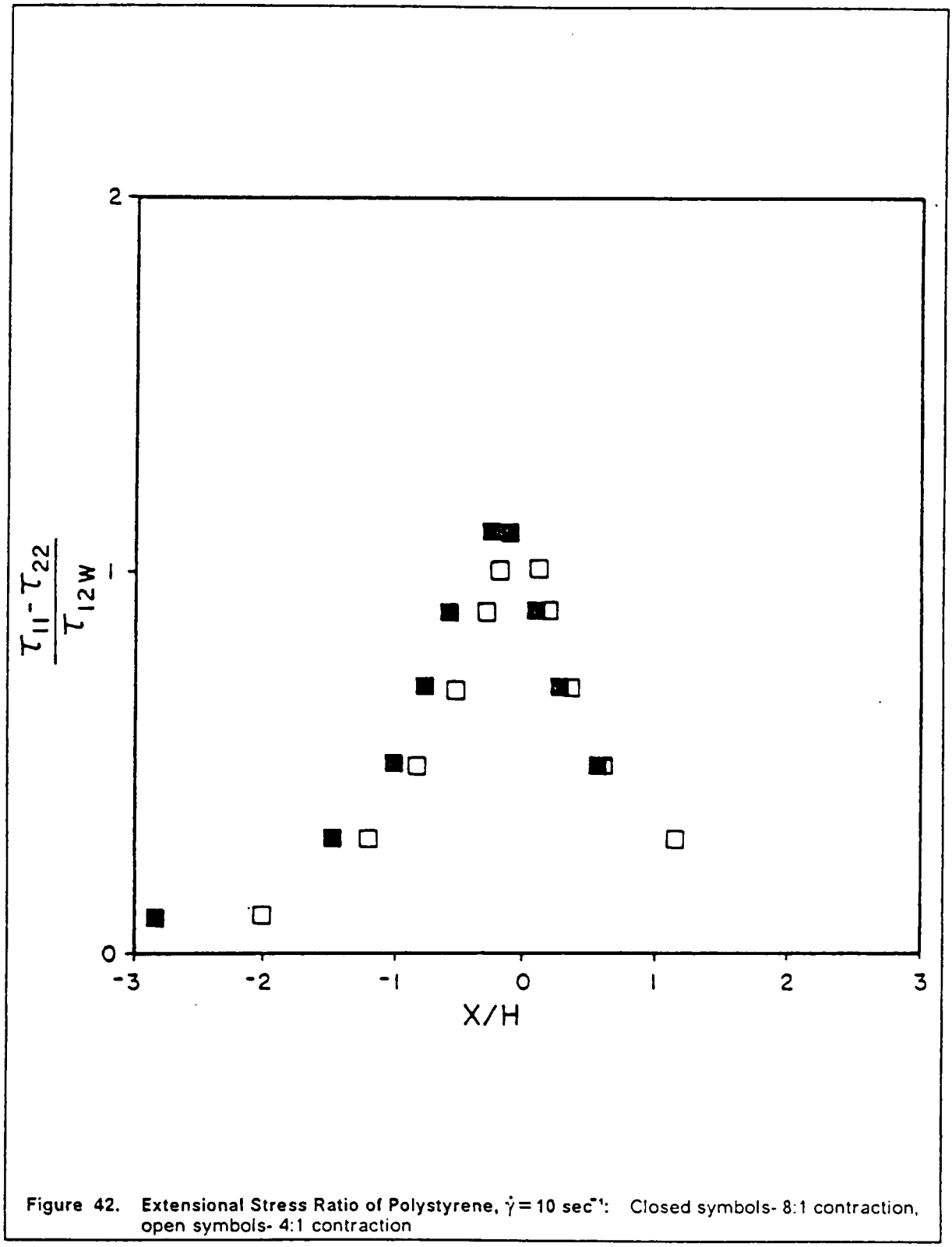

Figure 42. **Extensional Stress Ratio of Polystyrene, $\dot{\gamma} = 10\ sec^{-1}$:** Closed symbols- 8:1 contraction, open symbols- 4:1 contraction

rheological properties of the polymers studied. The results presented in the previous paragraphs, in regards to extensional stresses measured in the entry region, can also be used to support this hypothesis. In Figure 36 and Figure 37 on page 136 it was shown that there was a higher level of extensional stress in LDPE as it flowed through the contraction than there was in polystyrene. Therefore, not only do independent rheological measurements indicate that higher extensional stresses should be expected in LDPE in contraction flow but actual measurements of the stress in the flowing polymer corroborate this. These measurements show that although entry flow has components of both shear and extensional flow, in the region near the contraction extensional flow dominates and is therefore the more likely cause of vortex growth.

In addition, the explanation for the effect of contraction ratio on vortex growth can also be supported by the birefringence measurements. It was stated in section 5.1 that by increasing the contraction ratio there should be a corresponding increase in the acceleration of the fluid through the contraction and therefore an increase in the strain rate applied. This reasoning was used to explain the increase in detachment length observed for LDPE on going from the 4:1 to 8:1 contraction ratios. It was stated that the higher stain rates imposed on the polymer would cause higher extensional stresses to result and cause the detachment length to increase. From Figures 27-29 it is seen that birefringence measurements prove this to be true. For LDPE, which is rate sensitive, the extensional stresses measured in the entry region increase with contraction ratio. In contrast, polystyrene, which is relatively rate insensitive, shows a negligible change in measured stresses with increasing contraction ratio.

Although the response of a polymer to extensional strains can for the most part be used to explain vortex growth there is still a question which remains to be answered. It has been repeatedly stated that vortex growth in LDPE is due to the large extensional stresses which develop in it in the entry region. Ample experimental data has been provided to support this. However, it is possible to generate the same magnitude of extensional stress in polystyrene as was observed in LDPE by increasing the flow rate of the polystyrene. In Figure 43 on page 144 is compared the magnitude of the extensional stress in LDPE at 5 sec^{-1} and polystyrene

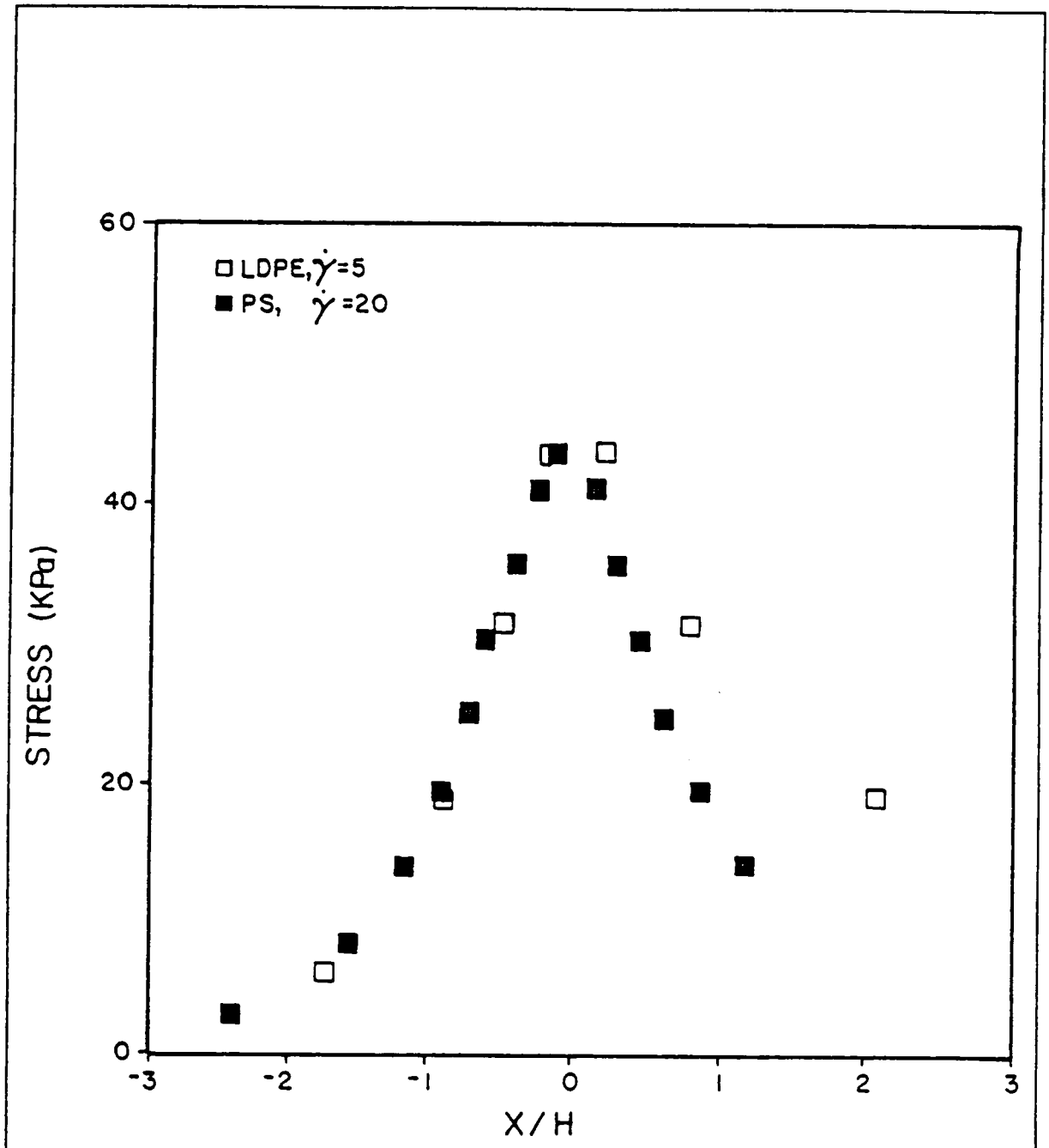

Figure 43. Extensional Stress of LDPE at 150° C and Polystyrene at 190° C, 4:1 Contraction

at 20 sec^{-1} (note this is a plot of $\tau_{11} - \tau_{22}$ and not its ratio to the shear stress). It can be seen that under these conditions both polymers have the same magnitude of centerline extensional stress yet LDPE was shown to exhibit vortex growth but polystyrene did not. Also, by increasing the flow rate even higher the extensional stresses in polystyrene should become higher than those in LDPE. However, at 80 sec^{-1} polystyrene did not exhibit vortex growth similar to that seen in LDPE at 5 sec^{-1} even though the magnitude of extensional stress in polystyrene must have been much higher than in LDPE. In addition, it was noted that vortex growth did not continue above 10 sec^{-1} in LDPE although the extensional stresses kept increasing.

Therefore, it appears that the ratio of extensional stress to shear stress, presented in the previous figures, determines the presence or absence of vortex growth. It has been explained why the extensional stress should be important but it not understood why its ratio with the shear stress should be significant. It's as if there is a competing process, which is coupled with the value of the shear stress, that acts to reduce or limit vortex growth at higher flow rates. It might be thought that inertia effects become significant at high flow rates and act to limit vortex growth in LDPE and prevent vortex growth in in polystyrene even though extensional stresses are high. However, inertia effects should be negligible at the Reynolds numbers encountered in the entry region (typically around 10^{-5}). Therefore, it is not known why the ratio of extensional and shear stresses would correlate with vortex growth but it is clear from the work presented so far in this chapter that knowledge of the extensional properties is necessary in explaining entry flow behavior and as such should be incorporated in the numerical simulation of the flow.

5.5 *Fit of the Rheological Properties of LDPE and Polystyrene by the PTT Model*

In the first part of this chapter the experimental work on entry flow has been presented. It was found in this work that the viscometric properties of a polymer alone could not be used to explain differences in flow behavior observed in the entry region. Through the observation of the entry flow behavior of polymers of different topology, molecular weight, and MWD through contractions of different geometries it was found that the rheological property of primary importance in explaining flow behavior was the extensional viscosity. Knowledge of both the steady-state and transient growth behavior of this property is needed to explain entry flow. As discussed in Chapter 2 many of the numerical studies of entry flow have failed to incorporate a constitutive equation which provides a realistic prediction of the extensional properties. Many of the models used predicted that the extensional viscosity goes to infinity at some critical value of the strain rate. Clearly this is not realistic and it could be expected that erroneous results would occur with the use of such an equation. Having determined experimentally the importance of extensional properties on entry flow behavior it was decided to incorporate in this study a constitutive equation which not only describes the viscometric properties of a fluid but in addition gives a good representation of the extensional properties. Based on this criteria it was decided to use the PTT model.

The PTT model is a differential constitutive equation which has two adjustable parameters for control over rheological properties. The first parameter, ξ, has control over the predictions of N_1 while the second parameter, ε, can be used to vary the magnitude of the extensional viscosity. This latter parameter is what makes the PTT model of particular interest. With this parameter it is possible to evaluate the effect of extensional viscosity on numerical predictions without significantly changing other rheological properties. In addition to the adjustable parameters, it is possible to obtain better predictions of rheological properties with

the PTT model through the use of multiple relaxation times. However, in this study only a single relaxation time was used. As will be seen, adequate prediction of rheological properties was obtained and at the same time the computer storage requirements were kept at a minimum by eliminating additional relaxation modes.

5.5.1 Prediction of Shear Properties

In the numerical work only LDPE and polystyrene have been studied. Again, these two polymers best demonstrate experimentally the differences in flow behavior observed in entry flow and therefore seem the best choices for testing the ability of the constitutive equation and the numerical method to predict flow behavior. The modelling has been done for LDPE at 150° C and polystyrene at 190° C. The fit of the shear viscosity and the primary normal stress difference of these polymers by the PTT model is presented in Figure 44 and Figure 45 on page 148.

In order to obtain the predictions the program PTTFIT was used. Based on the input of experimental viscosity data and the chosen value of ξ the program then determined the values of η_1, η_2, and λ by fitting the data using equation 4.25 and using the relation between η_1 and η_2 described in Chapter 4. Values of N_1 were then calculated using the values of these parameters in equation 4.26. Calculations were made based on the assumption of steady shear flow and therefore ε was taken to be zero. The value of ξ was chosen based on the predicted fit of N_1.

From Figure 44 and Figure 45 it can be seen that the PTT model provides a good fit of the shear properties of both LDPE and polystyrene. In both cases the predictions of N_1 are slightly high but the fit is within reason and is the best that could be obtained by variation of the value of ξ. For polystyrene the fit of the viscosity is good out to shear rates of about 50 sec^{-1}. There is some deviation in the fit of the high and low end of the shear thinning region but it is not serious. For LDPE the fit of the shear thinning region is better than for polystyrene

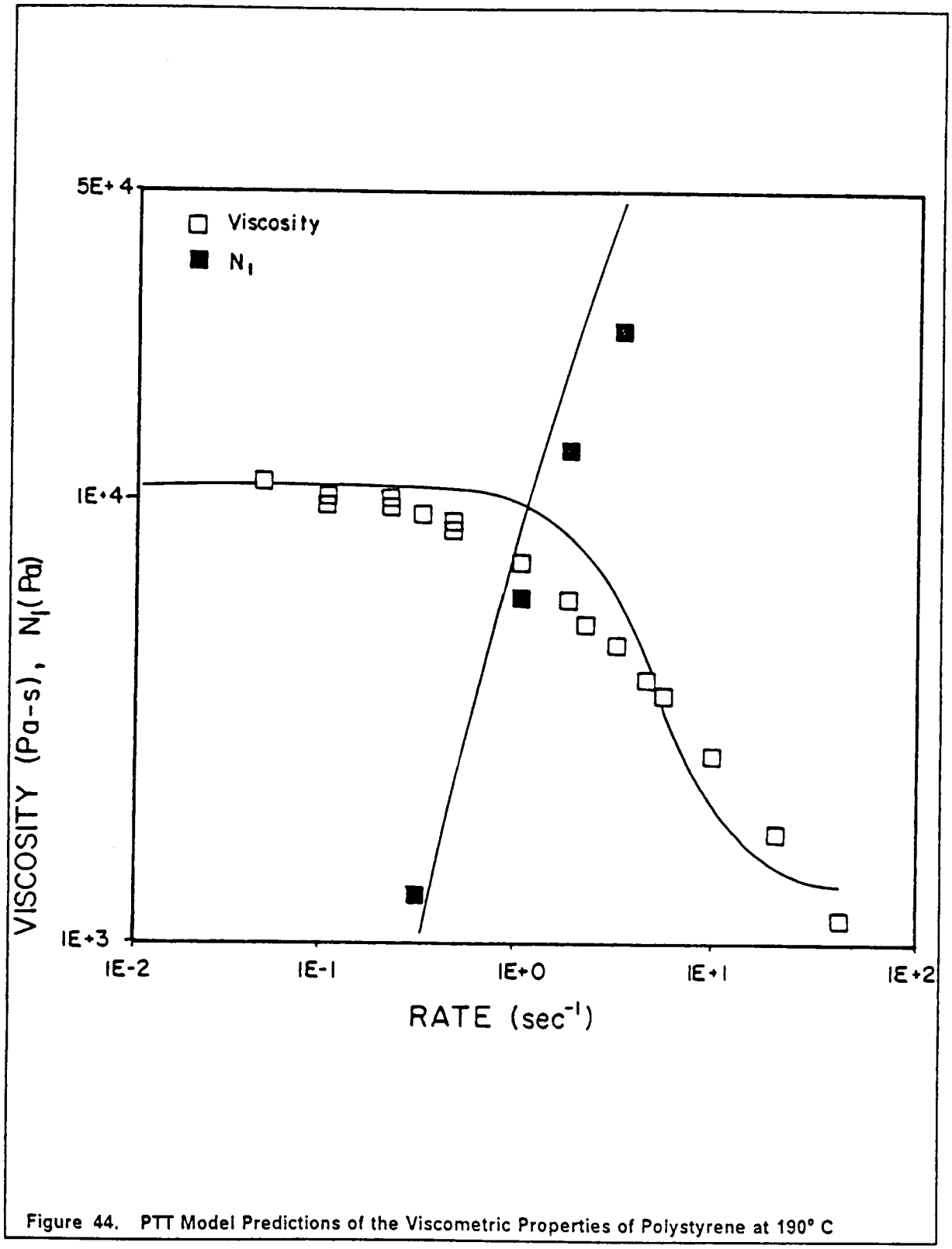

Figure 44. PTT Model Predictions of the Viscometric Properties of Polystyrene at 190° C

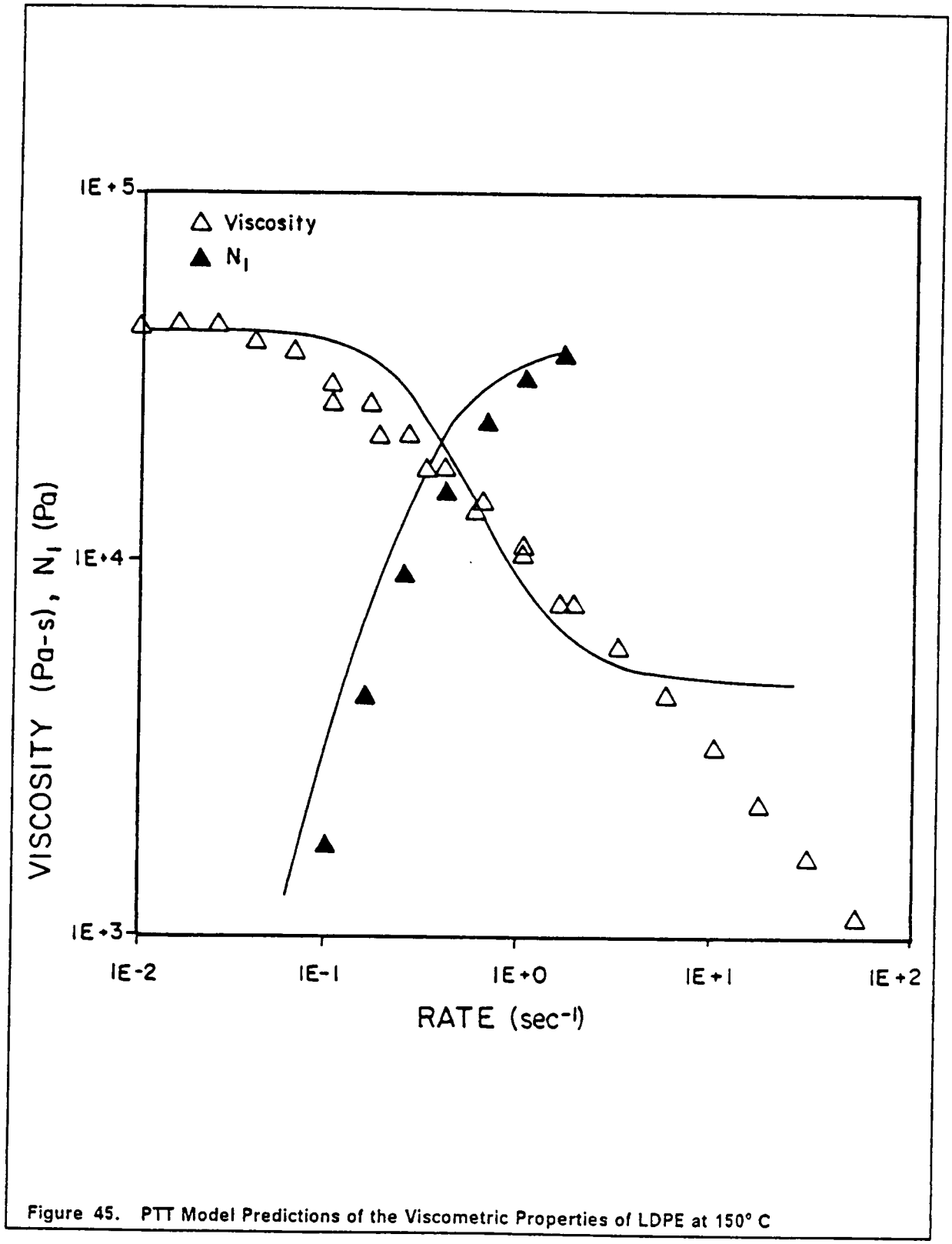

Figure 45. PTT Model Predictions of the Viscometric Properties of LDPE at 150° C

but the effect of the retardation term becomes apparent at fairly low shear rate ($\dot{\gamma} \cong 3sec^{-1}$). As was discussed in Chapter 4 it is necessary to use a retardation term with the PTT model to slow down the rapid shear thinning that the model predicts. If the retardation term were not used then the shear stress would go through a maximum and begin to decrease at higher shear rates. However, the incorporation of the retardation term results in the leveling off of the viscosity and a more rapid rise in stress than is experimentally observed. This will effectively limit the range over which numerical simulations should be done.

5.5.2 Prediction of Extensional Properties

In examining the predictions of the PTT model in extensional flow it was necessary to look at both the predictions of the steady-state extensional viscosity and the transient stress growth. Prediction of the steady-state extensional viscosity for polystyrene is presented in Figure 46 on page 151 along with a limited amount of experimental data. The predicted values were obtained using the program PTTEXTS. Values of η_E were calculated using equations 4.30 and 4.31 and input values of the parameters obtained from PTTFIT. The initial value of ε was chosen based on the fit of the experimental data. Although experimental data were available at low rates this data did not extend to higher rates where the maximum in η_E is predicted. Therefore two criteria were used in choosing ε. First, it was desired to keep the predicted values of η_E close to the experimental values at low strain rates. This would have required a large value of ε which would have significantly affected the viscometric property predictions. The second criterion was that the height of the maximum in η_E be comparable with data published in the literature. This would have required a smaller value of ε than was needed to fit the experimental data. A compromise between the two was chosen with ε being set at 0.1.

A different problem was encountered in fitting the extensional viscosity of LDPE. As was seen in section 5.1 no steady-state extensional viscosity was observed for LDPE. Whether the polymer ever reaches steady-state or not is not known due to the limited amount of strain that

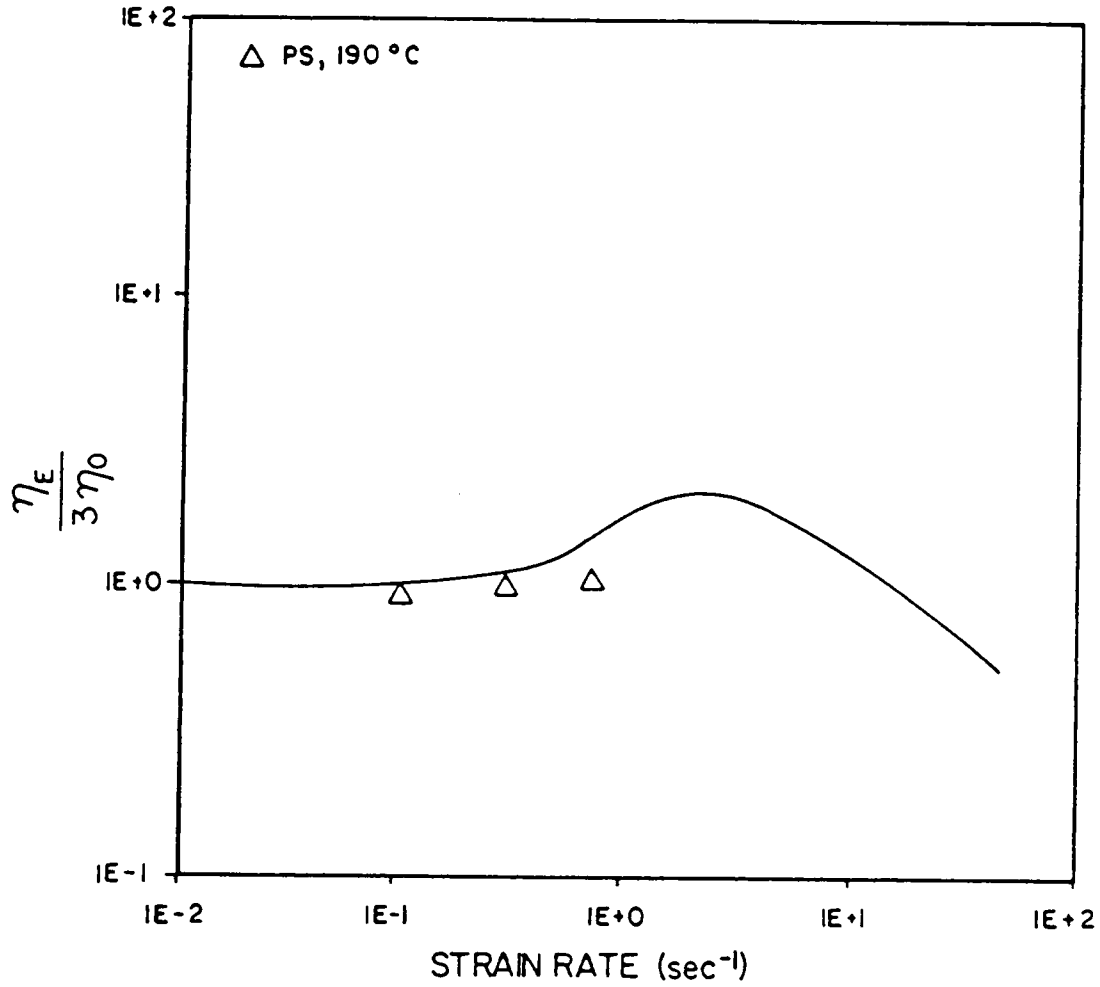

Figure 46. PTT Model Predictions of the Extensional Viscosity of Polystyrene at 190° C

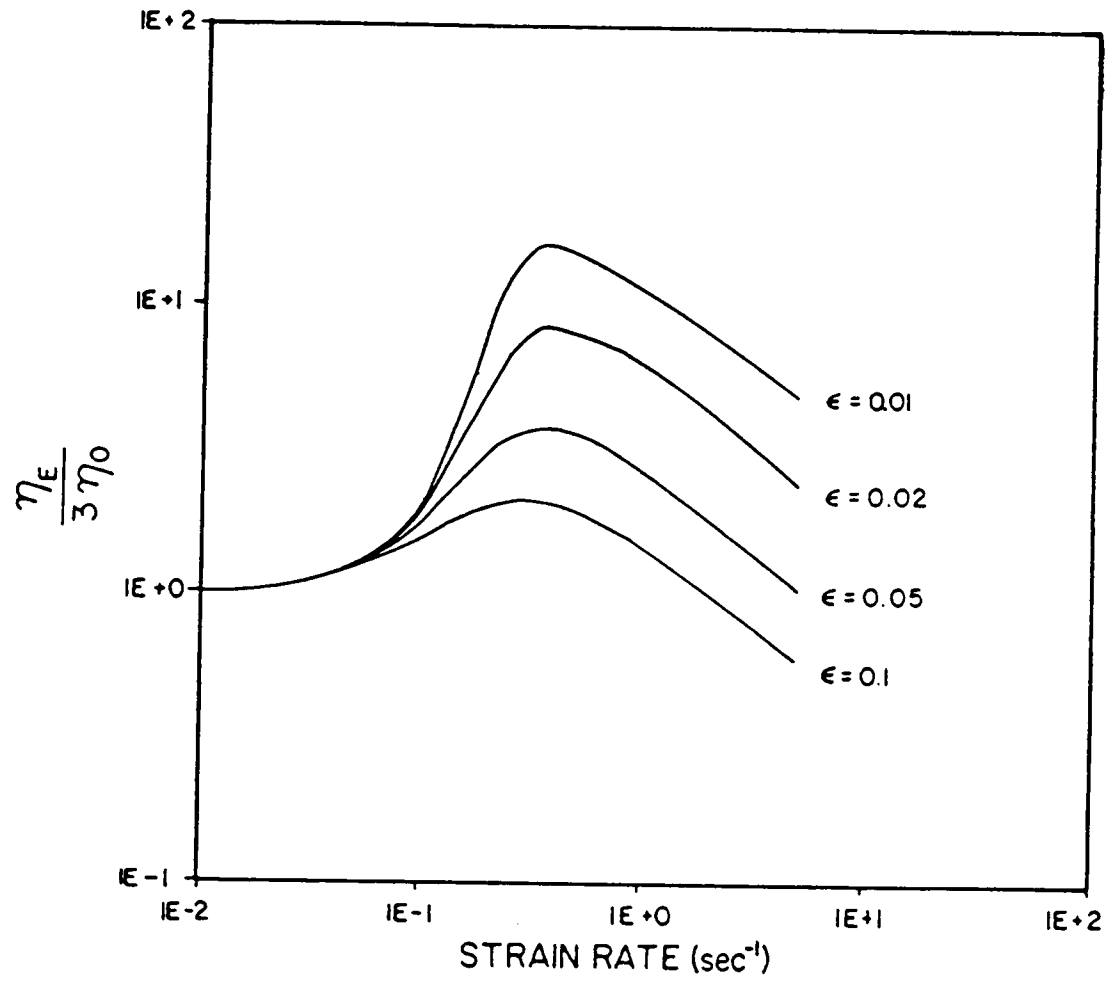

Figure 47. PTT Model Predictions of the Extensional Viscosity of LDPE at 150° C

could be achieved in the rheometer. However, the PTT model requires that a steady-state extensional viscosity be reached and the magnitude of the maximum value of η_E can take on a wide range of values depending on the value of ε chosen (see Figure 47 on page 152). There have been studies in which a steady-state extensional viscosity has been found for LDPE and values of $\frac{\eta_{Emax}}{\eta_0}$ have been reported. These values were used as the basis for choosing ε which was set at 0.01.

Comparison of the extensional viscosity versus strain rate curves for LDPE and polystyrene (Figure 48 on page 154) show that there are two major differences between the predictions for the two polymers which could affect the numerical simulations. The most obvious difference is the magnitude of $\frac{\eta_{Emax}}{3\eta_0}$ for the two polymers. For the values of ε chosen $\frac{\eta_{Emax}}{3\eta_0}$ is nearly 10 times as high for LDPE as it is for polystyrene. This ensures that the effect of high extensional stress on the numerical simulation of entry flow can be determined. The second difference between the polymers is the strain rate at which the maximum occurs. For LDPE it occurs at $\dot{\varepsilon} \cong 0.3\ sec^{-1}$ but it does not occur in polystyrene until the strain rate reaches $\dot{\varepsilon} \cong 2.0\ sec^{-1}$. This means that for low flow rate conditions at which the strain rates encountered in the flow are in the range 0.1 - 1.0 sec^{-1} the difference in the extensional response of the two polymers will be even greater than the values of η_{Emax} indicate since LDPE will be at its maximum values of η_E but polystyrene will not have risen much above the Trouton value.

In addition to the steady-state extensional viscosity, it was also necessary to examine the extensional stress growth predictions of the PTT model. This required the use of the program PTTEXTG. The program solved equations 4.32 an 4.33 using values of the parameters obtained from PTTFIT. The value of ε was chosen as described in the previous paragraphs. The predictions of the stress growth are presented in Figure 49 on page 155 and Figure 50 on page 156. As can be seen the model does well in predicting the the main difference between the two polymers in stress growth behavior. For polystyrene the model predicts the bounded stress growth behavior typical of this polymer. The fit to experimental data is quantitatively accurate at the low rates and qualitatively accurate at the higher rates. The deviation from the experimental data at high rates is attributable to the value of ε chosen. For $\varepsilon = 0.1$ the

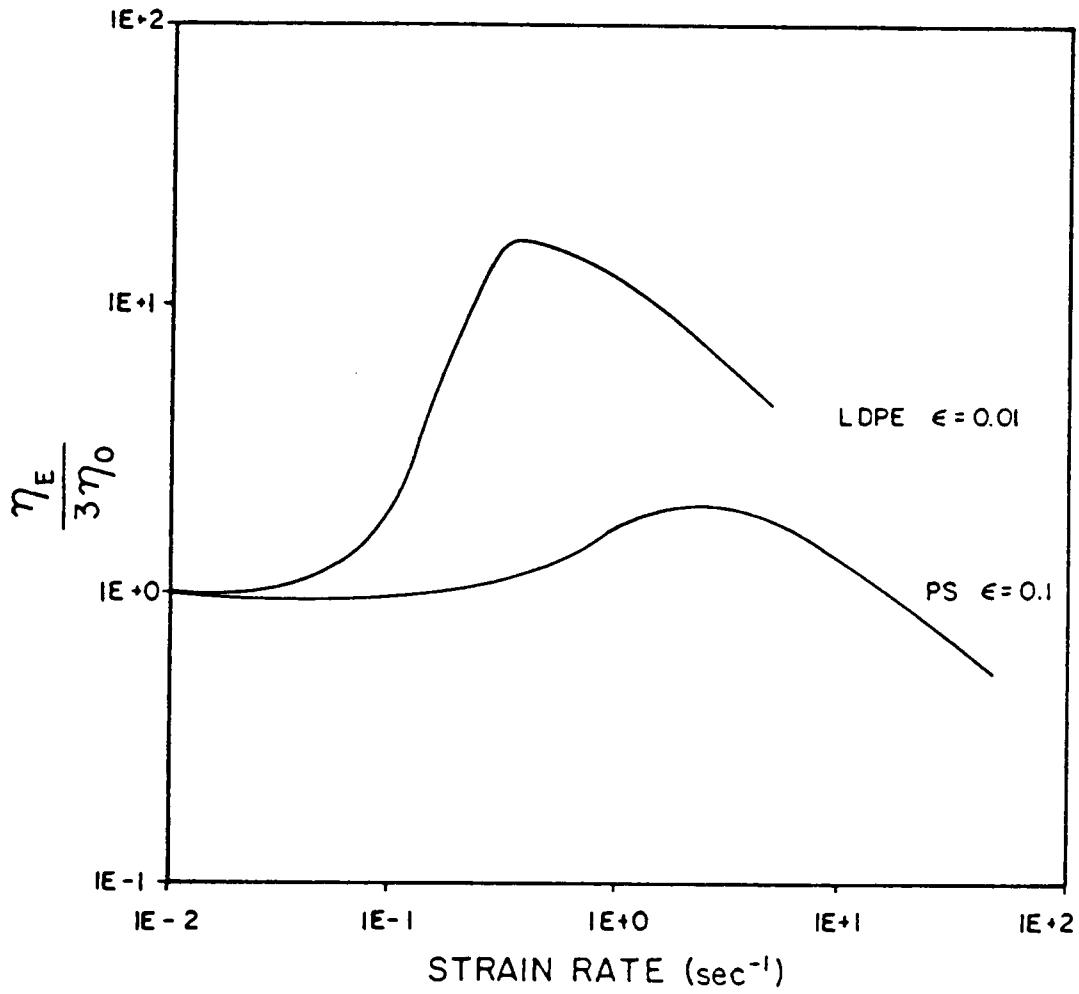

Figure 48. Comparison of the Extensional Viscosity Predictions for LDPE and Polystyrene

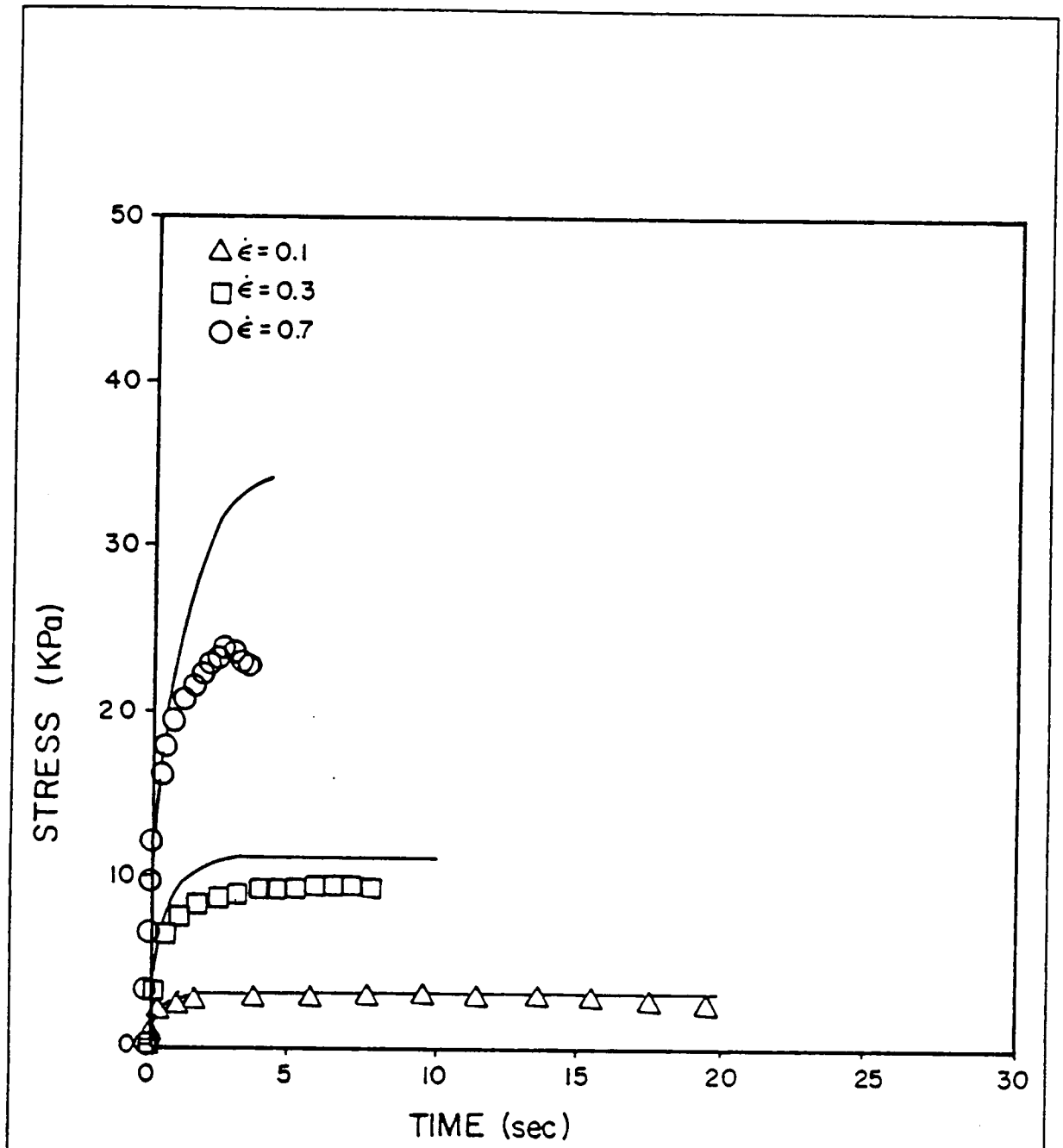

Figure 49. PTT Model Predictions of the Extensional Stress Growth of Polystyrene at 190° C

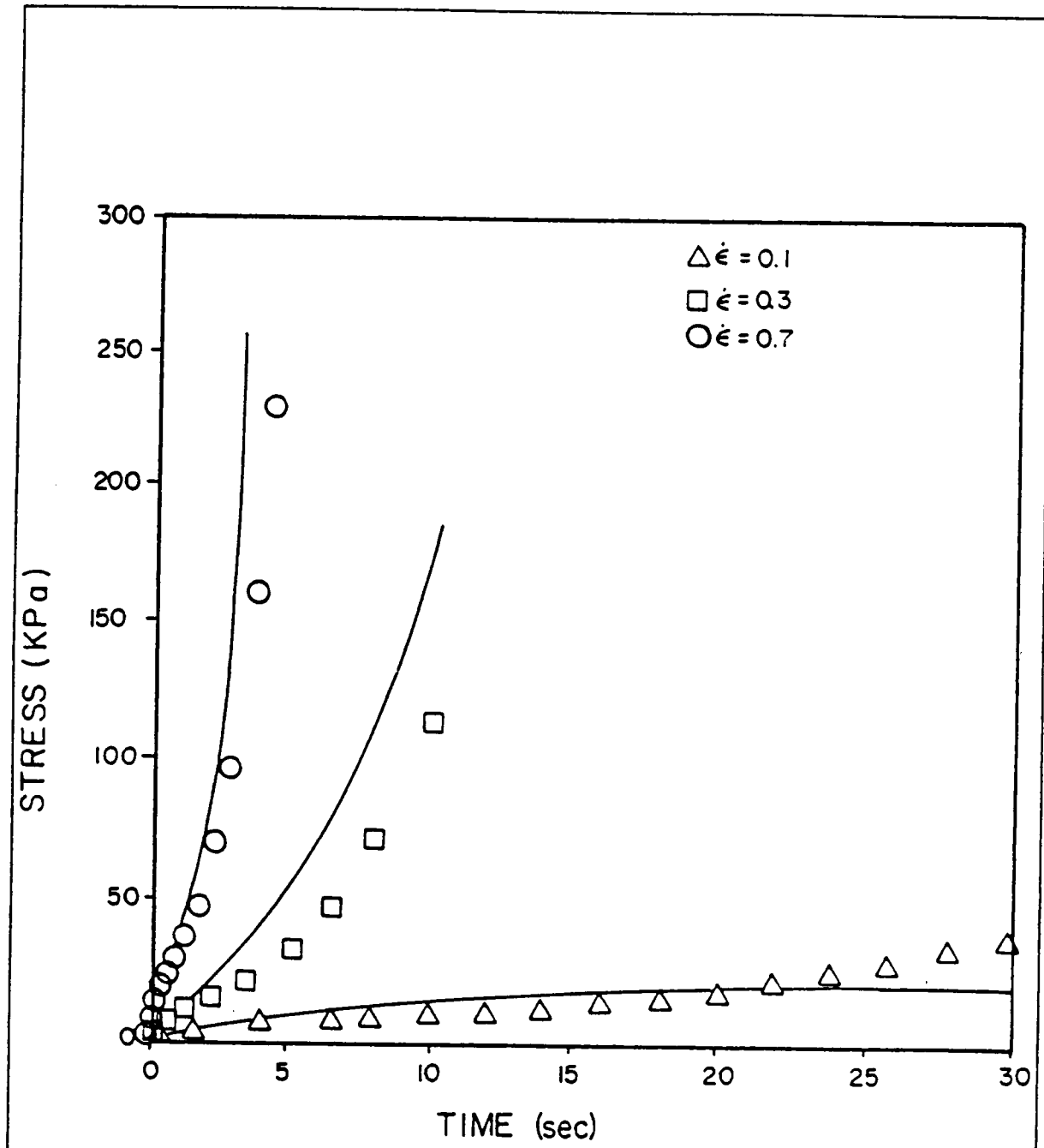

Figure 50. PTT Model Predictions of the Extensional Stress Growth of LDPE at 150° C

model predicts that η_E will have risen above the Trouton value at $\dot{\varepsilon} = 0.7\ sec^{-1}$, but the data do not. Again, ε could have been assigned a different value which would have made it fit the data better but the predictions of the shear properties would have been affected.

For LDPE the PTT model predicts the rapid stress growth behavior typical of this strain hardening material. Also, the fit to the experimental data is quite good. The predicted values are shown just for the range at which experimental data were available. At some point above the level of the graph both the curves for $\dot{\varepsilon} = 0.3$ and $0.7\ sec^{-1}$ would eventually level off to a steady-state value as shown for $\dot{\varepsilon} = 0.1\ sec^{-1}$. Again, this level of stress is determined by the value of ε.

It has been shown in this section that the PTT model provides a good fit of both the shear and extensional properties of LDPE and polystyrene. The model parameters that were used in this study are given in Table 6 on page 158. Using these parameters the constitutive equation is able to predict the major rheological differences between the two polymers. In a later section the effects of these predictions on entry flow simulation will be presented, but in the next section a discussion of the meshes used in the calculations will be given.

5.6 *Meshes Used and the Effect of Mesh Refinement*

Before it was possible to perform numerical simulations it was necessary to construct a finite element mesh over the flow domain. Only half of the entry region needed to be modelled since the flow was symmetric. The procedure used in constructing the mesh was to have relatively large elements far upstream and downstream of the contraction in the fully developed flow regions and small elements near the contraction where rapid changes in the stress and velocity were occurring. The upstream and downstream channel lengths were chosen such that the entry and exit planes would be in the fully developed flow region. This was a necessary criterion as the initial boundary conditions were calculated based on the assump-

Table 6. Values of the PTT Model Parameters

Parameter	LDPE	Polystyrene
η_1 (Pa-s)	37300	9520
η_2 (Pa-s)	4970	1270
λ (sec)	4.55	0.504
ξ	0.25	0.25
ε	0.01	0.1

tion of steady shear flow. The locations of the steady flow regions were determined from streamline and birefringence patterns. For the upstream channel it was chosen to use a 1.5 L/D and for the downstream channel an L/D of 3 was used.

Although the arrangement of elements and the lengths for the upstream and downstream channels were predetermined the actual number of elements used was based on the quality of the solution from the numerical method. As was discussed in Chapter 2 it has been found that the quality of solution and the limit of convergence can depend on mesh refinement. Keunings (R72) found that depending on the constitutive equation used mesh refinement only increases the limit of convergence to a certain point beyond which the limit decreases. Therefore, there should be an optimum mesh for a given flow problem. The effect of mesh refinement was not an objective of this study, but it was necessary to experiment with meshes of different size to see which would provide the best solution.

As will be discussed in the following section, numerical simulation of the flow of LDPE was carried out at conditions corresponding to the limit of convergence of the method. Since it was necessary to obtain the best possible solution it was required that there be optimization of the mesh. The procedure for optimization was by trial and error. Various mesh configurations were used in the simulation of the flow and for each mesh it was noted how close the simulation came to convergence before divergence occurred. Based on the behavior of the solution the number of elements was either increased or decreased. Initially a coarse mesh with 132 elements was used, but there was failure of the solution to converge and only three iterations took place before divergence occurred. Based on the work of Gotsis (85) it was thought that enlargement of the corner elements might improve convergence since it was found in that study that coarser meshes gave higher convergence limits, but just the opposite resulted. For a 114 element mesh, divergence of the solution occurred after only two iterations. From these results it was apparent that mesh refinement was necessary. It was found that increasing the number of elements to 290 significantly improved the solution but further refinement to 433 elements made the solution worse. Enlargement of the corner elements in

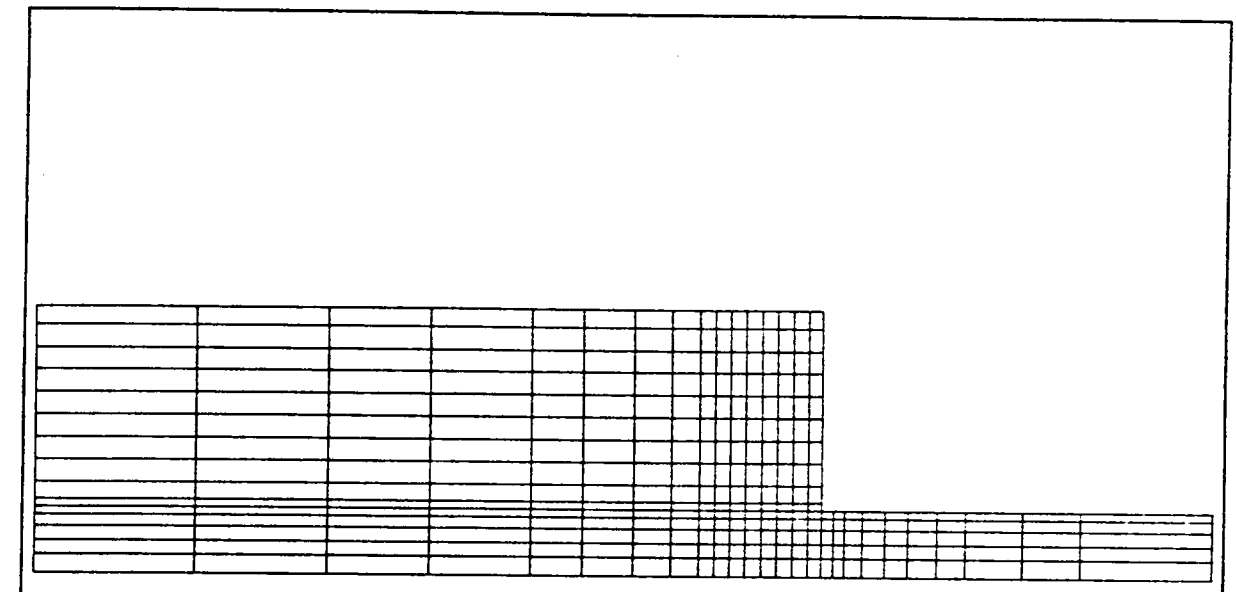

a

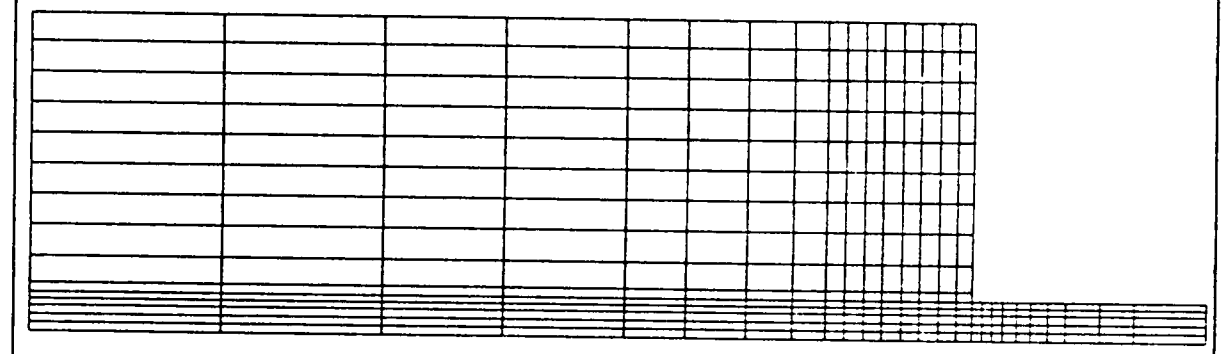

b

Figure 51. Meshes Used in the Finite Element Simulation: a) 4:1 contraction, 290 elements b) 8:1 contraction, 290 elements

the 290 element mesh again resulted in a worse solution. The optimum meshes for the 4:1 and 8:1 geometries derived from this trial and error method are shown in Figure 51.

In addition to the above described method, another mesh, based on this optimum configuration, was designed to be sure that the exit region of the mesh was long enough to be in the fully developed flow region. From birefringence patterns of LDPE it was observed that steady flow in the downstream channel did not occur within the viewing region of the slit die. Therefore, it was not known if a 3 L/D channel was long enough to reach the fully developed flow region. In response to those findings a mesh with a 10 L/D downstream channel was constructed. The mesh was the same as the optimized 4:1 mesh in Figure 51 except seven more columns of elements were added on to the exit of the die such that the 10 L/D channel was formed. Since the two meshes were identical except for the exit region the solutions for each mesh could be compared directly. The resulting solutions indicated no difference for the two meshes and it was concluded that the 3 L/D exit length was sufficient.

5.7 *Streamline Predictions Using the PTT Model*

In the previous sections descriptions have been given of the constitutive equation and finite element meshes used in this study. In this section the implementation of the FEM code NONEWT using the PTT model and the described mesh will be presented along with the streamline predictions made by the code. Comparison will be made between the numerical results and the experimentally measured detachment length and streamline patterns. The purpose of this work is to show to what degree the PTT model in conjunction with the penalty finite element method is successful in describing the distinctly different flow behavior of LDPE and polystyrene.

5.7.1 Predictions for Polystyrene

Simulation of the entry flow behavior of polystyrene was not a difficult task for the FEM code. Upon referring back to Figure 15 on page 98 it is remembered that the flow pattern of this polymer changed very little over the range of tested shear rates (1-80 sec^{-1}). The only difference observed was the increase in recirculation within the corners. As was shown in Figure 17 on page 100 the detachment length remained unchanged up to the highest flow rates. Since no vortex growth was exhibited there were little problems with the method simulating the flow.

Predictions of the streamline patterns of polystyrene in the 4:1 contraction are presented in Figure 52 on page 163 for shear rates of 1, 2.5, 5, and 10 sec^{-1}. As can be seen the predictions are very similar to the experimental results. The size of the corner vortex is nearly the same as that observed in the streak photographs and the only change with increasing shear rate is the increase in recirculation within the corner. (Although the value of the stream function shown in the figure stays the same with increasing $\dot{\gamma}$ the actual magnitude does increase. The stream functions shown in the figure have been normalized with respect to the centerline value. Therefore, with increasing shear rate there is an increase in the absolute magnitude of the stream function even though the normalized value remains the same.) The only difference between the experimental and numerical results is in regards to the recirculation within the cell. The experimental results indicate that recirculation is very weak, but the numerical results clearly indicate recirculation occurs. However, on closer examination it is seen that the two are not that different. First, although the numerical predictions show distinct recirculation, this recirculation is quite weak. The stream function in the cell is less than that at the centerline by a factor of 10^4. Therefore, the numerical method does indeed predict only a weak recirculation. In addition, the experimental patterns might have exhibited clearer recirculation if longer exposure times had been used. The photographs represent four minutes of flow time and although this is adequate time to define the recirculation at higher rates ($\dot{\gamma} > 20\ sec^{-1}$) it

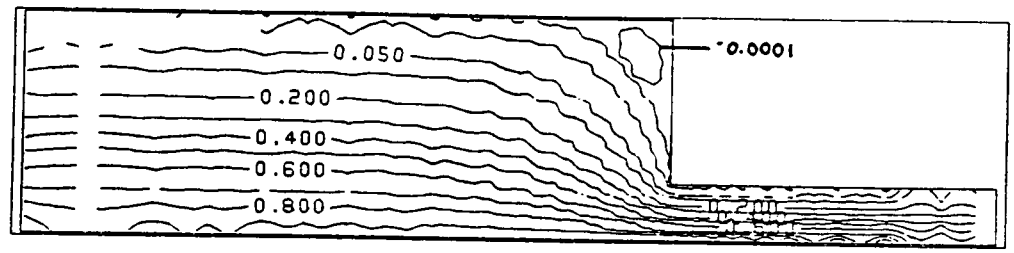

a

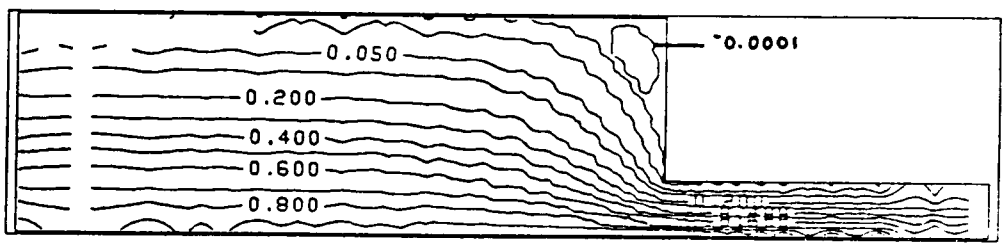

b

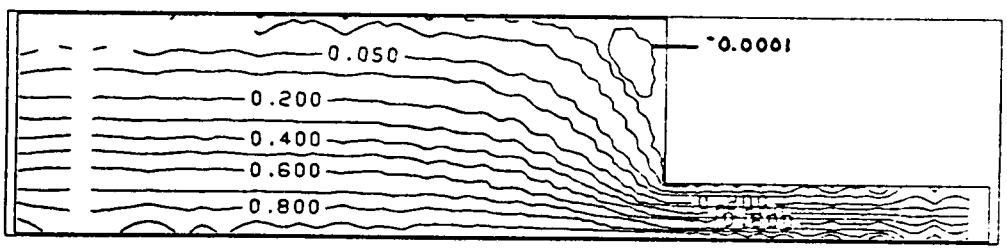

c

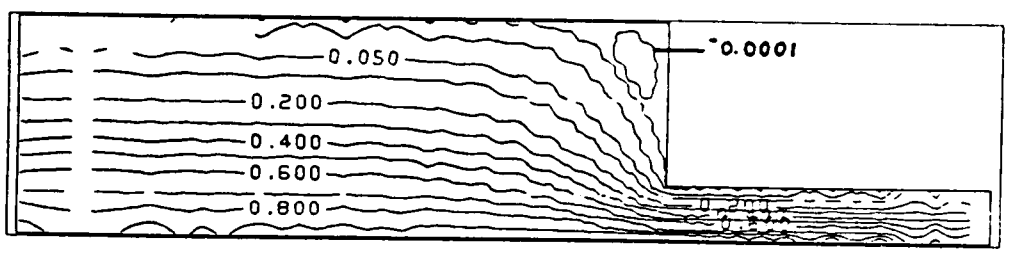

d

Figure 52. Streamline Pattern Predictions for Polystyrene at 190° C 4:1 Contraction: a) $\dot{\gamma} = 1\ sec^{-1}$ b) $\dot{\gamma} = 2.5\ sec^{-1}$ c) $\dot{\gamma} = 5\ sec^{-1}$ d) $\dot{\gamma} = 10\ sec^{-1}$

is not enough time for the lower rates. It is likely that longer exposures would have presented even stronger similarities between experimental and numerical results.

Similar results were predicted for the flow of polystyrene in the 8:1 geometry (Figure 53). Again it is seen that there is no increase in vortex size with increasing flow rate. Also, the detachment length is the same as that predicted in the 4:1 geometry. Both findings are in agreement with experimental results. As with the experimental results, no effect on flow behavior due to the contraction ratio was predicted for polystyrene.

It has been shown that the PTT model does well in predicting the entry flow behavior of polystyrene. However, there was no real challenge involved with the simulation since, as was found with the experimental results, there was no change in flow behavior with increasing flow rate. It was only necessary for the method to simulate what essentially corresponded to Newtonian flow. The situation was quite different for the simulation of LDPE's flow behavior since this polymer was found experimentally to exhibit vortex growth. The results of this work are presented in the following section.

5.7.2 Predictions for LDPE

The prediction of the entry flow behavior of LDPE provided a good test of the numerical methods ability to predict viscoelastic fluid flow. For polystyrene it was not necessary for the method to predict vortex growth as this was not observed experimentally but referring back to Figure 12 on page 94 it is shown that vortex growth does occur for LDPE and this growth begins at relatively low shear rates. The purpose of this section will be to report the results obtained in trying to numerically simulate this flow behavior.

The streamline predictions for LDPE in the 4:1 contraction at shear rates of 0.5, 1, and 2.5 sec^{-1} are presented in Figure 54 on page 166. As can be seen the predictions compare very well with the experimental results. At 0.5 and 1 sec^{-1} the predicted flow is Newtonian-like with the detachment length remaining constant and only weak recirculation occurring within the

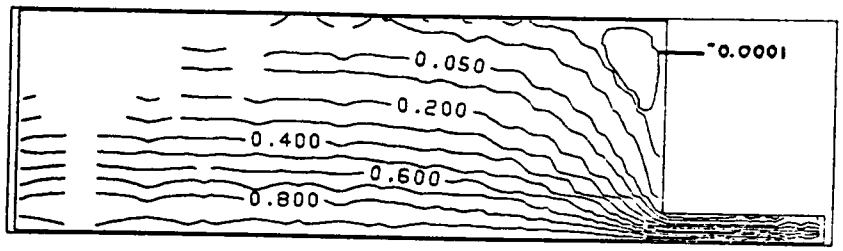

a

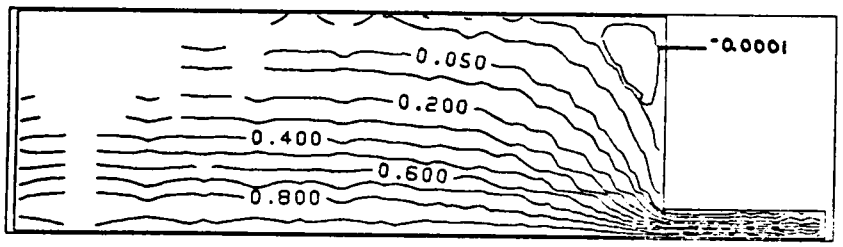

b

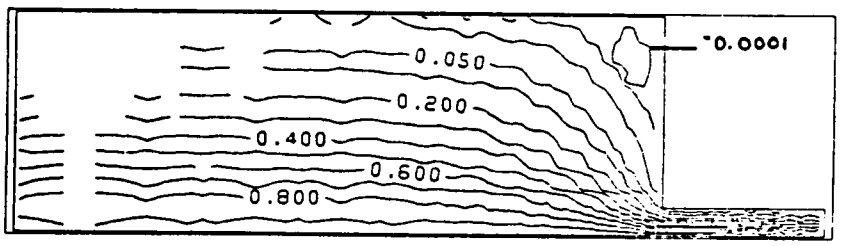

c

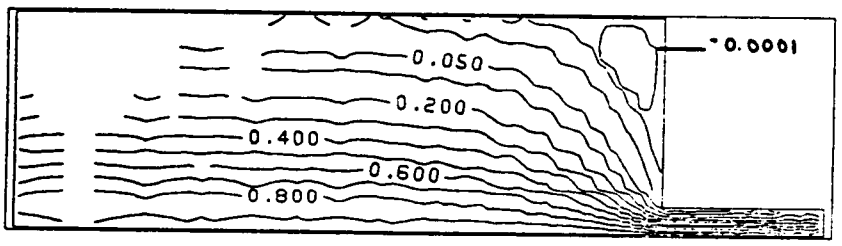

d

Figure 53. Streamline Pattern Predictions for Polystyrene at 190° C 8:1 Contraction: a) $\dot{\gamma} = 1\ sec^{-1}$ b) $\dot{\gamma} = 2.5\ sec^{-1}$ c) $\dot{\gamma} = 5\ sec^{-1}$ d) $\dot{\gamma} = 10\ sec^{-1}$

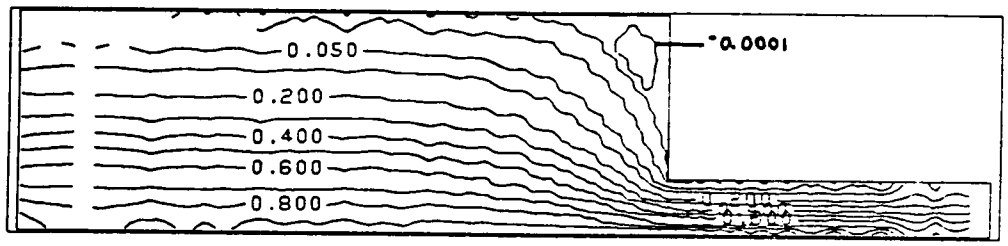

a

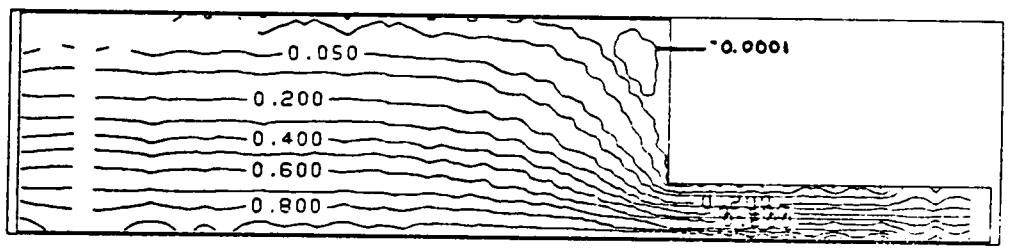

b

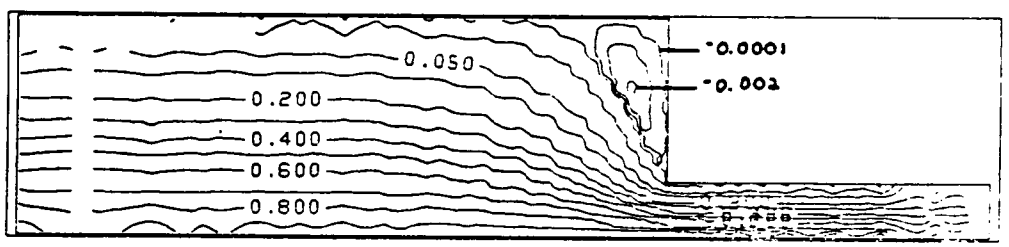

c

Figure 54. **Streamline Pattern Predictions for LDPE at 150° C 4:1 Contraction:** a) $\dot{\gamma} = 0.5\ sec^{-1}$ b) $\dot{\gamma} = 1.0\ sec^{-1}$ c) $\dot{\gamma} = 2.5\ sec^{-1}$

corners. This is what was found experimentally. Also, at these low rates the predicted behavior is identical to that for polystyrene. This result is in agreement with the previously made statement that at low flow rates the entry flow behavior of all polymers becomes the same in that it is Newtonian in nature. Upon increasing the shear rate from 1 to 2.5 sec^{-1} it is seen that the experimentally observed vortex growth is predicted numerically. There is both an increase in detachment length and in recirculation rate.

The same type of flow behavior was found for flow through the 8:1 contraction (Figure 55 on page 168), but for this case it appears that vortex growth may be occurring at a lower shear rate. This would be in agreement with what was found experimentally in that the contraction ratio does have an effect on the entry flow behavior of LDPE. Although experimental data were not reported at these low of rates it was shown in Figure 17 on page 100 that above $\dot{\gamma} = 5\ sec^{-1}$ the detachment length observed in the 8:1 contraction was larger than that found in the 4:1 contraction. Therefore, these predictions by the numerical method are reasonable. The numerically determined detachment length is compared with experimental values in Figure 56 on page 169 and for the limited range of the calculations it is seen that predicted values for both polymers in both geometries agree well with experimental data. However, there is a limit in how high in flow rate it is possible to obtain numerical solutions and this will be the subject of the following paragraphs.

5.7.3 Convergence Limit of the Method

The numerical results presented in the previous sections represent the range over which it was possible to obtain convergence. Although, according to the work of Gotsis (85), it actually would have been possible to go higher in rate in the simulation of polystyrene's flow behavior, this was not considered important since no change in flow behavior was expected to occur based on experimental results. However, the problem of convergence limit was particularly important in the simulation of LDPE's flow behavior.

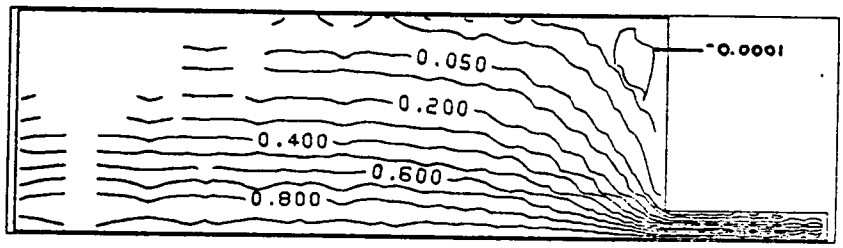

a

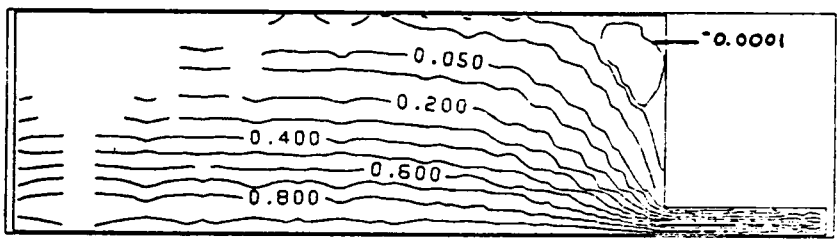

b

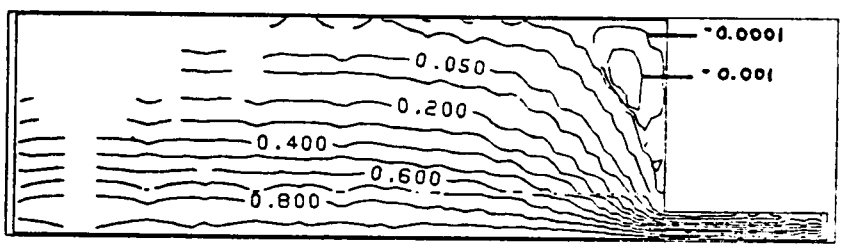

c

Figure 55. Streamline Pattern Predictions for LDPE at 150° C 8:1 Contraction: a) $\dot{\gamma} = 0.5\ sec^{-1}$ b) $\dot{\gamma} = 1.0\ sec^{-1}$ c) $\dot{\gamma} = 2.5\ sec^{-1}$

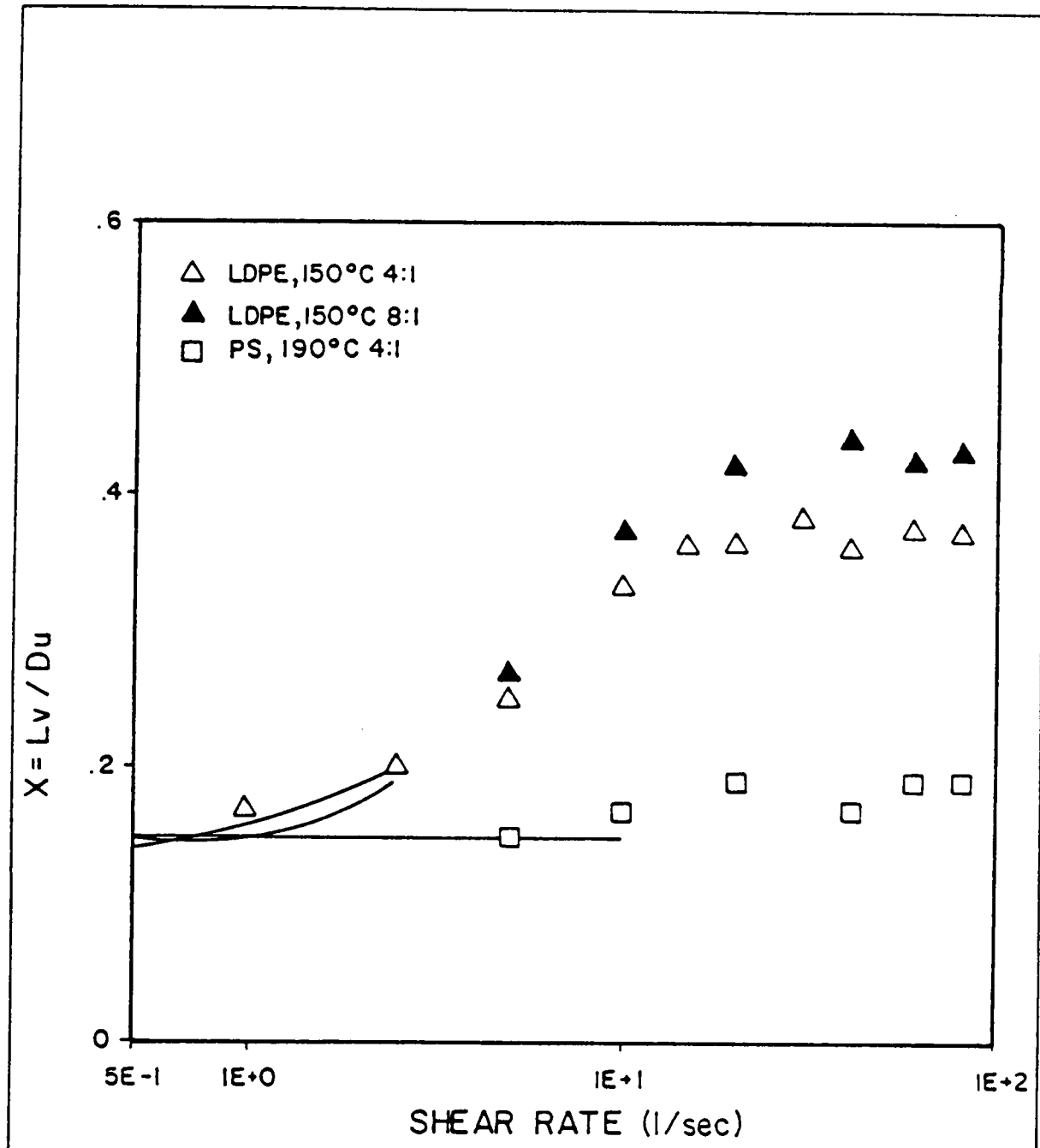

Figure 56. Predicted Detachment Length Versus Shear Rate for LDPE and Polystyrene

For LDPE it was found that the numerical method would not converge for shear rates higher than 1 sec^{-1}. At first it was thought that failure might be due to the rapid increase in shear stress at higher rates associated with the retardation term. However, at $\dot{\gamma} = 2.5\,sec^{-1}$, which is the rate at which the simulation was being attempted, the effect of the retardation term should not be significant. For these flow conditions the shear rates encountered in the entry region are all lower than 2.5 sec^{-1} except right at the wall of the downstream channel. Since the effect of the retardation term should not be noticed except at higher rates a different source of solution failure was sought.

From the experimental results it is seen that $\dot{\gamma} = 2.5\,sec^{-1}$ corresponds to the point at which vortex growth first begins. Therefore, something may happen to the flow field in conjunction with vortex growth which limits the convergence of the method. From the birefringence measurements made on LDPE it is recalled that this polymer exhibited steep stress gradients leading up to and away from the re-entrant corner and that significant stress overshoot also occurred at the corner. It was believed in this study, and has been stated in other studies, that failure of the method may be due to its inability to approximate these gradients. Based on this the FEM code was modified to reduce the stresses in the corner region. This was accomplished by setting the relaxation time of the polymer equal to zero at those elements which were in contact with the re-entrant corner. In doing so the PTT model was reduced to the Newtonian model at these elements and no normal stresses were predicted and the shear stress was calculated by telling the computer what the value of η_1 was at those elements. (The value of η_1 was chosen based on the value of η calculated when λ was not zero.) Incorporating this method it was possible to increase the limit of convergence and the onset of vortex growth was predicted at $\dot{\gamma} = 2.5\,sec^{-1}$ as shown in the previous section. However, this method did not result in convergence at any higher rates.

Based on these results it is apparent that high stress gradients right at the corner are not the entire cause of convergence limit. If this were so convergence should have occurred at rates higher than 2.5 sec^{-1}. However, it may be that it is necessary to provide a more gradual smoothing of the stress gradients by reducing the relaxation time at more elements

than those just in contact with the corner. Although stress reduction at the corner may have improved convergence slightly it may have been in this study that non-convergence at even higher rates was due to the presence of an additional gradient at the corner. By just changing the corner elements the stress could have still been rising rapidly on approach to the corner but dropped rapidly at the corner, because of the zero relaxation time, and then increased again going downstream. Although artificial changes to the stress gradients such as these may help improve the convergence limit it must be remembered that this is just a means to identify the cause on non-convergence since incorporating a zero relaxation time only masks the true situation. Ultimately, another method will have to be developed if solutions at higher rates are to be obtained.

5.7.4 Effect of Extensional Properties on Numerical Predictions of Vortex Growth

In the previous sections the ability of the PTT model in conjunction with the penalty finite element method to predict the entry flow behavior of LDPE and polystyrene has been discussed. It was shown that both the Newtonian-like flow of polystyrene as well as the initial stages of the vortex growth of LDPE could be predicted quite well. However, it was not stated to what degree the extensional properties of the polymer affected the flow simulations. As it was because of the PTT model's ability to predict the differences in extensional properties of LDPE and polystyrene that it was chosen for use in the numerical simulations it is appropriate that the effect of extensional properties be examined.

It was shown earlier that direct control over the PTT model's prediction of extensional properties is obtained through the parameter ε. Small values of ε lead to large predictions of η_E while large values of ε lead to predictions of η_E closer to the Trouton value. The effect of ε on shear properties is negligible for small values and there are only minor changes in the

shear thinning behavior of η when ε is increased to 0.1. With this in mind the effect of ε, and therefore the extensional properties, on the numerical simulation of entry flow behavior was examined by varying ε from 0.1 to 0.001.

For the case of the Newtonian-like flow of polystyrene and LDPE at low rates it was found that the value of ε had no effect on the flow predictions. The results for LDPE would be expected since at low flow rates the strain rates encountered in the entry region would be low and in the range where the PTT model predicts η_E to be at the Trouton value. In this range of strain rates ε has no effect on η_E. The same reasoning can be applied to the behavior of polystyrene.

At higher flow rates it was found that ε had an effect on the streamline predictions. Streamline plots for LDPE at 2.5 sec^{-1} are presented in Figure 57 on page 173 for a range of ε values. For this shear rate, which represents the beginning of the vortex growth region, ε has a significant effect on the predicted flow behavior. It is seen that as ε is increased the vortex decreases in size and recirculation rate decreases in intensity. This shows the relation between vortex growth and the extensional properties of the polymer. For small ε (high η_E) vortex size and recirculation rate are large but for large ε (small η_E) just the opposite occurs. Therefore, based on these results it would seem necessary, in the numerical simulation of entry flow, to incorporate a constitutive equation which is capable of giving realistic predictions of the extensional properties of the fluid.

5.8 *Stress Predictions Using the PTT Model*

In the previous section the accuracy of the numerical solutions was evaluated by comparison of numerical and experimental streamline patterns. It was found for the range over which solutions were obtained that the numerical method did well in predicting the entry flow behavior of polystyrene and LDPE. In this section a more quantitative evaluation of the nu-

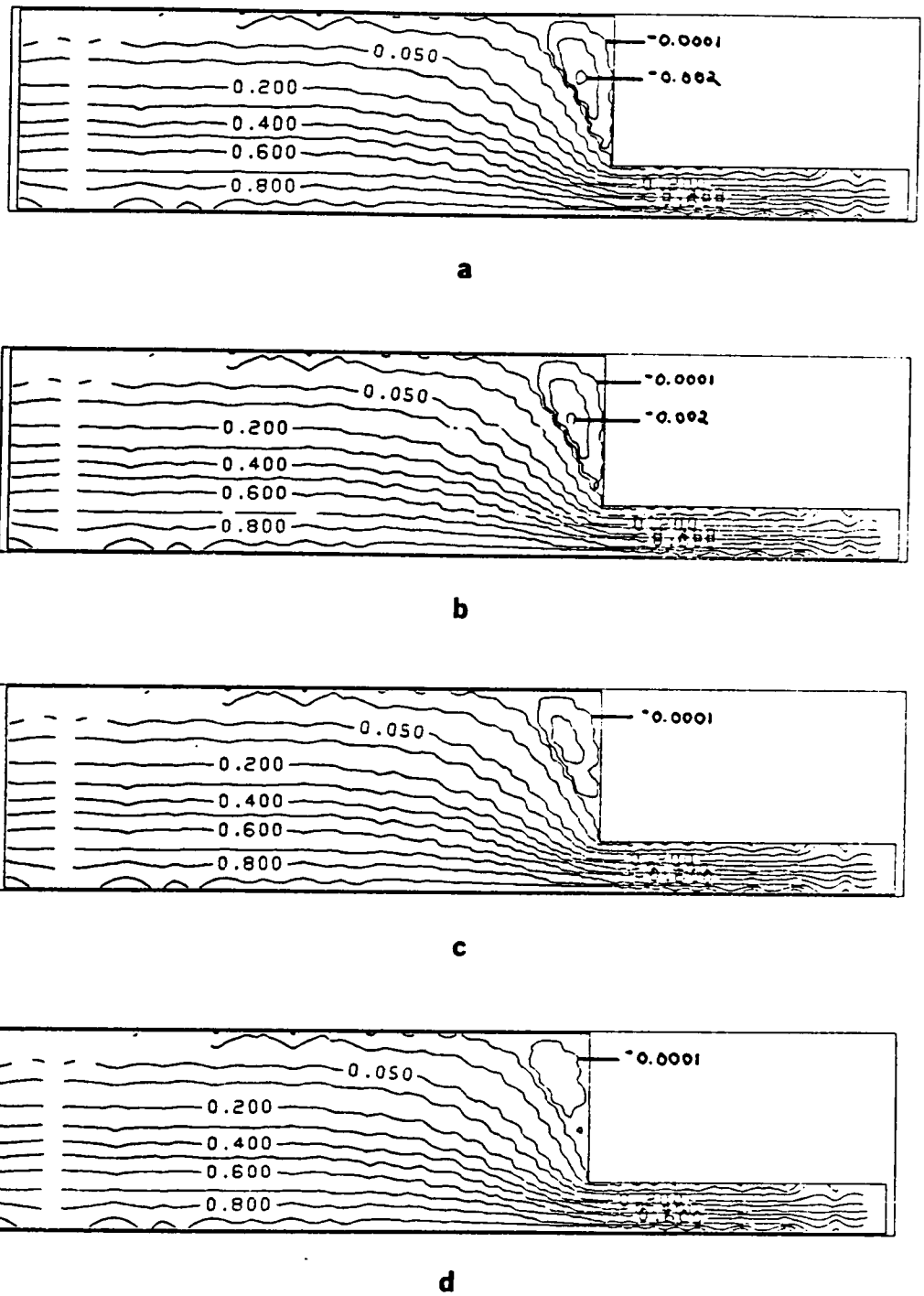

Figure 57. Effect of ε on Streamline Pattern Predictions of LDPE at $\dot{\gamma}=2.5\ sec^{-1}$, 4:1 Contraction: a) ε = 0.001 b) ε = 0.01 c) ε = 0.05 d) ε = 0.1

merical method is given by comparison of numerical and experimental stress distributions. As vortex growth has been attributed to the development of large extensional stresses in the entry region the ability of the numerical method to predict these stresses is of importance.

Comparison between numerical and experimental values of the centerline extensional stress in polystyrene is presented in Figure 58 and Figure 59 on page 175. The plots are again of the ratio for the centerline extensional stress to the downstream wall shear stress. It can be seen from these figures that the PTT model does very well in predicting the stress in both the 4:1 and the 8:1 geometries. The peak stress predicted by the model is slightly higher than that found experimentally but other than that the fit is good. The model does well in predicting both the rise in stress up to the corner and the relaxation of stress downstream of the corner. It also does well in predicting the increase in stress with increasing shear rate.

Comparison of numerical and experimental results is not as easy for LDPE. Since numerical solutions were only obtained at low flow rates the number of experimental points available is limited. The results are shown in Figure 60 on page 177 for the 4:1 contraction and in Figure 61 on page 178 for the 8:1 contraction. For a shear rate of 1 sec^{-1} the PTT model does well in predicting the stresses in LDPE. It also does well in predicting the increase in stress with increasing shear rate in the 8:1 geometry. However, in the 4:1 geometry there is a prediction of lower stress at 2.5 sec^{-1} than at 1 sec^{-1}. Obviously this cannot be the case and it is believed that this result is due to the incorporation of a zero relaxation time at the corner elements for $\dot{\gamma} = 2.5\,sec^{-1}$. The use of the zero relaxation time allowed for the convergence of the method by the reduction of stresses at the corner. This effect was felt at the centerline and resulted in a prediction of lower stress than actually occurred in the flowing system. Based on this result it would also be expected that the stress in the 8:1 contraction at $\dot{\gamma} = 2.5\,sec^{-1}$ should also be higher. Overall the prediction of stress by the PTT model in both LDPE and polystyrene appears to be good.

In addition to the comparison of numerical and experimental results, comparison can also be made between the predictions for the two polymers and the two geometries. Figure 62 on page 179 and Figure 63 on page 180 compare the predicted extensional stress ratio in LDPE

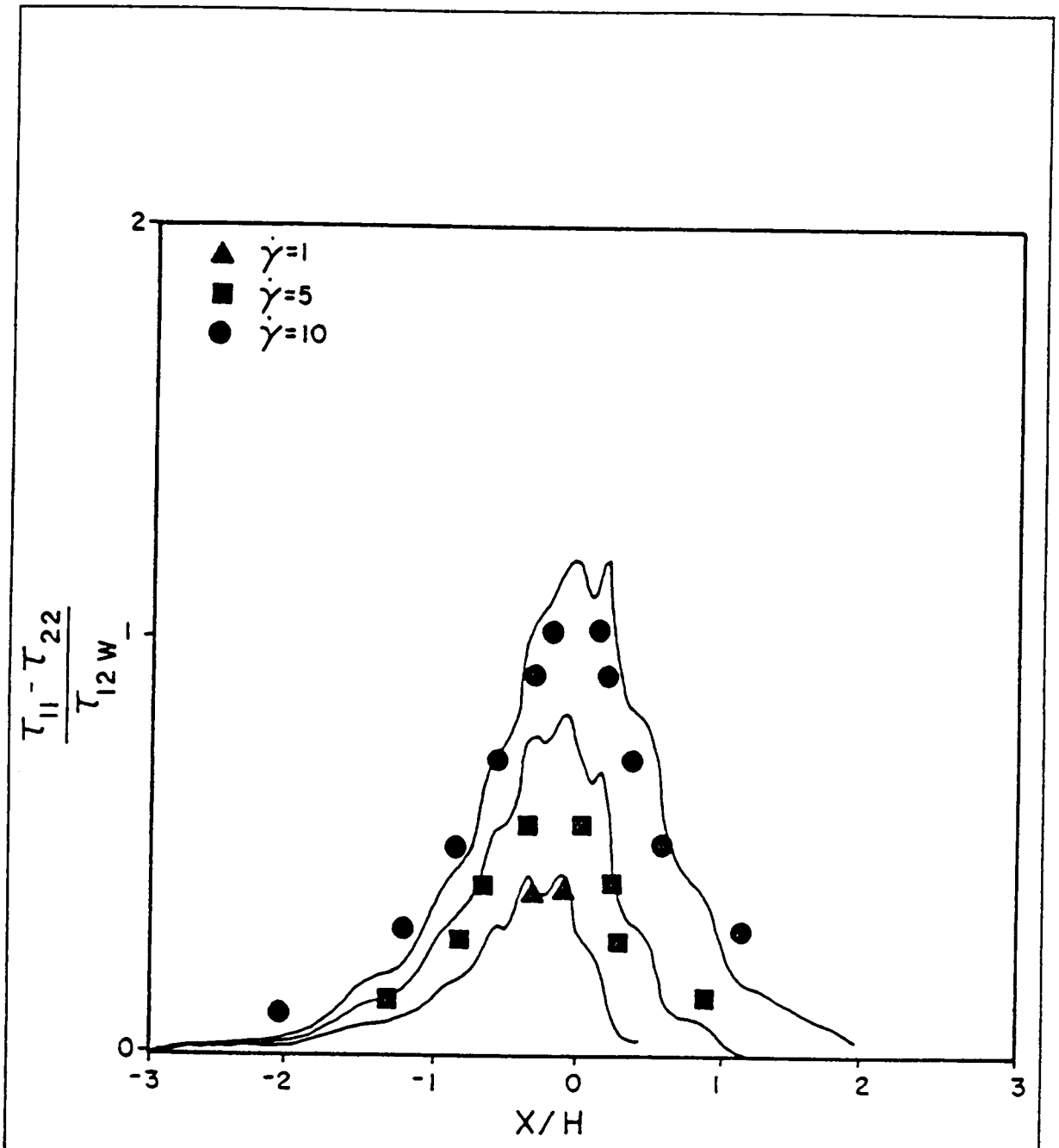

Figure 58. Extensional Stress Ratio Predictions for Polystyrene at 190° C, 4:1 Contraction: Symbols represent experimental data

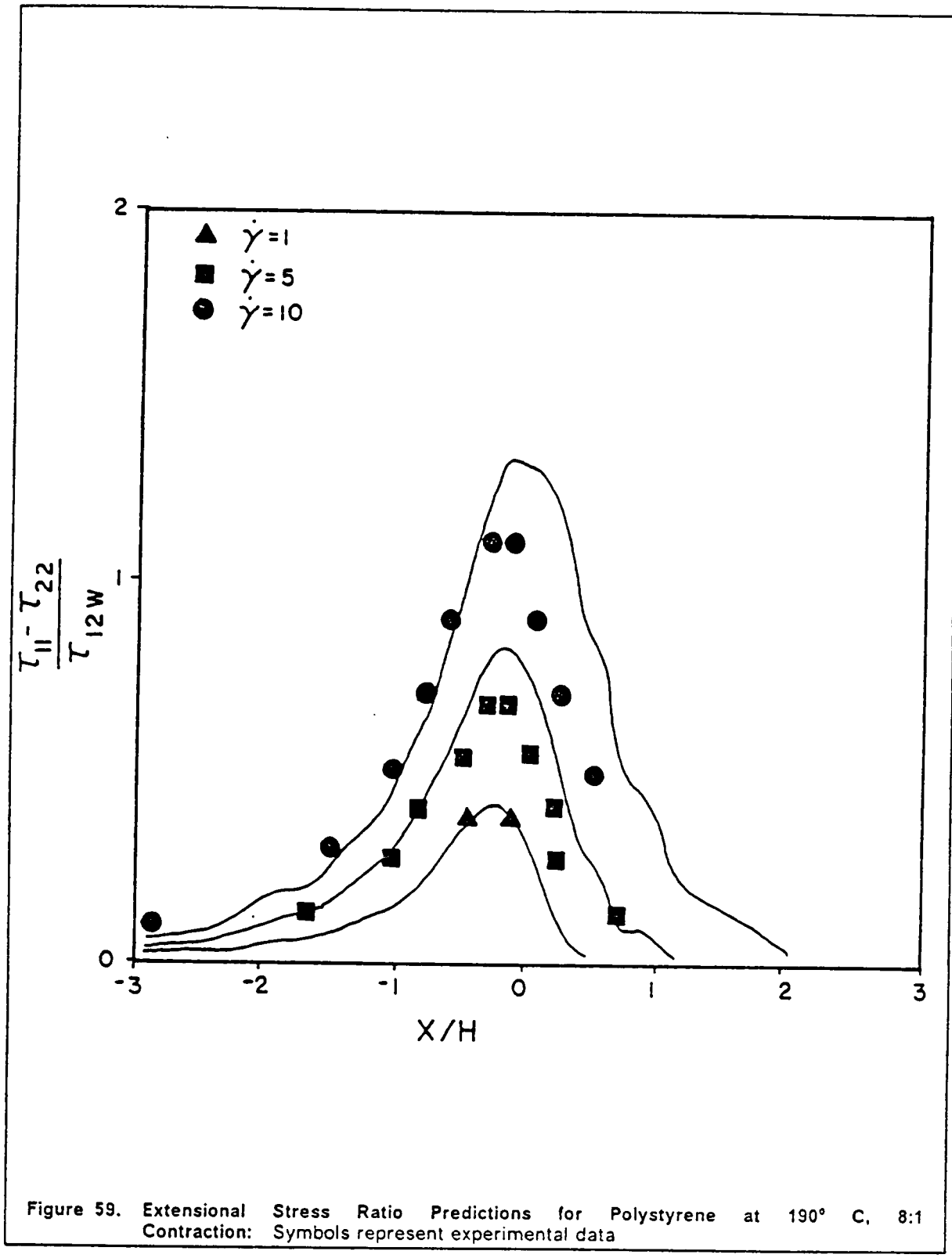

Figure 59. Extensional Stress Ratio Predictions for Polystyrene at 190° C, 8:1 Contraction: Symbols represent experimental data

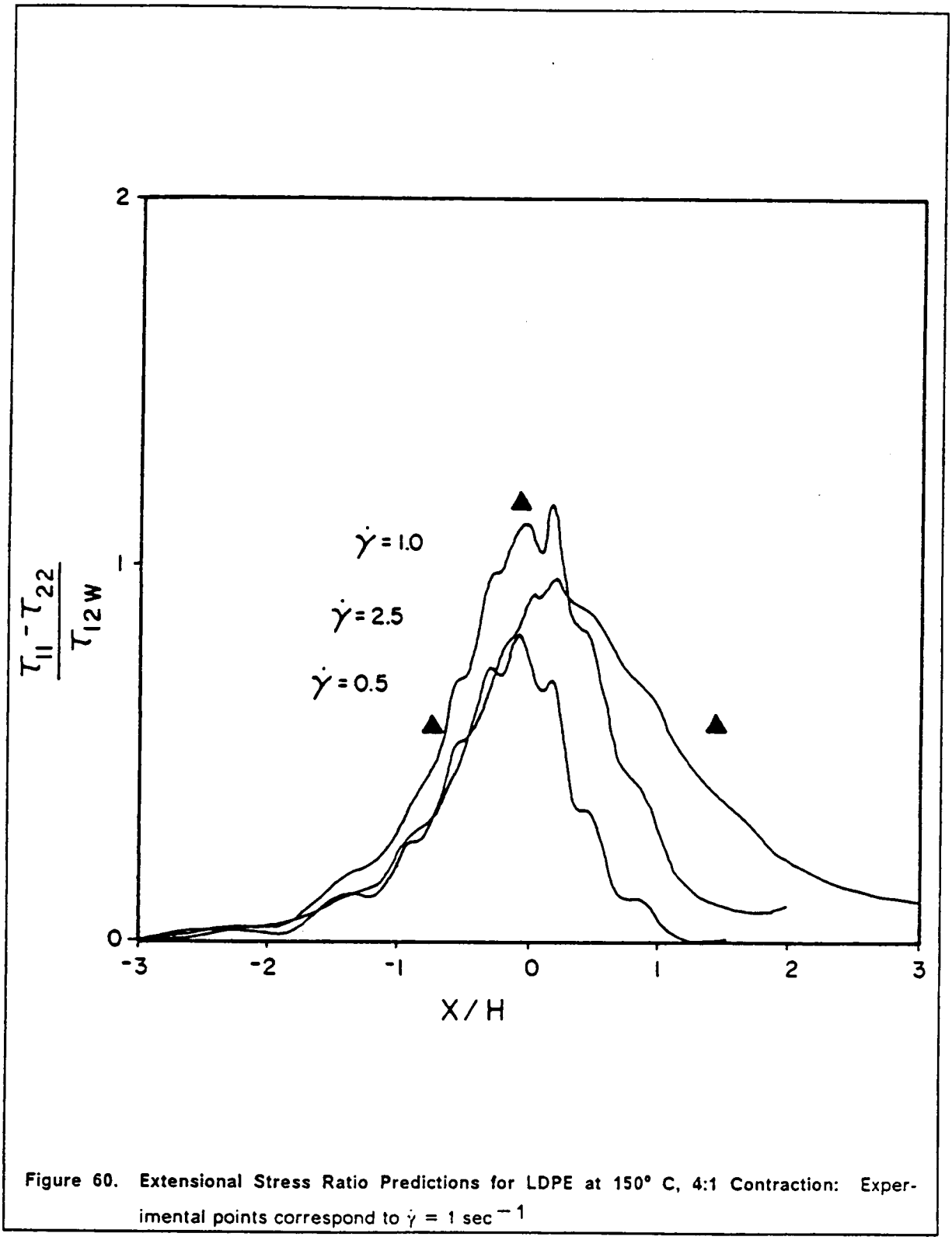

Figure 60. **Extensional Stress Ratio Predictions for LDPE at 150° C, 4:1 Contraction:** Experimental points correspond to $\dot{\gamma} = 1\ sec^{-1}$

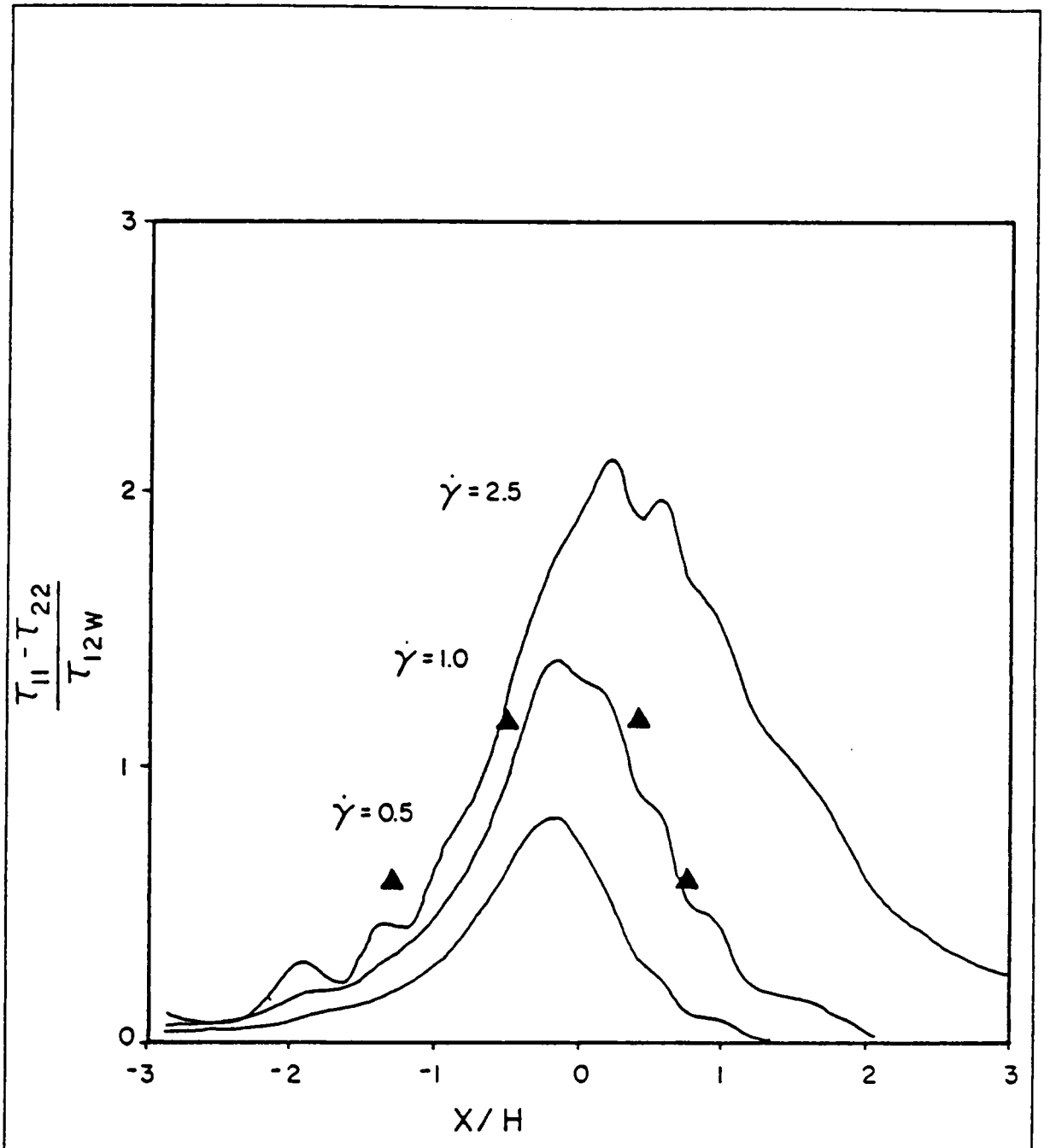

Figure 61. **Extensional Stress Ratio Predictions for LDPE at 150° C, 8:1 Contraction:** Experimental points correspond to $\dot{\gamma} = 1\ sec^{-1}$

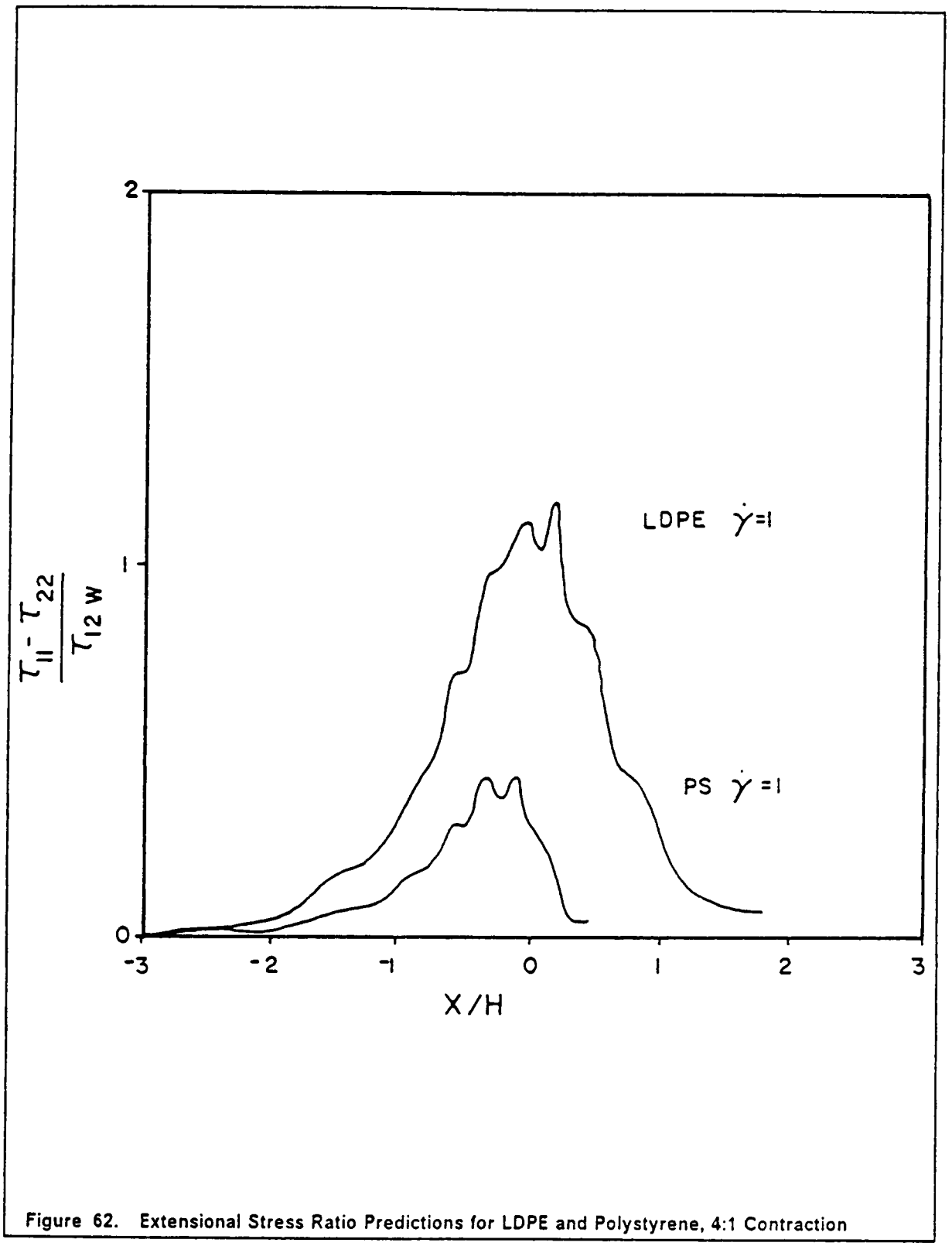

Figure 62. Extensional Stress Ratio Predictions for LDPE and Polystyrene, 4:1 Contraction

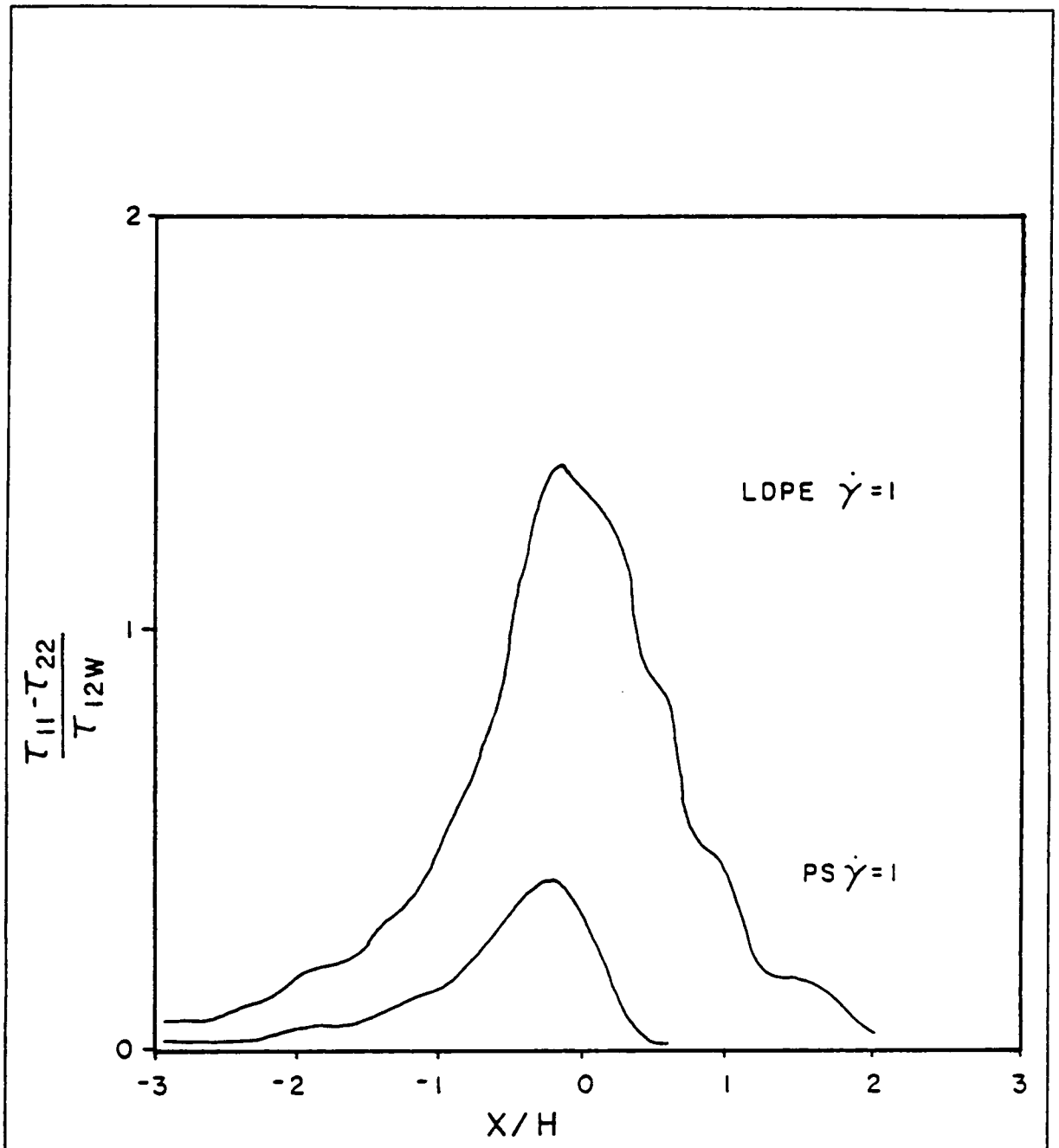

Figure 63. Extensional Stress Ratio Predictions for LDPE and Polystyrene, 8:1 Contraction

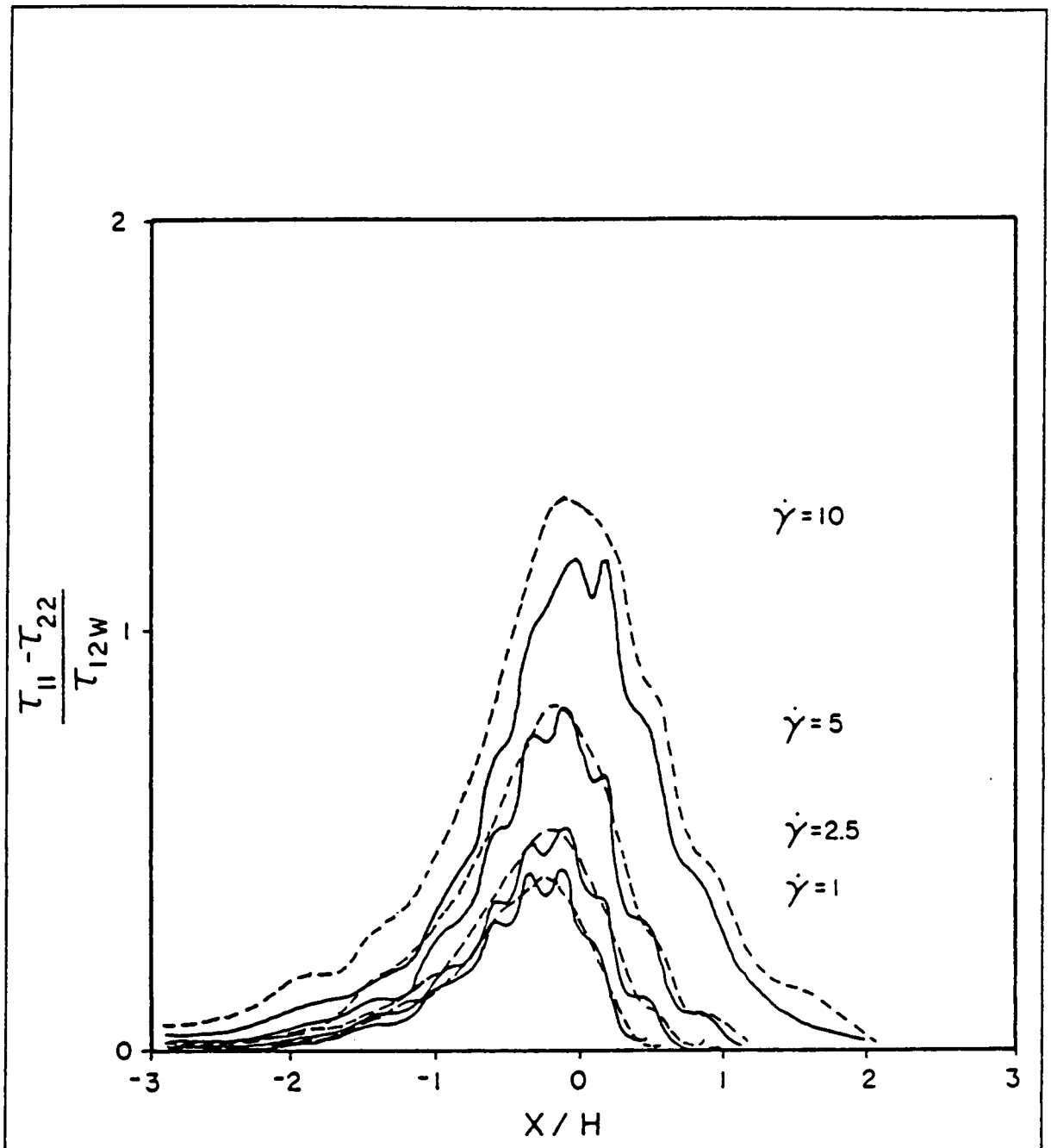

Figure 64. Extensional Stress Ratio Predictions for Polystyrene at 190° C, 4:1 and 8:1 Contractions: Dashed curve corresponds to 4:1 contraction

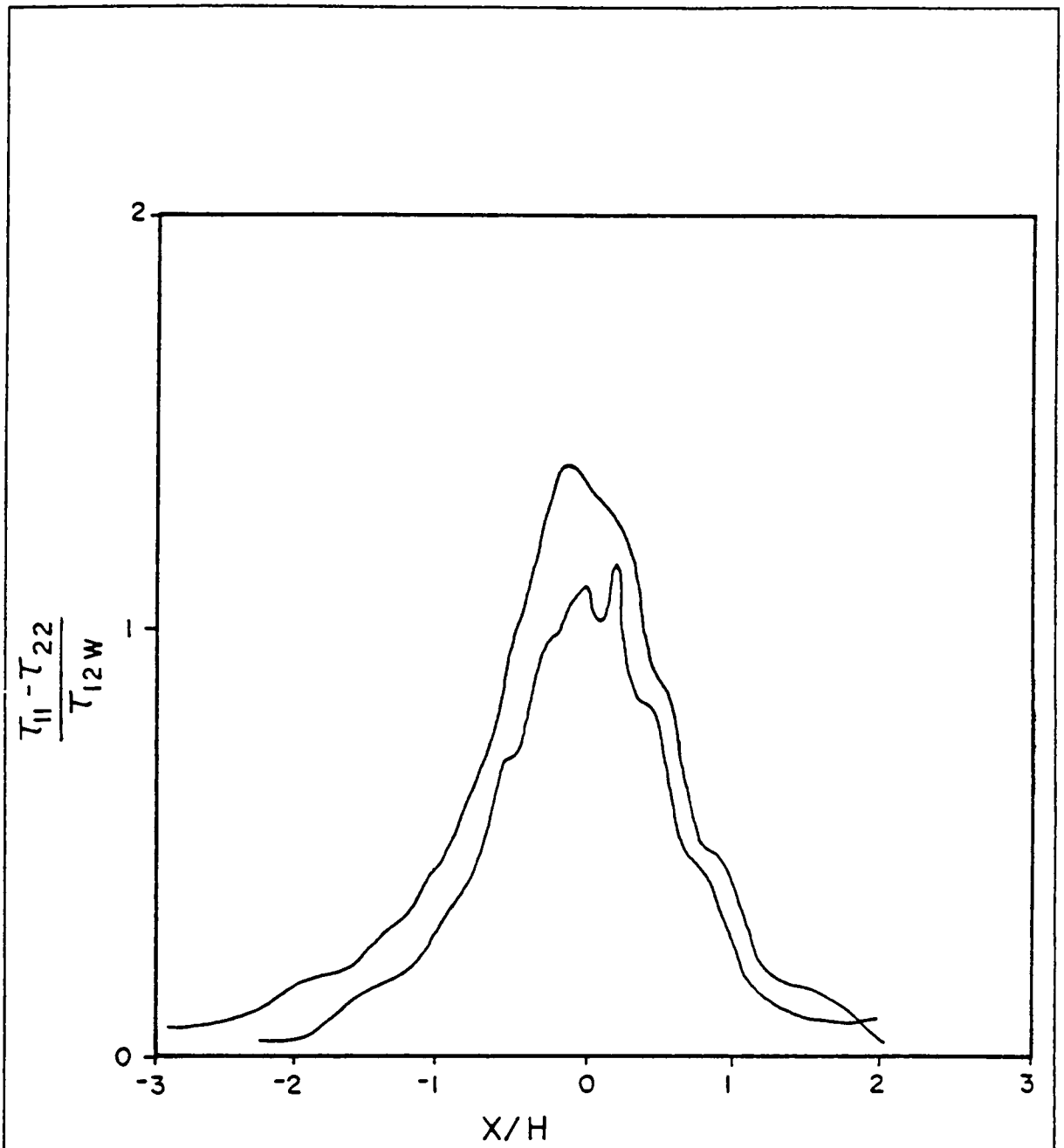

Figure 65. **Extensional Stress Ratio Predictions for LDPE at 150° C, 4:1 and 8:1 Contractions,** $\dot{\gamma}=1\ sec^{-1}$: Lower curve- 4:1 contraction

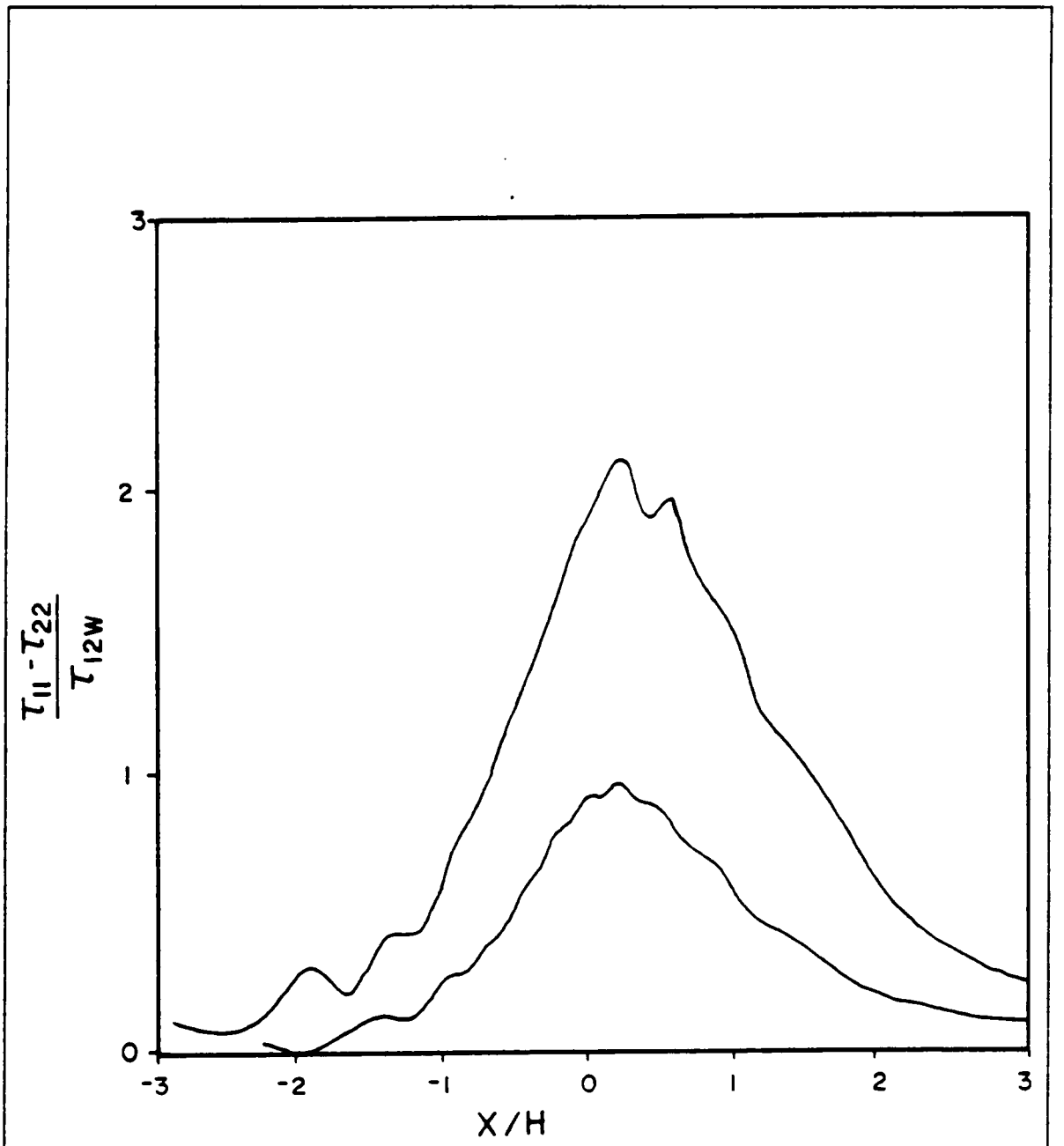

Figure 66. Extensional Stress Ratio Predictions for LDPE at 150° C, 4:1 and 8:1 Contractions, $\dot{\gamma}$=2.5 sec^{-1}: Lower curve- 4:1 contraction

and polystyrene. It is seen that the level of extensional stress in LDPE is significantly higher than that in polystyrene even at these low rates. The difference becomes even greater in the 8:1 contraction. These results are in agreement with what was found experimentally at higher rates (Figure 36 on page 135 and Figure 37 on page 136). Also, agreement is found for the effect of contraction ratio on extensional stress. Results for the 4:1 and 8:1 geometries are presented in Figure 64 on page 181 for polystyrene. It is seen that over the range of shear rates for which solutions were obtained there is very little effect due to the contraction ratio. However, in LDPE higher levels of stress are found in the 8:1 contraction than in the 4:1 (Figure 65 on page 182 and Figure 66 on page 183). These results agree with what was found in section 5.4 and as such provide numerical support for the statements on vortex growth which were presented there.

In this section and sections 5.5 and 5.7 it has been shown to what degree the PTT model in conjunction with the finite element method is capable of predicting the rheological properties, entry flow streamline patterns, and entry flow stress distribution of LDPE and polystyrene. It was shown for the most part that the predictions are in good agreement with experimental data. As such the numerical results provide support for the relationship between extensional properties and entry flow behavior and therefore provide an additional basis upon which conclusions can be made.

6.0 CONCLUSIONS AND RECOMMENDATIONS

6.1 Conclusions: Experimental Study

In Chapter 5 results were presented and discussed in regards to the experimental and numerical study of the entry flow behavior of polymer melts. The conclusions about these results are presented in this chapter. In regards to the experimental work there have been two main objectives. The first was to provide an understanding of why vortices form in the first place. As was pointed out in Chapter 2, in previous studies the presence or absence of vortices was taken as a given and correlation of flow behavior with rheological properties proceeded from that point. In this study, the position taken was that it was necessary to first understand why vortices form and then, based on that understanding, fulfil the second objective of this study which was to correlate the flow behavior with rheological, geometrical, and molecular parameters. Conclusions regarding vortex formation are presented in statements 1-3 and those regarding correlation of flow behavior are presented in statements 4-8.

1. Vortex growth occurs due to a polymer's resistance to flow under the influence of extensional strain. As was seen for LDPE the restriction to flow, caused in this case by the high degree of branching in the polymer, resulted in the flow streamlines pulling up out of the

corners and effectively funneling the polymer from the upstream channel to the smaller downstream channel. As a result secondary flow cells formed in the corner. For polystyrene, a linear molecule, there was much less restriction to extensional deformation and no vortex growth was exhibited.

2. Recirculation within the secondary flow cell is due to the transfer of momentum across the cell interface. Therefore, it is possible to have a secondary flow cell but no apparent recirculation if the fluid is highly viscous. This was observed for polystyrene at 165° C and for the HDPE's for which their extensional stresses were large enough to form secondary flow cells but their shear viscosity was too high to initiate recirculation within the cell. In contrast, LDPE had both large secondary flow cells and high intensity recirculation. It is believed that both effects were due to long chain branching. The branching resulted in the large extensional stresses needed to form the secondary flow cell but the branching also resulted in a lower shear viscosity for this material than would be found in a linear polymer of the same molecular weight. The lower viscosity resulted in the high intensity recirculation.

3. There is an upper limit to the amount of vortex growth exhibited by a polymer. Although this is not completely understood it is believed that there might be a competing process which acts to prevent vortex growth at higher rates. As shown by birefringence measurements, extensional stresses in LDPE continue to increase with increasing flow rate yet vortex size reaches an upper limit beyond which no further growth is observed. Also, polystyrene exhibits no vortex growth even though at high flow rates the extensional stresses in the polymer are higher than those in LDPE when vortex growth first begins.

4. Although elasticity can be used to correlate entry flow behavior of a given type of polymer it cannot be used to correlate the flow behavior of different types of polymers. It was shown that We could be used to correlate the entry flow behavior of HDPE's of different M_w but when compared with LDPE and polystyrene it was found that the relation did not hold. The detachment lengths exhibited by the polymers did not order with the values of G'/G'' of the polymers.

5. There is not a critical value of We above which vortex growth occurs for all polymers. It was found that vortex growth began in LDPE at We$\cong$1 but no vortex growth was observed in polystyrene at 190° C up to We =1.6. Therefore, We by itself cannot be used to predict the onset of vortex growth.

6. Based on statements 3-5 it is concluded that vortex growth cannot be predicted based on shear or extensional properties by themselves but on a combination of the two. It was found that the ratio of the centerline extensional stress to the downstream wall shear stress correlated best with the flow behavior. The ratio was 2-3 times greater in magnitude for LDPE, which exhibited vortex growth, than for polystyrene which did not.

7. Flow geometries with large contraction ratios result in larger vortices due to the higher strain rates imposed in the entry region. This was seen for LDPE in the 4:1 and 8:1 geometries for which larger vortices were observed in the 8:1 contraction. It was reasoned that the increased vortex size was due to the higher strain rates imposed on the fluid in the 8:1 contraction due to the greater acceleration experienced in this geometry than in the 4:1 geometry. The higher strain rates resulted in higher extensional stresses because the polymer's extensional viscosity is an increasing function of strain rate. No change was observed for polystyrene in going from the 4:1 to the 8:1 contraction since this polymer's extensional viscosity is relatively rate insensitive.

8. Changes in a polymer's molecular characteristics which result in an increase in the polymer's resistance to flow in extension results in larger vortices. This was observed for the polystyrene blend and the different M_w HDPE's. For the polystyrene blend it was found that the addition of a small amount of high molecular weight chains resulted in a minimal change in the viscometric properties of the polymer at the shear rates of the flow experiments but there was a doubling of the magnitude of the extensional viscosity. The result was a slight increase in detachment length observed in the blend. The same results were observed for the HDPE's for which the differences in M_w were much greater.

6.2 Conclusions: Numerical Study

The final objective of this study was to provide some improvement to the numerical prediction of entry flow based on the experimental findings of this work. From the experimental work it was found that the extensional properties of a polymer are most important in determining if vortex growth will occur. As such it was necessary to incorporate in the numerical method a constitutive equation which was capable of predicting not only the viscometric properties but more importantly the extensional properties of the polymer. In the numerical work the flow behavior of LDPE and polystyrene was to be simulated. Therefore, it was also necessary that the constitutive equation be able to predict the significantly different responses of the two polymers in extension. Based on these considerations the Phan-Thien Tanner (PTT) model was chosen. Conclusions regarding the ability of this model to predict the rheological properties of the polymers that were used in the numerical work follow. Also, conclusions are given regarding the ability of the PTT model in conjunction with the finite element method to simulate entry flow behavior of LDPE and polystyrene.

1. The PTT model gives good predictions not only of the viscometric properties but also of the transient and steady-state extensional properties of LDPE and polystyrene. It was found experimentally that polystyrene exhibits a bounded stress growth in extension whereas that of LDPE is unbounded within the strain range of the rheometer. The PTT model was able to predict this significant difference in the stress growth behavior for the two polymers. Also, by means of an adjustable parameter in the model, it was possible to predict the difference in $\frac{\eta_{Emax}}{\eta_0}$ of these two polymers.

2. The PTT model in conjunction with the finite element method gives good qualitative agreement with the experimentally obtained streamline patterns and good quantitative agreement with the experimentally obtained extensional stress ratio, $\frac{\tau_{11} - \tau_{22}}{\tau_{12w}}$, for LDPE and polystyrene. Although there was not much of a challenge in modelling the flow behavior of polystyrene there was one for LDPE and the method was able to predict the vortex growth

exhibited by LDPE. Also, the experimentally observed effects of contraction ratio on streamline patterns and stress within the entry region were predicted numerically.

3. An increase in the convergence limit of the method is achieved by incorporating a zero relaxation time at the corner elements. It was found for LDPE that the solution would not converge at a rate corresponding to that at which vortex growth was observed experimentally. By using a zero relaxation time at the corner elements the limit of convergence was increased slightly and vortex growth was predicted. It is thought that steep stress gradients near the corner reduced by the zero relaxation time thereby allowing solution at higher rates.

4. The numerical predictions provide independent support to the statement that vortex growth is related to the extensional properties of the polymer. It was possible to adjust the predicted extensional response of a polymer through adjustment of the ε parameter in the PTT model. The parameter controls the value of $\frac{\eta_{E_{max}}}{\eta_0}$. It was found that under Newtonian-like flow conditions the predicted flow behavior did not depend on the value of $\frac{\eta_{E_{max}}}{\eta_0}$. However, under vortex growth conditions the size of the vortex was dependent on this value. For LDPE it was found that, holding all other conditions equal, reducing $\frac{\eta_{E_{max}}}{\eta_0}$ reduced vortex size thereby providing a numerically proven link between vortex growth and extensional properties.

5. An optimum mesh exists for a given flow geometry. In regards to mesh refinement it was found that there was an optimum number of elements for a mesh. Increase or decrease in this number and arrangement of elements led to worse solutions. In regards to the L/D of the exit region it was found, for the case of the optimum mesh, that an increase in L/D from 3 to 10 did not change the solution thereby indicating that L/D=3 is adequate even for predicting the flow behavior of polymers which exhibit slow stress relaxation.

6.3 Recommendations

Although many questions have been answered in regards to entry flow there are many which remain to be addressed. Given below are recommendations for further work in this area:

1. Examine other polymers to further verify the relation, presented in this study, between vortex growth and the extensional stress ratio $\frac{\tau_{11} - \tau_{22}}{\tau_{12w}}$. Ideally, to achieve this goal it would be desirable to examine a number of samples of a given polymer, such as polystyrene, of a given M_w which differ only by the degree of branching. The purpose would be to have different polymers which exhibit a range of entry flow patterns from that observed in this study for polystyrene to that of LDPE. It would then be possible to track the change in entry flow behavior with that of the extensional stress ratio.

2. Observe the entry flow behavior of polystyrene at flow rates up to the point of melt fracture to see if vortex growth occurs. Vortex growth was not observed in this study for polystyrene up to the highest flow rates obtainable in the apparatus. However, it would be of interest to see if the extensional stress ratio ever becomes comparable to that of LDPE and if vortex growth occurs before the onset of any instability.

3. Determine the extensional strains and strain rates encountered in the entry region. It was noted that the extensional stress exhibited by LDPE rises rapidly with strain and that this higher level of stress contributes to vortex growth. It is not known though, what strains or strain rates are encountered in the entry region. Therefore, it is not known what point on the stress-strain curve corresponds to the conditions encountered in the flow. Such information would be helpful in determining the magnitude of the extensional stresses in the entry region.

4. Examine axisymmetric entry flow. Although there are experimental difficulties in observing axisymmetric flow this type of geometry would be useful in evaluating the relation between vortex growth and extensional stress. It would be expected that the strain rates en-

countered in an axisymmetric contraction would be higher than those in a planar contraction and the degree of vortex growth would correspondingly be affected.

5. Obtain extensional viscosity measurements at higher strains and higher temperatures. It was noted earlier that because of the limits of the extensional rheometer it was not possible to determine if there was a steady-state extensional viscosity for LDPE. Therefore, fit of the constitutive equation parameters was based on literature data. Knowledge of such information would be useful in fitting model parameters. Also, if extensional measurements could be obtained at higher temperatures other polymers of interest could be used in relating flow behavior to extensional properties.

6. Obtain velocity and entrance pressure loss data. This information would be useful in the evaluation of the accuracy of the numerical calculations.

7. Incorporate slip at the corner in the numerical simulation. It was found in this study that the incorporation of a zero relaxation time at the corner resulted in an increase in the convergence limit. Use of slip may similarly improve convergence by reducing steep gradients at the corner.

REFERENCES

1. H. Giesekus, Rheol. Acta, 7:2 (1968) 127.
2. R.L. Boles, H.L. Davis, and D.C. Bogue, Polym. Eng. & Sci., 10:1 (1970) 24.
3. T.F. Ballenger and J.L. White, Chem. Eng. Sci., 25 (1970) 1191.
4. T.F. Ballenger, I-Jen Chen, J.W. Crowder, G.E. Hagler, D.C. Bogue, and J.L. White, Trans. Soc. Rheol., 15:2 (1971) 195.
5. Y. Tomita and T. Shimbo, Appl. Polym. Symp., 20 (1973) 137.
6. T.Hasagawa and T. Iwaida, J. Non-Newt. Fluid Mech., 15 (1984) 279.
7. H. Nugyen and D.V. Boger, J. Non-Newt. Fluid Mech., 5 (1979) 353.
8. P.J. Cable and D.V. Boger, AIChE J., 24:5 (1978) 869.
9. K.P. Jackson, K. Walters, and R.W. Williams, J. Non-Newt. Fluid Mech., 14 (1984) 173.
10. T.R. Fields and D.C. Bogue, Trans. Soc. Rheol., 12:1 (1968) 39.
11. J.H. Southern and D.R. Paul, Polym. Eng. & Sci., 14:8 (1974) 560.
12. G.D. Eisenbrand and J.D. Goddard, J. Non-Newt. Fluid Mech., 11 (1982) 37.
13. A.L. Halmos and D.V. Boger, Trans. Soc. Rheol., 20:2 (1976) 253.
14. R.J. Binnington, G.J. Troup, and D.V. Boger, J. Non-Newt. Fluid Mech., 12 (1983) 255.
15. D.R. Oliver and R. Bragg, Can. J. Chem. Eng., 51 (1973) 287.
16. A.B. Metzner, E.A. Uebler, and C.F. Chan Man Fong, AIChE J., 15:5 (1969) 750.
17. T. Cochrane, K. Walters, and M.F. Webster, Phil. Trans. R. Soc. Lond., A301 (1981) 163.

18. K. Walters and M.F. Webster, Phil. Trans. R. Soc. Lond., A308 (1982) 199.

19. T. Cochrane, K. Walters, and M.F. Webster, J. Non-Newt. Fluid Mech., 10 (1982) 95.

20. P.J. Cable and D.V. Boger, AIChE J., 24:6 (1978) 992.

21. P.J. Cable and D.V. Boger, AIChE J., 25:1 (1979) 152.

22. J.L. Dudas and J.S. Vrentas, Trans. Soc. Rheol., (1973) 89.

23. J.L. White and A. Kondo, J.Non-Newt. Fluid Mech., 3 (1978/79) 41.

24. D.V. Boger, Pure & Appl. Chem., 57:7 (1985) 921.

25. D.V. Boger, *Rheology Volume 1: Principles*, Ed. G. Astarita, G. Marrucci, and L. Nicolais, New York : Plenum Press, 1980.

26. F.N. Cogswell, Polym. Eng. & Sci., 12:1 (1972) 64.

27. C.Y. Ma, J.L. White, F.C. Weissert, and K. Min, J. Non-Newt. Fluid Mech., 17 (1985) 275.

28. W. Philippoff and F.H. Gaskins, Trans Soc. Rheol., 2 (1958) 263.

29. C.D. Han and L.H. Drexler, J. Appl. Polym. Sci., 17 (1973) 2329.

30. L.H. Drexler and C.D. Han, J. Appl. Polym. Sci., 17 (1973) 2355.

31. C.D. Han and L.H. Drexler, J. Appl. Polym. Sci., 17 (1973) 2369.

32. J.P. Tordella, Trans. Soc. Rheol., 1 (1957) 203.

33. H. Schott and W.S Kaghan, Ind. Eng. Chem., 51 (1959) 844.

34. E.B. Bagley and A.M. Birks, J. Appl. Physics, 31:3 (1960) 556.

35. T.F. Ballenger and J.L. White, J. Appl. Polym. Sci., 15 (1971) 1949.

36. P.L. Clegg, Trans. J. Plast. Inst., 26 (1958) 151.

37. J.L. den Otter, Plastics & Polym., 38 (1970) 1555.

38. J.L. White, Appl. Polym. Symp., 20 (1973) 155.

39. H. Münstedt, J. Rheol., 23:4 (1979) 421.

40. J.M. Dealy, J. Non-Newt. Fluid Mech., 4 (1978) 9.

41. J.M. Dealy, *Rheometers for Molten Plastics*, New York : Van Nostrand Rheinhold Co., 1982.

42. Y. Ide and J.L. White, J. Appl. Polym. Sci., 22 (1978) 1061.

43. R. Muller, J.L. Barea, D. Froelich, B. Morese-Seguela, and D. Constantin, Society of Plastics Engineers ANTEC Technical Papers, 31 (1985) 616.

44. L.A. Utracki and A.M.Catani, Polym. Eng. & Sci., 25:11 (1985) 690.

45. V.S. Au-Yeung and C.W. Macosko, J. Rheol., 25:4 (1982) 445.

46. A. Franck and J. Meissner, Rheol. Acta, 23 (1984) 117.

47. H. Münstedt, J. Rheol., 24:6 (1980) 847.

48. H. Münstedt, *Rheology Volume 2: Fluids*, Ed. G. Astarita, G. Marrucci, and L. Nicolais, New York : Plenum Press, 1980.

49. J.L. White, Appl. Polym. Symp., 33 (1978) 31.

50. H. Münstedt and H.M. Laun, Rheol. Acta., 20 (1981) 211.

51. D.M. Kalyon and E.H. Moy, Society of Plastics Engineers ANTEC Technical Papers, 31 (1985) 680.

52. T. Raible, A. Demarmels, and J. Meissner, Polymer Bulletin, 1 (1979) 397.

53. F.N. Cogswell, Appl. Polym. Symp., 27 (1975) 1.

54. R.J. Binnington and D.V. Boger, In Press J. Rheol.

55. R.J. Binnington and D.V. Boger, In Press Polm. Eng. & Sci.

56. K. Walters, Proc. IX Intl. Congress on Rheology, (1984) 31.

57. T. Ballenger, M.S. Thesis, Univ. of Tenn., 1971.

58. J. Meissner, Society of Plastics Engineers ANTEC Technical Papers, 31 (1985) 606.

59. M.J. Crochet and K. Walters, Ann. Rev. Fluid Mech., 15 (1983) 241.

60. M. A. Mendelson, P.W. Yeh, R.A. Brown, and R.C. Armstrong, J. Non- Newt. Fluid Mech., 10 (1982) 31.

61. P.W. Yeh, M.E. Kim-E, R.C. Armstrong, and R.A. Brown, J. Non-Newt. Fluid Mech., 16 (1984) 173.

62. S.L. Josse and B.A. Finlayson, J. Non-Newt. Fluid Mech., 16 (1984) 13.

63. G.V. Vinogradov and V.N. Manin, Kolloid Z.-Z Polymere, 201 (1964) 93.

64. D.V. Boger and A.M. Rama Murthy, Rheol. Acta, 11 (1972) 61.

65. J.R.A. Pearson and T.J.F. Pickup, Polymer, 14 (1973) 209.

66. K. Strauss and R. Kinast, Colloid Polym. Sci., 252:9 (1974) 753.

67. M. Shirakashi, Y. Ishida, and S. Wakiya, Rheol. Acta, 22 (1983) 462.

68. E.B. Bagley and H.P. Schreiber, Trans. Soc. Rheol., 5 (1961) 341.

69. J.P. Tordella, J. Appl. Polym. Sci., 7 (1963) 215.

70. N.I. Insarova, Polym. Mech., 5:3 (1969) 487.

71. Y. Oyanagi and Y. Yamaguchi, J. Soc. Mater. Sci. Jap., 20 (1971) 659.

72. G.V. Vinogradov, N.I. Insarova, B.B. Boiko, and E.K. Borisenkova, Polym. Eng. & Sci.,12 (1972) 323.

73. Y. Oyanagi, Appl. Polym. Symp., 20 (1973) 123.

74. A.I. Isayev and R.K. Upadhyay, J. Non-Newt. Fluid Mech., 19 (1985) 135.

75. M. Kawahara and W. Takeuchi, Comp. and Fluids, 5 (1977) 33.

76. M.F. Malone and S. Middleman, Annual Meeting of AIChE, Nov. 1979.

77. M.J. Crochet and M. Bezy, J. Non-Newt. Fluid Mech., 5 (1979) 201.

78. P. Chang, T.W. Patten, and B.A. Finlayson, Comp. and Fluids, 7 (1979) 267.

79. A.R. Davies, S.J. Lee, and M.F. Webster, J. Non-Newt. Fluid Mech., 16 (1984) 117.

80. R. Keunings and M.J. Crochet, J. Non-Newt. Fluid Mech., 14 (1984) 279.

81. R.K. Upadhyay, Ph.D. Dissertation, Cornell Univ., 1982.

82. E. Mitsoulis, J. Vlachopolous, and F.A. Mirza, "Finite Element Analysis of Isothermal and Anisothermal Polymer Melt Flow", presented at IMRI/NRCC mini symposium "Mathematical Modelling of Plastics Processing and Control", Montreal Feb. 1983.

83. E. Mitsoulis, J. Vlachopolous, and F.A. Mirza, "A Numerical Study of the Effect of Normal Stresses and the Elongational Viscosity on Entry Vortex Growth and on Extrudate Swell", presented at IMRI/NRCC symposium on "Mathematical Modelling of Plastics Processing", Montreal Jan. 1984.

84. E. Mitsoulis, J.Vlachopolous, and F.A. Mirza, Polym. Eng. & Sci., 24:9 (1984) 707.

85. A.D. Gotsis, Ph.D. Dissertation, VPI&SU, Blacksburg, Virginia (1986).

86. A.V. Rama Murthy, Trans. Soc. Rheol., 18:3 (1974) 431.

87. E.T. Busby and W.C. MacSporran, J. Non-Newt. Fluid Mech., 1 (1976) 71.

88. E.B. Adams, J.C. Whitehead, and D.C. Bogue, AIChE J., 11:6 (1965) 1026.

89. K. Walters and D.M. Rawlinson, Rheol. Acta, 21 (1982) 547.

90. D.F. James and J.H. Saringer, J. Fluid Mech., 97 (1980) 655.

91. D.F. James and J.H. Sarimger, J. Rheol., 26 (1982) 321.

92. A.K. Chakraborty and A.B. Metzner, J. Rheol., 30 (1986) 29.

93. R.E. Evans and K. Walters, J. Non-Newtonian. Fluid Mech., 20 (1986) 11.

94. G. Dembek, Rheol. Acta, 21 (1982) 553.

95. D.V. Boger, D.U. Hur, and R.J. Binnington, J. Non-Newtonian Fluid Mech., 20 (1986) 31.

96. A.R. Davies, S.J. Lee, and M.F. Webster, J. Non-Newt. Fluid Mech., 16 (1984) 117.

97. R. Keunings, J. Non-Newt. Fluid Mech., 20 (1986) 209.

98. Rheometrics Inc., *Rheometrics Mechanical Spectrometer Operations Manual*, Union, New Jersey (1978).

99. R. D. Pike, Ph.D. Dissertation, VPI&SU, Blacksburg, Virginia (1984).

100. M. D. Read, Ph.D. Dissertation, VPI&SU, Blacksburg, Virginia (1986).

101. H. Janeschitz-Kriegl, *Polymer Melt Rheology and Flow Birefringence*, Springer-Verlag, New York (1983).

102. J. N. Reddy, *An Introduction to the Finite Element Method*, McGraw Hill, New York (1984).

103. N. Phan-Thien and R. I. Tanner, J. Non-Newt. Fluid Mech., 2 (1977) 353.

104. N. Phan-Thien, J. Rheol., 22:3 (1978) 259.

105. M. J. Crochet and M. Bezy, J. Non-Newt. Fluid Mech., 5 (1979) 201.

106. D. H. Pelletier, "GEN2D", Virginia Tech (1984).

107. J. L. S. Wales, *The Application of Flow Birefringence to Rheological Studies of Polymer Melts*, Delft University Press (1976).

108. L. R. G. Treloar, *The Physics of Rubber Elasticity*, 3rd Ed., Clarendon Press, Oxford (1975).

109. H. Münstedt, Trans. Soc. Rheol., 23 (1979) 421.

Appendix A. Rheological Data

Table 7. Shear Data: NPE-952, 150° C (100)

Steady Shear

$\dot{\gamma}$ (1/sec)	η (Pa-s)	N_1 (Pa)
1.00 E-2	4.24 E4	
1.59 E-2	4.30 E4	
2.51 E-2	4.31 E4	
3.98 E-2	3.83 E4	
6.31 E-2	3.61 E4	
1.00 E-1	3.00 E4	1.75 E3
1.59 E-1	2.62 E4	4.35 E3
2.51 E-1	2.16 E4	9.02 E3
3.98 E-1	1.76 E4	1.51 E4
6.31 E-1	1.41 E4	2.31 E4
1.00 E0	1.07 E4	3.09 E4
1.59 E0	7.75 E3	3.56 E4

Dynamic

ω (rad/sec)	η^* (Pa-s)	G′ (Pa)	G″ (Pa)
1.00 E-1	2.60 E4	1.24 E3	2.29 E3
1.78 E-1	2.13 E4	2.03 E3	3.21 E3
3.16 E-1	1.71 E4	3.14 E3	4.39 E3
5.62 E-1	1.33 E4	4.67 E3	5.87 E3
1.00 E0	1.03 E4	6.77 E3	7.73 E3
1.78 E0	7.78 E3	9.61 E3	9.95 E3
3.16 E0	5.80 E3	1.33 E4	1.27 E4
5.62 E0	4.26 E3	1.79 E4	1.59 E4
1.00 E1	3.09 E3	2.38 E4	1.98 E4
1.78 E1	2.22 E3	3.10 E4	2.43 E4
3.16 E1	1.57 E3	3.98 E4	2.97 E4
5.62 E1	1.10 E3	5.02 E4	3.64 E4
1.00 E2	7.70 E2	6.24 E4	4.50 E4

Table 8. Shear Data: Styron 678, 165° C (99)

Steady Shear

$\dot{\gamma}$ (1/sec)	η (Pa-s)	N_1 (Pa)
1.00 E-2	1.07 E5	
1.39 E-2	1.04 E5	
1.93 E-2	9.33 E4	
5.18 E-2	7.30 E4	
7.20 E-2	6.20 E4	2.90 E3
1.39 E-1	5.36 E4	6.73 E3
1.93 E-1	4.98 E4	9.99 E3
2.68 E-1	4.63 E4	1.52 E4

Dynamic

ω (rad/sec)	η^* (Pa-s)	G′ (Pa)	G″ (Pa)
1.00 E-1	5.61 E4	2.11 E3	5.20 E3
1.59 E-1	4.96 E4	3.64 E3	6.97 E3
2.51 E-1	4.29 E4	5.56 E3	9.22 E3
3.98 E-1	3.57 E4	8.14 E3	1.17 E4
6.31 E-1	2.97 E4	1.18 E4	1.45 E4
1.00 E0	2.41 E4	1.64 E4	1.77 E4
1.59 E0	1.90 E4	2.18 E4	2.08 E4
2.51 E0	1.49 E4	2.84 E4	2.42 E4
3.98 E0	1.14 E4	3.60 E4	2.76 E4
6.31 E0	8.56 E3	4.43 E4	3.10 E4
1.00 E1	6.36 E3	5.35 E4	3.44 E4

Table 9. Shear Data: Styron 678, 190° C (99)

Steady Shear

$\dot{\gamma}$ (1/sec)	η (Pa-s)	N_1 (Pa)
1.00 E-2	1.11 E4	
4.64 E-2	1.11 E4	
1.00 E-1	9.80 E3	
2.16 E-1	1.01 E4	
3.16 E-1	9.21 E3	1.27 E3
4.64 E-1	8.86 E3	
1.00 E0	7.20 E3	6.13 E3
1.78 E0	6.01 E3	1.28 E4
3.16 E0	4.80 E3	2.45 E4
5.62 E0	3.70 E3	3.76 E4

Dynamic

ω (rad/sec)	η^* (Pa-s)	G′ (Pa)	G″ (Pa)
1.00 E-1	1.03 E4	1.00 E2	1.03 E3
2.16 E-1	9.69 E3	4.31 E2	2.04 E3
4.64 E-1	8.43 E3	1.29 E3	3.69 E3
1.00 E0	6.33 E3	2.90 E3	6.24 E3
2.16 E0	5.34 E3	6.05 E3	9.31 E3
4.64 E0	3.93 E3	1.15 E4	1.42 E4
1.00 E1	2.71 E3	1.92 E4	1.92 E4
2.16 E1	1.80 E3	2.99 E4	2.46 E4
4.64 E1	1.14 E3	4.34 E4	2.99 E4
1.00 E2	6.94 E2	6.00 E4	3.50 E4

Table 10. Shear Data: Polystyrene Blend, 190° C

Steady Shear

$\dot{\gamma}$ (1/sec)	η (Pa-s)	N_1 (Pa)
1.00 E-2	2.28 E4	
2.16 E-2	2.16 E4	
4.64 E-2	1.77 E4	
1.00 E-1	1.61 E4	
2.16 E-1	1.32 E4	4.17 E2
4.64 E-1	1.07 E4	4.55 E3
1.00 E0	8.06 E3	1.07 E4
2.16 E0	5.43 E3	2.34 E4

Dynamic

ω (rad/sec)	η^* (Pa-s)	G′ (Pa)	G″ (Pa)
1.000 E-1	1.540 E4	4.511 E2	1.472 E3
2.155 E-1	1.256 E4	8.847 E2	2.557 E3
4.642 E-1	1.047 E4	2.054 E3	4.405 E3
1.000 E0	7.931 E3	3.681 E3	7.025 E3
2.155 E0	6.370 E3	8.066 E3	1.111 E4
4.642 E0	4.538 E3	1.388 E4	1.585 E4
1.000 E1	3.104 E3	2.253 E4	2.134 E4
2.155 E1	2.024 E3	3.413 E4	2.714 E4
4.642 E1	1.263 E3	4.829 E4	3.326 E4
1.000 E2	7.626 E2	6.442 E4	4.085 E4

Table 11. Dynamic Shear Data: EMN TR-885, 190° C

ω (rad/sec)	η* (Pa-s)	G′ (Pa)	G″ (Pa)
2.155 E-1	5.874 E2	1.308 E1	1.259 E2
4.642 E-1	5.022 E2	3.328 E1	2.307 E2
1.000 E0	4.936 E2	1.020 E2	4.829 E2
2.155 E0	4.077 E2	1.923 E2	8.572 E2
4.642 E0	3.772 E2	4.169 E2	1.700 E3
1.000 E1	3.372 E2	9.025 E2	3.249 E3
2.155 E1	2.959 E2	1.916 E3	6.080 E3
4.642 E1	2.540 E2	3.913 E3	1.112 E4
1.000 E2	2.131 E2	7.621 E3	1.990 E4

Table 12. Dynamic Shear Data: HHM-5502, 190° C

ω (rad/sec)	η* (Pa-s)	G′ (Pa)	G″ (Pa)
1.000 E-1	2.883 E4	1.523 E3	2.448 E3
2.155 E-1	2.200 E4	2.618 E3	3.951 E3
4.642 E-1	1.649 E4	4.411 E3	6.255 E3
1.000 E0	1.223 E4	7.325 E3	9.795 E3
2.155 E0	8.856 E3	1.202 E4	1.482 E4
4.642 E0	6.321 E3	1.928 E4	2.212 E4
1.000 E1	4.380 E3	2.986 E4	3.204 E4
2.255 E1	3.007 E3	4.592 E4	4.570 E4
4.642 E1	2.024 E3	6.875 E4	6.404 E4
1.000 E2	1.335 E3	9.972 E4	8.879 E4

Table 13. Dynamic Shear Data: HXM-50100, 190° C

ω (rad/sec)	η* (Pa-s)	G′ (Pa)	G″ (Pa)
1.000 E-1	1.005 E5	6.819 E3	7.379 E3
2.155 E-1	6.975 E4	1.041 E4	1.084 E4
4.642 E-1	4.739 E4	1.556 E4	1.555 E4
1.000 E0	3.224 E4	2.386 E4	2.169 E4
2.155 E0	2.124 E4	3.147 E4	3.045 E4
4.642 E0	1.395 E4	4.940 E4	4.187 E4
1.000 E1	9.052 E3	7.097 E4	5.620 E4
2.155 E1	5.780 E3	9.987 E4	7.440 E4
4.642 E1	3.625 E3	1.375 E5	9.699 E4
1.000 E2	2.238 E3	1.848 E5	1.263 E5

Table 14. Transient Extensional Data: NPE 952, 150° C

$\dot{\varepsilon} = 0.1\ \text{sec}^{-1}$

Time (sec)	Stress (Pa)	Viscosity (Pa-s)
0	0	0
1.992 E0	4.331 E3	4.514 E4
3.984 E0	6.075 E3	6.298 E4
5.977 E0	7.408 E3	7.702 E4
7.969 E0	8.647 E3	8.982 E4
9.961 E0	9.923 E3	1.029 E5
1.195 E1	1.126 E4	1.169 E5
1.395 E1	1.279 E4	1.328 E5
1.594 E1	1.469 E4	1.524 E5
1.793 E1	1.691 E4	1.753 E5
1.992 E1	1.945 E4	2.010 E5
2.191 E1	2.285 E4	2.364 E5
2.391 E1	2.655 E4	2.747 E5
2.590 E1	3.032 E4	3.138 E5
2.789 E1	3.526 E4	3.647 E5
2.988 E1	3.921 E4	4.058 E5

Table 15. Transient Extensional Data: NPE 952, 150° C

$\dot{\varepsilon} = 0.3\ \text{sec}^{-1}$

Time (sec)	Strain	Stress (Pa)	Viscosity (Pa-s)
0	0	0	0
6.445 E-1	1.880 E-1	7.745 E3	2.697 E4
1.289 E0	3.822 E-1	1.156 E4	4.016 E4
1.934 E0	5.767 E-1	1.473 E4	5.102 E4
2.578 E0	7.718 E-1	1.772 E4	6.131 E4
3.223 E0	9.684 E-1	2.097 E4	7.253 E4
3.867 E0	1.163 E0	2.443 E4	8.472 E4
4.512 E0	1.358 E0	2.869 E4	9.926 E4
5.156 E0	1.554 E0	3.388 E4	1.170 E5
5.801 E0	1.749 E0	4.004 E4	1.385 E5
6.445 E0	1.944 E0	4.770 E4	1.650 E5
7.090 E0	2.139 E0	5.747 E4	1.985 E5
7.734 E0	2.334 E0	6.877 E4	2.380 E5
8.379 E0	2.529 E0	8.248 E4	2.854 E5
9.024 E0	2.724 E0	9.770 E4	3.366 E5
9.668 E0	2.920 E0	1.130 E5	3.896 E5

Table 16. Transient Extensional Data: NPE 952, 150° C

$\dot{\varepsilon} = 0.7\,\text{sec}^{-1}$

Time (sec)	Strain	Stress (Pa)	Viscosity (Pa-s)
0	0	0	0
2.832 E-1	1.897 E-1	1.186 E4	1.771 E4
5.664 E-1	3.890 E-1	1.818 E4	2.707 E4
8.496 E-1	5.878 E-1	2.359 E4	3.497 E4
1.133 E0	7.885 E-1	2.908 E4	4.329 E4
1.416 E0	9.858 E-1	3.482 E4	5.166 E4
1.699 E0	1.185 E0	4.154 E4	6.170 E4
1.983 E0	1.384 E0	4.964 E4	7.365 E4
2.266 E0	1.583 E0	5.976 E4	8.864 E4
2.549 E0	1.782 E0	7.226 E4	1.072 E5
2.832 E0	1.981 E0	8.815 E4	1.304 E5
3.115 E0	2.180 E0	1.082 E5	1.600 E5
3.398 E0	2.379 E0	1.329 E5	1.968 E5
3.682 E0	2.578 E0	1.624 E5	2.406 E5
3.965 E0	2.777 E0	1.905 E5	2.884 E5
4.248 E0	2.976 E0	2.286 E5	3.384 E5

Table 17. Transient Extensional Data: STYRON 678, 165° C

$\dot{\varepsilon} = 0.1\ \text{sec}^{-1}$

Time (sec)	Strain	Stress (Pa)	Viscosity (Pa-s)
0	0	0	0
1.992 E0	1.894 E-1	9.418 E3	9.800 E4
3.984 E0	3.879 E-1	1.227 E4	1.274 E5
5.977 E0	5.883 E-1	1.400 E4	1.452 E5
7.969 E0	7.902 E-1	1.519 E4	1.576 E5
9.961 E0	9.920 E-1	1.629 E4	1.694 E5
1.195 E1	1.192 E0	1.706 E4	1.770 E5
1.395 E1	1.393 E0	1.775 E4	1.842 E5
1.594 E1	1.594 E0	1.844 E4	1.911 E5
1.793 E1	1.795 E0	1.893 E4	1.963 E5
1.992 E1	1.996 E0	1.932 E4	2.003 E5
2.191 E1	2.197 E0	1.954 E4	2.021 E5
2.391 E1	2.398 E0	1.952 E4	2.021 E5
2.590 E1	2.599 E0	1.959 E4	2.028 E5
2.789 E1	2.800 E0	1.931 E4	1.997 E5

Table 18. Transient Extensional Data: STYRON 678, 165° C

$\dot{\varepsilon} = 0.3\ \text{sec}^{-1}$

Time (sec)	Strain	Stress (Pa)	Viscosity (Pa-s)
0	0	0	0
6.445 E-1	1.831 E-1	1.675 E4	5.819 E4
1.289 E0	3.761 E-1	2.416 E4	8.389 E4
1.934 E0	5.719 E-1	2.944 E4	1.024 E5
2.578 E0	7.679 E-1	3.380 E4	1.174 E5
3.223 E0	9.619 E-1	3.758 E4	1.302 E5
3.867 E0	1.158 E0	4.106 E4	1.420 E5
4.512 E0	1.353 E0	4.417 E4	1.531 E5
5.156 E0	1.547 E0	4.706 E4	1.627 E5
5.801 E0	1.743 E0	4.988 E4	1.726 E5
6.445 E0	1.938 E0	5.236 E4	1.810 E5
7.090 E0	2.133 E0	5.450 E4	1.882 E5
7.734 E0	2.329 E0	5.581 E4	1.931 E5
8.379 E0	2.524 E0	5.611 E4	1.941 E5

Table 19. Transient Extensional Data: STYRON 678, 165° C

$\dot{\varepsilon} = 0.7\ \text{sec}^{-1}$

Time (sec)	Strain	Stress (Pa)	Viscosity (Pa-s)
0	0	0	0
2.637 E-1	1.807 E-1	2.343 E4	3.499 E4
5.274 E-1	3.670 E-1	3.588 E4	5.378 E4
7.910 E-1	5.542 E-1	4.553 E4	6.833 E4
1.055 E0	7.393 E-1	5.389 E4	8.082 E4
1.318 E0	9.238 E-1	6.150 E4	9.198 E4
1.582 E0	1.111 E0	6.903 E4	1.033 E5
1.846 E0	1.296 E0	7.616 E4	1.139 E5
2.109 E0	1.483 E0	8.304 E4	1.243 E5
2.373 E0	1.669 E0	9.013 E4	1.347 E5
2.637 E0	1.855 E0	9.664 E4	1.444 E5
2.900 E0	2.041 E0	1.030 E5	1.535 E5
3.164 E0	2.227 E0	1.092 E5	1.626 E5
3.428 E0	2.413 E0	1.146 E5	1.722 E5
3.691 E0	2.599 E0	1.197 E5	1.785 E5
3.955 E0	2.785 E0	1.235 E5	1.844 E5
4.219 E0	2.971 E0	1.267 E5	1.889 E5

Table 20. Transient Extensional Data: STYRON 678, 190° C

$\dot{\varepsilon} = 0.1\ \text{sec}^{-1}$

Time (sec)	Strain	Stress (Pa)	Viscosity (Pa-s)
0	0	0	0
2.4 E-1	2.4 E-2	1.00 E3	1.04 E4
6.0 E-1	6.0 E-2	1.94 E3	2.01 E4
1.2 E0	1.2 E-1	2.44 E3	2.53 E4
1.95 E0	1.92 E-1	2.76 E3	2.86 E4
3.91 E0	3.88 E-1	3.00 E3	3.11 E4
5.86 E0	5.87 E-1	3.06 E3	3.17 E4
7.81 E0	7.83 E-1	3.07 E3	3.18 E4
9.77 E0	9.81 E-1	3.06 E3	3.17 E4
1.17 E1	1.18 E0	3.03 E3	3.14 E4
1.37 E1	1.38 E0	2.97 E3	3.08 E4
1.56 E1	1.57 E0	2.94 E3	3.05 E4
1.76 E1	1.77 E0	2.83 E3	2.94 E4
1.95 E1	1.97 E0	2.70 E3	2.80 E4

Table 21. Transient Extensional Data: STYRON 678, 190° C

$\dot{\varepsilon} = 0.3\ sec^{-1}$

Time (sec)	Strain	Stress (Pa)	Viscosity (Pa-s)
0	0	0	0
8.0 E-2	2.4 E-2	1.67 E3	5.86 E3
2.0 E-1	6.0 E-2	3.83 E3	1.34 E4
4.0 E-1	1.2 E-1	6.56 E3	2.30 E4
6.64 E-1	1.97 E-1	6.73 E3	2.36 E4
1.33 E0	3.99 E-1	8.10 E3	2.82 E4
1.99 E0	5.99 E-1	8.73 E3	3.03 E4
2.66 E0	7.99 E-1	9.14 E3	3.17 E4
3.32 E0	1.00 E0	9.30 E3	3.22 E4
3.98 E0	1.20 E0	9.51 E3	3.30 E4
4.65 E0	1.40 E0	9.63 E3	3.34 E4
5.31 E0	1.60 E0	9.77 E3	3.38 E4
5.98 E0	1.80 E0	9.83 E3	3.40 E4
6.64 E0	2.01 E0	9.83 E3	3.40 E4
7.31 E0	2.21 E0	9.78 E3	3.39 E4
7.97 E0	2.41 E0	9.74 E3	3.37 E4
8.63 E0	2.61 E0	9.61 E3	3.33 E4
9.30 E0	2.81 E0	9.28 E3	3.21 E4

Table 22. Transient Extensional Data: STYRON 678, 190° C

$\dot{\varepsilon} = 0.7\ \text{sec}^{-1}$

Time (sec)	Strain	Stress (Pa)	Viscosity (Pa-s)
0	0	0	0
3.4 E-2	2.4 E-2	3.47 E3	5.20 E3
8.6 E-2	6.0 E-2	7.08 E3	1.06 E4
1.71 E-1	1.20 E-1	1.00 E4	1.50 E4
2.73 E-1	1.85 E-1	1.23 E4	1.84 E4
5.47 E-1	3.77 E-1	1.60 E4	2.41 E4
8.20 E-1	5.71 E-1	1.81 E4	2.72 E4
1.09 E0	7.63 E-1	1.96 E4	2.95 E4
1.37 E0	9.57 E-1	2.07 E4	3.11 E4
1.64 E0	1.15 E0	2.17 E4	3.25 E4
1.91 E0	1.34 E0	2.24 E4	3.35 E4
2.19 E0	1.54 E0	2.30 E4	3.45 E4
2.46 E0	1.73 E0	2.34 E4	3.52 E4
2.73 E0	1.92 E0	2.38 E4	3.57 E4
3.01 E0	2.12 E0	2.37 E4	3.55 E4
3.28 E0	2.31 E0	2.34 E4	3.51 E4
3.56 E0	2.50 E0	2.29 E4	3.43 E4
3.83 E0	2.69 E0	2.17 E4	3.25 E4
4.10 E0	2.89 E0	1.98 E4	2.97 E4

Table 23. Transient Extensional Data: Polystyrene Blend, 190° C

$\dot{\varepsilon} = 0.1\ sec^{-1}$

Time (sec)	Strain	Stress (Pa)	Viscosity (Pa-s)
0	0	0	0
2.40 E-1	2.40 E-2	1.11 E3	1.16 E4
6.00 E-1	6.00 E-2	2.50 E3	2.61 E4
1.20 E0	1.20 E-1	3.42 E3	3.57 E4
1.97 E0	1.90 E-1	4.13 E3	4.31 E4
3.95 E0	3.88 E-1	4.91 E3	5.11 E4
5.92 E0	5.88 E-1	5.65 E3	5.53 E4
7.89 E0	7.87 E-1	5.68 E3	5.90 E4
9.86 E0	9.86 E-1	5.89 E3	6.10 E4
1.18 E1	1.19 E0	6.08 E3	6.30 E4
1.38 E1	1.38 E0	6.13 E3	6.35 E4
1.58 E1	1.58 E0	6.18 E3	6.40 E4
1.78 E1	1.78 E0	6.17 E3	6.40 E4
1.97 E1	1.98 E0	6.06 E3	6.27 E4
2.17 E1	2.18 E0	5.83 E3	6.01 E4
2.37 E1	2.38 E0	5.34 E3	5.52 E4

Table 24. Transient Extensional Data: Polystyrene Blend, 190° C

$\dot{\varepsilon} = 0.3\ \text{sec}^{-1}$

Time (sec)	Strain	Stress (Pa)	Viscosity (Pa-s)
0	0	0	0
8.00 E-2	2.40 E-2	1.81 E3	6.29 E3
2.00 E-1	6.00 E-2	4.44 E3	1.54 E4
4.00 E-1	1.20 E-1	6.67 E3	2.32 E4
6.64 E-1	1.93 E-1	8.40 E3	2.94 E4
1.33 E0	3.94 E-1	1.09 E4	3.81 E4
1.99 E0	5.97 E-1	1.24 E4	4.30 E4
2.66 E0	7.96 E-1	1.35 E4	4.68 E4
3.32 E0	9.97 E-1	1.44 E4	4.98 E4
3.98 E0	1.20 E0	1.52 E4	5.28 E4
4.65 E0	1.40 E0	1.59 E4	5.49 E4
5.31 E0	1.60 E0	1.64 E4	5.66 E4
5.98 E0	1.80 E0	1.68 E4	5.81 E4
6.64 E0	2.00 E0	1.69 E4	5.86 E4
7.31 E0	2.20 E0	1.67 E4	5.80 E4
7.97 E0	2.40 E0	1.61 E4	5.59 E4
8.63 E0	2.61 E0	1.49 E4	5.17 E4

Table 25. Transient Extensional Data: Polystyrene Blend, 190° C

$\dot{\varepsilon} = 0.7\ \text{sec}^{-1}$

Time (sec)	Strain	Stress (Pa)	Viscosity (Pa-s)
0	0	0	0
2.73 E-1	1.87 E-1	1.39 E4	2.10 E4
5.47 E-1	3.81 E-1	1.94 E4	2.93 E4
8.20 E-1	5.74 E-1	2.29 E4	3.46 E4
1.09 E0	7.65 E-1	2.57 E4	3.86 E4
1.37 E0	9.59 E-1	2.81 E4	4.23 E4
1.64 E0	1.15 E0	3.01 E4	4.54 E4
1.91 E0	1.34 E0	3.20 E4	4.80 E4
2.19 E0	1.54 E0	3.37 E4	5.06 E4
2.46 E0	1.73 E0	3.53 E4	5.30 E4
2.73 E0	1.92 E0	3.65 E4	5.49 E4
3.01 E0	2.12 E0	3.73 E4	5.59 E4
3.28 E0	2.31 E0	3.71 E4	5.55 E4
3.56 E0	2.50 E0	3.07 E4	4.61 E4

Table 26. Transient Extensional Data: EMN TR-885,150° C

$\dot{\varepsilon} = 0.1\ \text{sec}^{-1}$

Time (sec)	Stress (Pa)
0	0
2.0 E-1	8.290 E2
4.0 E-1	9.570 E2
6.0 E-1	1.100 E3
8.0 E-1	1.286 E3
1.0 E0	1.471 E3
1.2 E0	1.714 E3
1.4 E0	2.000 E3
1.6 E0	2.314 E3
1.8 E0	2.686 E3
2.0 E0	3.100 E3
2.2 E0	3.643 E3
2.4 E0	4.329 E3
2.6 E0	5.071 E3
2.8 E0	6.129 E3
3.0 E0	7.429 E3

Table 27. Transient Extensional Data: HHM-5502, 190° C

$\dot{\varepsilon} = 0.1\ \text{sec}^{-1}$

Time (sec)	Stress (Pa)	Viscosity (Pa-s)
0	0	0
1.984 E0	5.973 E3	6.205 E4
2.977 E0	7.719 E3	8.008 E4
4.969 E0	9.229 E3	9.562 E4
6.961 E0	1.092 E4	1.136 E5
8.195 E0	1.301 E4	1.349 E5
1.095 E1	1.545 E4	1.601 E5
1.294 E1	1.806 E4	1.870 E5
1.493 E1	2.104 E4	2.174 E5
1.692 E1	2.392 E4	2.476 E5
1.891 E1	2.648 E4	2.738 E5
2.091 E1	2.940 E4	3.043 E5
2.290 E1	3.055 E4	3.161 E5
2.489 E1	2.878 E4	2.970 E5

Table 28. Transient Extensional Data: HXM-50100, 190° C

$\dot{\varepsilon} = 0.1\ \text{sec}^{-1}$

Time (sec)	Stress (Pa)	Viscosity (Pa-s)
0	0	0
1.984 E0	9.428 E3	9.870 E4
2.977 E0	2.512 E4	2.631 E5
4.969 E0	3.471 E4	3.616 E5
6.961 E0	4.339 E4	4.576 E5
8.195 E0	5.458 E4	5.690 E5
1.095 E1	6.603 E4	6.846 E5
1.294 E1	7.762 E4	8.036 E5
1.493 E1	8.696 E4	9.025 E5
1.692 E1	8.882 E4	9.191 E5

Appendix B. Flow Birefringence Theory

Flowing polymer melts can be characterized in terms of shear and normal stresses which act on the fluid. These stresses can be resolved into components which act along the principal axes of the flow. As a result of the stress there is an orientation of molecules within the melt which leads to a corresponding anisotropy of the optical properties of the polymer. A tensoral optical property, such as the refractive index, can similarly be resolved into components along its principal axes. The technique of flow birefringence makes use of the change in optical properties to determine the state of stress in the melt by means of the stress-optical law which relates the two properties. The objective here is to provide the theory behind flow birefringence.

For simple shear flow the stress tensor $\underline{\pi}$, is symmetric (i.e. $\pi_{ij} = \pi_{ji}$). For Newtonian fluids the normal stresses are zero however, for non-Newtonian fluids they are not and the stress tensor takes on the following form where $\underline{\pi} = P\underline{\delta} + \underline{\tau}$,

$$\pi = \begin{pmatrix} \tau_{11} + P & \tau_{12} & 0 \\ \tau_{12} & \tau_{22} + P & 0 \\ 0 & 0 & \tau_{33} + P \end{pmatrix} \qquad (B.1)$$

The principal stresses are at an angle χ' relative to the flow lines of the system. However, since both the principal stress axes (I, II) and the laboratory axes (x,y) are in the same plane it is possible to obtain expressions relating the principal stress

difference, $\Pi = \Pi_{\prime} - \Pi_{\prime\prime}$, to the shear stress, τ_{12}, and the first normal stress difference, $\tau_{11} - \tau_{22}$.

$$\Pi \sin 2\chi' = 2\tau_{12} \tag{B.2}$$

$$\Pi \cos 2\chi' = \tau_{11} - \tau_{22} \tag{B.3}$$

Division of the first equation by the second eliminates the principal stress difference and leads to an expression relating the orientation angle to the shear stress and the first normal stress difference.

$$\tan 2\chi' = \frac{2\tau_{12}}{\tau_{11} - \tau_{22}} \tag{B.4}$$

It has been found that there are expressions relating the birefringence in stressed materials to the applied stress (107). These are based on the stress optic law which states the following,

1. The polarization axes and the principal stress axes are coincident at any point in a stressed solid (i.e. the axes are coaxial).

2. At that point the differences of the velocities of the two oppositely polarized rays are proportional to the difference of the two principal stresses.

For the refractive index tensor $\underline{n}$, which has the same form as the stress tensor, the following expressions can be written based on the first statement of the stress-optic law,

$$\Delta n \sin 2\chi = 2n_{12} \tag{B.5}$$

$$\Delta n \cos 2\chi = n_{11} - n_{22} \tag{B.6}$$

where χ is the extinction angle. From the second statement it was found that,

$$n_{12} = C\tau_{12} \tag{B.7}$$

$$n_{11} - n_{22} = C(\tau_{11} - \tau_{22}) \tag{B.8}$$

where C is the stress optic coefficient. These last two equations provide a direct means of obtaining the shear stress and the first normal stress difference based on measurements of the refractive indices and knowledge of the stress optic coefficient.

The same results were obtained later based on a molecular theory of the behavior of polymeric systems (107,108). According to this theory the components of the stress tensor could be expressed as (107),

$$\tau_{ij} = \sum_k \frac{N_a c_k}{M_k} < x_i F_{jk} > \tag{B.9}$$

This represents the summation of the contribution of k chains to the overall stress of the system where N_a is Avogadro's number, c is the concentration, and M is the molecular weight. F_j represents the x_j component of the statistical force between chain ends and x is the coordinate of the end of the chain whose other end is located at the origin of the coordinate system.

An expression for the observed birefringence can be obtained by starting with the Lorentz-Lorenz equation,

$$\frac{n^2 - 1}{n^2 + 2} = \frac{4}{3}\pi \sum_k B_k \frac{N_k c_k}{M_k} \tag{B.10}$$

where B is the polarization per molecule and n is the refractive index.

When the above equation is rewritten in terms of the components of the refractive index tensor and the polarizability tensor, the following equation for the birefringence is obtained,

$$n_{ii} - n_{jj} = \frac{2}{9}\pi \frac{(\bar{n}^2 + 2)^2}{\bar{n}} \sum_k \frac{N_a c_k}{M_k} (B_{ii} - B_{jj})_k \tag{B.11}$$

where $\bar{n}$ represents the average index of refraction.

An expression is now needed to replace the molecular polarizability B . This is done by summing the polarizability contributions of chain segments. This leads to the following expression,

$$B_{ll} - B_{jj} = N(\alpha_1 - \alpha_2)\frac{3 < \cos^2\theta > - 1}{2} \qquad (B.12)$$

where N is the number of segments, α_1 is the molecular polarizability parallel to the segment, α_2 is the polarizability perpendicular to the segment, and θ is the angle between the reference axis and the segment. This can be simplified to give,

$$B_{ll} - B_{jj} = \frac{3}{5}(\alpha_1 - \alpha_2)\frac{< x_i x_j >}{r_0^2} \qquad (B.13)$$

where r_0^2 is the mean squared end-to-end distance of the chain. If this expression is substituted into equation B.11 the following is obtained,

$$n_{ll} - n_{jj} = \frac{6}{45}\pi\frac{(\bar{n}^2 + 2)^2}{\bar{n}}(\alpha_1 - \alpha_2)\sum_k \frac{N_a c_k}{M_k}\frac{< x_i^2 - x_j^2 >_k}{r_0^2} \qquad (B.14)$$

The force between chain ends has been found to be $F = -\frac{3kTr}{r_0^2}$ .When this is inserted into equation B.9 and the result is combined with the birefringence equation above the following results are obtained,

$$n_{11} - n_{22} = C(\tau_{11} - \tau_{22}) \qquad (B.15)$$

$$n_{11} - n_{33} = C(\tau_{11} - \tau_{33}) \qquad (B.16)$$

$$n_{12} = C\tau_{12} \qquad (B.17)$$

Assuming coaxiality then leads to,

$$\Delta n \sin 2\chi = 2C\tau_{12} \qquad (B.18)$$

$$\Delta n \cos 2\chi = C(\tau_{11} - \tau_{22}) \qquad (B.19)$$

where C is the stress optic coefficient,

$$C = \frac{2}{45}\frac{\pi}{kT}\frac{(\bar{n}^2 + 2)^2}{\bar{n}}(\alpha_1 - \alpha_2) \qquad (B.20)$$

Therefore, it is seen that the previously postulated equations for birefringence can be derived based on a molecular theory of polymer behavior. There are, however, assumptions included in the derivation. These are that segmental polarizabilities are additive, only small chain deformations are occurring, and that the real chain can be described by a statistical chain.

The vita has been removed from the scanned document